MANCHESTER 1824
The University of Manchester

Application of the State Space Approach to Cross-Laminated Timber Panels

A thesis submitted to the University of Manchester for the degree of
Doctor of Philosophy
in the Faculty of Science and Engineering

2019

Asad Shukri Albostami

School of Mechanical, Aerospace and Civil Engineering

The University of Manchester

TABLE OF CONTENTS

Word count: 37582

LIST OF PUBLISHED WORKS

Parts of this research have been presented or submitted for publication as follows:

Journal published papers:

Albostami, A., Wu, ZJ. and Zou, Z. 2017. State space approach with FEM for the determination of structural behaviour of composite plates. *International Journal of Structural Integrity*. 8(4), 468-483.

Albostami, A., Wu ZJ. and Cunningham LS. 2017. Structural behaviour of Cross-Laminated Timber panels by the State Space Approach. *International Journal of Computational Methods and Experimental Measurements*. 5(6), 834-846.

Journal submitted paper:

Albostami, A., Wu ZJ. and Cunningham LS. 2018. Assessment of Cross-Laminated Timber Panels by the State Space Approach. *Advances in Structural Engineering*.

Conference papers:

Albostami, A., Wu, ZJ. and Zou, Z. 2015. Precise Determination of Structural Behaviour of Composite Plates. MACE PGR Conference, University of Manchester, 22nd March, Manchester, UK.

Albostami, A., Wu, ZJ. and Zou, Z. 2015. State Space Approach with FEM for Composite Plates. 5th International Workshop on Aerostructures, 2nd - 4th September, Manchester, UK.

Albostami, A., Wu ZJ. and Cunningham LS. 2017. Structural behaviour of Cross-Laminated Timber panels by the State Space Approach. 1st International Conference on Timber Structures and Engineering, 13th - 15th June, New Forest, UK.

Albostami, A., Wu ZJ., Cunningham LS. and Han C. 2018. Numerical Modelling of Cross-Laminated Timber Panels. 1st International Conference on Theoretical, Analytical and Computational Methods for Composite Materials and Composite Structures, ICOMP 2018, 23rd - 25th May, Wuhan, China.

LIST OF FIGURES

LIST OF TABLES

LIST OF NOTATIONS

a	Length
b	Width
C	Elastic constant
$[D_{mn}]$	System matrix with the number of Fourier series terms
$E_{1,2,3}$	Young's Moduli
EI_{eff}	Effective bending stiffness of the initial cross-section
F_{mn}	State vector
G	Shear Moduli
$[G]$	System state matrix
h	Thickness of plate
h_{board}	Thickness of each CLT panel board
h_{panel}	Thickness of CLT panel
h/a	Thickness-to-width ratio
K	Composition factor
l_{panel}	Length of CLT panel
m, n	Number of Fourier series terms
q_o	Unit load
u, v, w	Displacement components
W_{board}	Width of each CLT panel board
W_{panel}	Width of CLT panel
γ	Shear strain
ε	Strain vector
ν	Poisson's ratio
σ	Stress vector
σ^*, τ^*	Strength properties
τ	Shear stress

LIST OF ABBREVIATIONS

BS EN	British Standards/European norm
C3D8	3D 8-node linear brick element
C3D20	3D 20-node linear brick element
C3D8R	Reduced integrated 3D 8-node linear brick element
C3D20R	Reduced integrated 3D 20-node linear brick element
CLT	Cross-Laminated Timber
CLPT	Classical Laminated Plate Theory
CPT	Classical Plate Theory
ESLT	Equivalent Single Layer Plate Theory
FEM	Finite Element Method
FRP	Fibre-Reinforced Polymer
FSDT	First-Shear Order Deformation Theory
GLT	Glued-Laminated Timber
MEMS	Micro-Electro-Mechanical-System
HSDT	Higher-order Shear Deformation Theory
MDF	Medium Density Fibreboard
MUF	Melamine-Urea-Formaldehyde
OSB	Oriented Strand Board
SLS	Serviceability Limit State
SSA	State Space Approach
SSL	Sinusoidal Load
UDL	Uniformly Distributed Load
ULT	Ultimate Limit State
1K-PUR	One Part Polyurethane

ABSTRACT

In many countries today, cross-laminated timber (CLT) panels are increasingly being used in structural applications. CLT has many key advantages such as high strength-to-weight ratio in comparison to other common construction materials, excellent sustainability credentials, easy handling in construction, quick erection time, and good thermal and sound insulation.

CLT exhibits complex behaviour; therefore, powerful theories are required to provide a better understanding of the mechanical behaviour of CLT panels and to enable their efficient and safe application in structural engineering. From that point of view, developing theoretical and numerical solutions for the analysis of CLT panels is an active research topic.

A CLT panel is a laminated composite panel and, from an engineering design point of view, it can be considered as an orthotropic composite material with an elastic behaviour. Existing analytical approaches for CLT panels have limitations in applicability and accuracy. Hence, the State Space Approach (SSA) has the potential to improve the accuracy and range of applicability over these existing methods. The SSA provides theoretically accurate three-dimensional solutions that guarantee continuous transverse stress distributions across the thickness of the plates. Also, the boundary conditions and the continuity at the interfaces are satisfied (Ye, 2003). Thus, the research presented in this thesis will investigate CLT panels using the novel application of this approach.

Before focusing on the specific application to CLT, the general SSA is explored for simply supported orthotropic composite plates under different types of out-of-plane loads. A new analytical solution by using the SSA for the case of a plate with three sides simply supported and one free edge under different out-of-plane loads will be developed and the derivations for the equations will be shown in detail. Note that this is the first time the SSA formulation for this particular boundary condition has been developed. For both the aforementioned and fully simply supported boundary conditions, the results obtained by using the SSA are compared with existing experimental works, various existing analytical approaches and numerical methods.

To provide more knowledge and understanding of this particular application, numerical modelling of CLT using the Finite Element Method (FEM) via ABAQUS is conducted. Although the FEM is very applicable in understanding the general structural behaviour of the panel, it shows discontinuity of the transverse shear stresses at the interfaces of each ply of the CLT since, in the case of solid elements, the transverse stresses are obtained from the displacement field not from the equilibrium equations. Crucially, the SSA overcomes this problem and shows continuous stress distributions between the plies. Ultimately, this work shows that, for the boundary conditions examined, the SSA provides an accurate and efficient way to capture the structural behaviour of CLT panels subject to out-of-plane loads and can outperform some of the existing analytical methods commonly used in practice.

DECLARATION

No portion of the work referred to in the thesis has been submitted in support of an application for another degree or qualification of this or any other university or other institute of learning.

COPYRIGHT STATEMENT

This thesis is dedicated to the memory of my father, Shukri Albostami. I miss him every day, but I am glad to know he saw this process through to its completion. It is also dedicated to my mother, Hana Abu Dahab, who has always supported me.

Asad Shukri Albostami

ACKNOWLEDGEMENTS

Firstly, I would like to express my sincere thanks to my supervisor, *Dr Lee Cunningham*, for the continuous support of my PhD study, for his patience, motivation and knowledge. His guidance has helped me throughout my research and he is always pushing me to be the best. Also, I would like to thank *Dr Jack Wu* for his guidance, comments and knowledge during my journey.

Besides my supervisors, I would like to thank *Prof Benedict D. Rogers* and *Prof Martin Gillie* for their support during my research, and their appreciable comments and advice that enabled to me to conduct my research in the way that I am now presenting.

I would like to thank *Miss Christine Jinks* for making me always feel supported, and for her wonderful personality that makes me love being part of the school of MACE.

Many thanks to my sponsoring university, *the University of Petra*, for funding me during my PhD journey.

Great thanks to my family in Jordan, for believing in me and supporting me during my journey to finish my PhD.

Thanks to my friend *Miss Rwayda Al Hamad* for being a true friend and for supporting me all the time during my PhD.

Big thanks to my special friends *Dr Andrew Bennett* and *Robert Lovelace* for supporting me and welcoming me here in the UK and showing me all the wonderful places and the kind traditions in the UK.

Finally, special thanks to my friends who supported me during my PhD, especially *Cara Aoibheann*, *Daniel Gunn* and *his family*, *Dr Darcy Gillie*, *Maher Ajour*, *Matteo Izzi*, *Rana Shabber*, *Sergio Oliveira Formoso* and *Yazan Al Qaisi*.

CHAPTER 1
INTRODUCTION

1.1 Introduction and motivation

Cross-laminated timber (CLT) elements exhibit complex behaviour. Therefore, rigorous theories are required to provide a clear understanding of their structural performance and enable their efficient and safe application in construction. In view of this, developing theoretical and numerical solutions for the analysis of CLT panels is an active research topic.

Concerning theoretical solutions, two-dimensional theories can provide a good prediction of some global responses of thin plates. However, as the thickness of the plate increases, the accuracy of the results will decrease, and these theories can give only inaccurate inter-laminar stresses. Hence, in this research, a 3D approach called the State Space Approach (SSA) has been applied to overcome these limitations and give more accurate results.

The SSA provides theoretically accurate three-dimensional solutions that guarantee continuous transverse stress distributions across the thickness of the plates. Also, the boundary conditions and the continuity at the interfaces are satisfied. In addition, the SSA can give a full range of elastic structural behaviour exactly for various thicknesses from thin to very thick plates (Sheng and Ye, 2003).

In this research, the SSA will be adopted and applied to CLT as a structural engineering application; there are, however, inherent limitations in the SSA approach, principally the fact that the glued joints are ignored. However, even with this simplification, the superior ability of the SSA compared to other standard approaches in capturing the stress distributions across the range of practical CLT plate span-to-thickness ratios

justifies it being a focus of investigation. For practical design purposes, timber is considered to be an elastic material. Similarly, since CLT can be described as essentially an orthotropic laminated plate, it would seem the SSA is highly applicable.

1.2 Research impact

The outcomes from this research have significant application in structural engineering and the construction industry. Increased understanding of the behaviour of CLT panels under different types of out-of-plane loads and different boundary conditions and an increased range of applicability in terms of panel span-to-depth ratio will lead to design efficiencies.

The primary output of this research aims to create a new analytical solution and apply it to the CLT panel for more understanding about the effect of the thickness-to-width ratio on the structural behaviour.

Ultimately, it is intended that the SSA (when applied through a user-friendly interface, in this case, the software MATHEMATICA) may provide the engineer with an easy way to design CLT panels with different types of loads and boundary conditions. Also, this approach has the potential to overcome the limitations inherent in commonly used design approaches such as the Gamma method in Eurocode 5, as will be discussed in chapters 4 and 5.

1.3 Thesis outline

This thesis is constructed as follows:

Chapter 2 introduces the background to CLT panels in structural engineering applications, associated material properties and the design guidance currently available for CLT. Also, it reviews different existing experimental work, analytical approaches and numerical methods applied to CLT panels under different types of load.

Chapter 3 reviews the development and the fundamental concepts of the existing two-dimensional and three-dimensional plate approaches that will be used later in this research.

Chapter 4 presents the concept of the State Space Approach (SSA) for simply supported orthotropic composite plates. For the application of the SSA, different case studies are analysed by using the SSA for the determination of structural behaviour of general composite plates under different types of out-of-plane load. Then, finite element method (FEM) models are validated with SSA results. Following this, the SSA is extended to consider laminated composite plates, and a comparison between the SSA and an existing analytical approach will be shown.

Chapter 5 applies the SSA to CLT panels as a novel application subjected to out-of-plane loads to obtain the 3D analytical solutions that satisfy the boundary conditions and the continuity conditions between different laminates. Different case studies will be included in this chapter; firstly, the SSA and different existing 2D and 3D analytical methods will be validated with different existing experimental tests, then the 3D SSA will be compared with different existing 2D and 3D methods with the FEM.

Chapter 6 presents a new analytical solution using the SSA for boundary conditions consisting of three sides simply supported and one free edge. In this chapter, the SSA together with the state transfer matrix will be presented to investigate general homogenous orthotropic composite plate behaviour with the new boundary condition and then existing analytical and FEM results will be compared with the SSA. Subsequently, the new analytical solution provided by the SSA will be applied to CLT panels. Two case studies will be presented. The studies will consider the CLT panels under different types of out-of-plane load.

Chapter 7 summarises the work carried out in this research, draws the main conclusions of this work and gives recommendations for future work.

1.4 Objectives

As will be seen from the next chapter, developing theoretical and numerical solutions for the analysis of CLT panels is still an important area of research in order to provide a better understanding of structural performance and enable efficient and safe application in construction. From this point of view, the main objectives of the work presented here are:

1. To investigate and review the prevailing plate theories applied to the CLT panels.
2. To introduce and develop a 3D analytical approach called the SSA for CLT panels with simply supported boundary conditions under different types of loads, and analyse and compare the stresses and the displacements with different existing experimental works and analytical approaches. Such theories are required to better understand the mechanical potential of CLT panels in timber construction and to enable their efficient and safe application in structural engineering.
3. To develop numerical models by using finite element methods via ABAQUS for CLT panels, considering the bonding between the plies, and compare the performance with the 3D SSA.
4. To further develop the simply supported boundary conditions by using the SSA that has been discussed in the second objective and explore a new analytical solution for three sides simply supported and one free edge, and apply the new solution to the CLT panels and compare the new solution with existing analytical approaches and numerical FEM under different types of loads.

Ultimately, these overall objectives of the research will be to apply the SSA to CLT panels and compare the predictions against existing test data, current analytical approaches and FEM. Various boundary conditions and stress states reflecting real-life CLT elements will be explored.

CHAPTER 2
BACKGROUND TO STRUCTURAL TIMBER AND CLT

2.1 Background and characteristics of structural timber

The use of timber as a structural material dates back millennia. In previous centuries, those building with timber did so with an intuitive and inherited understanding of the material and its capabilities. Advances in structural engineering in the last 150 years have resulted in greater understanding of material behaviour; this is driven by the increasing performance demands of today's built environment. In today's world, the environmental credentials afforded by timber have led to an increased interest in this natural material. In parallel with this, new manufacturing technologies for engineered timber products such as glulam and cross-laminated timber have enabled timber to attain greater applicability than ever before, allowing it to compete with concrete and steel in many cases.

Softwood and Hardwood are the two categories for timber as a structural material (Ozelton and Baird, 2006). Softwoods are obtained from coniferous trees and are used commonly for structural timber for the following reasons: material availability, ease of handling, low cost and fast growth rate. In contrast, hardwood is obtained from broad-leaved trees and normally has superior durability compared to softwood; for that reason, it is often used for claddings. Typically, broad-leaved type trees need a very long time to grow and the sourcing of hardwood can be less sustainable compared to softwood (McKenzie, 2000).

For context, in the same span and load scenario, softwood timber in terms of weight can be up to six times more efficient than concrete panels and three times more efficient than lightweight composites such as graphite-fibre composites (Harris, 2015).

Timber is considered an elastic orthotropic composite material, which implies that it will recover completely from any deformation after the load is removed. Timber strength based on the direction of the component cellular fibres is often referred to as the grain; normally these run parallel to the growth direction of the parent tree (in the case of timber sourced from the trunk). In reference to the grain direction, timber has three principal axes: longitudinal axis parallel to the grain, radial and tangential axes, as shown in Figure 2-1.

The strength and stiffness of timber is much greater parallel to the grain than in the radial or tangential directions (i.e. the axes perpendicular to the grain) (McKenzie, 2000). For commonly used softwoods, the tangential stiffness is usually slightly lower than the radial stiffness; this varies depending on the species, Dinwoodie (2000). For example, typically for spruce timber, the tangential stiffness would be expected to be around 60% of the radial stiffness, Dinwoodie (2000).

In the present research, the timber material within each CLT lamina is treated as orthotropic and the mechanical properties in the two perpendicular directions, i.e. radial and tangential to the grain, are assumed to be the same as is common in design practice (McKenzie, 2000; American Institute of Timber Construction, 2012; Stürzenbecher *et al*., 2010).

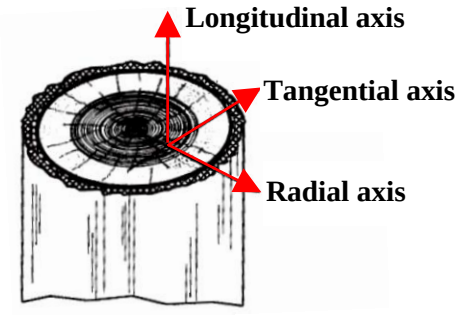

Figure 2-1 Timber structure (McKenzie, 2000).

Figure 2-2 shows the typical stress-strain curves for tension and compression behaviour of timber when the load is parallel and perpendicular to the grain. In this figure, when the load is parallel to the grain (as shown in Figure 2-2(a)), timber shows stronger behaviour compared with when the load is perpendicular to the grain as shown in Figure 2-2(b). In tension, timber exhibits an essentially linear behaviour up to rupture in the parallel and perpendicular to the grain directions. In compression, timber exhibits some softening behaviour characterised by post-peak crushing.

Due to its elastic behaviour (Dinwoodie, 2000), as shown in Figure 2-2, Hooke's law can be applied to timber, i.e. the deformations induced when subjected to an external force will be directly proportional to the magnitude of the applied force (McKenzie, 2000).

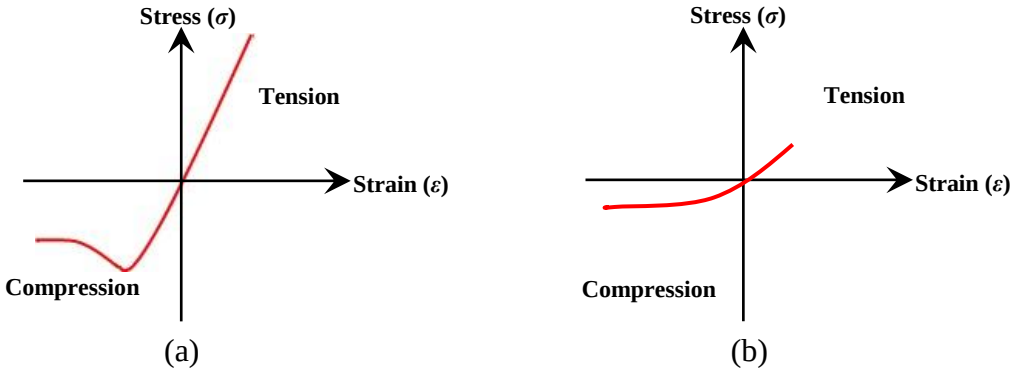

Figure 2-2 Typical stress-strain diagram of timber for (a) load parallel to the grain and (b) load perpendicular to the grain (McKenzie, 2000).

As a natural material, solid timber exhibits various imperfections such as knots, shakes and wanes. Various engineered timber products have been developed as a means of creating a more uniform strength and stiffness behaviour as well as reducing the frequency and effect of defects, e.g. Glued Laminated Timber (GLT), Oriented Strand Board (OSB), Plywood, Particleboard, Medium Density Fibreboard (MDF) and Cross-Laminated Timber (CLT) (Kutnar and Muthu, 2016).

The work presented in this thesis focuses on CLT. By cross-laminating the softwood panels, the dimensional stability of boards along the grain stabilises the cross-grain movement of boards laid orthogonally, creating a renewable, low-cost panel product of remarkable efficiency (Harris, 2015). The material efficiency of a CLT panel can be expressed using the equation proposed by Gordon (1988), i.e. $\sqrt[3]{E}/\rho$; where E is the modulus of elasticity and ρ is the density. Further detail of CLT characteristics will be presented in the following section.

2.2 Cross-laminated timber (CLT): Background and characteristics

CLT is a laminated composite panel used in structural engineering applications forming walls, floors and roofs, etc. It was first developed in Switzerland and Austria in the mid-1990s (Harris, 2015).

The CLT panel consists of at least three plies of boards orthogonally cross-stacked and glued together on their wide faces and, in some cases, on the narrow faces too, typically in a symmetric layup, as shown in Figure 2-3. In some specific conditions, double plies in the same orientation may be used to improve the structural capacity of the CLT members, as shown in Figure 2-4. In material terms CLT can be considered as an orthotropic composite.

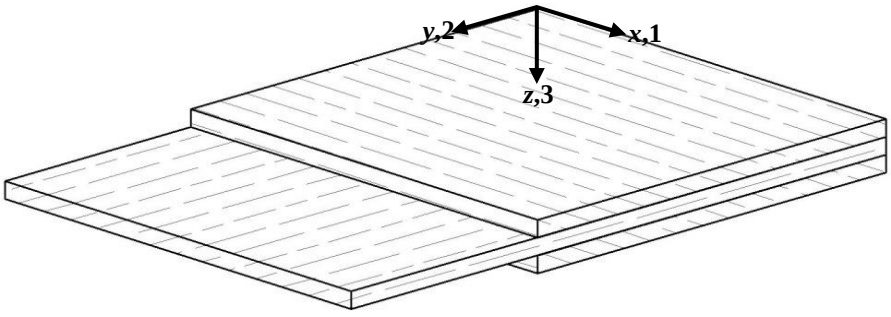

Figure 2-3 Schematic of a CLT panel.

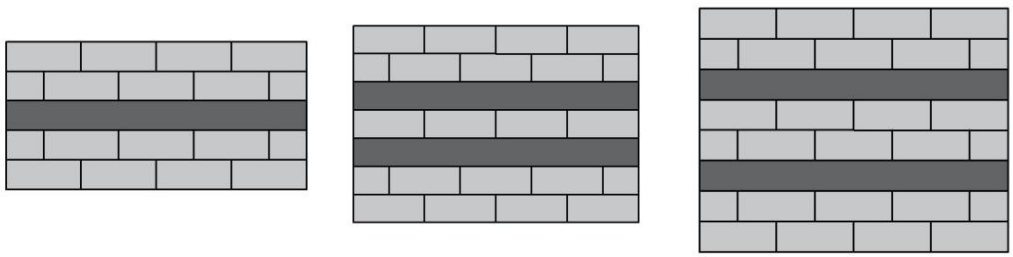

Figure 2-4 Specific conditions of CLT panel structure.

The principle of CLT is similar to plywood, whereby the natural timber's reduction in strength and stiffness perpendicular to the grain compared to parallel to the grain is ‘evened out’ with successive laminates with alternate grain orientation. Therefore, the crossed layers will improve the structural integrity and dimensional stability (Sutton *et al*., 2011). CLT panels differ from regular plywood and similar engineered timber products by their size; typically, CLT sections have a comparable thickness to masonry or concrete walls.

Consequently, CLT panels have significant strength and this has allowed timber to compete with concrete and steel in multi-storey applications. Currently, CLT buildings of nine storeys or more have been constructed (Stauder, 2013). CLT panels may act as one- or two-way systems depending on their application, e.g. walls or floor slabs; see Figure 2-5.

The behaviour of CLT panels as one- or two -way systems is dependent on the supporting system. If the panel is supported from two opposite ends only then it will behave as a one-way spanning system. Two-way action will be derived the panel is supported on all four edges (Lewis *et al*., 2016). Also, in the case of a rectangular panel supported on four edges, the degree of two-way action is dependent on the ratio of the long to the short edge.

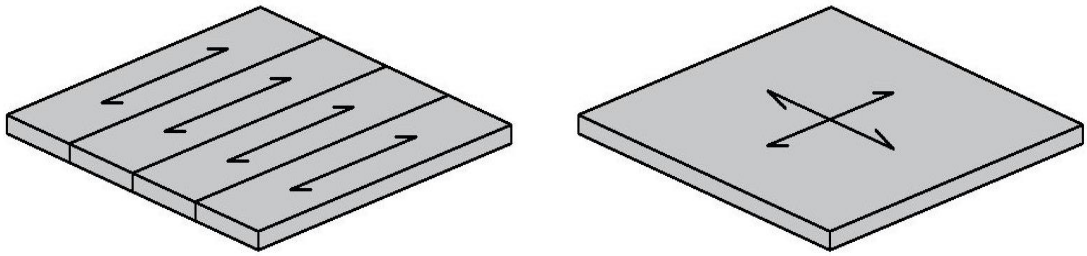

(a) (b)

Figure 2-5 CLT panels (a) one-way and (b) two-way.

The use of CLT panels has increased in the construction sector over the last 10 years due to the significant advantages they offer. The high strength-to-weight ratio, ease of handling in construction, quick erection time, and good thermal and sound insulation are all key advantages of CLT panels that make them ideal for structural engineering applications. The dimensions of each board as shown in Figure 2-6 may vary, with ranges in thickness (h_{board}) from 10 mm to 50 mm and width (W_{board}) from 60 mm to 240 mm. Panel sizes can vary according to manufacturers; common ranges of panel widths (W_{panel}) are from 0.6 m to 3 m, while thicknesses (h_{panel}) can be up to 400 mm. In practice, panel sizes are limited by handling and transportation constraints; typically, lengths (l_{panel}) up to 18 m are possible (FPInnovations, 2013).

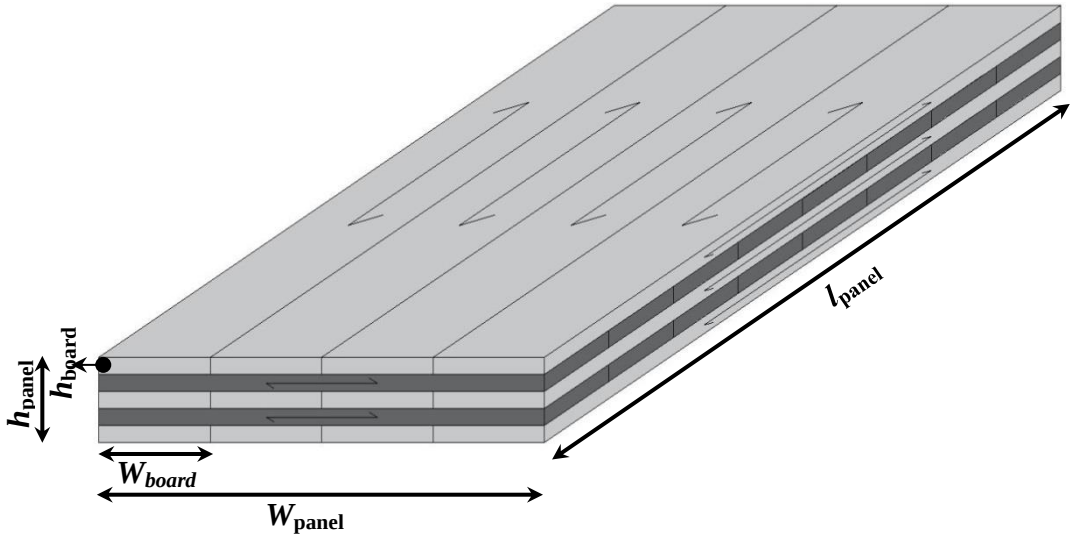

Figure 2-6 Typical dimensions of a CLT panel.

As mentioned previously in regards to the advantages of CLT as a structural material, the inherent sustainability of the material and the financial benefits mean that CLT panels are being used for a large range of buildings (Pearson, 2014).

2.2.1 Adhesive bonding

Adhesive bonding plays a very important role in the strength of the CLT panel. For CLT panels, two key parts need to be connected using adhesive bonding, the first one is between the boards in the same ply, and the second one is the connection between the different plies, as shown in Figure 2-7. Although glueing the edges will give a very effective and strong CLT panel, many manufacturers avoid doing so due to the extra cost this process incurs (FPInnovations, 2013).

The use of adhesives follows codified approaches which are often based on manufacturers' experience of using CLT over the last 20 years or so, such as BS EN 386 (2001) and BS EN 15425 (2008). But also, to use the adhesive bonding properly, the applied quantity of adhesive, the bonding pressure and the curing procedure need to be accurate and consistent; this is normally done in a controlled, factory environment (Harris, 2015).

There are different types of adhesives; two types that are commonly used in CLT manufacture will be presented. The first type is One Part Polyurethane (1K-PUR) and the second type is Melamine-Urea-Formaldehyde (MUF). Both of them are colourless and are resistant to exposure to sunlight and humidity. Generally, 1K-PUR adhesives are more flexible but also more vulnerable to higher temperatures (greater than 60°C) if not modified properly; temperatures beyond 60°C lead to rapid loss of stiffness and strength. In contrast, the MUF adhesive provides higher resistance to high temperatures, and also it is used to fill gaps in the CLT (Brandner, 2014).

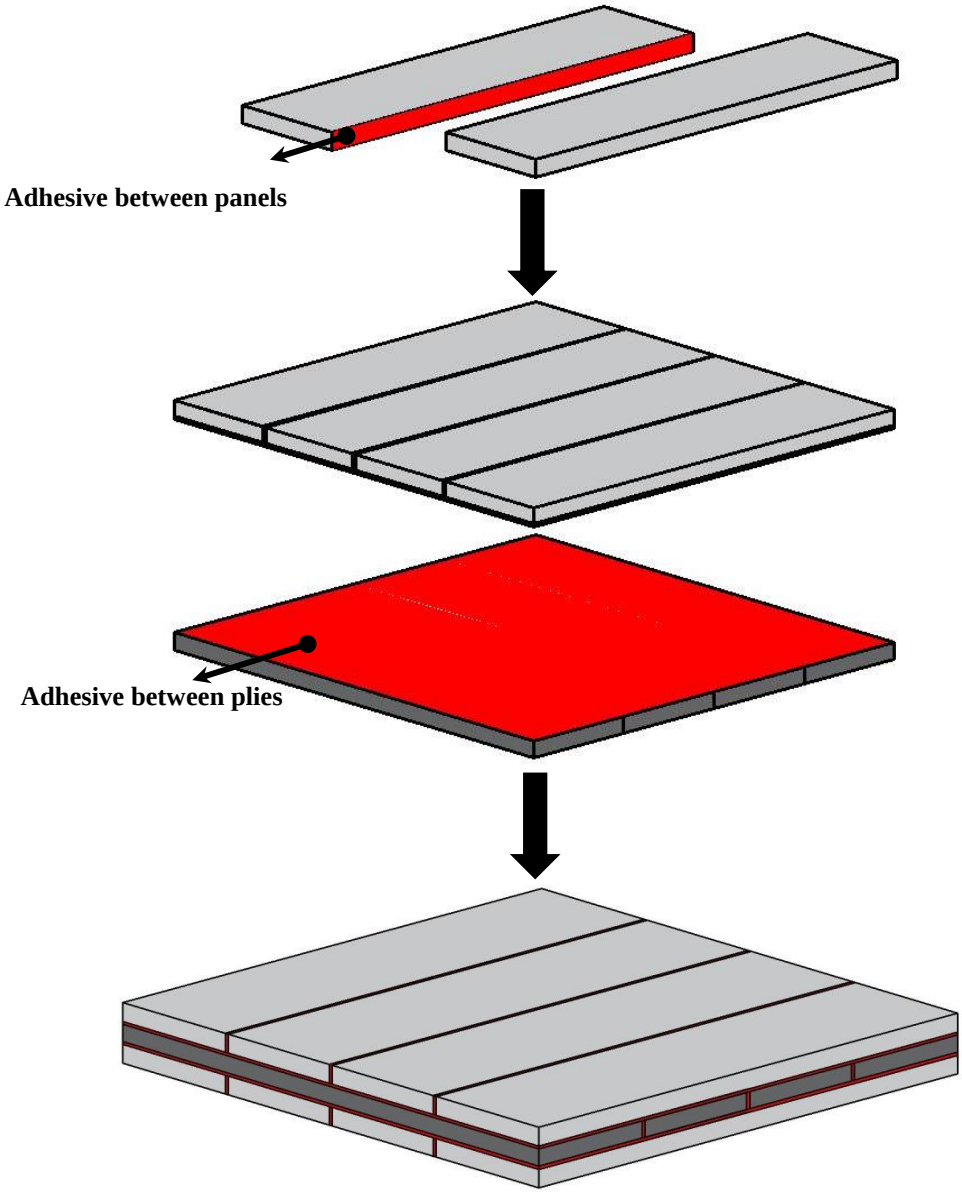

Figure 2-7 Adhesive bonding layers between the panels and the plies for CLT.

2.3 Mechanical characteristics of CLT and strength grading

To understand the behaviour of the CLT panels, the mechanical properties of CLT will be studied in this section.

Mechanical properties of the CLT panel as whole can be found in one of two ways. The first is to determine the properties of the individual plies (the characteristic values are known for each particular grade or category of structural timber). Some form of equation is then used to predict the property of the CLT composite. The second option

is more direct and accurate; this consists of testing the full CLT panel itself as opposed to individual plies (Brandner *et al*., 2016).

For both ways, certain guidance documents are required when designing and understanding the CLT mechanical material properties, such as the Canadian CLT handbook (FPInnovations, 2013) and national codes such as British Standards/European Norm (BS EN 408, 2012; BS EN 384, 2010 and BS EN 338, 2009).

In the Eurocode approach, timber is classified as a particular strength class or grade in accordance with BS EN 338 (2009); each class has specific characteristic properties which are used for design.

To determine the grade properties for timber through BS EN 408 (2012) and BS EN 384 (2010), strength, stiffness and density are the three key grade-determining properties in Europe. Depending on these key properties, two sets can be specified. The first one is related to the bending strength, stiffness and density, and it is based on data from the bending test. The second one is related to tension strength, stiffness and density, and it is based on data from the tension tests. The bending grade is commonly used for general construction timber. But the tensile grade is more suitable for grading of lamellas for the glued laminated timber beams (Ridley-Ellis *et al*., 2016).

The two grades, bending and tension, are not equivalent to each other, and should not be combined together. In some cases, if the bending data test is available, the tension properties can be estimated conservatively from bending properties and density. Also, if the tension data test is available, the bending properties can be estimated from the tension properties and density (Ridley-Ellis *et al*., 2016).

The other secondary properties such as tension and compression strength perpendicular to the grain, shear strength and shear modulus could be estimated conservatively from either one of the two grades bending or tension (Ridley-Ellis *et al*., 2016).

Due to the natural uncertainty of the timber as a natural material, the strength and the density are defined by a lower 5^{th} percentile value, but the stiffness is defined by a mean. Because of that, timber properties exceed those stated in the different guidance such as BS EN 338 (2009), especially the secondary properties. Timber strength classes are reports of populations not pieces, so the grading does not work on an individual piece level. Although certain pieces of timber are assigned to a specific strength class they might not all have the same strength and so some pieces may be under the requirements of the strength class (Ridley-Ellis *et al*., 2016).

As mentioned before, in section 2.1, softwood and hardwood are the two classes of timber depending on the strength and the uses of them in the construction field. For softwood species, the strength classes are C14, C16, C18, C20, C22, C24, C27, C30, C35, C40, C45 and C50. For hardwood species, the strength classes are D18, D24, D30, D35, D40, D50, D60 and D70. To make it clear, Table 2-1 shows one example of the characteristic strength properties of C24-grade timber; this is the most commonly used grade for CLT plies in Europe. In this table, according to BS EN 384 (2010), the number of tested specimens in each sample shall be more than 40. For the bending strength, the sample depth is 150 mm and the overall span is 18 times the specimen depth. For the tensile strength, the sample width should be 150 mm. However, for the strength properties of shear, tension and compression perpendicular to the grain, the specimen section should be in a position that can be tested and at failure is expected to happen (BS EN 384, 2010).

If the values of the bending strength and density of the set of timber are equal to or greater than the values of the strength class shown in Table 2-1, the set of timber may be assigned to this specific strength class, and its mean modulus of elasticity in bending is equal to or exceeds the 95th percentile of the value of the specific strength class that has been assigned for it.

Table 2-1 C24-Grade timber strength properties of CLT in accordance with BS EN 338 (2009) and BS EN 14080 (2013) in MPa.

Bending = 24
Tension parallel to the grain (σ^*_{1t}) = 14
Tension perpendicular to the grain (σ^*_{2t}) = (σ^*_{3t}) = 0.4
Compression parallel to the grain (σ^*_{1c}) = 21
Compression perpendicular to the grain (σ^*_{2c}) = (σ^*_{3c}) = 2.5
Shear (τ^*_{12}) =(τ^*_{13}) = 4
Rolling shear (τ^*_{23}) = 1.2

In the design procedures for CLT, there are three main types of loads that need to be considered: the in-plane axial loads, the in-plane shear loads and the out-of-plane loads. Also, rolling shear strength and stiffness has a big effect on the behaviour of CLT and may control its design since the loads transfer between the different plies of the CLT through the rolling shear (Harris, 2015).

In this research, CLT under out-of-plane loads will be the focus area, and, in the next chapter, detailed reviews of different experimental, theoretical and numerical analysis for CLT will be presented.

2.4 Overview of existing plate theories for modelling out-of-plane behaviour

When a CLT panel is loaded in bending, alternate layers (the parallel and perpendicular) are loaded parallel and perpendicular to the grain. As mentioned previously, the elastic modulus of the CLT loaded across the grain is small compared to that along the grain, so according to that the plies loaded perpendicular to the grain can be assumed to be relatively unstressed (Harris, 2015).

For the safety of the structure, the out-of-plane bending stress resulting from the applied load should be checked against the design bending strength. The Eurocodes adopt a Limit State Approach to the design of CLT structures, with the two main states being Ultimate Limit State (ULS) and Serviceability Limit State (SLS) (Harris, 2015).

SLS relates to specific in-service requirements for a structure such as deflection and vibration. ULS is concerned with ultimate strength and avoiding structural failure (McKenzie, 2000). For ULS, the ultimate stress is determined by multiplying the characteristic stress by a factor of safety, then comparing it with the ultimate capacity of the material itself.

2.4.1 Existing experimental work on out-plane behaviour of CLT

To understand CLT itself, a significant number of experimental investigations have been undertaken over the last 10 to 15 years. To gain an insight into the accuracy of current design approaches, particularly for bending, Hochreiner *et al*. (2014) focused on the global failure mechanisms and the different rupture patterns in CLT panels with three and five plies. Also, Czaderski *et al*. (2007) investigated the mechanical behaviour of 3-ply CLT panels with different thickness-to-width ratios from 0.025 to 0.25 under three different types of load. The tests aimed to estimate the actual modulus of elasticity and the strength of the bonded panels. They also compared their data with existing beam and plate methods. Similarly, a detailed plate-bending experiment on CLT panels was carried out by O'Dowd *et al*. (2016).

O'Dowd *et al*. (2016) found the bending stiffness of CLT panels experimentally. They used three different specimen sizes to develop a detailed understanding of the accurate bending stiffness. The CLT panel used in the test consisted of a five-lamina panel. Crucially, specimens from each lamina were tested in order to define their properties to accuracy greater than the declared standard grade strengths. It was reported that the

failure was inclined towards a brittle mode. The bending stiffness obtained experimentally was compared with three different theoretical methods: the mechanically jointed beam theory (Gamma-method), the composite theory (*K*-method) and shear analogy method. It was concluded that the *K*-method and shear analogy method underestimate the experimental stiffness, although the Gamma method gives reliably conservative results compared with the experimental results. A similar trend has been reported by other researchers, e.g. Thiel and Schickhofer (2010) and Vilguts *et al*. (2015).

Using the three theoretical methods investigated by O'Dowd *et al*. (2016), Sikora *et al*. (2016) studied the effect of the thickness of the CLT panels on the bending and shear strength. They found for the three analytical methods that, as the thickness of the CLT panel increases, the nominal ultimate bending strength decreases. The same trend was also observed for the shear strength. In addition, it was noticed that the bonding process used to form the CLT panel and the resulting quality of the bond are influential in the type of failure.

Failure modes are classified into different possible modes; the first one is the tensile failure in the longitudinal direction and perpendicular to the grain of the CLT plate. The second one is the compressive failure in the longitudinal direction; this failure is usually associated with fibre composites. The third one is a tensile failure in the radial direction; this one may occur due to shear stress parallel to the grain or rolling shear perpendicular to the grain. The fourth type is a tensile failure in the tangential direction. This type as a result of the lateral tensile bending stress or rolling shear. The fifth one is the shear failure parallel to the grain. The sixth one is the failure of edge glueing and the final one is the interface failure between single layers (Hochreiner *et al*., 2014).

Of the three theoretical methods commonly used in design calculations by O'Dowd *et al*. (2016) and Sikora *et al*. (2016), the first one, the Gamma-method, was introduced by Möhler and is derived using simple beam theory (Möhler, 1955); therefore, all its basic assumptions are valid. It assumes the normal to the plate remains normal to the deformed plate and the normal undergoes no extension or shortening.

Consequently, transverse shear strains γ_{xz}, γ_{yz}, and the normal strain in the *z*-direction ε_z disappear. Also, the mid-plane of the plate undergoes no in-plane deformation, i.e. $u_{(\text{at } z = 0)} = v_{(\text{at } z = 0)}$ are equal to zero.

Furthermore, the normal out-of-plane stress σ_z is negligible in comparison with other stress components. The gamma method was originally developed for mechanically jointed I'beams. In the original method, the gamma factor (connection efficiency factor) denoted the degree of fixity and slip associated with the mechanical fasteners (gamma = 0 for no connection and gamma = 1 for full connectivity). The method has been adapted for CLT such that the gamma factor represents the slip associated with the rolling shear in the laminae with grains orientated perpendicular to the outer panel grain, typically gamma may vary between 0.85 and 1 for CLT (FPInnovations, 2013). The premise of the adaptation to CLT is that the longitudinal boards take most of the load, then it could be assumed that these boards are connected by imaginary fasteners which have stiffness equal to that of the cross layers' rolling shear stiffness (Zhou *et al*., 2017). Using the gamma factor, an effective bending stiffness (EI_{eff}) can be derived for the CLT panel as a whole. In the gamma method, shear deformations are neglected in the longitudinal layers of the CLT, however, the shear deformations are included in the cross layers as these are equal to the rolling shear deformations.

With regard to the *K*-method described by O'Dowd *et al*. (2016) and Sikora *et al.* (2016), the *K*-factor depends on loading and panel orientation but does not account for

shear deformation in individual boards. The third approach is a shear analogy method introduced by Kreuzinger, and it is the most accurate method among the three methods for the analysis of CLT panels, as shown in Figure 2-8, because this method takes into account the shear deformation of the cross-ply (FPInnovations, 2013).

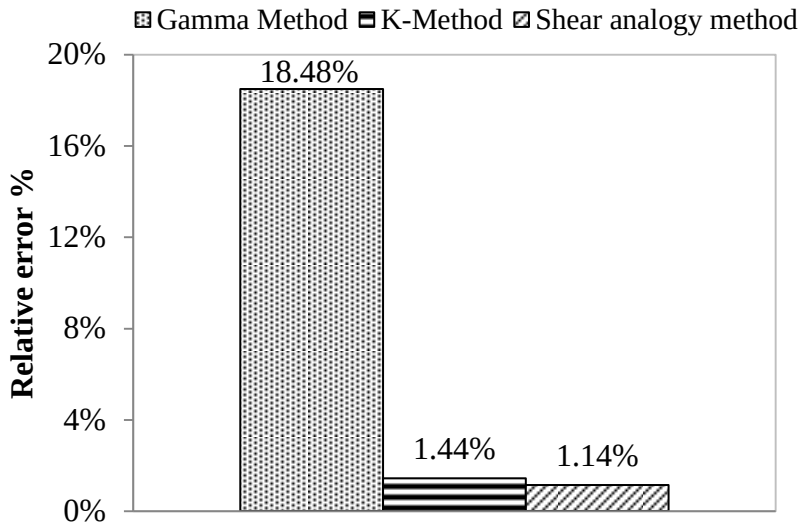

Figure 2-8 Relative errors for different theoretical methods based on O'Dowd *et al*.'s (2016) experiment.

By combining different types of experimental tests on the CLT panels, Saavedra Flores *et al*. (2015) obtained different CLT stiffness by applying bending, shear and compression loads. For the bending load, the experiment was the same as O'Dowd *et al*. (2016) and its purpose was to determine the bending stiffness of the CLT panels parallel to the grain. For the in-plane shear test, the Chilean standard to determine the in-plane shear stiffness was adopted (Saavedra Flores *et al*., 2015). Finally, for the axial compression test, they obtained the axial stiffness of CLT panels.

CLT panels can be manufactured having different combinations of ply grade and thickness. Therefore, evaluating the strength of CLT experimentally can be time-consuming and expensive (Oh *et al*., 2015). In response to this, numerical and analytical models are adopted to define the panel strength.

In the following section, various prevalent analytical approaches for CLT will be explored and discussed in detail.

2.4.2 Existing analytical approaches for CLT

The mathematical description of the structural behaviour of CLT regarding the accurate calculation for engineering purposes has not yet been fully developed. Therefore, many researchers have used different types of plate theories to analyse CLT, especially 2D theories. Due to the limitations of the 2D plate theories, as will be mentioned, researchers have started to apply 3D approaches to analyse and fully understand the behaviour of CLT (Albostami *et al*., 2017).

In an investigation of common existing plate theories for CLT, Sturzenbecher *et al*. (2010) and Sturzenbecher and Hofstetter (2011) applied both 2D and 3D approaches to CLT panels, comparing the accuracy of each. 2D theories explored included Classical Plate Theory (CPT), First-order Shear Deformation Theory (FSDT) and more advanced theories such as those outlined by Ren (1986). The 3D approach utilised what is termed as an exact solution as outlined by Pagano (1970). In reference to the Pagano approach, the term ‘exact solution’ refers to a solution that captures the entire physics of the problem within the context of an idealised, perfectly elastic material (Wolfram Research, 2016). Also, Bailey (1976) defines the exact solution as a solution that satisfies the equilibrium of the differential equation and the boundary condition equation.

The accuracy of these theories was evaluated for different laminate layups with three to seven layers, having different thickness-to-width ratios from 0.025 to 0.25 under different transverse loading conditions. In addition, experimental data by Czaderski *et al*. (2007) was used as a comparison for the various analytical solutions. Unfortunately, for thick plates with a thickness-to-width ratio of 0.2 and larger, and for concentrated

loads, the 2D theories fail to obtain accurate results in comparisons with results from numerical models and analytical solutions. Interestingly, Sturzenbecher *et al*. (2010) and Sturzenbecher and Hofstetter (2011) found that the Ren (Ren, 1986) approach is the most efficient and accurate 2D theory in describing the structural behaviour of CLT panels. Sturzenbecher and Hofstetter (2011) compared the results from the 2D Ren theory with the 3D elasticity solutions given by Pagano (1970) (as shown in Figure 2-9) and obtained a good agreement. These approaches will be studied and analysed in Chapter 5. However, the approaches implemented by Sturzenbecher *et al*. (2010) and Sturzenbecher and Hofstetter (2011) had limitations; primarily, the effect of the transverse normal stress σ_z is neglected and the deflection w is assumed to be a constant across the thickness of the plate.

Albostami *et al*. (2017) first applied the State Space Approach to CLT. This is a 3D analytical approach which has the potential to overcome some of the shortcomings of existing plate theories commonly used for CLT. The basis and formulation of the SSA will be discussed in detail in Chapter 4. The SSA results for 5-ply CLT panels under different types of load were compared with existing 2D and Pagano's approach that have been studied by Sturzenbecher and Hofstetter (2011). Experimental data from Czaderski *et al*. (2007) was used to validate the SSA results. The SSA approach was shown to solve the problem of the existing approaches concerning the thickness limitation.

In the next chapter, more detailed discussion of the plate theories that are commonly applied to composite plate will be provided for more understanding about the theories themselves.

In the following section, the existing numerical models for CLT panels will be explored and discussed in detail.

2.4.3 Existing numerical modelling for CLT

Several studies have been carried out in this field including some of the analytical approaches previously described, but, unfortunately, some of these approaches can be cumbersome to use. For that reason, researchers have studied the complex behaviour of CLT by using numerical methods like the Finite Element Method (FEM). When using FEM, it is important to understand the associated limitations and the sensitivities to different factors such as element mesh size and element types.

In 2015, Shahnewaz *et al*. validated the numerical model by the experimental data that was conducted on CLT beams and walls by FPInnovations (2013) to measure the load versus displacement response and to determine the in-plane stiffness behaviour of CLT panels. The FEM model was developed using the commercially available software ANSYS. As one of the most important considerations when modelling of CLT panels is how to represent contact and bond between the panels' different layers, Shahnewaz *et al*. used contact elements and a high frictional coefficient based on the high stiffness of the glue. The FEM model gave accurate results with an approximate 10% difference to the experimental data in predicting the elastic stiffness of CLT panels. Using the validated model, a parametric study was conducted to explore the effect of panel thickness on the in-plane stiffness of CLT panels. Shahnewaz *et al*. found that, when the thickness of the panels is doubled, the stiffness is increased by up to 24%. The resulting increase would seem lower than what would be expected from first principles, i.e. elastic stiffness is proportional to the cube of the depth. Some of the shortfalls may be attributed to the efficiency of the bond between laminae. Serrano and Enquist (2010) simulated the experimental compression tests on a square 3-ply CLT panel. The compression force was uniformly distributed over the complete top surface. The main aim of the tests was to investigate the effect of the load distribution within the test specimen. For the FEM model, Serrano and Enquist recommended that the interaction

between the individual boards within the specimen be taken into account for more accurate results.

Their tests found that, at low load levels, large strains have already developed at the interface between the plies of the CLT. Therefore, in order to fully capture the actual response, particularly post-peak behaviour observed in the test, they suggested an orthotropic plastic material model.

Vilguts *et al*. (2015) simulated via ANSYS an experiment on two CLT panels with a total thickness of 95 mm under distributed load. They compared the stresses acting on the edge of the plate and the maximum vertical displacement with boundary conditions consisting of two simply supported sides with free edges. The comparisons between the models and the corresponding experimental results were in reasonable agreement and had a maximum observed difference of 20%. As is the case with any FEM model, the present research found that a sensitivity investigation (described later) for the model should be undertaken as the choice of mesh size and element type will affect the simulation results.

To gain an improved understanding of the behaviour of CLT panels including shear failure, 5- and 7-ply CLT panels under centred concentrated loads were studied by Bogensperger and Jöbstl (2015). The different parameters that affect the shear behaviour, e.g. span-to-thickness ratio, etc., are investigated numerically. Non-linear analysis was carried out by using FEM. For simplification in their model, all the stresses in the interactions between the layers were neglected. The FEM stress-strain behaviour was compared with corresponding experimental data and both the linear elastic and non-linear parts of the curves were studied. It was found that the agreement between the experiment and the FEM results was good with approximate differences less than 20% in the linear elastic response, but, for the non-linear stage, the mechanical strength in the

experimental specimen was overestimated by a greater margin. The results were improved after the softening of the material was added to the model.

In the same way, Saavedra Flores *et al*. (2015) investigated the mechanical behaviour of CLT panels by FEM within a multi-scale model. Saavedra Flores *et al*. validated their models against a series of experimental tests for bending, in-plane shear and axial stiffness properties. The numerical models gave good agreement compared with the data from the experiments; in particular, the relative error was around 11%. The work was aimed at capturing the natural randomness found in the mechanical properties of the timber by introducing uncertainty in the definition of the material itself that was making up the CLT panels and to introduce corresponding detailed material properties. To study the uncertainty in the material, Saavedra Flores *et al*. (2015) proposed a specific strategy for the simulation modelling that can consider some of the not well-known or variable properties when measuring any experiments for the material. In each simulation, these parameters are studied one-by-one within a specific range of variation, while the other parameters are kept fixed.

To make it easy to follow the existing numerical studies mentioned before in this section, Table 2-2 shows these studies with a summary of the focus area for each one.

In view of the existing numerical work on modelling CLT via FEM, a comparison of the proposed SSA with FEM (both methods conducted by the present author) will be presented in chapters 5 and 6 of this thesis.

Table 2-2 Existing numerical modelling for CLT.

Name of the researcher	Year of the research	Relative error compared to the experimental data	Main focus points
Serrano and Enquist	2010	-	• The interaction between the individual boards within the specimen is recommended to be taken into account for more accurate results. • An orthotropic plastic material model is suggested to fully capture the actual response of the CLT panels.
Shahnewaz *et al*.	2015	10%	• Contact elements and a high frictional coefficient based on the high stiffness of the glue were used in the model. • A parametric study was conducted to explore the effect of panel thickness on the in-plane stiffness of CLT panels. • The thickness of the panels is doubled when the stiffness is increased by up to 24%.
Vilguts *et al*.	2015	Less than 20%	• A sensitivity investigation for the model should be undertaken as the choice of mesh size and element type will affect the simulation results.
Bogensperger and Jöbstl	2015	Less than 20%	• Non-linear analysis was carried out on the CLT model under centred concentrated loads. • For the non-linear stage, the mechanical strength in the experimental specimen was overestimated by a greater margin. The results were improved after the softening of the material was added in the model.
Saavedra Flores *et al*.	2015	Around 11%	• Capturing the natural randomness found in the mechanical properties of the timber.

2.5 Summary

In this chapter, an overview of structural timber and CLT has been presented. The associated material characteristics and behaviour of CLT under different types of loads have been discussed. The various available design guides and in particular the associated Eurocodes have been introduced.

Also, an investigation of the existing experimental, analytical and numerical methods used to obtain proper and accurate solutions for CLT panel stress states has been presented in this chapter.

A summary of the literature review presented in this chapter is provided in Figure 2-9. This figure also provides an overview of the salient work that researchers have carried out so far concerning the existing studies on CLT panels and the engineering applications.

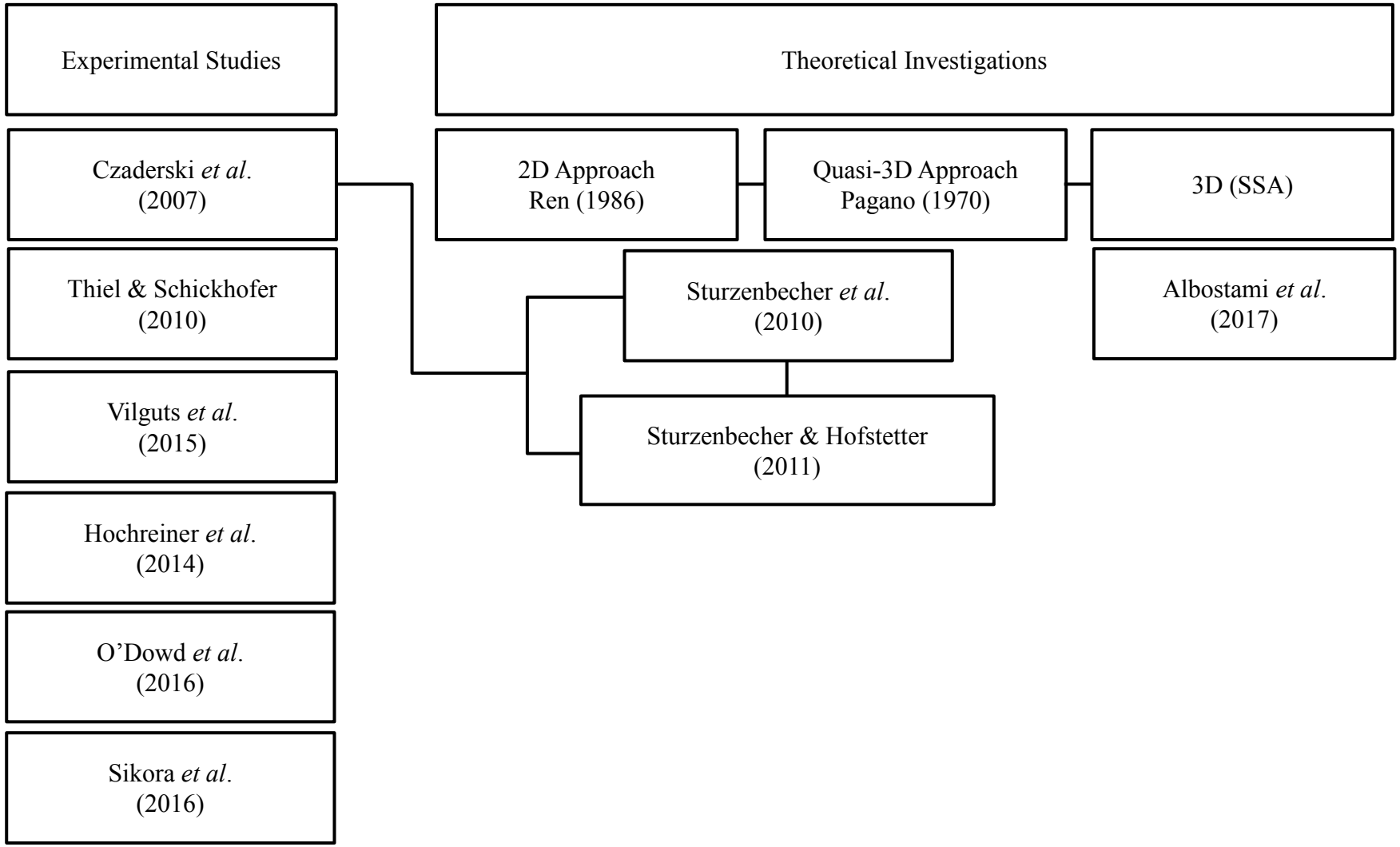

Figure 2-9 Flowchart of a summary of the existing studies of CLT panels.

CHAPTER 3
PLATE THEORIES: REVIEW OF EXISTING THEORIES AND APPROACHES

3.1 Introduction

According to Reddy (2004) and Ghugal and Shimpi (2002), many approaches have been used for the analysis of composite plates including Classical Plate Theory (CPT) and shear deformation plate theories. However, the accurate behaviour of the composite material should be based on 3D rather than 2D approaches due to the limitations of the 2D theories, as will be discussed later in this chapter. Also, in this chapter, the fundamental concepts of the existing 2D and 3D approaches that will be used later in the upcoming chapters will be reviewed.

3.2 General plate theories

Plate theories are classified as Two-Dimensional (2D) theories, Layerwise theories and Three-Dimensional (3D) approaches. In this section, some of the plate theories will be discussed in detail. In regards to Two-Dimensional (2D) plate theories, the following are explored: Classical Plate Theory (CPT), First-order Shear Deformation Theory (FSDT) and Higher-order Shear Deformation Theories (HSDT). Following this, Layerwise Theories and, finally, Pagano's approach and the SSA will be explored as 3D plate theories.

In this research, the 3D SSA will be adopted for the next analysis chapters.

3.2.1 Two-dimensional (2D) plate theories

2D plate theories are derived from 3D elasticity formulation theory by making appropriate assumptions to reduce 3D to a 2D problem relating to the kinematics of deformation or the stress state as a linear combination of unknown functions through the thickness coordinate (Reddy, 2004).

For laminated structures, the deformations are assumed to be continuous functions of the thickness coordinate, as shown in Figure 3-1 and Figure 3-2. As a result of that, the resultant transverse strains are continuous too; moreover, the inter-laminar stresses in 2D plate theories are discontinuous between adjacent layers at the interface of dissimilar materials (Han, 2014).

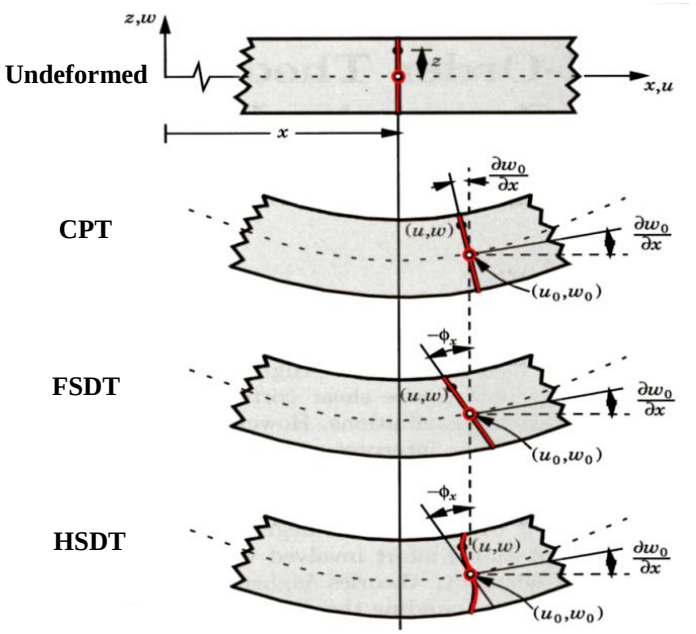

Figure 3-1 Deformation of a transverse normal according to the Classical Plate Theory, First-order and Higher-order Shear Deformation Theories (Reddy, 2004).

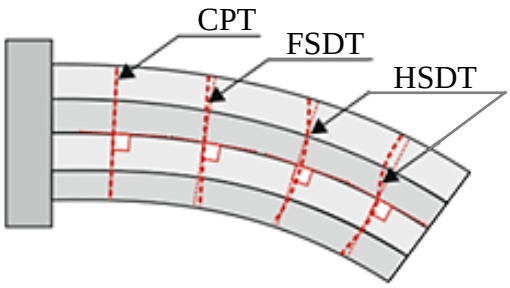

Figure 3-2 Deformation profiles represented by different shear deformation models (Kreja, 2011).

3.2.1.1 Classical Plate Theory (CPT)

The CPT, as the first plate theory, which was proposed by Kirchhoff in 1850, is the simplest plate theory. The Love-Kirchhoff plate theory is an extension to the CPT for composite plates.

The Love-Kirchhoff plate hypothesis is a generalisation of the plane section assumption in the beam theory. It assumes that, firstly, the normal to the plate remains normal to the deformed plate and the normal undergoes no extension or shortening. Consequently, transverse shear strains γ_{xz}, γ_{yz}, and the normal strain in the z-direction ε_z disappear.

$$\gamma_{xz} = {}^1\!/_2\left(\frac{\partial w}{\partial x} + \frac{\partial u}{\partial z}\right) = 0 \ , \ \gamma_{yz} = {}^1\!/_2\left(\frac{\partial w}{\partial y} + \frac{\partial v}{\partial z}\right) = 0 \text{ and } \varepsilon_z = \frac{\partial w}{\partial z} = 0 \qquad (3\text{-}1)$$

Where u and v are the in-plane deformations and w is the out-of-plane deformation. Also, γ_{xz} is the shear strain along the x and z-axes, γ_{yz} is the shear strain along the y and z-axes and ε_z is the normal strain along the z-axis.

Secondly, the mid-plane of the plate undergoes no in-plane deformation, i.e. $u_{(\text{at } z = 0)} = v_{(\text{at } z = 0)}$ are equal to zero. Thirdly, the normal out-of-plane stress σ_z is negligible in comparison with the other stress components.

In spite of its inaccurate results, CPT is still widely used as a basic analysis method for the composite plate. Furthermore, it gives quick predictions for the behaviour of thin plates and estimates of the global response such as gross deflection, bending analysis and buckling (Han, 2014).

3.2.1.2 First-order Shear Deformation Theory (FSDT)

In order to overcome the limitations of the CPT, another 2D plate theory was proposed by Reissner (1945). Reissner's theory is based on modelling the plate structure as two-dimensional structures with the assumption of the stress variation through the thickness of the plate. The theory takes into account the shear deformation and the transverse normal stresses. It is considered as a stress-based shear deformable plate theory. Mindlin (1951) proposed a displacement field through the plate thickness to account for the effect of shear deformation. Mindlin and Reissner's theory is called the First-order Shear Deformation Theory (FSDT) as it proposes a linear variation of the displacements through the plate thickness (Rashed, 2000). The most important feature of the plate theories in regard to shear deformation is that they can be used to analyse both thin and medium thickness plates (i.e. a thickness-to-width ratio 0.2 and less) (Onate, 1989).

The FSDT extends the kinematics of the CPT by including a gross transverse shear deformation in its kinematics assumptions; the transverse shear strain is assumed to be constant through the thickness; it follows that the transverse shear stress will also be constant. To adjust the transverse shear stiffness, the shear correction factors are required due to a constant shear strain distribution across the plate thickness resulting from the linear interpolation of the displacement field in the direction of the plate thickness (Kreja, 2011), and it depends on the following factors: the lamination parameters, geometry, loading and boundary conditions (Reddy, 2004).

The accuracy of the results mainly depends on the shear correction factor (Han, 2014). In order to analyse and calculate the transverse stresses accurately and to consider other complicated boundary conditions, the Higher-order Shear Deformation Theories are introduced.

3.2.1.3 Higher-order Shear Deformation Theory (HSDT)

Second- and Higher-order Shear Plate Theories (HSDT) are based on the same assumptions as the CPT and FSDT, except that HSDT considers higher-order polynomials in the expansion of the displacement components through the thickness of the plate. Levinson (1980) proposed a Third-order Shear Deformation Theory for isotropic plates of uniform thickness, and it was found there was no need to use the shear correction factor in this theory. In addition, these theories are seen to provide a better approximation to the results obtained from FSDT and can give more accurate inter-laminar stress distribution. However, they involve higher-order stress resultants that are difficult to understand physically and require much more computational effort (Reddy, 2004). Moreover, the HSDT does not guarantee the inter-laminar continuity (Carrera, 1996). Therefore, such theories should be used only when necessary.

3.3 Layerwise theories

The previous 2D theories, defined as Equivalent Single Layer Plate Theories (ESLT), show the computational convenience that the number of independent variables does not depend on the number of layers. The layerwise theories were developed by assuming separate displacement field expansions within each material layer; in this case, each layer has the same number of independent variables (Sturzenbecher *et al*., 2010). In these theories, each layer is modelled as an independent plate, and then, at the layer interfaces, the compatibility of the displacement component is introduced as a polynomial function. Also, the displacement components are assumed to be continuous through the laminate thickness, but the derivatives of the displacements with respect to the thickness may be discontinuous (Guo *et al*., 2014).

Many researchers have studied and reviewed the efficiency of the layerwise theories compared to ESLTs, e.g. Noor and Burton (1990) and Reddy (1993).

Zigzag behaviour describes the changes in the slope of the displacement and the stresses through the thickness. Lekhnitskii (1968) was the first to propose a zigzag theory, which was obtained by solving the elasticity problem involving a layered beam. The general distribution of the displacements and transverse stresses through the thickness of 1-ply and 3-ply composite laminate has been given by Carrera (2003), as shown in Figure 3-3. From this figure, the displacements must be continuous for compatibility reasons and the layers assumed to be perfectly bonded between each other and the transverse stresses are continuous through the thickness due to equilibrium reasons (Carrera, 1997).

Based on a new variation principle proposed by Reissner (1984), Murakami (1986) achieved an improvement by including a zigzag-shaped function to approximate thickness variation of in-plane displacements. Ren (1986) takes into account the influence of Poisson’s ratio and the transverse shear stresses and in-plane displacements are continuous between layers. Murakami and Ren's methods lead to very accurate results for displacements and stresses examined by the 3D analytical solution obtained by Pagano (1969).

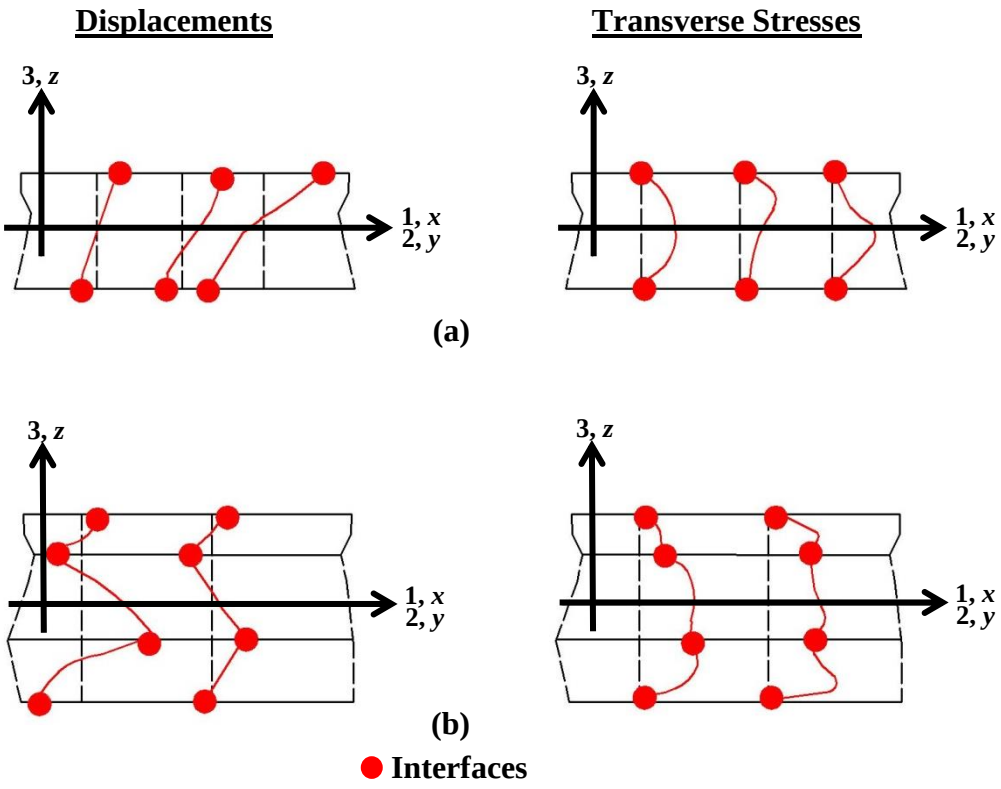

Figure 3-3 General distribution of the displacements and transverse stresses through the thickness of (a) one isotropic and (b) multi-layered composite laminate (Carrera, 2003).

2D plate theories provide an accurate description of global response for thin to moderately thick plates (thickness-to-width ratio 0.2 and less) (Onate, 1989). Furthermore, the 2D models often inaccurately describe the state of stress and strain at the ply level near geometric and material discontinuities or near regions of intense loading. In such cases, 3D theories are required (Reddy, 2004).

3.4 Three-dimensional (3D) plate theories

To overcome the limitations of the 2D solutions for plates, the 3D solutions take into account the constitutive equations of linear 3D elasticity, the kinematic equations and the stress equilibrium equations. The boundary conditions and the continuity at the interfaces are satisfied. 3D solutions provide detailed investigations into global and local responses of plates and give accurate estimates of the mechanical behaviour (Han, 2014).

Two approaches will be explored in this review. The first one is Pagano's approach and the second one is the State Space Approach (SSA).

3.4.1 Pagano's approach

In this approach, Pagano transferred the three-dimensional partial differential equations to a set of ordinary differential equations with respect to the thickness coordinate. The ordinary differential equations are then solved analytically.

Pagano initiated this approach in 1969. He studied the plane strain problem of the isotropic and orthotropic laminates under cylindrical bending. For cylindrical bending, the boundary conditions and the load can vary only in the *x*-direction, as the *y*-direction is assumed to be infinite (Jairazbhoy *et al.*, 2008; Nimbolkar and Jain, 2005). As this did not include the normal transverse stress in the equilibrium equation, the solution was still considered as a quasi-3D solution. However, Pagano did compare his result with that from CPT.

It was found the CPT solution for stresses and displacements converged to the quasi-3D solution as span-to-depth ratio increased and the laminates became thinner and thinner. This approach was extended to the 3D structural behaviour of rectangular bidirectional composites and sandwich plates (Pagano, 1970).

In Pagano (1970), the in- and- out of plane displacements *u*, *v* and *w* are defined by Fourier series, and the accuracy of the solution depends on the number of Fourier series terms (*m* and *n*). To obtain a 3D solution for a singly-ply orthotropic plate with simply supported four edges, a sixth-order differential equation governing the out-of-plane displacement w_{mn} was obtained:

$$\frac{\partial^6 w_{mn}}{\partial z^6} + A\frac{\partial^4 w_{mn}}{\partial z^4} + B\frac{\partial^2 w_{mn}}{\partial z^2} + Cw_{mn} = 0 \qquad (3\text{-}2)$$

Where *A*, *B* and *C* are constants that can be determined by the number of Fourier series terms (*m* and *n*) and the material properties of the plate (Pagano, 1970; Han, 2014).

3.4.2 State Space Approach (SSA)

The approach that has been introduced here for the 3D plate theory is called the State Space Approach (SSA) (Wu *et al*., 2015). The term 'state space' derives from the linear control system where the principal concern is the relationship between inputs (or source) and outputs (or responses) (Ye, 2003). In general terms, the SSA describes the state of the system at a given time or point in space.

For 3D analysis of laminated plates, after introducing the boundary conditions, the displacements and the transverse stresses at the bottom surface of the plate (termed as the initial state of the system) are determined. The displacements and stresses at the top surface of the plate can be found at any *x* and *y* locations; then, any displacements and transverse stresses could be found through the thickness of the plate. Once the displacements and the transverse stresses are found, the in-plane stresses can be calculated directly. For a homogeneous anisotropic plate, the three-dimensional equations can be represented by the system of partial differential equations (Ye, 2003) as follows:

$$\frac{\partial}{\partial z}\{\mathrm{F}\}=[\mathrm{G}]\{\mathrm{F}\}+\{\mathrm{B}\} \tag{3-3}$$

Herein, $\{\mathrm{F}\} = [u\ v\ \sigma_z\ \tau_{xz}\ \tau_{yz}\ w]^T$ is called the state vector of the plate; [G] is named as the system state matrix whose elements are functions of material and geometric constants of the plate and also partial differential operators with respect to the other two in-plane coordinates; and {B} is a vector associated with initial stresses, strains and temperatures.

The SSA provides theoretically accurate three-dimensional solutions that guarantee continuous transverse stress distributions across the thickness of the plates. Also, the boundary conditions and the continuity at the interfaces are satisfied. Additionally, the SSA can give a full range of structural behaviour exactly for various thicknesses from thin to very thick plates (Sheng and Ye, 2003).

The SSA considers all displacement and transverse stress components as the primary state variables simultaneously. The boundary conditions on the top and the bottom surfaces are directly related to them. Initially, the approach originated from Vlasov (1957), who stated a state variable equation for the solution of the 3D elasticity by using the method of initial functions. Later, it was considered by Bahar (1975) as a state space setting for homogeneous and isotropic plates. As one of the pioneering researchers in 3D elastic theory, Wu (1987) introduced SSA to a 3D thick plate analysis. Fan and Ye (1990) presented a theoretically exact solution based on the state space method for statics and dynamics of orthotropic thick plates with simply supported edges. All fundamental equations of three-dimensional elasticity can be exactly satisfied, and the nine elastic constants for orthotropic materials can be considered. In addition, the approach extended by Fan and Ye can be applied to the buckling of a thick orthotropic plate. Likewise, Wu and Wardenier (1998) achieved a theoretically exact 3D elasticity solution for simply supported thick, orthotropic and rectangular plates subjected to arbitrary loading. In fact, they obtained a sixth-order differential equation governing the transverse displacement for the first time in comparison with the fourth-order differential equation that is used in CPT.

In 2012, Kamis presented the structural behaviour of Fibre-Reinforced Polymer (FRP) laminated composites by using the SSA. The investigation focused on the performance

of a laminated rectangular plate of length *a* and width *b* subjected to different loading conditions with fully fixed edges, as shown in Figure 3-4.

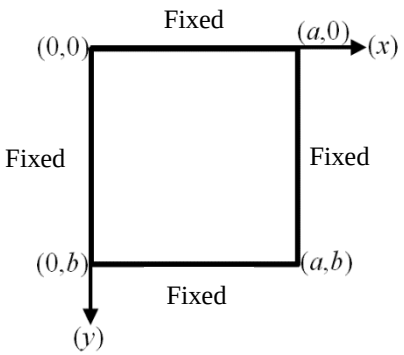

Figure 3-4 Fully fixed boundary conditions of a plate.

The 3D SSA solution was derived for the first time and the transfer matrix and the recursive solutions were used to produce the analytical solution. The idea to obtain a solution for this particular boundary condition is to analyse the fixed edges by applying traction to the edges of simply supported by the superposition principle for the in-plane displacements (*U* and *V*), as shown in the following equations:

$$U = \overline{U} + f_u \tag{3-4}$$

$$V = \overline{V} + f_v \tag{3-5}$$

Where $\overline{U}$ and $\overline{V}$ are the in-plane displacements, and f_u and f_v can be assumed to be any function that can satisfy the boundary conditions. In Kamis (2012), these functions are assumed to be linear, as per the following equations:

For f_u, the functions along the *x*-axis when $x=0$ is $1-\frac{x}{a}$ and when $x=a$ is $\frac{x}{a}$ (3-6)

For f_v, the functions along the *y*-axis when $y=0$ is $1-\frac{y}{b}$ and when $y=b$ is $\frac{y}{b}$ (3-7)

This work can be used as a benchmark for further investigation with the same boundary conditions. Recently, with different boundary conditions and different material application, Han (2014) extended the SSA to the theoretically exact analysis of thick

piezoelectric laminates in the application of a Micro-Electro-Mechanical-System (MEMS) with simply supported sides and free edges, as shown in Figure 3-5.

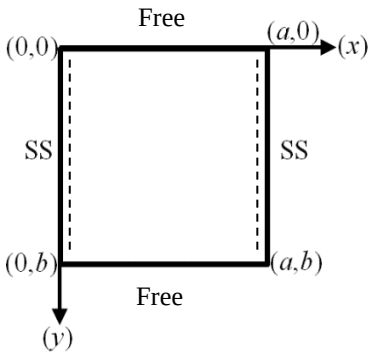

Figure 3-5 Simply supported sides with two free edges boundary conditions of a plate.

Han (2014) followed the same procedures that Kamis (2012) used to solve the boundary condition problem, but adopted different assumptions for the traction functions, as shown in the following equations:

For f_u, the functions along the y-axis when y=0 is $\frac{b}{2}(1-\frac{y}{b})^2$ and when y=b is $\frac{b}{2}(\frac{y}{b})^2$ (3-8)

For f_v, the functions along the y-axis when y=0 is $1-\frac{y}{b}$ and when y=b is $\frac{y}{b}$ (3-9)

In this research, the SSA is adopted and used to formulate the solution for new boundary conditions; these have not been previously derived. Also, this work focuses on application to CLT, which is entirely novel.

3.5 Summary

An investigation of the existing 2D and 3D approaches that will be used in the upcoming chapters for different case studies has been presented in this chapter.

2D theories can provide a good prediction of some global responses of thin plates. As the thickness of the plate increases, the accuracy of the results will decrease, and these theories can give only inaccurate inter-laminar stresses. Hence, SSA as a 3D approach

has been developed to overcome these limitations and give more accurate results. Therefore, the SSA will be adopted for the upcoming analysis.

In Figure 3-6, a summary of the plate theories covered through existing research studies is shown.

In the following chapter of this thesis, as a 3D analytical approach, the SSA will be applied to a general composite material for more understanding of the method and its capability to capture the behaviour of a composite panel.

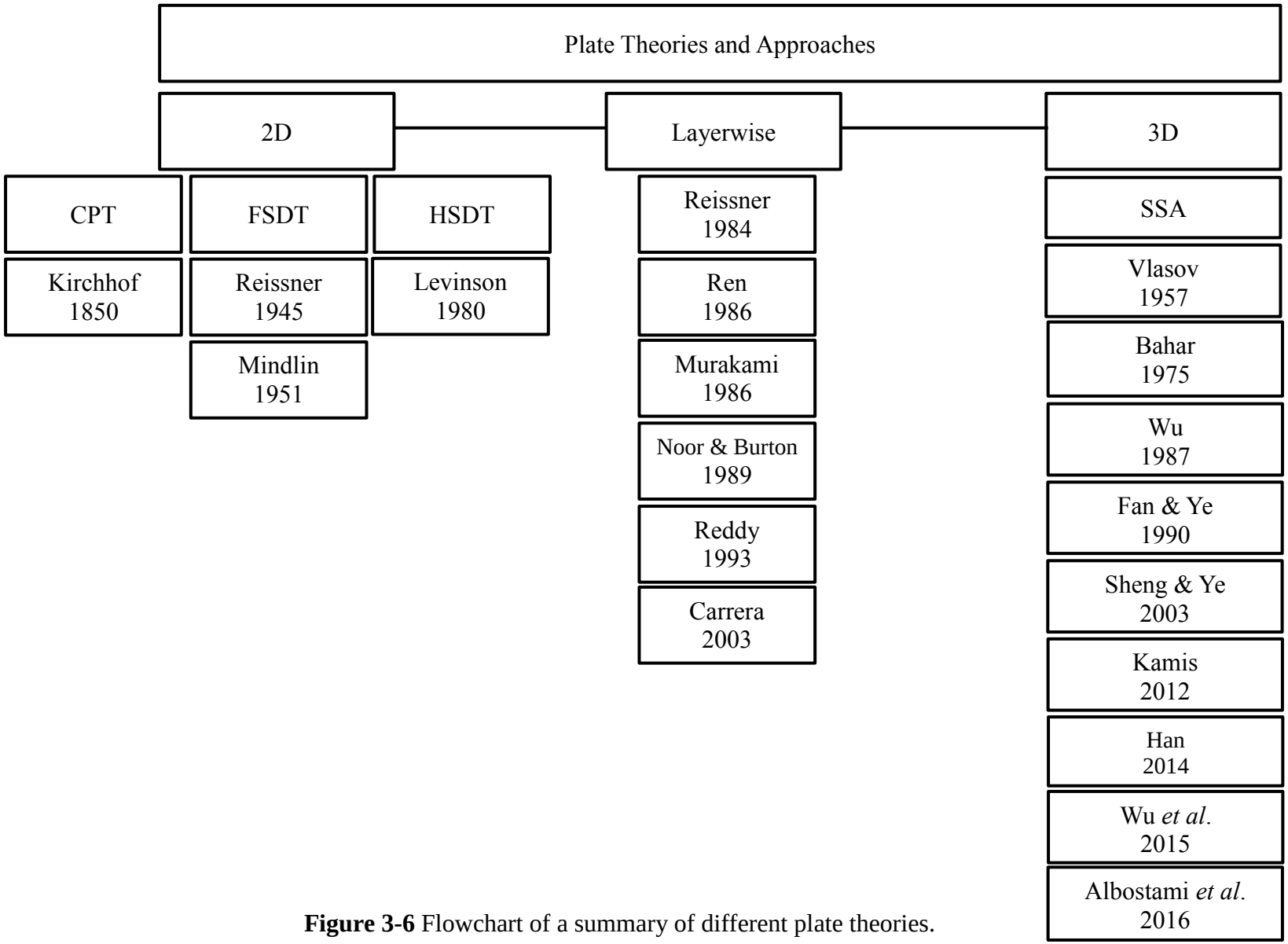

Figure 3-6 Flowchart of a summary of different plate theories.

CHAPTER 4
GENERAL APPLICATION OF THE 3D STATE SPACE APPROACH TO COMPOSITE PLATES

4.1 Introduction

The State Space Approach (SSA), as mentioned in the previous chapter, is an analytical approach based on the application of the equilibrium and compatibility equations, together with the stress and strain relations (Hooke's law) to produce governing equations which need to be solved to find all the displacements and stresses. In this chapter, the concept equations and procedures of the SSA for a simply supported composite plate will be introduced.

For the application of SSA, in this chapter, different case studies are analysed to determine the structural behaviour of simply supported orthotropic composite plates. Then, the FEM models are validated with the SSA results. After that, investigation of a single-ply composite plate will be extended to a laminated composite plate, and the SSA equations will be applied to consider more than one ply. In this part, a case study will be explored by the SSA and various existing analytical 2D approaches will be compared with the SSA.

4.2 Formulation of the equation (single-ply plate)

Consider an elastic homogenous orthotropic rectangular plate of length *a*, width *b* and uniform thickness *h*, as shown in Figure 4-1; the elasto-static equilibrium equations of the plate (Ye, 2003) – ignoring the body forces – can be written as:

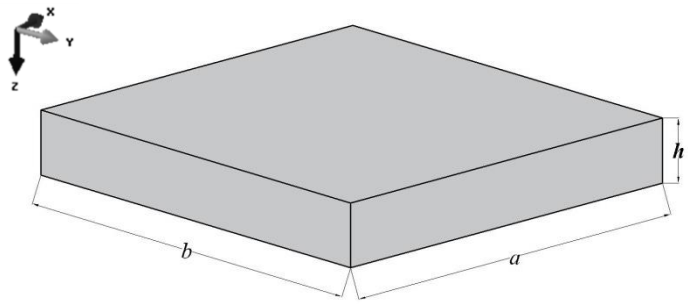

Figure 4-1 Geometry of a single-ply plate.

$$\frac{\partial \sigma_x}{\partial x}+\frac{\partial \tau_{xy}}{\partial y}+\frac{\partial \tau_{xz}}{\partial z}=0$$

$$\frac{\partial \tau_{xy}}{\partial x}+\frac{\partial \sigma_y}{\partial y}+\frac{\partial \tau_{yz}}{\partial z}=0 \qquad (4\text{-}1)$$

$$\frac{\partial \tau_{xz}}{\partial x}+\frac{\partial \tau_{yz}}{\partial y}+\frac{\partial \sigma_z}{\partial z}=0$$

Where σ_x, σ_y and σ_z are normal stresses along x, y and z-axes, and τ_{xy}, τ_{yz} with respect to x-y, y-z and τ_{xz} with respect to x-z planes.

Since Hooke's law can be applied to elastic materials, the stress-strain relation becomes:

$$\begin{Bmatrix}\sigma_x\\ \sigma_y\\ \sigma_z\\ \tau_{yz}\\ \tau_{xz}\\ \tau_{xy}\end{Bmatrix}=\begin{bmatrix}C_{11} & C_{12} & C_{13} & 0 & 0 & 0\\ C_{21} & C_{22} & C_{23} & 0 & 0 & 0\\ C_{31} & C_{32} & C_{33} & 0 & 0 & 0\\ 0 & 0 & 0 & C_{44} & 0 & 0\\ 0 & 0 & 0 & 0 & C_{55} & 0\\ 0 & 0 & 0 & 0 & 0 & C_{66}\end{bmatrix}\begin{Bmatrix}\varepsilon_x\\ \varepsilon_y\\ \varepsilon_z\\ \gamma_{yz}\\ \gamma_{xz}\\ \gamma_{xy}\end{Bmatrix} \qquad (4\text{-}2)$$

In equation (4-2), the strain-displacement relations can be written as:

$$\varepsilon_x=\frac{\partial u}{\partial x},\ \varepsilon_y=\frac{\partial v}{\partial y},\ \varepsilon_z=\frac{\partial w}{\partial z},$$

$$\gamma_{yz}=\frac{\partial v}{\partial z}+\frac{\partial w}{\partial y},\ \gamma_{xz}=\frac{\partial u}{\partial z}+\frac{\partial w}{\partial x},\ \gamma_{xy}=\frac{\partial u}{\partial y}+\frac{\partial v}{\partial x} \qquad (4\text{-}3)$$

and

$$
\begin{aligned}
C_{11} &= \frac{E_1(1 - v_{23}v_{32})}{Q} & C_{12} = C_{21} &= \frac{E_1(v_{21} + v_{31}v_{23})}{Q} \\
C_{22} &= \frac{E_2(1 - v_{13}v_{31})}{Q} & C_{13} = C_{31} &= \frac{E_1(v_{31} + v_{21}v_{32})}{Q} \\
C_{33} &= \frac{E_3(1 - v_{12}v_{21})}{Q} & C_{23} = C_{32} &= \frac{E_2(v_{32} + v_{12}v_{31})}{Q} \\
C_{44} &= G_{23} & C_{55} &= G_{31} \\
C_{66} &= G_{12} \\
Q &= 1\text{-}v_{12}v_{21}\text{-}v_{23}v_{32}\text{-}v_{31}v_{13}\text{-}2v_{12}v_{23}v_{31} \\
\frac{v_{ij}}{E_i} &= \frac{v_{ji}}{E_j} \qquad (i, j = 1, 2, 3)
\end{aligned}
\tag{4-4}
$$

Where E_1, E_2 and E_3 are Young's moduli of the plate among the material coordinates. The subscripts 1, 2 and 3 indicate fibre direction, transverse and perpendicular to the plate respectively. G_{12} is shear moduli with respect to 1-2, G_{23} with respect to 2-3 and G_{13} with respect to 1-3 planes. v_{12}, v_{23} and v_{13} are the Poisson's ratios correspondingly.

From equation (4-2), all stress components can be expressed explicitly:

$$
\begin{aligned}
\sigma_x &= C_{11}\frac{\partial u}{\partial x} + C_{12}\frac{\partial v}{\partial y} + C_{13}\frac{\partial w}{\partial z} \\
\sigma_y &= C_{12}\frac{\partial u}{\partial x} + C_{22}\frac{\partial v}{\partial y} + C_{23}\frac{\partial w}{\partial z} \\
\sigma_z &= C_{13}\frac{\partial u}{\partial x} + C_{23}\frac{\partial v}{\partial y} + C_{33}\frac{\partial w}{\partial z} \\
\tau_{yz} &= C_{44}\left(\frac{\partial v}{\partial z} + \frac{\partial w}{\partial y}\right) \\
\tau_{xz} &= C_{55}\left(\frac{\partial u}{\partial z} + \frac{\partial w}{\partial x}\right) \\
\tau_{xy} &= C_{66}\left(\frac{\partial u}{\partial y} + \frac{\partial v}{\partial x}\right)
\end{aligned}
\tag{4-5}
$$

$$\frac{\partial u}{\partial z} = \frac{\tau_{xz}}{C_{55}} - \frac{\partial w}{\partial x}$$

$$\frac{\partial v}{\partial z} = \frac{\tau_{yz}}{C_{44}} - \frac{\partial w}{\partial y}$$

$$\frac{\partial w}{\partial z} = \frac{\sigma_z}{C_{33}} - \frac{C_{13}}{C_{33}}\frac{\partial u}{\partial x} - \frac{C_{23}}{C_{33}}\frac{\partial v}{\partial y}$$

$$\frac{\partial \sigma_z}{\partial z} = -\frac{\partial \tau_{xz}}{\partial x} - \frac{\partial \tau_{yz}}{\partial y}$$

$$\frac{\partial \tau_{xz}}{\partial z} = -\frac{\partial \sigma_x}{\partial x} - \frac{\partial \tau_{xy}}{\partial y} = [-(C_{11} - \frac{C_{13}^2}{C_{33}})\frac{\partial^2}{\partial x^2} - C_{66}\frac{\partial^2}{\partial y^2}]u - [(C_{12} - \frac{C_{13}C_{23}}{C_{33}}) + C_{66}]\frac{\partial^2 v}{\partial x \partial y} - \frac{C_{13}}{C_{33}}\frac{\partial \sigma_z}{\partial x} \quad (4\text{-}6)$$

$$\frac{\partial \tau_{yz}}{\partial z} = -\frac{\partial \tau_{xy}}{\partial x} - \frac{\partial \sigma_y}{\partial y} = -[(C_{12} - \frac{C_{13}C_{23}}{C_{33}}) + C_{66}]\frac{\partial^2 u}{\partial x \partial y} + [-C_{66}\frac{\partial^2}{\partial x^2} - (C_{22} - \frac{C_{23}^2}{C_{33}})\frac{\partial^2}{\partial y^2}]v - \frac{C_{23}}{C_{33}}\frac{\partial \sigma_z}{\partial y}$$

Three displacements in *x*-*y*-*z* directions, labelled with *u*, *v* and *w*, and the transverse stresses σ_z, τ_{xz} and τ_{yz}, are solved with respect to the *z* coordinate directly from the equations (4-1), (4-3) and (4-5).

Denoting:

$$C_1 = -\frac{C_{12}}{C_{33}} \qquad C_2 = C_{11} - \frac{C_{12}^2}{C_{33}}$$

$$C_3 = C_{12} - \frac{C_{13}C_{23}}{C_{33}} \qquad C_4 = C_{22} - \frac{C_{23}^2}{C_{33}}$$

$$C_5 = -\frac{C_{23}}{C_{33}} \qquad C_6 = C_{66} \quad (4\text{-}7)$$

$$C_7 = \frac{1}{C_{33}} \qquad C_8 = \frac{1}{C_{55}}$$

$$C_9 = \frac{1}{C_{44}}$$

and rearranging equation (4-6) leads to a matrix form as:

$$\frac{\partial}{\partial z}\{\mathrm{F}\}=[\mathrm{G}]\{\mathrm{F}\} \tag{4-8}$$

Herein, $\{\mathrm{F}\}= [u\ v\ \sigma_z\ \tau_{xz}\ \tau_{yz}\ w]^T$ is called the state vector of the plate and [G] is named as the system state matrix:

$$[\mathrm{G}]=\begin{bmatrix} 0 & 0 & 0 & C_8 & 0 & -\frac{\partial}{\partial x} \\ 0 & 0 & 0 & 0 & C_9 & -\frac{\partial}{\partial y} \\ 0 & 0 & 0 & -\frac{\partial}{\partial x} & -\frac{\partial}{\partial y} & 0 \\ -C_2\frac{\partial^2}{\partial x^2}-C_6\frac{\partial^2}{\partial y^2} & -(C_3+C_6)\frac{\partial^2}{\partial x\partial y} & C_1\frac{\partial}{\partial x} & 0 & 0 & 0 \\ -(C_3+C_6)\frac{\partial^2}{\partial x\partial y} & -C_6\frac{\partial^2}{\partial x^2}-C_4\frac{\partial^2}{\partial y^2} & C_5\frac{\partial}{\partial y} & 0 & 0 & 0 \\ C_1\frac{\partial}{\partial x} & C_5\frac{\partial}{\partial y} & C_7 & 0 & 0 & 0 \end{bmatrix} \tag{4-9}$$

Once the state vector containing the three displacements and the transverse stresses [σ_z, τ_{xz}, τ_{yz}] has been found, the three in-plane stresses in the *x*-*y* plane can be calculated from equation (4-5) as follows:

$$\begin{Bmatrix} \sigma_x \\ \sigma_y \\ \tau_{xy} \end{Bmatrix}=\begin{bmatrix} C_2\frac{\partial}{\partial x} & C_3\frac{\partial}{\partial y} & -C_1 & 0 & 0 & 0 \\ C_3\frac{\partial}{\partial x} & C_4\frac{\partial}{\partial y} & -C_5 & 0 & 0 & 0 \\ C_6\frac{\partial}{\partial y} & C_6\frac{\partial}{\partial x} & 0 & 0 & 0 & 0 \end{bmatrix}\begin{Bmatrix} u \\ v \\ \sigma_z \\ \tau_{xz} \\ \tau_{yz} \\ w \end{Bmatrix} \tag{4-10}$$

To consider a rectangular plate with the four sides simply supported (SS) (Figure 4-2), the following boundary condition should be satisfied:

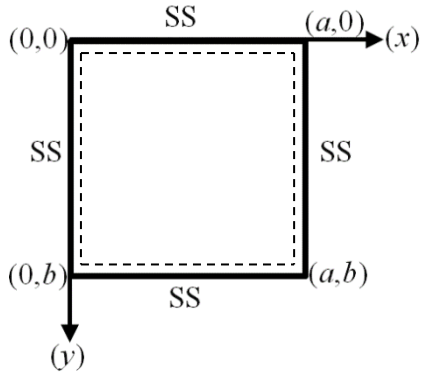

Figure 4-2 Boundary conditions of the plate.

$$\begin{aligned} \sigma_x = v = w = 0 \qquad & (\text{at } x = 0,\ a) \\ \sigma_y = u = w = 0 \qquad & (\text{at } y = 0,\ b) \end{aligned} \tag{4-11}$$

In order to satisfy the boundary conditions specified in equation (4-11), the following six state variables of the state vector can be expressed by double Fourier series by:

$$\begin{aligned} u\,(x,y,z) &= \sum_{m=1}\sum_{n=1} U_{mn}(z)\cos(m\pi x/a)\sin(n\pi y/b) \\ v\,(x,y,z) &= \sum_{m=1}\sum_{n=1} V_{mn}(z)\sin(m\pi x/a)\cos(n\pi y/b) \\ w\,(x,y,z) &= \sum_{m=1}\sum_{n=1} W_{mn}(z)\sin(m\pi x/a)\sin(n\pi y/b) \\ \tau_{xz}(x,y,z) &= \sum_{m=1}\sum_{n=1} X_{mn}(z)\cos(m\pi x/a)\sin(n\pi y/b) \\ \tau_{yz}(x,y,z) &= \sum_{m=1}\sum_{n=1} Y_{mn}(z)\sin(m\pi x/a)\cos(n\pi y/b) \\ \sigma_z(x,y,z) &= \sum_{m=1}\sum_{n=1} Z_{mn}(z)\sin(m\pi x/a)\sin(n\pi y/b) \end{aligned} \tag{4-12}$$

Let $\zeta = m\pi/a$ and $\eta = n\pi/b$ where m and n are the number of Fourier series terms of the analytical solution in the x and y directions, and substituting equation (4-12) into equation (4-8) yields for each combination of m and n:

$$\frac{d}{dz}\{F_{mn}(z)\} = [D_{mn}]\{F_{mn}(z)\} \tag{4-13}$$

Herein, $\{F_{mn}(z)\} = [U_{mn}(z)\ V_{mn}(z)\ Z_{mn}(z)\ X_{mn}(z)\ Y_{mn}(z)\ W_{mn}(z)]^T$ is the state vector of the plate with the m-n^{th} and the system matrix is:

$$[D_{mn}] = \begin{bmatrix} 0 & 0 & 0 & C_8 & 0 & -\zeta \\ 0 & 0 & 0 & 0 & C_9 & -\eta \\ 0 & 0 & 0 & \zeta & \eta & 0 \\ C_2\zeta^2 + C_6\eta^2 & (C_3+C_6)\zeta\eta & C_1\zeta & 0 & 0 & 0 \\ (C_3+C_6)\zeta\eta & C_6\zeta^2 + C_4\eta^2 & C_5\eta & 0 & 0 & 0 \\ -C_1\zeta & -C_5\eta & C_7 & 0 & 0 & 0 \end{bmatrix} \tag{4-14}$$

4.3 Solution of the equation

By solving the differential equation (4-13) based on the classical solution method of a linear differential equation (Stroud, 2013), the solution can be found as:

$$\{F_{mn}(z)\} = [G_{mn}(z)]\{F_{mn}(0)\} \tag{4-15}$$

where $[G_{mn}(z)] = \exp\{[D_{mn}]z\}$, and when $z = h$,

$$\{F_{mn}(h)\} = [G_{mn}(h)]\{F_{mn}(0)\} \tag{4-16}$$

$\{F_{mn}(0)\}$ and $\{F_{mn}(h)\}$ are the values of the state variables on the top (z=0) and bottom (z=h) surfaces. They can be determined uniquely based on the load conditions on the top and bottom surfaces of the plate. For example, if the plate is subjected to an arbitrarily distributed external transverse pressure $q(x,y)$ on the top surface only, the state vectors on the top and bottom surfaces of the plate can be expanded into Fourier series, as shown in equations (4-17) and (4-18), respectively:

$$\{\mathrm{F}_{mn}(0)\} = \begin{Bmatrix} U_{mn}(0) \\ V_{mn}(0) \\ \frac{4}{ab}\int_0^a \int_0^b q(x,y)\sin(m\pi x/a)\sin(n\pi y/b)\,\mathrm{d}x\mathrm{d}y \\ 0 \\ 0 \\ W_{mn}(0) \end{Bmatrix} \tag{4-17}$$

And:

$$\{\mathrm{F}_{mn}(h)\}^T = [U_{mn}(h)\ \ V_{mn}(h)\ \ 0\ \ 0\ \ 0\ W_{mn}(h)] \tag{4-18}$$

Further formulation simplification can be used if $q(x,y)=q$ is a constant (e.g. in case of a uniformly distributed load), and:

$$\frac{4}{ab}\int_0^a \int_0^b q(x,y)\sin(m\pi x/a)\sin(n\pi y/b)\,\mathrm{d}x\mathrm{d}y = \begin{cases} 0 & (m, n = 2, 4, 6,\ldots..) \\ \frac{-16q}{mn\pi^2} & (m, n = 1, 3, 5,\ldots..) \end{cases} \tag{4-19}$$

One of the most challenging aspects of the work presented here is the accurate calculation of the exponential matrix$\mathrm{G}_{mn}(z)$, especially with a high number of Fourier series terms (m and n) in thicker plates. To solve this problem, the precision can be improved for all elements in the matrix $[D_{mn}]$ should be adopted before solving the corresponding exponential matrix. The computer coding routine used here for the exponential matrix function is MatrixExp, which is embedded in the commercially available software MATHEMATICA (Wolfram Research, 2016); for the associated code, see Appendix A. This can give sufficiently accurate results for thicker plates, as will be shown later in section 4.4.3.5 (depending on the element precision in $[D_{mn}]$).

Substituting equations (4-17) and (4-18) into (4-16), all displacement components on the top and the bottom surfaces of the plate can be obtained; that is, $U_{mn}(0)$, $V_{mn}(0)$, $W_{mn}(0)$ and $U_{mn}(h)$, $V_{mn}(h)$, $W_{mn}(h)$.

After finding all the displacements and the transverse stresses, the in-plane stresses can be found by using the following equation:

$$\begin{Bmatrix}\sigma_x\\ \sigma_y\\ \tau_{xy}\end{Bmatrix}=\begin{bmatrix}-C_2\zeta & -C_3\eta & -C_1 & 0 & 0 & 0\\ -C_3\zeta & -C_4\eta & -C_5 & 0 & 0 & 0\\ C_6\eta & C_6\zeta & 0 & 0 & 0 & 0\end{bmatrix}\begin{Bmatrix}u\\ v\\ \sigma_z\\ \tau_{xz}\\ \tau_{yz}\\ w\end{Bmatrix} \tag{4-20}$$

Although all the stresses and displacements can be calculated by using the SSA, as shown in equation (4-12), the six state variables are expressed as a Fourier series and, by that, these six states will be continuous and the accuracy will depend on the number of Fourier series terms.

For the next sections, different case studies will explore the capability of the SSA in comparison to various analytical and numerical methods. The studies will start with a general application of the SSA to composite plate (single ply), and Classical Plate Theory (CPT) will be compared with the SSA. Then, different FEM models will be validated with the SSA under different types of load. Meanwhile, new findings will be explored by using the SSA.

Finally, the SSA will be extended to consider laminated plates with more than one ply, and a comparison between the SSA results with various existing analytical approaches will be studied.

4.4 SSA application to a general composite single-ply plate

In this section, three case studies are analysed by using SSA, different existing analytical approaches and FEM for the determination of the structural behaviour of simply supported orthotropic composite plates under different types of load. For the first case, the plate is under sinusoidal load with a maximum magnitude of 1 MPa. The SSA will be explored for this study and the CPT results will be compared. The second case study is a composite plate under anti-symmetrical half-single sine distributed out-of-plane load, and, in the third case, the load is uniformly distributed. For the second and third case studies, the numerical results from a finite element model developed in ABAQUS, for comparison, are provided with those obtained by using the SSA with different parametric studies.

4.4.1 Case Study 1: Orthotropic square single-ply plate under different types of load - SSA and CPT comparison

The focused-on plate has the same geometry as that examined analytically by Reddy (2004). The in-plane dimensions of the plate are $a = b = 100$ mm and h/a is equal to 0.01. Here, a is the length of the plate along the x-axis, b is the dimension of the plate along the y-axis and h is the total thickness of the plate (z-axis), as shown in Figure 4-3. The set of elastic material parameters used and given as shown in Table 4-1 for the plies are as per the reference (Reddy, 2004).

Table 4-1 Elastic material properties of a single-ply composite plate (Reddy, 2004).

$E_1/E_2 = 25$; $E_3 = E_2$
$G_{12} = G_{13} = 0.5\ E_2$
$G_{23} = 0.2\ E_2$
$\nu_{12} = \nu_{13} = \nu_{23} = 0.25$

The plate is simply supported from four sides as per Reddy (2004) and is under two types of out-of-plane load, as shown in Figure 4-3. The first load is sinusoidal load (SSL) with a maximum magnitude of 1 MPa ($q(x,y) = q_0 \sin(\pi x/a) \sin(\pi y/b)$ where q_0= 1 MPa), and the second one is uniformly distributed load (UDL) with $q(x,y) = q$.

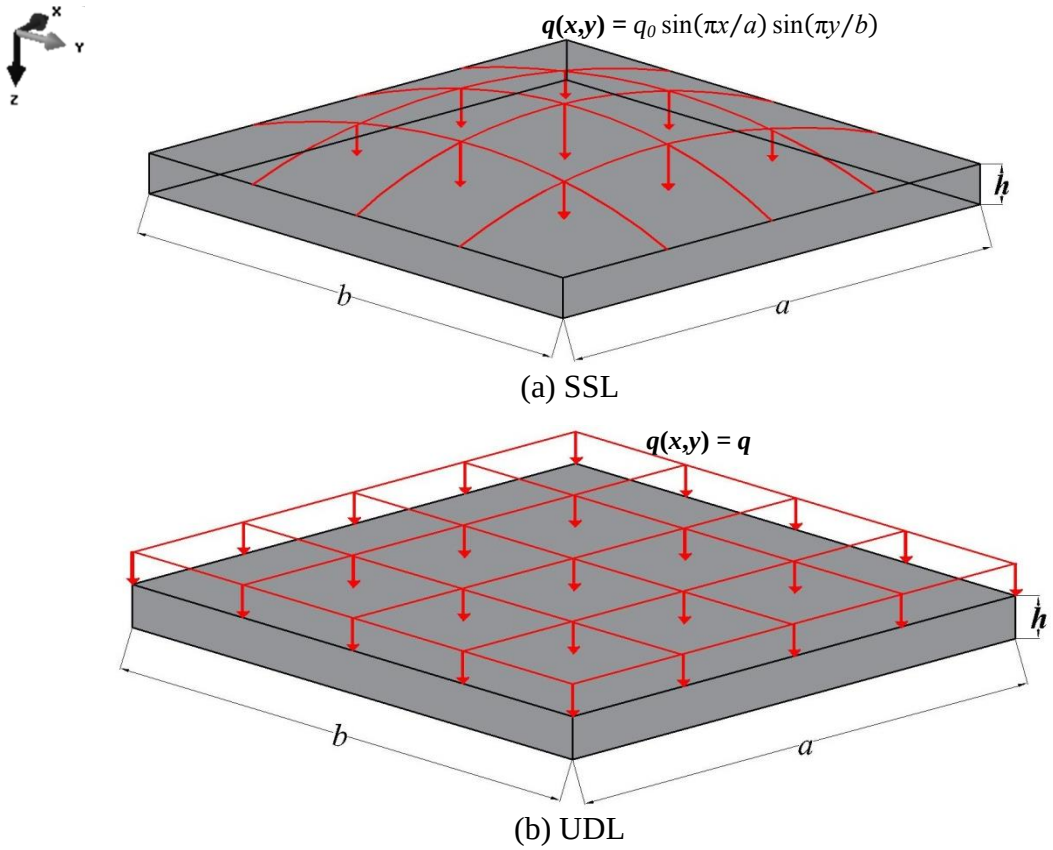

Figure 4-3 The geometry of a single-ply orthotropic plate under (a) sinusoidal load and (b) uniformly distributed load.

4.4.1.1 Analytical comparison

Table 4-2 shows the theoretical results for the out-of-plane displacement w, the in-plane stresses σ_x, σ_y and τ_{xy} and the transverse shear stress τ_{xz} on different locations under two types of load. The comparison is between the SSA and CPT results with the thickness-to-width ratio (h/a) equal to 0.01.

For SSL, the number of Fourier series terms (m and n) in the SSA is set to equal 1; also, for UDL the m and n are set to be equal to 19, as per Reddy (2004).

As shown in Table 4-2, the CPT gives lower results compared to the SSA for the out-of-plane displacement w and the in-plane-stresses σ_x and σ_y for both loads, but, in general, the results show very good agreement between each other and this is expected as the plate is thin.

Table 4-2 Theoretical results for out-of-plane displacements and stresses of the orthotropic plate for $a = b$ and $h/a = 0.01$.

(a) SSL			
	(x,y,z)	**SSA**	**CPT** (Reddy, 2004)
$(WE_2h^3/b^4q_0)\times10^2$	$(\frac{a}{2},\frac{b}{2},\frac{h}{2})$	0.4333	0.4312
$\sigma_x h^2/b^2q_0$	$(\frac{a}{2},\frac{b}{2},h)$	0.5390	0.5387
$\sigma_y h^2/b^2q_0$	$(\frac{a}{2},\frac{b}{2},h)$	0.0268	0.0267
$\tau_{xy} h^2/b^2q_0$	$(a,b,0)$	0.0213	0.0213
$\tau_{xz} h/bq_0$	$(0,\frac{b}{2},\frac{h}{2})$	0.4396	0.4398
(b) UDL			
$(WE_2h^3/b^4q_0)\times10^2$	$(\frac{a}{2},\frac{b}{2},\frac{h}{2})$	0.6527	0.6497
$\sigma_x h^2/b^2q_0$	$(\frac{a}{2},\frac{b}{2},h)$	0.7870	0.7866
$\sigma_y h^2/b^2q_0$	$(\frac{a}{2},\frac{b}{2},h)$	0.0245	0.0244
$\tau_{xy} h^2/b^2q_0$	$(a,b,0)$	0.0465	0.0463
$\tau_{xz} h/bq_0$	$(0,\frac{b}{2},\frac{h}{2})$	0.7746	0.7758

For the upcoming case studies, using ABAQUS, the numerical analysis will be explored for different types of loads and models and compared with the SSA; also, the effect of the thickness-to-width ratios will be studied by applying the SSA. Before that, a brief overview of the FEM approach by ABAQUS will be presented.

4.4.2 Introduction to the numerical solution: Finite element method (FEM) by ABAQUS

The FEM is commonly used to solve problems for which analytical solutions are not readily available or do not necessarily exist. Also, it can be used to produce satisfactory solutions with reasonable accuracy for composite plate and shell structures. The FEM is based on the idea of discretising a structure into small elements, describing the behaviour of each element in a simple way, then reconnecting elements at nodes (Cook, 1995).

In this section, the parameters that affect the FEM modelling will be presented such as material properties, element types, boundary conditions and mesh element types. Then, the specific parameters for different case studies that will be used in this chapter will be specified. Following this, the FEM will be adopted to model different case studies and compared with the SSA.

4.4.2.1 Material properties

Selecting the appropriate material properties of the composite material is an important task. A composite plate has different moduli directions. For the material properties, ABAQUS needs to insert the material properties as Isotropic, Engineering Constants (which is to define Young's moduli, Shear moduli and Poisson's ratios directly related to the local coordinates of the plate), Lamina and Orthotropic.

In this study, the composite plate has been assigned as an elastic material with associated input in the FEM model as shown in Table 4-3.

4.4.2.2 Element types

In ABAQUS, a wide range of elements can be used depending on the problem to be simulated. The types of element families include continuum (solid), shell, beam, rigid, membrane and truss elements. For each of these elements there are more types of elements depending on the degrees of freedom, number of nodes, formulation and integration (ABAQUS, 2013). The first letter or letters of an element name indicate the family to which the element is related; for example, the S in S4R indicates a shell element.

The degrees of freedom are the essential variables evaluated during the analysis in ABAQUS; the use of solid elements is limited to 3D elements that have only displacement degrees of freedom. On the other hand, conventional shell elements have displacement and rotational degrees of freedom at each node. At any other points in the element, the displacements are obtained by interpolating from the nodal displacements; the interpolation order is determined by the number of nodes used in the element, as shown in Figure 4-4.

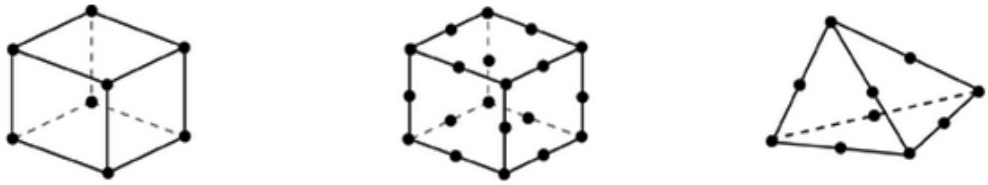

(a) Linear element 8-nodes | (b) Quadratic element 20-nodes | (c) Modified second-order element 10-nodes

Figure 4-4 Number of nodes used in each element type (ABAQUS, 2013).

Some elements can use full or reduced integration; however, reduced integration uses a lower-order integration to form the element stiffness and reduces the running time of the module.

- Solid element

The solid elements in ABAQUS include first-order (linear) interpolation elements and second-order (quadratic) interpolation elements. The second-order elements provide higher accuracy than the first-order ones for simple and smooth problems. When the normal stresses cannot be ignored and when the inter-laminar stresses are required, the composites with solid elements should be used.

- Shell element

For 3D shell elements in ABAQUS, there are three different formulations: general purpose, thin-only and thick-only shells. The general purpose shells allow the shell thickness to change with the element deformation (ABAQUS, 2013).

In this study, after an element type sensitivity study, the 3D fully integrated solid element with 20 nodes has been assigned for the FEM models, as shown in Table 4-3.

4.4.2.3 Mesh element size

Meshing is one of the most important processes since the accuracy of the results may depend on the meshing of the assemblies.

In this research, the shape of the mesh chosen is Quad-dominated type and the optimum mesh size will be derived from a mesh sensitivity study detailed in the next section.

Table 4-3 Different FEM parameters of ABAQUS.

FEM parameters	ABAQUS options	Assigned option
Material properties	Isotropic, Engineering Constants, Lamina and Orthotropic	Engineering Constants by defining Young's moduli, Shear moduli and Poisson's ratios directly related to the local coordinates of the plate
Element type	Continuum (solid), shell, beam, rigid, membrane and truss elements	3D fully integration solid element with 20 nodes
Mesh element type and size	Different mesh sizes	Quad-dominated type and the optimum mesh size

4.4.3 Case Study 2: Orthotropic square plate under anti-symmetrical half single sine distributed out-of-plane load - numerical comparison

In this case, the geometry of the composite plate is $a = b = 5$ mm and $h/a = 0.2$, 0.3 and 0.5. Where a is the length of the plate along the x-axis, b is the width of the plate along the y-axis and h is the thickness of the plate along the z-axis, as shown in Figure 4-5. The set of elastic material parameters used is given as shown in Table 4-4 as per Wu (1987).

Table 4-4 Elastic material properties of the composite plate (Wu, 1987).

$E_1 = 10\ E_2 = 10\ E_3$
$G_{12} = G_{13} = 0.6\ E_3$
$G_{23} = 0.5\ E_3$
$v_{12} = v_{13} = v_{23} = 0.25$

The plate is simply supported for all sides and the load is an anti-symmetrical half-sinusoidal distributed out-of-plane load $\frac{q}{2}\sin\left(\frac{\pi x}{a}\right)\sin\left(\frac{\pi y}{b}\right)$. Hence, $Z_{mn}(z)$ at the top ($z = 0$) and the bottom ($z = h$) surfaces of the plate are equal to $-q/2$ and $q/2$, respectively, as shown in Figure 4-5.

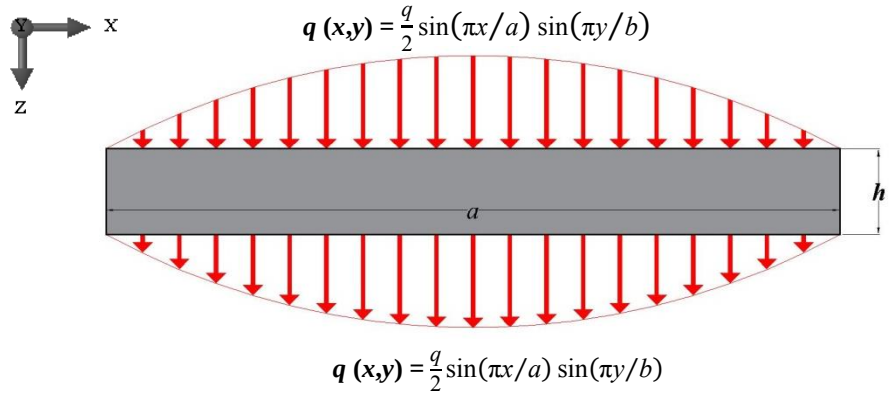

Figure 4-5 The geometry of a single-ply orthotropic plate under anti-symmetrical half-sinusoidal distributed out-of-plane load.

In the next section, the numerical results are given by using ABAQUS and the results are compared with those from the SSA analytical solution in order to illustrate the precision of these methods.

4.4.3.1 FEM model for Case Study 2: Parametric study

To provide a fair comparison and illustration of the advantages of the SSA, the numerical precision in the FEM model should be as accurate as possible. In order to determine an accurate FEM model, different element types and mesh sizes are considered first and compared with the SSA results. Then, the effect of thickness-to-width ratios of the plate on the analytical results can be presented and discussed systematically.

In this section, element type, mesh size and boundary condition sensitivity will be studied and explored for the FEM model. The FEM and the SSA results will be compared with each other to see the compatibility of the SSA with the FEM. Then, since the SSA is theoretically applicable to any thicknesses of plate (from thin to thick plates), the thickness-to-width ratio will be explored for SSA and FEM.

4.4.3.2 Element type for Case Study 2

As shown in Figure 4-6 and Table 4-5, four different solid elements have been studied: Reduced integrated 3D 8-node linear brick element (C3D8R), Fully integrated 3D 8-node linear brick element (C3D8), Reduced integrated 3D 20-node linear brick element (C3D20R) and Fully integrated 3D 20-node linear brick element (C3D20) (ABAQUS, 2013) with a mesh composed of elements with a unit length of 0.0625 mm. The mesh size sensitivity study will be discussed in detail in a later section.

The FEM and the SSA results have been compared with each other for the in- and out-of plane displacements and stresses. The solid element is used in this chapter instead of the shell element because the solid element can capture all the displacements and the stresses through the thickness of the plate, as shown in Table 4-5. Also, in this table, the in-plane stress σ_x, σ_y and τ_{xy} for the shell element are less than the FEM solid elements and the SSA result.

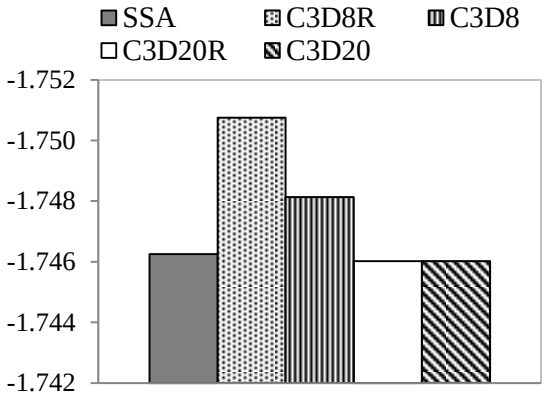

$u.E_3/qh$ at $(0,\frac{b}{2},h)$

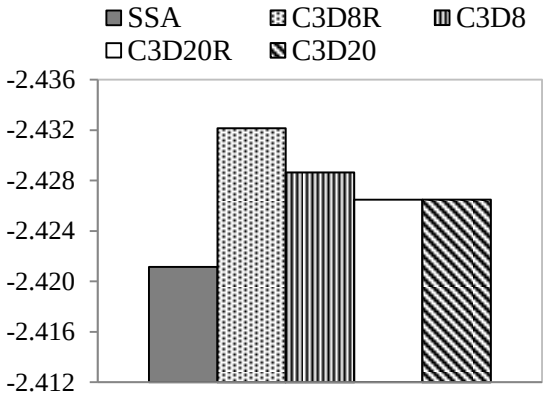

$v.E_3/qh$ at $(\frac{a}{2},0,h)$

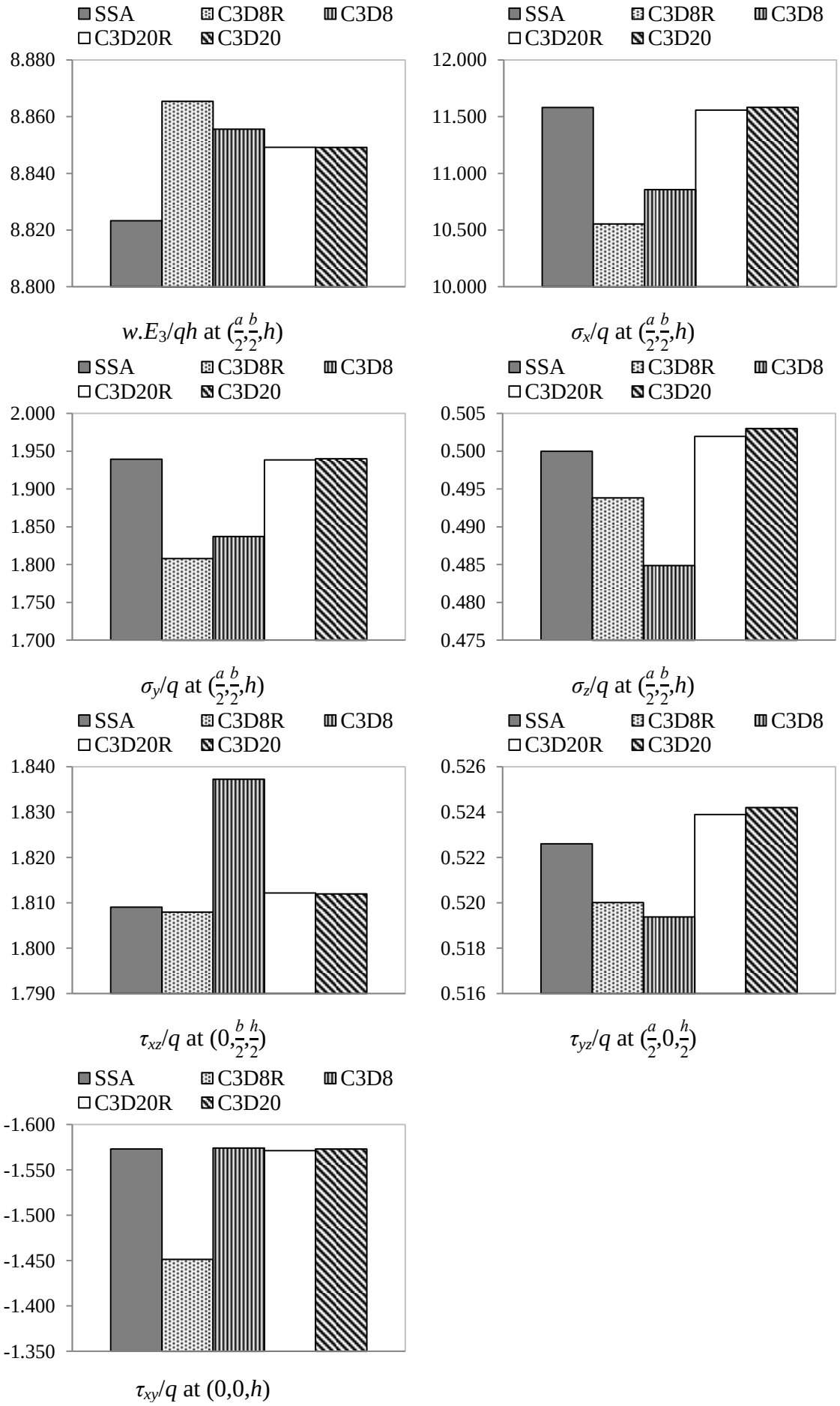

Figure 4-6 SSA with FEM results for different solid element types (h/a = 0.2).

In Table 4-5, the FEM and the SSA results for all the stresses and displacements are compared between each other; the negative relative errors mean the FEM gives less value than the SSA. From this table, it is apparent that the 8-node models gave more relative errors than the 20-node ones, especially for the stresses (in- and out-of-plane), although, in general, all the results are within the acceptable error and some of them are very close to each other and give an excellent agreement between each other. From this quantitative comparison with SSA, the FEM element type that gives more consistent results with a minimum relative error between each other is C3D20. On the basis of this observation, the numerical model with this element type will be adapted accordingly in the following numerical calculations to compare between the SSA and FEM results.

Table 4-5 Relative errors for different element types of a single-ply plate for $h/a = 0.2$.

		SSA	C3D8R		C3D8		C3D20R		C3D20		S8R	
			Values	Relative error (%)	Values	Relative error (%)	Values	Relative error (%)	Values	Relative error (%)	Values	Relative error (%)
$u.E_3/qh$	$(0,\frac{b}{2},h)$	-1.7463	-1.7508	0.26	-1.7481	0.11	-1.7460	-0.01	-1.7460	-0.01	0.0000	-
$v.E_3/qh$	$(\frac{a}{2},0,h)$	-2.4212	-2.4321	0.45	-2.4286	0.31	-2.4265	0.22	-2.4265	0.22	0.0000	-
$w.E_3/qh$		8.8233	8.8655	0.48	8.8556	0.37	8.8492	0.29	8.8492	0.29	9.4761	7.40
σ_x/q	$(\frac{a}{2},\frac{b}{2},h)$	11.5818	10.5554	-8.86	10.8575	-6.25	11.5582	-0.20	11.5827	0.01	9.9759	13.87
σ_y/q		1.9394	1.8080	-6.77	1.8373	-5.26	1.9385	-0.05	1.9401	0.04	1.6730	13.74
σ_z/q		0.5000	0.4938	-1.23	0.4849	-3.02	0.5020	0.39	0.5030	0.60	0.0000	-
τ_{xz}/q	$(0,\frac{b}{2},\frac{h}{2})$	1.8091	1.8080	-0.06	1.8373	1.56	1.8122	0.17	1.8120	0.16	1.0114	44.09
τ_{yz}/q	$(\frac{a}{2},0,\frac{h}{2})$	0.5226	0.5200	-0.50	0.5194	-0.62	0.5239	0.25	0.5242	0.30	0.0000	-
τ_{xy}/q	$(0,0,h)$	-1.5732	-1.4514	-7.74	-1.5742	0.06	-1.5713	-0.12	-1.5732	0.00	0.0000	-

4.4.3.3 Mesh size for Case Study 2

A mesh sensitivity test was performed to check which mesh size from four different sizes would be more appropriate for particular cases. The four meshes have lengths equal to 0.25, 0.125, 0.0625 and 0.03125 mm. Due to anti-symmetric half-single sine distributed out-of-plane load, the numerical results for the out-of-plane stress σ_z should be equal to $-q/2$ or $q/2$ on the top and bottom surfaces of the plate. These values can be used to confirm the accuracy of the numerical results from FEM, as shown in Figure 4-7, Figure 4-8 and Table 4-7.

For the out-of-plane stress σ_z results, when the mesh size of the element decreases, its relative error with respect to the SSA will be smaller and the results will be more accurate. Although the mesh sizes 0.0625 and 0.03125 mm give very close results to each other, the mesh size 0.0625 will be used in the current FEM analysis for time-efficiency, as shown in Table 4-6.

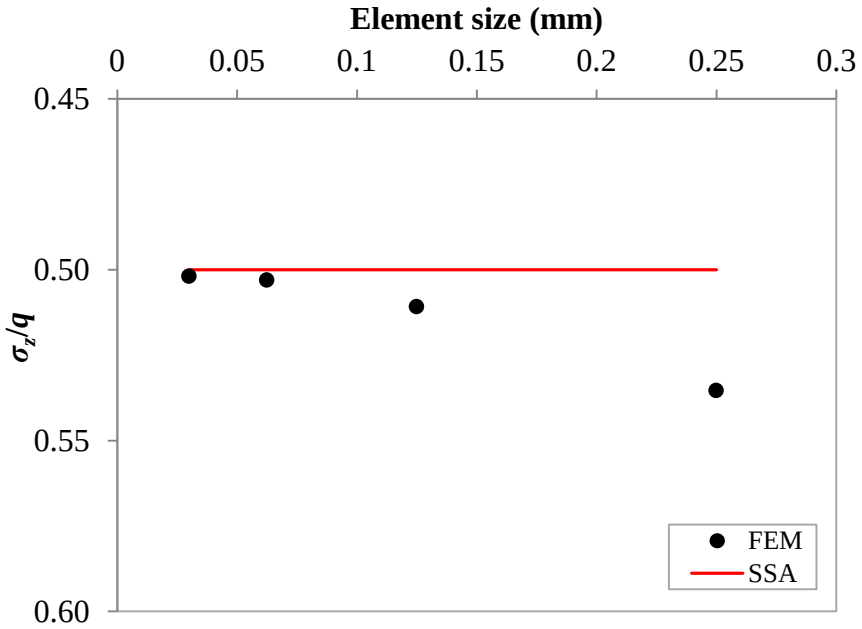

Figure 4-7 Different mesh size results of a single-ply plate for σ_z/q at $z = h$ for $h/a = 0.2$.

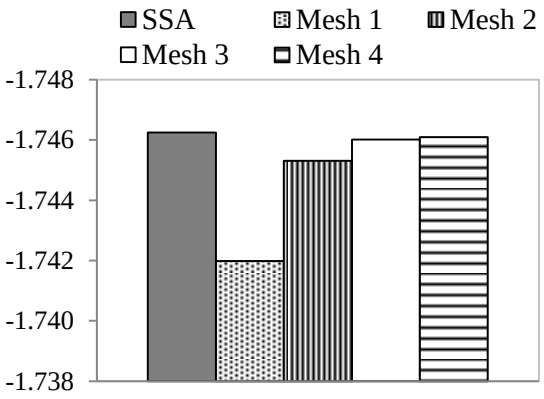

$u.E_3/qh$ at $(0,\frac{b}{2},h)$

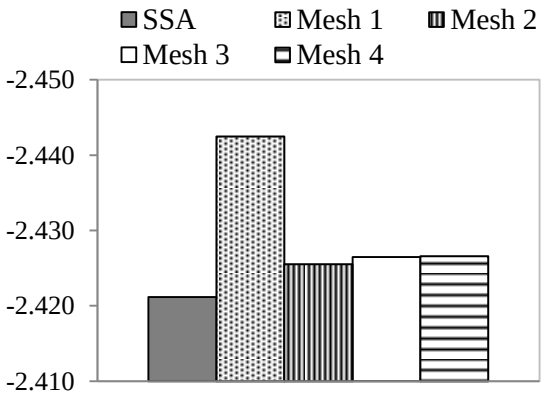

$v.E_3/qh$ at $(\frac{a}{2},0,h)$

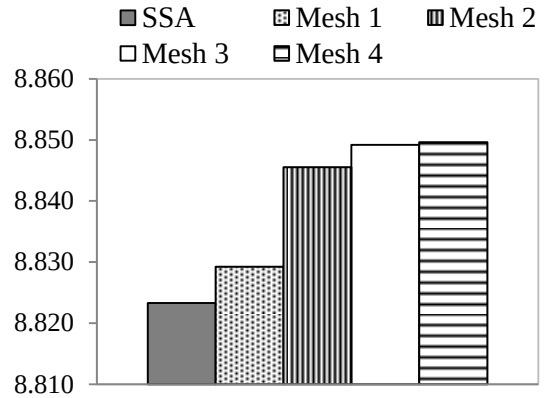

$w.E_3/qh$ at $(\frac{a}{2},\frac{b}{2},h)$

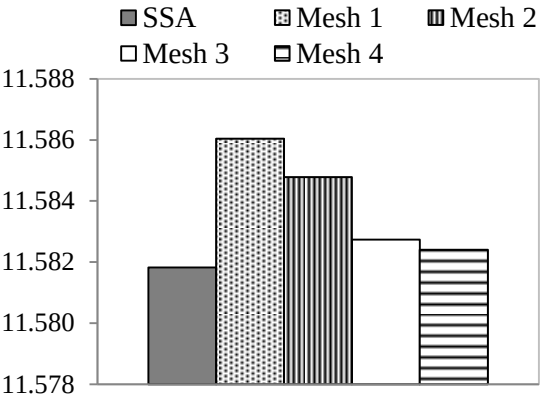

σ_x/q at $(\frac{a}{2},\frac{b}{2},h)$

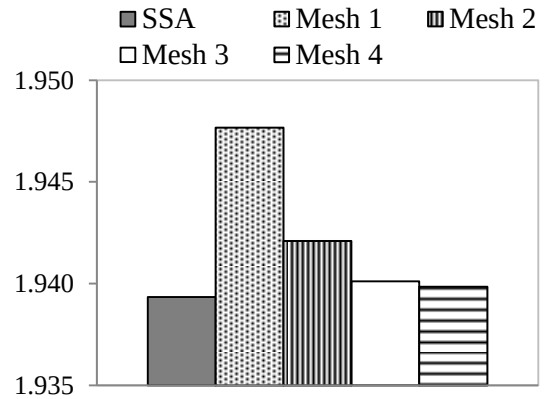

σ_y/q at $(\frac{a}{2},\frac{b}{2},h)$

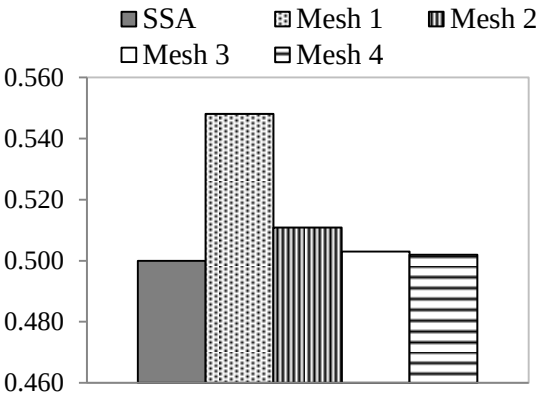

σ_z/q at $(\frac{a}{2},\frac{b}{2},h)$

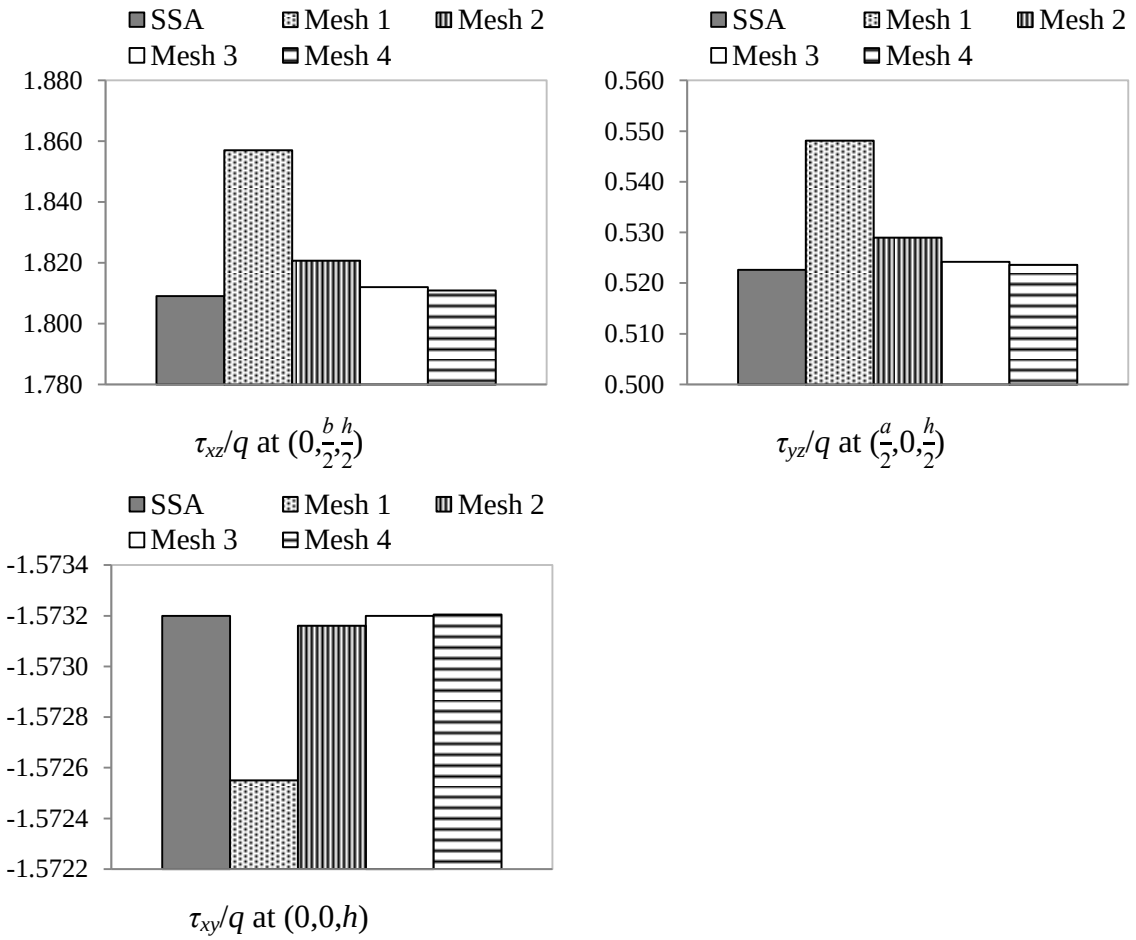

Figure 4-8 SSA with FEM results of a single-ply plate for different mesh sizes (h/a = 0.2).

Table 4-6 FEM models' running time for different mesh sizes for Case Study 2.

	Mesh 1 0.25 mm	Mesh 2 0.125 mm	Mesh 3 0.0625 mm	Mesh 4 0.03125 mm
Running time (s)	11	36	2452	3723.54

Table 4-7 Relative errors for different mesh sizes of a single-ply plate for h/a = 0.2.

		SSA	Mesh 1 (0.25×0.25)		Mesh 2 (0.125×0.125)		Mesh 3 (0.0625×0.0625)		Mesh 4 (0.03125×0.03125)	
			Values	Relative error (%)	Values	Relative error (%)	Values	Relative error (%)	Values	Relative error (%)
$u.E_3/qh$	$(0,\frac{b}{2},h)$	-1.7463	-1.7420	-0.24	-1.7453	-0.05	-1.7460	-0.01	-1.7461	-0.01
$v.E_3/qh$	$(\frac{a}{2},0,h)$	-2.4212	-2.4425	0.88	-2.4255	0.18	-2.4265	0.22	-2.4266	0.23
$w.E_3/qh$		8.8233	8.8292	0.07	8.8455	0.25	8.8492	0.29	8.8496	0.30
σ_x/q	$(\frac{a}{2},\frac{b}{2},h)$	11.5818	11.5860	0.04	11.5848	0.03	11.5827	0.01	11.5824	0.00
σ_y/q		1.9394	1.9477	0.43	1.9421	0.14	1.9401	0.04	1.9399	0.03
σ_z/q		0.5000	0.5481	9.63	0.5109	2.17	0.5030	0.60	0.5020	0.39
τ_{xz}/q	$(0,\frac{b}{2},\frac{h}{2})$	1.8091	1.8571	2.66	1.8207	0.65	1.8120	0.16	1.8109	0.10
τ_{yz}/q	$(\frac{a}{2},0,\frac{h}{2})$	0.5226	0.5481	4.89	0.5290	1.22	0.5242	0.30	0.5236	0.20
τ_{xy}/q	$(0,0,h)$	-1.5732	-1.5726	-0.04	-1.5732	0.00	-1.5732	0.00	-1.5732	0.00

4.4.3.4 Boundary condition sensitivity for Case Study 2

The boundary conditions occupied a significant role in obtaining accurate FEM results. For simply supported edges, ABAQUS gives options to determine the BC. Hence, in ABAQUS, as shown in Figure 4-9, there are two options to simulate the simply supported edges. To make the same simulation for the boundary conditions as the SSA, these boundary conditions are applied over the whole face. For this particular condition, one of the limitations of the SSA is that to satisfy the boundary conditions, the whole face will need to be satisfied (according to equation 4-11). The first one is BC1, whereby U3 is equal to zero along all the edges. The second, BC2, is where U2 and U3 are equal to zero along the *y*-axis, and U1 and U3 are equal to zero along the *x*-axis (whereby U is a translation).

The BC1 structural mechanism is unstable as the movement is not allowed just for the *z*-direction, although, as the plate is just under the out-of-plane loading, this mechanism is acceptable to simulate in this case study. For the BC2, the structural mechanism is statically indeterminate, and it will restrain the elongation of the tension face and the shorting of the compression face as it will be applied along the whole face the same as the analytical solution to enable a consistent comparison to be made between the FEM and the SSA.

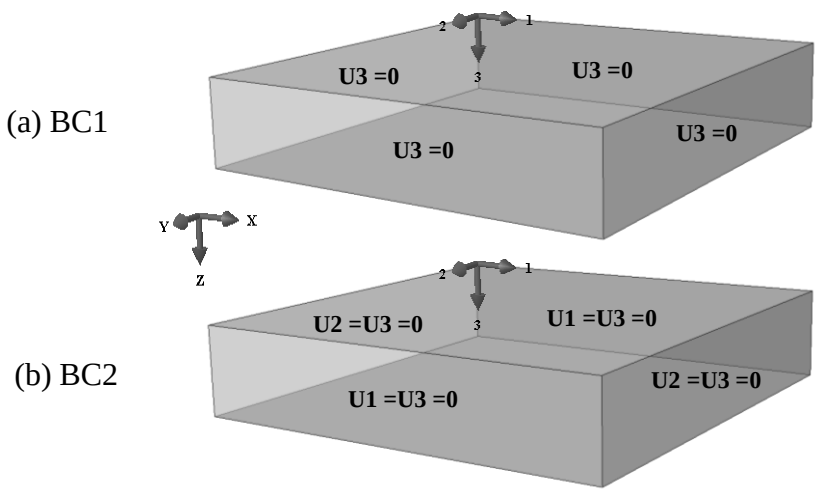

Figure 4-9 Different options for a simply supported boundary condition for Case Study 2.

Figure 4-10 and Table 4-8 show the different options to create simply supported edges by using ABAQUS and compare the results with the SSA. It is clear that BC2 is more reasonable and it gives better agreement with the SSA as it is the same boundary condition as the one used before in the SSA equations. In some cases, it could be easier to apply BC1, but, in this chapter, BC2 will be adopted.

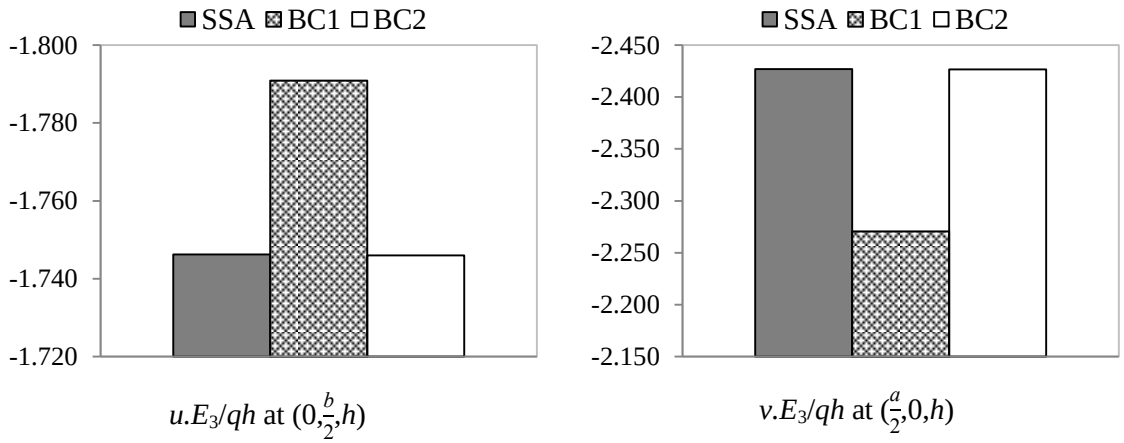

$u.E_3/qh$ at $(0,\frac{b}{2},h)$ $v.E_3/qh$ at $(\frac{a}{2},0,h)$

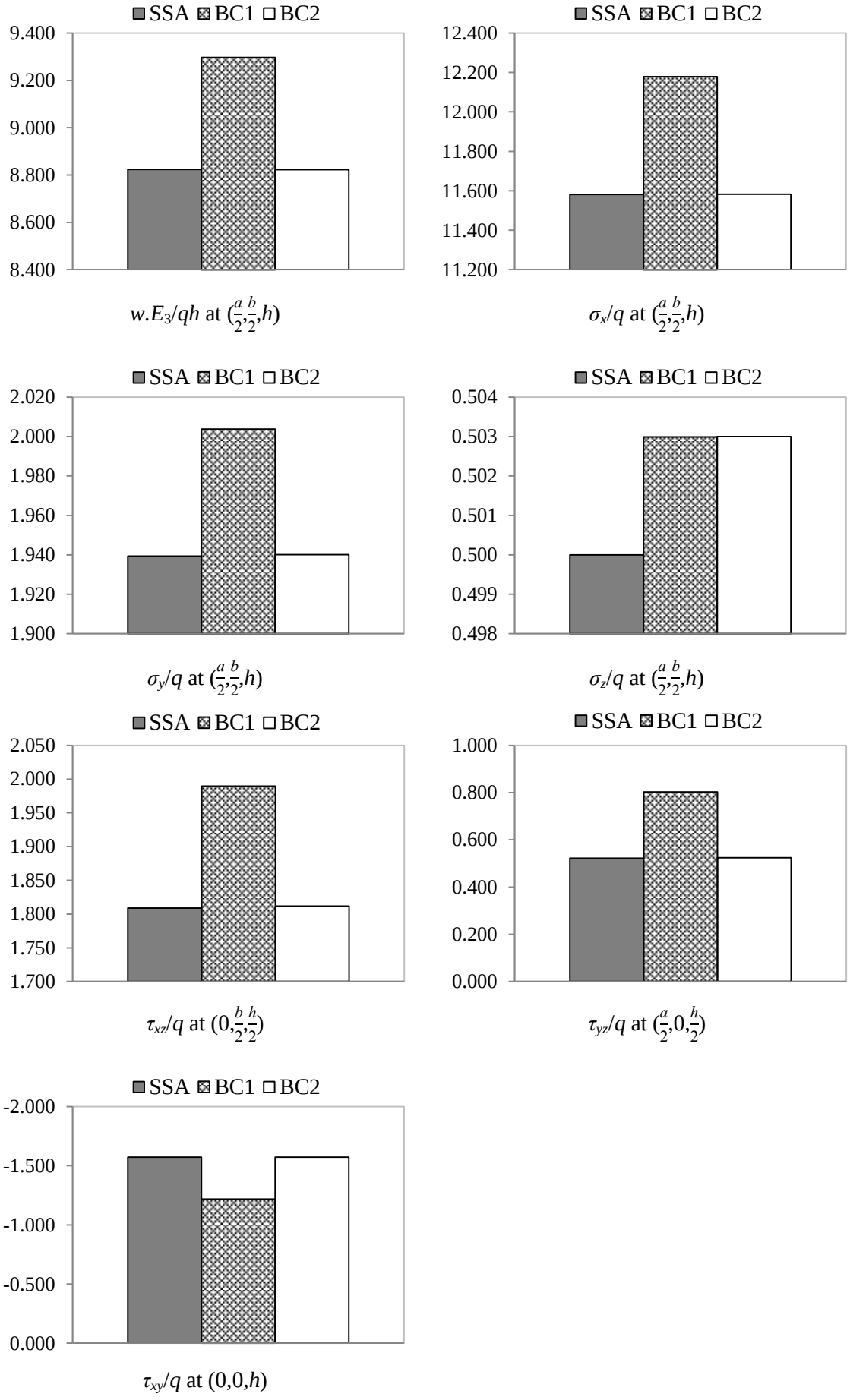

Figure 4-10 SSA with FEM results of a single-ply plate for different BCs (h/a = 0.2).

Table 4-8 SSA with FEM results of a single-ply plate for different BCs (h/a = 0.2).

	(x,y,z)	SSA	*FEM	
			BC 1	BC 2
$u.E_3/qh$	$(0,\frac{b}{2},h)$	-1.7463	-1.7909	-1.7460
$v.E_3/qh$	$(\frac{a}{2},0,h)$	-2.4212	-2.2706	-2.4265
$w.E_3/qh$	$(\frac{a}{2},\frac{b}{2},h)$	8.8233	9.2975	8.8492
σ_x/q	$(\frac{a}{2},\frac{b}{2},h)$	11.5818	12.1793	11.5827
σ_y/q	$(\frac{a}{2},\frac{b}{2},h)$	1.9394	2.0037	1.9401
σ_z/q	$(\frac{a}{2},\frac{b}{2},h)$	0.5000	0.5030	0.5030
τ_{xz}/q	$(0,\frac{b}{2},\frac{h}{2})$	1.8091	1.9895	1.8120
τ_{yz}/q	$(\frac{a}{2},0,\frac{h}{2})$	0.5226	0.8023	0.5242
τ_{xy}/q	$(0,0,h)$	-1.5732	-1.2176	-1.5732

*All the FEM models are 3D 20-node linear brick element (C3D20) with mesh size 0.0625 mm.

For detailed in-plane stress distribution σ_x through the thickness, Figure 4-11 shows σ_x for the two boundary conditions and accordingly with the results of the SSA. From this figure, the SSA gives a good distribution through the thickness when compared to both boundary condition options by the FEM models, but the SSA is closer to the FEM with BC2 than BC1 and that is expected as the BC2 simulates the same boundary conditions as the SSA. So, as mentioned before, the BC2 will be adopted.

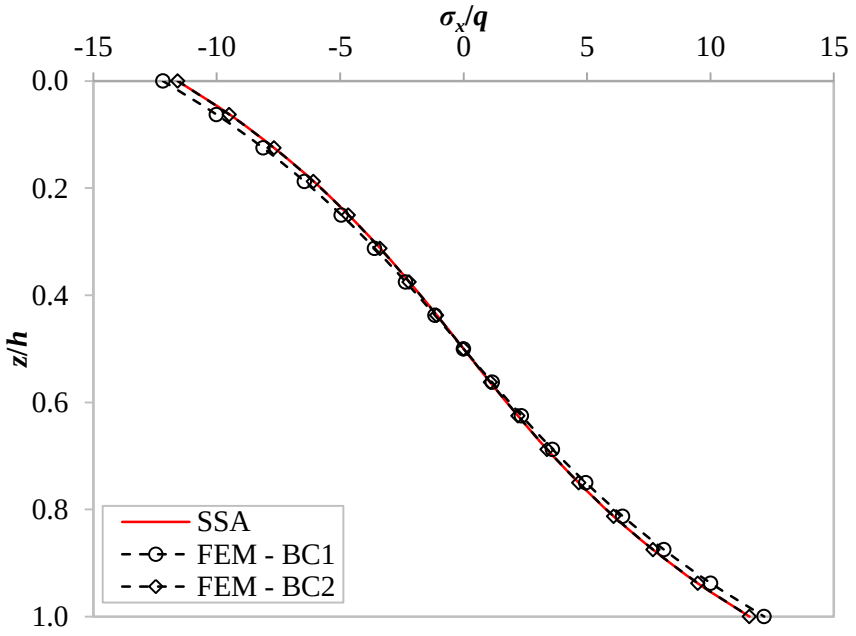

Figure 4-11 The effect of BC sensitivity on the in-plane stress (σ_x/q) through the thickness of a single-ply plate (h/a = 0.2).

4.4.3.5 Thickness-to-width ratio (h/a) for Case Study 2

Since the loading in this study is anti-symmetric, one of the advantages of using the SSA is that the capability of this approach to obtain an exact solution is demonstrated. This is because all boundary conditions of the six edge surfaces (four sides, together with the top and bottom surfaces; each surface has been described by three mixture stresses and/or displacements) are satisfied exactly. All equilibrium equations, kinematic equations and Hooke's law of 3D elasticity are fully covered and considered without any assumption and omission under the frame of the SSA. It is hence safe to say that the solution sought under this case is exact and the effect of the thickness-to-width ratios (h/a) on the plate structural behaviour can be determined quantitatively.

Figure 4-12 shows the effect of h/a on the in-plane stress σ_x through the half of the thickness as the behaviour will be symmetrical for the other half. The non-linear behaviour of the stress across the thickness can be observed clearly as h/a increases.

This figure shows that the linear stress distribution assumption through the thickness direction in the CPT assumption is inappropriate. From the same figure, it can be seen that, for all h/a ratios, there is a good agreement between the FEM (BC2) and the SSA including thin, medium and thick plates.

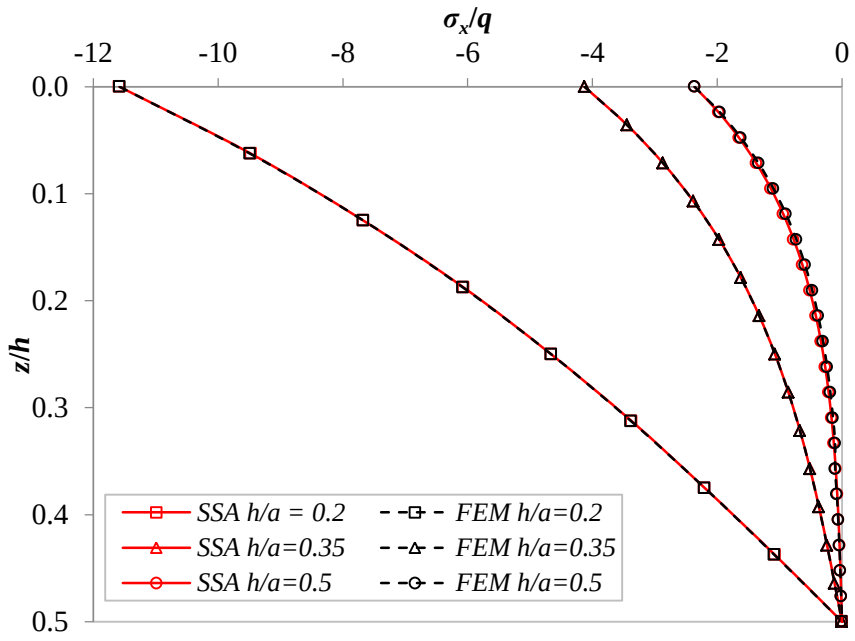

Figure 4-12 The effect of different h/a on the in-plane stress (σ_x/q) through the thickness (note: data is provided in Appendix B-Table B.1).

After the previous case studies, the next study will explore applying the SSA and the FEM to an orthotropic thick plate under uniformly distributed load. This section aims to show the accuracy of the SSA when high values are set to m and n.

4.4.4 Case Study 3: Orthotropic square plate under uniformly distributed load - numerical comparison

In this case, the geometry, material properties and the boundary conditions of the plate are the same as Case 2 (section 4.4.3). The only difference from Case 2 is that the load on the top surface of the plate is uniformly distributed $q(x,y) = q$ and the load on the bottom surface of the plate is nil, as shown in Figure 4-13.

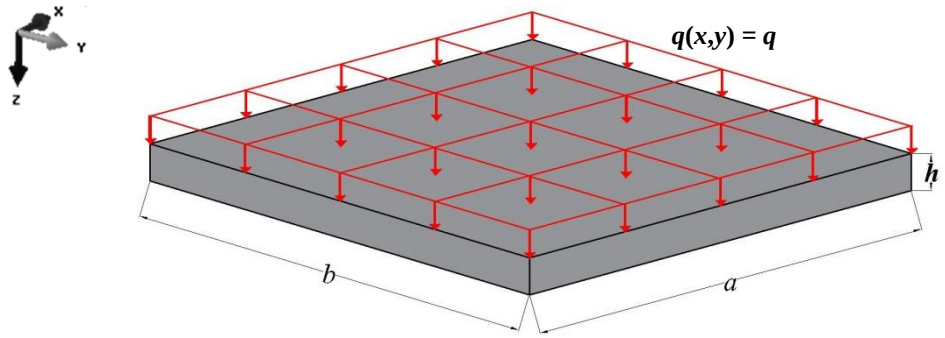

Figure 4-13 The geometry of a single-ply orthotropic plate under uniformly distributed load.

For a uniformly distributed load, to give an accurate analytical solution, Figure 4-14 shows different values for the number of Fourier series terms m along x/a, and, from this figure, as the value of m is higher, the load distribution σ_z shows more uniformity. For this reason, the highest number of Fourier series terms (m and n) in the solution.

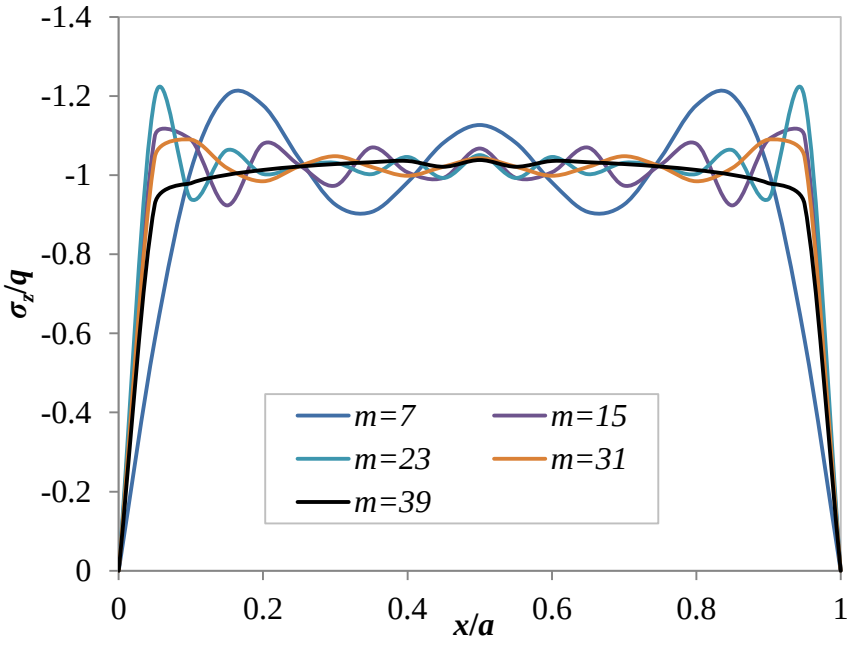

Figure 4-14 The load at the top ply (z=0) distribution along x/a for Case Study 3.

For the same reason as the selection of the element type, as stated in Case 2, the precision comparison in this case study would be the element type C3D20 with the mesh size 0.0625×0.6025 mm. Table 4-9 shows the SSA and FEM results for the displacements and stresses of the composite plate. The results show that the FEM and SSA results are very close to each other, but the FEM has overestimated the results; e.g.

for in-plane stress σ_x the relative error is around 0.70% between the SSA and the FEM results.

To give the variation of the results between the SSA and the FEM, Figure 4-15 shows the distribution of the out-of-plane displacement w through the thickness. Apparently, the FEM gives larger values compared to the exact solution. For u, v and τ_{xy}, the FEM gives the same values for the top and bottom of the plate with different signs, and this is a weakness of the FEM program as it should not be the same according to the SSA solution. Additionally, the FEM results for τ_{xz} at the top and the bottom of the plate, as shown in Figure 4-16, are equal to -0.082 and 0.019 respectively. Although these values are small, the FEM results are not very precise in this case, as the transverse shear stress τ_{xz} should be zero at the top and the bottom of the plate. Hence, this problem can be reduced by using finer mesh size; however, this means longer computational running time by ABAQUS. Note that the average FEM computational running time for this particular model was approximately two hours, and this compared to the seconds taken when using the SSA code, as shown before in Table 4-6.

In practice, it is important to control the values of the inter-laminar stresses such as τ_{xz} as their presence leads to de-lamination if they exceed the shear strength (Ealias and Mattam, 2013).

Table 4-9 In- and out-of-plane displacements and stresses of Case 3 for h/a = 0.2.

	(x,y)	z	SSA	FEM
$u.E_3/qh$	$(0,\frac{b}{2})$	*T	2.8917	2.9010
		*B	-2.8001	-2.9010
$v.E_3/qh$	$(\frac{a}{2},0)$	*T	4.2289	4.4203
		*B	-4.4203	-4.4203
$w.E_3/qh$	$(\frac{a}{2},\frac{b}{2})$	*T	13.7081	13.7169
		*B	13.2274	13.2274
σ_x/q	$(\frac{a}{2},\frac{b}{2})$	*T	-17.0107	-17.1240
		*B	16.9643	16.9666
σ_y/q	$(\frac{a}{2},\frac{b}{2})$	*T	-2.4682	-2.5590
		*B	2.4175	2.4837
τ_{xy}/q	(0,0)	*T	3.7305	4.0943
		*B	-3.0743	-4.0943
τ_{xz}/q	$(0,\frac{b}{2})$	$h/2$	3.2006	3.2035
τ_{yz}/q	$(\frac{a}{2},0)$	$h/2$	1.3266	1.3518

* Where T and B are the top and bottom of the single-ply plate through the thickness respectively.

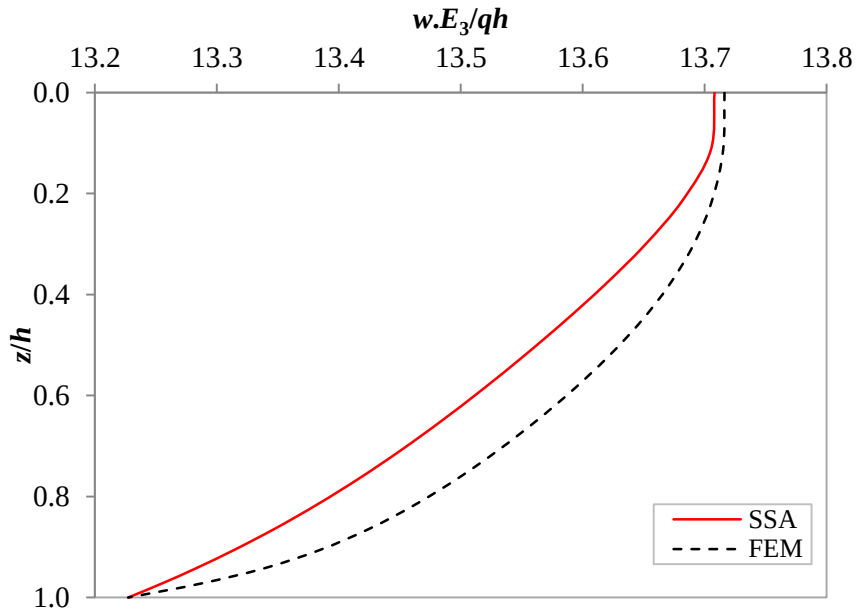

Figure 4-15 Out-of-plane displacement ($w.E_3/qh$) distribution through the thickness of the plate with h/a = 0.2 (note: data is provided in Appendix B-Table B.2).

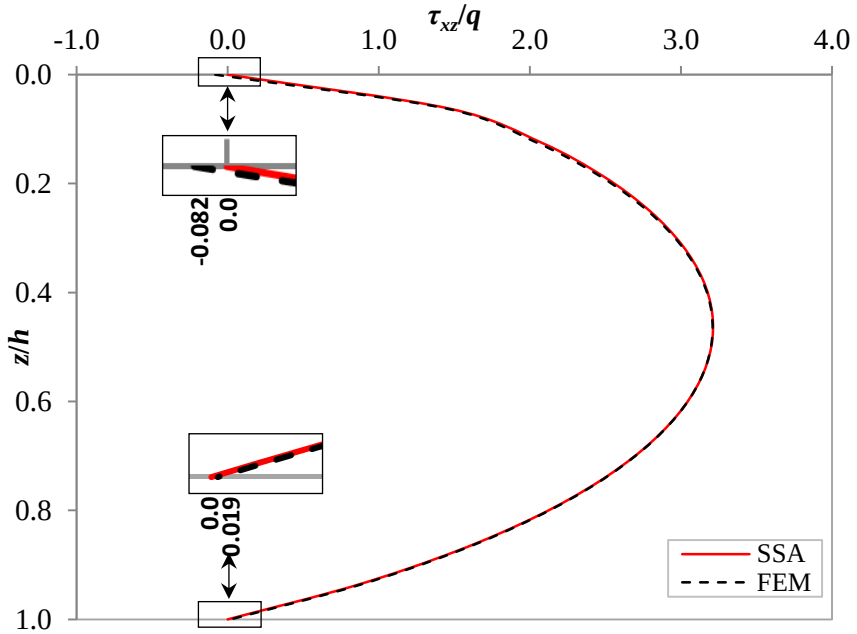

Figure 4-16 Transverse shear stress (τ_{xz}/q) distribution through the thickness of the plate with h/a = 0.2 (note: data is provided in Appendix B-Table B.3).

After applying the SSA to one general composite ply, in the next section, the SSA will be extended to include a laminated composite plate. Then, the SSA results will be compared with different existing analytical approaches.

4.5 SSA applied to a general laminated composite plate

For general laminated plates, as shown in Figure 4-17, if the plate is *j*-plied laminate, equation (4-16) ($\{F_{mn}(h)\} = [G_{mn}(h)]\{F_{mn}(0)\}$) will be applied first to each of the individual layers of the plate, where $\{F_{mn}(h)\}$ is called the state vector at the bottom of the plate, $\{F_{mn}(0)\}$ at the top of the plate, and $[G_{mn}(h)]$ is the system state matrix. Equation (4-16) is extended to:

$$\{F_{mn}(d_j)\}_j = \left[G(d_j)\right]_j \{F_{mn}(0)\}_j \tag{4-21}$$

where j is the number of layers, d_j is the thickness of each layer.

Then, if equation (4-21) is applied for $(j+1)^{th}$ layer; the equation becomes:

$$\{F_{mn}(d_{j+1})\}_{j+1}=\left[G(d_{j+1})\right]_{j+1}\{F_{mn}(0)\}_{j+1} \tag{4-22}$$

Therefore; $\{F_{mn}(0)\}_{j+1}=\{F_{mn}(d_j)\}_j$, then equation (4-22) becomes:

$$\{F_{mn}(d_{j+1})\}_{j+1}=\left[G(d_{j+1})\right]_{j+1}\left[G(d_j)\right]_j\{F_{mn}(0)\}_j \tag{4-23}$$

To summarise, equation (4-23) can be written as the following equation:

$$\{F_{mn}(d_{j+1})\}_{j+1}=[\Pi]\{F_{mn}(0)\}_{j+1} \tag{4-24}$$

Where:

$$\Pi=\left[G(d_{j+1})\right]_{j+1}\left[G(d_j)\right]_j$$

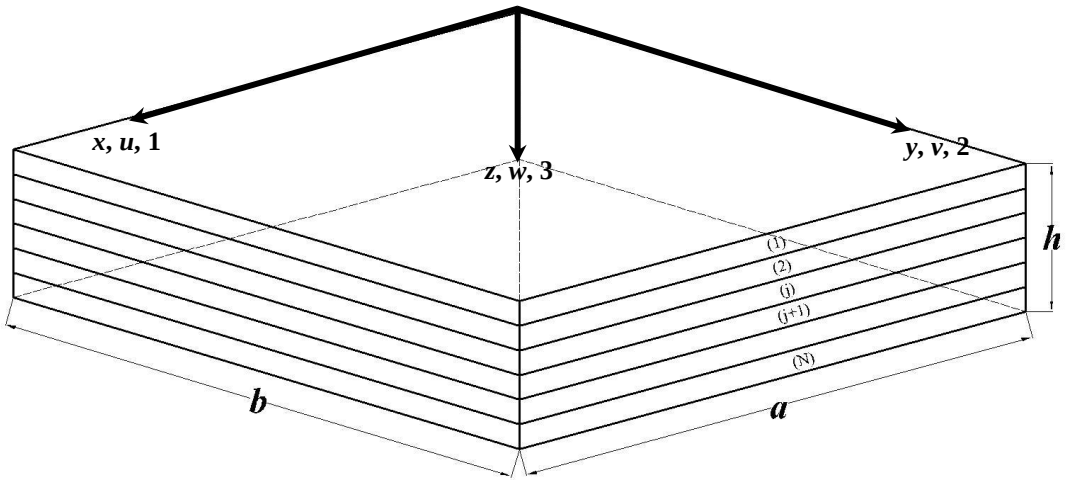

Figure 4-17 Nomenclature of an orthotropic rectangular laminated plate.

In this section, the SSA will be applied to a cross-ply plate as a laminated composite plate and different analytical approaches will be compared with the SSA result.

4.5.1 Antisymmetric cross-ply plate (two plies) comparison with various analytical solutions

The focused-on panel has the same geometry as that examined analytically by Reddy (2004). The panel or plate is symmetrical, with two plies of alternate orientation, i.e. [0/ 90]°, as shown in Figure 4-18. The in-plane dimensions of the plate are $a = b$ = 100 mm and h/a is equal to 0.2. Here, a is the length of the plate along the x-axis, b is the

dimension of the plate along the *y*-axis and *h* is the total thickness of the plate (*z*-axis), as shown in Figure 4-18. The set of elastic material parameters used, as shown in Table 4-10, for the plies is as per the reference (Reddy, 2004).

Table 4-10 Elastic material properties of the composite plate (Reddy, 2004).

$E_1/E_2 = 25;\ E_3 = E_2$
$G_{12} = G_{13} = 0.5\ E_2$
$G_{23} = 0.2\ E_2$
$\nu_{12} = \nu_{13} = \nu_{23} = 0.25$

The plate is simply supported from four sides as per Reddy (2004) and the load on the top surface of the panel is a sinusoidal load, as shown in Figure 4-18.

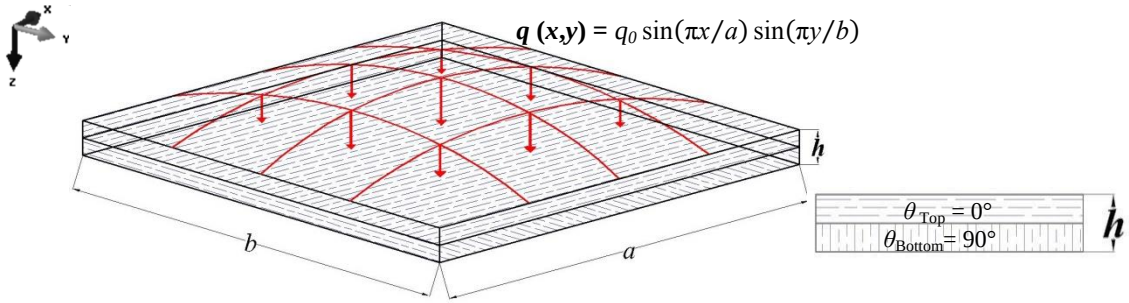

Figure 4-18 The geometry of the antisymmetric cross-ply plate under sinusoidal load and the orientation angles through *h*.

Figure 4-19 and Table 4-11 show the results of the different analytical approaches for the out-of-plane displacement w and the in-plane stresses σ_x and σ_y of antisymmetric cross-ply for $a = b$ and $h/a = 0.2$ for the simply supported boundary condition.

The analytical approaches that are used are Classical Laminated Plate Theory (CLPT), First-order Shear Deformation Theory (FSDT) and Higher-order Shear Deformation Theory (HSDT) and they are validated with the SSA. For more information about each approach, see Chapter 3, section 3.2.

The values in Figure 4-19 and Table 4-11 for the out-of-plane displacement w will be at the top of the plate, for the in-plane stress σ_x, the results will be at the top of the plate and for σ_y, they will be at the bottom of the plate, as per Reddy (2004). These locations are chosen to find the maximum out-of-plane displacements w and the in-plane stresses σ_x and σ_y.

The SSA shows the closest result for the out-of-plane displacement w to the FSDT compared to the other approaches. Also, the SSA shows a good agreement with the HSDT. Thus, in this case, the CLPT has underpredicted the results compared to the other approaches as the plate is considered to be a thick plate (Reddy, 2004).

For the in-plane stresses σ_x and σ_y, the values are the same as here the plate is square and the stresses are in the same position due to the plate's symmetry. The HSDT and the SSA are the closest to each other.

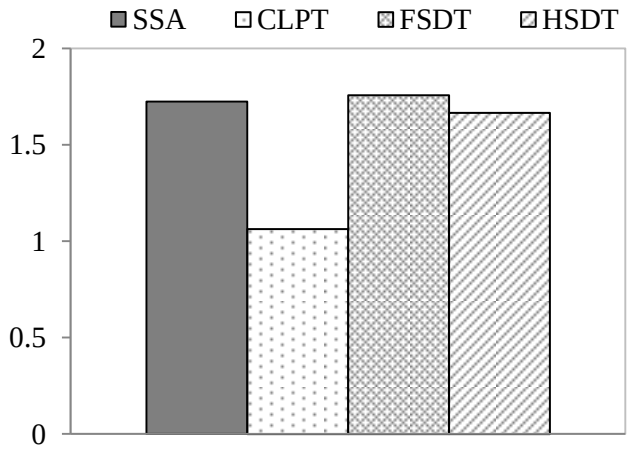

(a) $\frac{WE_2h^3}{b^4q_0}\times 10^2$

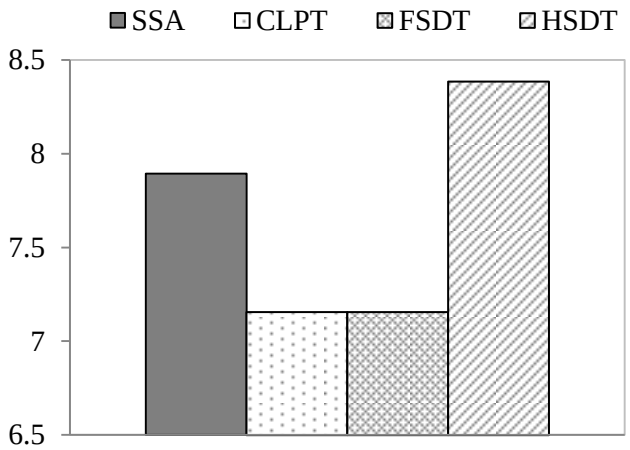

(b) $\frac{-\sigma_x h^2}{b^2 q_0} \times 10$

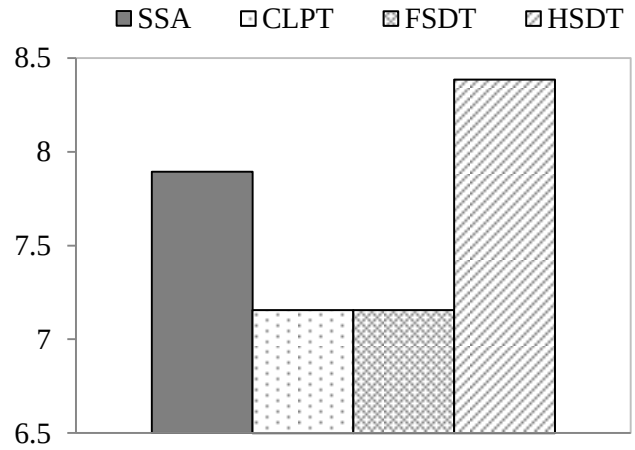

(c) $\frac{-\sigma_y h^2}{b^2 q_0} \times 10$

Figure 4-19 Theoretical results for displacements and in-plane stresses of antisymmetric cross-ply for $a = b$ and $h/a = 0.2$.

Table 4-11 Theoretical results for displacements and in-plane stresses of antisymmetric cross-ply for $a = b$ and $h/a = 0.2$.

	(x, y, z)	SSA	CLPT	FSDT	HSDT
$\frac{WE_2 h^3}{b^4 q_0} \times 10^2$	$(\frac{a}{2}, \frac{b}{2}, 0)$	1.725	1.064	1.758	1.667
$\frac{-\sigma_x h^2}{b^2 q_0} \times 10$	$(\frac{a}{2}, \frac{b}{2}, 0)$	7.894	7.157	7.157	8.385
$\frac{-\sigma_y h^2}{b^2 q_0} \times 10$	$(\frac{a}{2}, \frac{b}{2}, h)$	7.894	7.157	7.157	8.385

4.6 Concluding Remarks

An analytical investigation has been carried out for a general composite simply supported rectangular plate with two different loading conditions by using 3D SSA. The SSA, as a powerful three-dimensional approach, satisfies all the boundary conditions and the continuity at the interfaces. The state space method can give theoretically precise results for all in- and out-of-plane stresses and displacements for various thicknesses from thin to very thick plates. By applying the SSA, it is found that the behaviour of the stresses through the thickness becomes non-linear, especially for plates with a higher thickness-to-width ratio (h/a).

Furthermore, for the case studies in this chapter, the finite element models developed in ABAQUS overestimate some of the results, such as almost all of the displacement components and in-plane normal stresses, while shear stresses in FEM are lower values in comparison with those of the SSA. Such accuracy is required when numerical results from the FEM are applied for real structural design and behaviour evaluation.

In the next chapter, the SSA will be extended to consider a laminated composite plate, and this material will be Cross-Laminated Timber (CLT). Different case studies experimentally, analytically and numerically will be compared with the SSA.

CHAPTER 5
APPLICATION OF THE 3D STATE SPACE APPROACH TO CLT PANELS

5.1 Introduction

In the previous chapter, the SSA was applied to a generic laminated composite plate. In this chapter, the SSA will be applied to Cross-Laminated Timber (CLT) panels.

In this chapter, Cross-Laminated Timber (CLT) panels are investigated as a novel engineering application of the State Space Approach (SSA). The 3D analytical method provided by the SSA offers the potential for improved accuracy over existing common approaches to the analysis of CLT. The SSA is applied to describe the behaviour of a number of CLT panel configurations previously examined experimentally, analytically and numerically. In order to demonstrate the capability of the SSA in this application, the results are compared with those from various 2D and 3D analytical approaches and finite element modelling. Furthermore, different failure criteria are explored to assess the ultimate strength and design of the panels compared to the experimental test. The SSA method demonstrates its superior capability to the various existing 2D approaches in capturing the non-linear distribution of the stresses through the thickness of the CLT panels over a range of thicknesses.

In this chapter, firstly, the SSA is validated with the experimental works by Czaderski *et al*. (2007) for 3-ply CLT panels and Hochreiner *et al.* (2014) for 5-ply CLT panels under different types of loads. Then, different 2D and 3D analytical solutions are validated with the SSA for different CLT panels. Subsequently, after all the theoretically exact stresses are obtained by the SSA for the experiment undertaken by Czaderski *et al*. (2007), three different failure criteria are studied for 3-ply CLT to explore and understand more about the structural behaviour and failure of the CLT used

in the experiment. Then, the 3-ply CLT panel is modelled by using the finite element program ABAQUS and different types of models are simulated with different element types, mesh sizes and simply supported boundary condition options. Then, the FEM results are compared with the SSA results. After this, for the final section, an experimental work undertaken by O'Dowd *et al*. (2016) is simulated by FEM followed by an associated parametric study.

For all the following validations and calculations, the CLT panel is considered as an orthotropic material with three principal axes: longitudinal axis parallel to the grain, radial and tangential axes. The last two axes are treated the same in value and regarded as having properties perpendicular to the grain (McKenzie, 2000; Forest Products Laboratory, 2010).

5.2 CLT panel experimental validation

The following discusses the SSA modelling of 3- and 5-ply CLT panels tested experimentally by Czaderski *et al*. (2007) and Hochreiner *et al*. (2014).

5.2.1 Case Study 1: 3-ply CLT panel

Czaderski *et al*. (2007) studied a number of 3-ply CLT panels with an h/a ratio of 0.03 and a total thickness of 70 mm in two layup configurations [10, 50, 10] and [25, 20, 25] mm. The plates were simply supported on all four edges under four different types of concentrated load (delivered via 150×150 mm^2 spreader plates).

In this case study, two concentrated load configurations will be examined; the first load configuration is a central point load and the second is based on a quarter point load, as shown in Figure 5-1. Each plate is based on the [10, 50, 10] mm layup; corresponding material properties including E_1, E_2 and E_3 are shown in Table 5-1 as per the original experiment (Czaderski *et al*., 2007).

The modulus of elasticity of each layer of the CLT used in the test is estimated by using non-destructive ultrasound testing before bonding is applied between the layers. After the CLT plies were bonded, the modulus of elasticity and the strength of the CLT as one unit for the parallel and perpendicular to the grain direction of the outer plies were derived from beam tests (Czaderski *et al*., 2007).

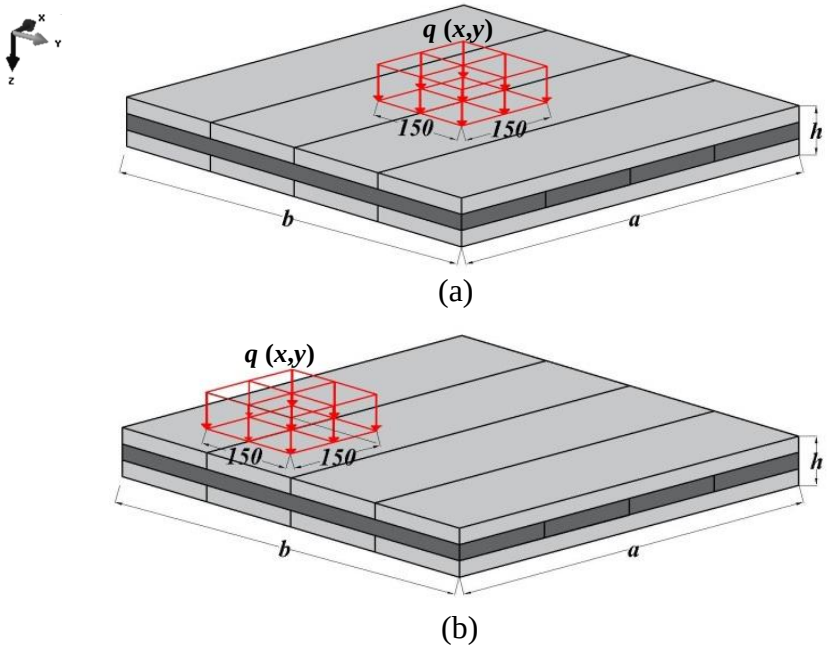

Figure 5-1 3-ply CLT panel under concentrated loads for (a) centred at the plate mid-point and (b) quarter point loads.

Deflections at the midpoint and quarter points were measured on the plate's lower surface directly under the load, so the quoted values for the out-of-plane deflection *w* will be at the lower surface. In the SSA models presented here, the number of Fourier series terms for the analytical solution, *m* and *n*, was set to 25, as per Sturzenbecher *et al*. (2010).

To ensure that the SSA can be applied in this case study and for comparison reasons, the experimental and SSA load-displacement curves for each specimen are shown in Figure 5-2. It can be seen that the SSA gives very good agreement with experimental results for the out-of-plane displacement *w* for both loading conditions.

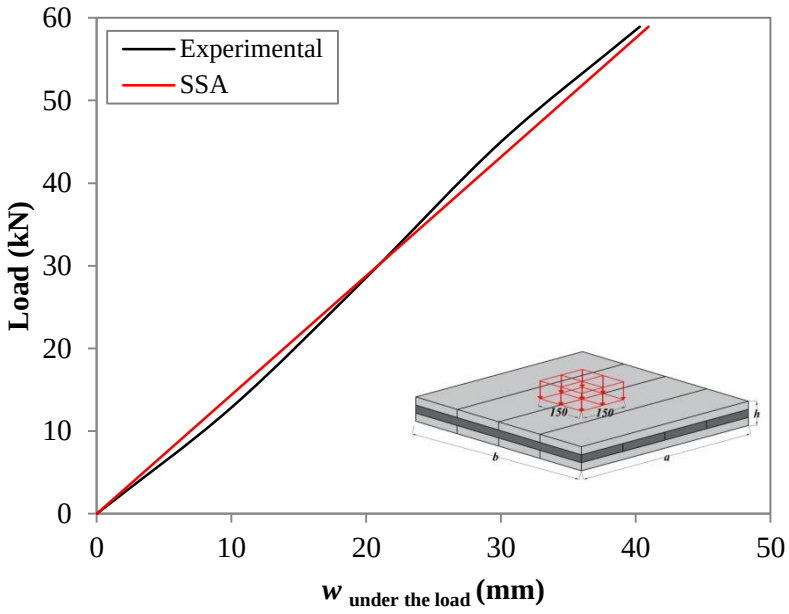

(a)

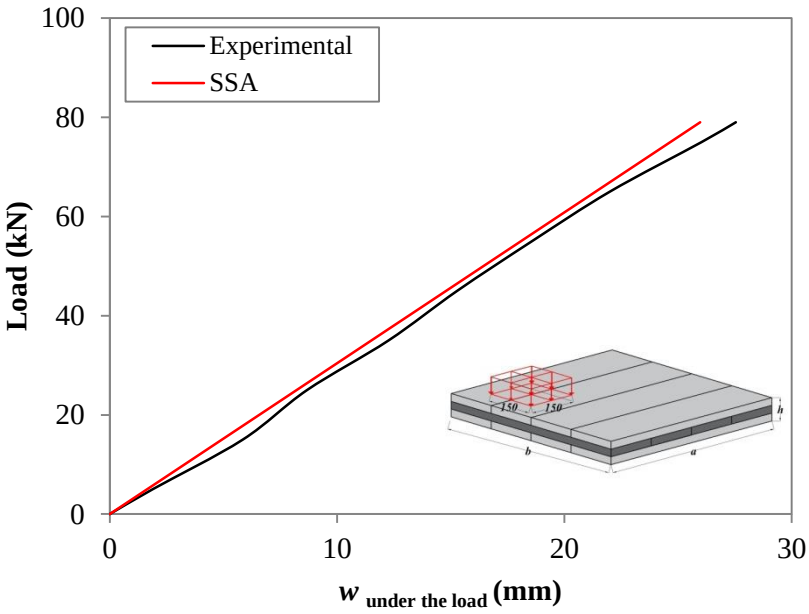

(b)

Figure 5-2 Load-displacement curves for the experimental and SSA for (a) central point (E_1 = 11,500 MPa) and (b) quarter point loads (E_1 = 12,000 MPa).

Subsequently, Table 5-1 and Figure 5-3 presents the experimental data along with the results from the SSA and other analytical approaches for each specimen at a total load of 30kN for the central point loaded plates and 45kN for the quarter point loaded plates. It can be observed that the SSA gives a good overall performance in modelling the

composites' behaviour. In the case of the central point load, the values for the SSA and the Pagano approach (as mentioned in detail before, in section 3.4.1) are exactly the same and both give good agreement with the experimental data. This demonstrates their suitability to deliver reliable output here. In the case of the quarter point load, the SSA method provides a closer match with the experimental results than either the Pagano or FSDT approaches.

The level of theoretical accuracy achieved by the SSA should be viewed within the context of the natural variation of timber itself. Typically, the co-efficient of variation for timber strengths will vary but it is frequently less than 15% (Dinwoodie, 2000).

Table 5-1 Experimental and theoretical results for displacements (mm) of the 3-ply CLT panel at total central load = 30kN, total quarter point loading = 45kN (h/a = 0.03, a=b= 2.5m)

Load	E_1 (MPa)	E_2 = E_3(MPa)	***w* (mm) at *z*=*h***			
			Exp. Data (Czaderski *et al*., 2007)	SSA	Pagano Sturzenbecher *et al*. (2010)	FSDT
*Central Point	11,500	575	20.90	20.84	20.84	20.89
	12,500	625	18.20	19.11	19.11	19.16
*Quarter Point	10,000	500	17.20	17.79	18.48	18.50
	12,000	600	15.00	14.80	15.35	15.34

*The Poisson's ratios of the CLT panels for both types of load are v_{12}= v_{13}= 0.02 and v_{23}= 0.3

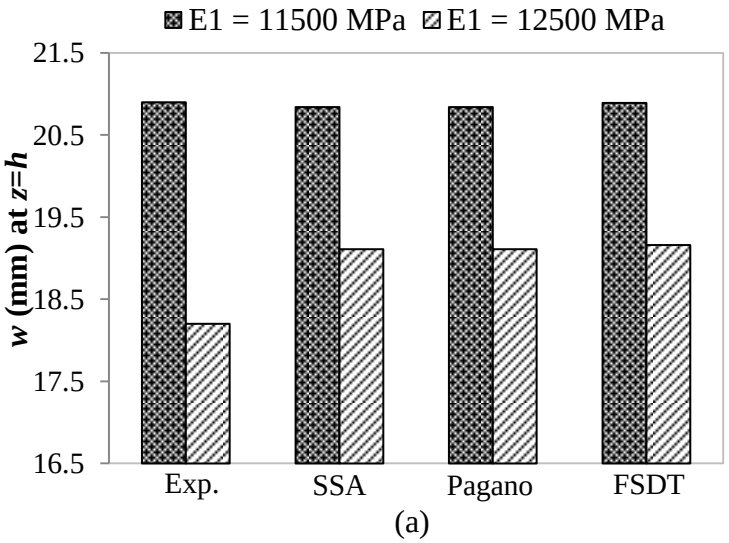

(a)

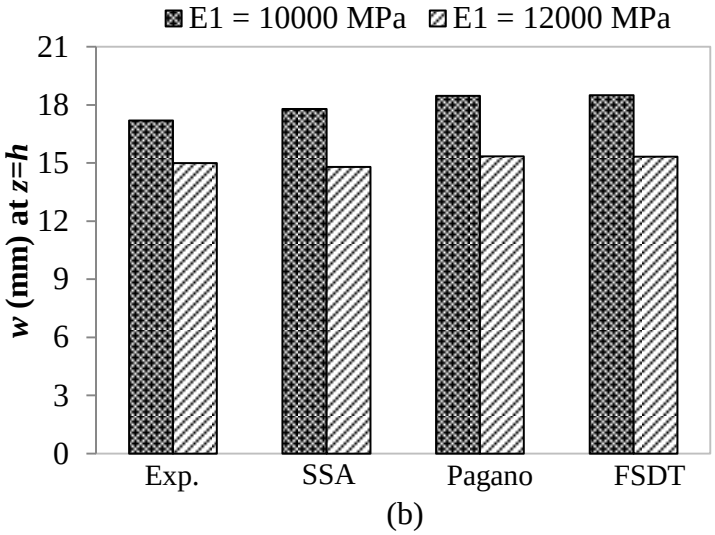

Figure 5-3 Experimental and theoretical results for displacements (mm) of the 3-ply CLT panel (h/a = 0.03) for (a) central point and (b) quarter point loads.

After validating the 3-ply CLT panel as an engineering application and for more thick plate application, the 5-ply CLT panel will be validated in the next section.

5.2.2 Case Study 2: 5-ply CLT panel

The panel in this study has the same geometry and properties as the experiment tested by Hochreiner *et al*. (2014). The panel is symmetrical with five plies of alternate grain orientation, i.e. [0/90/0/90/0]°, under centrally concentrated load acting uniformly on a patch area (c, d), as shown in Figure 5-4. Each ply has a thickness of 19 mm, so the total plate thickness is 95 mm. The in-plane dimensions of the plate are $a = b$ = 1900 mm and h/a is equal to 0.05. Here, a and b are the length of the plate along the x-axis and y-axis respectively, and h is the total thickness of the plate (z-axis), as shown in Figure 5-4. The set of elastic material parameters used for the timber plies is given in Table 5-2 and is as per the reference (Hochreiner *et al*., 2014).

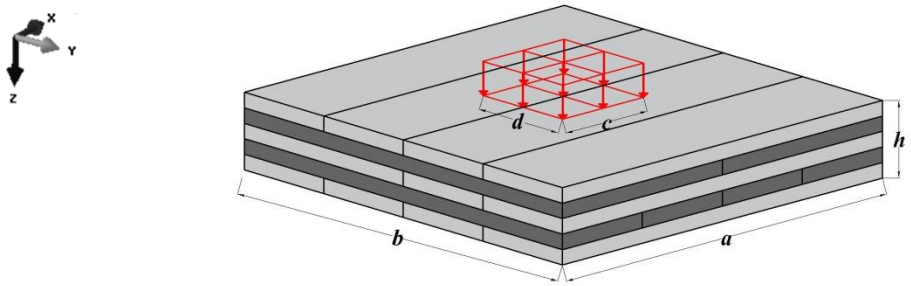

Figure 5-4 The geometry of the 5-ply CLT panel under central concentrated out-of-plane load.

Table 5-2 Elastic material properties for CLT panels (Hochreiner *et al.*, 2014).

E_1 = 11000 MPa; $E_2 = E_3$ = 370 MPa
$G_{12} = G_{13}$ = 690 MPa; G_{23} = 50 MPa
$v_{12} = v_{13}$ = 0.44; v_{23} = 0.64

As shown in Figure 5-5(a), the SSA gives very good agreement with experimental results for the out-of-plane displacement *w*. From this point of view, the SSA can be adopted for this case study and the out-of-plane displacement *w* can be drawn through the thickness of the CLT panel, as shown in Figure 5-5(b). From this figure, the non-linear behaviour of *w* is clear.

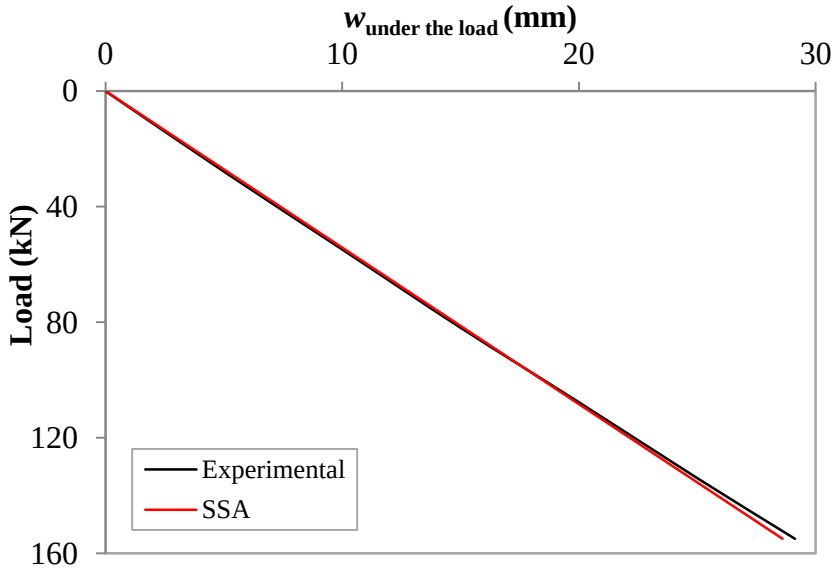

(a)

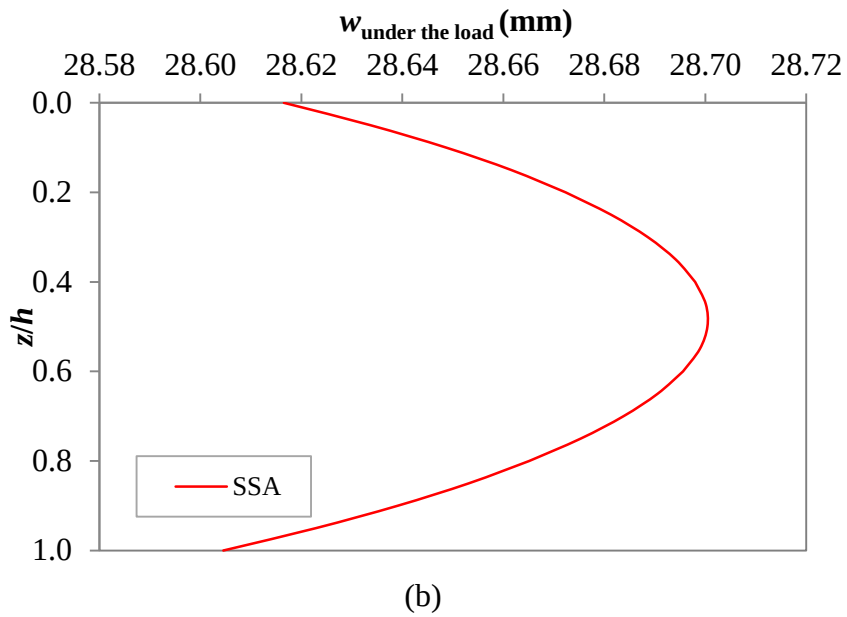

(b)

Figure 5-5 (a) Load-displacement curves for the experimental and SSA and (b) SSA out-of-plane displacement *w* distribution through the thickness.

As *h*/*a* is equal to 0.05, the CLT panel is considered to be a thin plate; however, by applying the SSA for this case study, the actual behaviour of the in-plane stresses σ_x through the thickness can be noticed, as shown in Figure 5-6, and the application can be extended to thicker plates, where the 2D methods are unable to capture the stresses accurately. Also as shown in the same figure, the in-plane stresses σ_x decrease as the thickness of the plate is increased. In addition, in the first layer as the thickness is increased the stresses will change the sign from negative to positive.

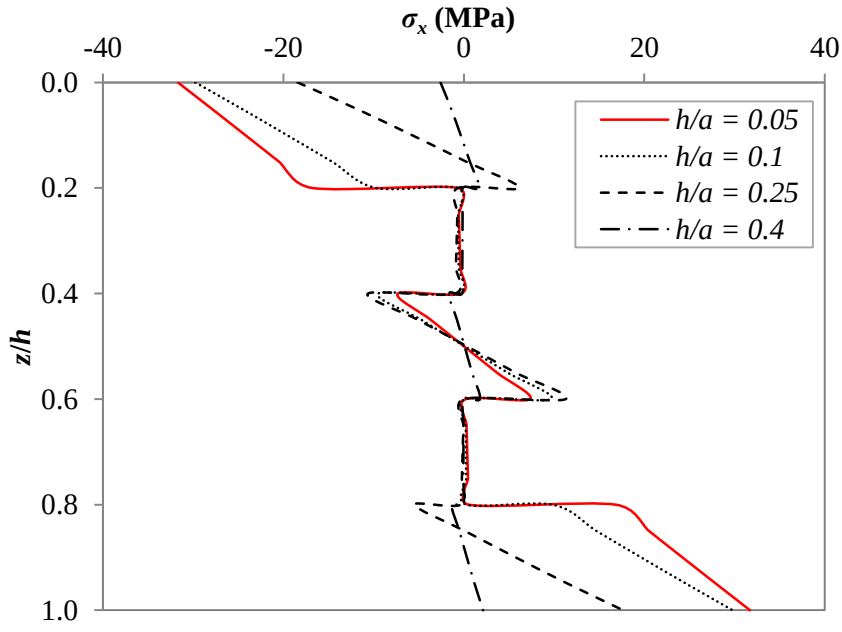

Figure 5-6 The in-plane stress σ_x by the SSA through the thickness for different h/a for Case Study 2 (note: data is provided in Appendix C-Table C.1).

As mentioned before, in order to demonstrate the capabilities of the SSA in this application, in the next section, the CLT panel will now be analysed using a variety of approaches including the SSA.

5.3 CLT panel detailed comparison with various analytical solutions

In this section, two case studies are explored analytically. The first one is three plies of CLT panel examined analytically by Sturzenbecher and Hofstetter (2011), and the second one is five plies of CLT panel examined analytically by Sturzenbecher *et al.* (2010).

5.3.1 Case Study 3: 3-ply CLT panel

The focused-on panel has the same geometry as that examined analytically by Sturzenbecher and Hofstetter (2011). The panel or plate is symmetrical with three plies of alternate grain orientation, i.e. [0/90/0]°, as shown in Figure 5-7.

Each board or ply has a thickness of 30 mm so that the total plate thickness is 90 mm. The in-plane dimensions of the plate are $a = b = 360$ mm and h/a is equal to 0.25 as this is the thicker plate studied by Sturzenbecher and Hofstetter (2011). Here a is the length of the plate along the x-axis, b is the dimension of the plate along the y-axis and h is the total thickness of the plate (z-axis), as shown in Figure 5-7.

The set of elastic material parameters used for the timber plies is the same as per Sturzenbecher and Hofstetter (2011) and it is the same as Case 2. All the calculations are based on C24-grade timber as the constituent of the CLT boards, in accordance with BS EN 338.

The panel is simply supported on all sides, as per Sturzenbecher and Hofstetter (2011), and the load on the top surface of the panel is a sinusoidal load with a maximum magnitude of 1 MPa ($q(x,y) = q_0 \sin(\pi x/a) \sin(\pi y/b)$ where q_0= 1 MPa), as shown in Figure 5-7.

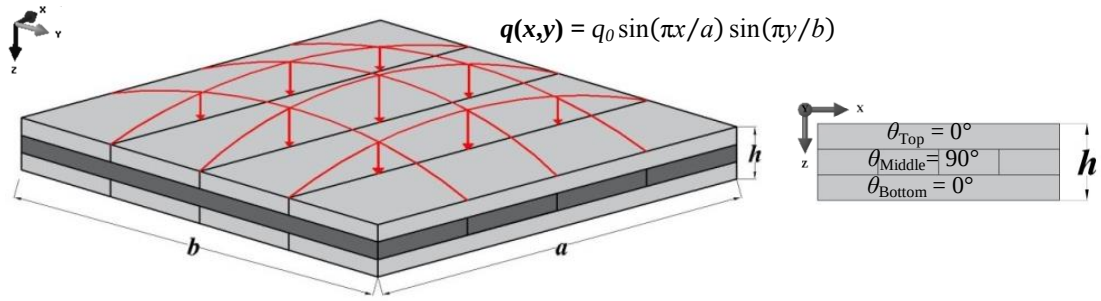

Figure 5-7 The geometry of the 3-ply CLT panel under sinusoidal load and the grain orientation angles through h.

Figure 5-8, Figure 5-9 and Table 5-3 show the theoretical results for the displacements and the stresses of the 3-ply CLT panel for the case of h/a = 0.25 using the SSA in comparison with results from Sturzenbecher and Hofstetter (2011), which utilised the previously mentioned 2D Ren approach and the 3D Pagano approach. It can be observed that the 3D Pagano approach results closely match that of the SSA; also, the 2D approach does not give good agreement with the SSA.

From the same figures and table, for the mid-plane ply, it is clear there are inconsistencies in the values of the inter-laminar stresses (τ_{xz} and τ_{yz}) between the SSA and the 2D approaches. The 2D results overestimated the values of τ_{xz} while they underestimated the value of τ_{yz}.

As can be noticed from Figure 5-9, the SSA and Pagano approaches match exactly through the thickness, although there is a difference between the SSA and the 2D approaches used by Sturzenbecher and Hofstetter (2011) with the distribution of out-of-plane τ_{xz} through the thickness of the CLT panel. The maximum value of τ_{xz} obtained using the 2D approaches occurs in the mid-plane. Using the SSA, the behaviour of the stress is continuous across layer interfaces and the maximum value for τ_{xz} is not in the mid-plane but in the interfaces of the mid-ply locally.

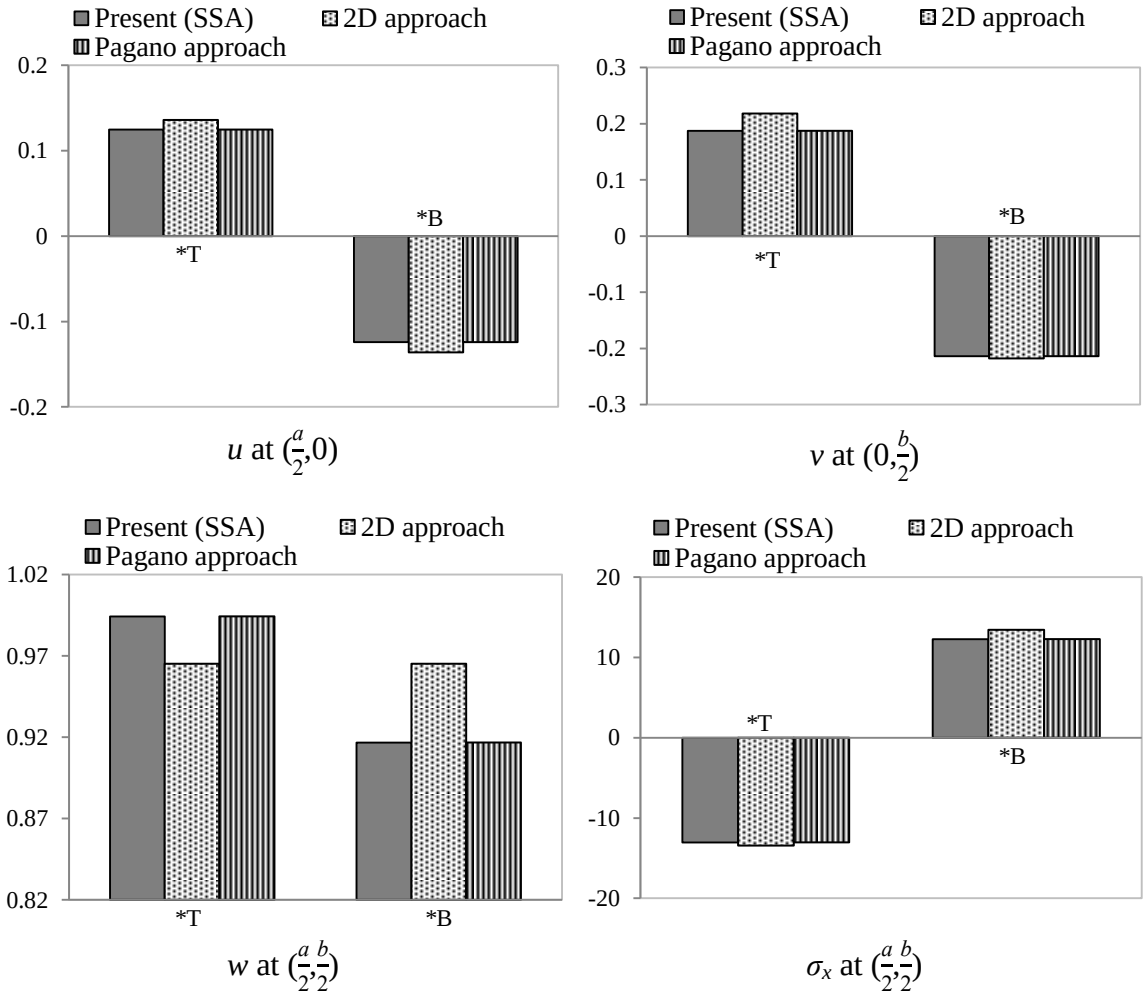

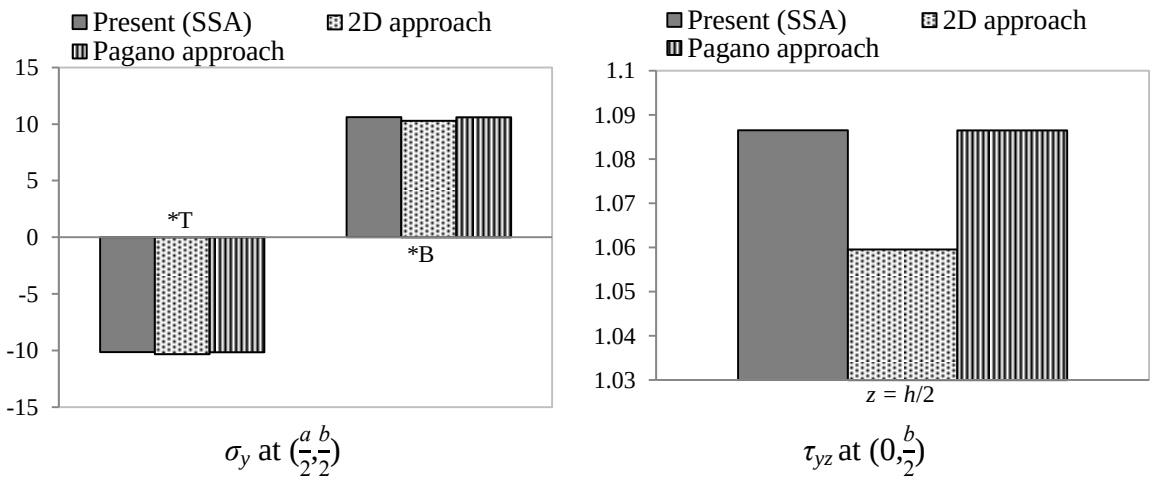

*Where T and B are the top and bottom of the panel through the thickness respectively.

Figure 5-8 Theoretical results for displacements (mm) and stress states (MPa) of the 3-ply CLT panel (h/a = 0.25).

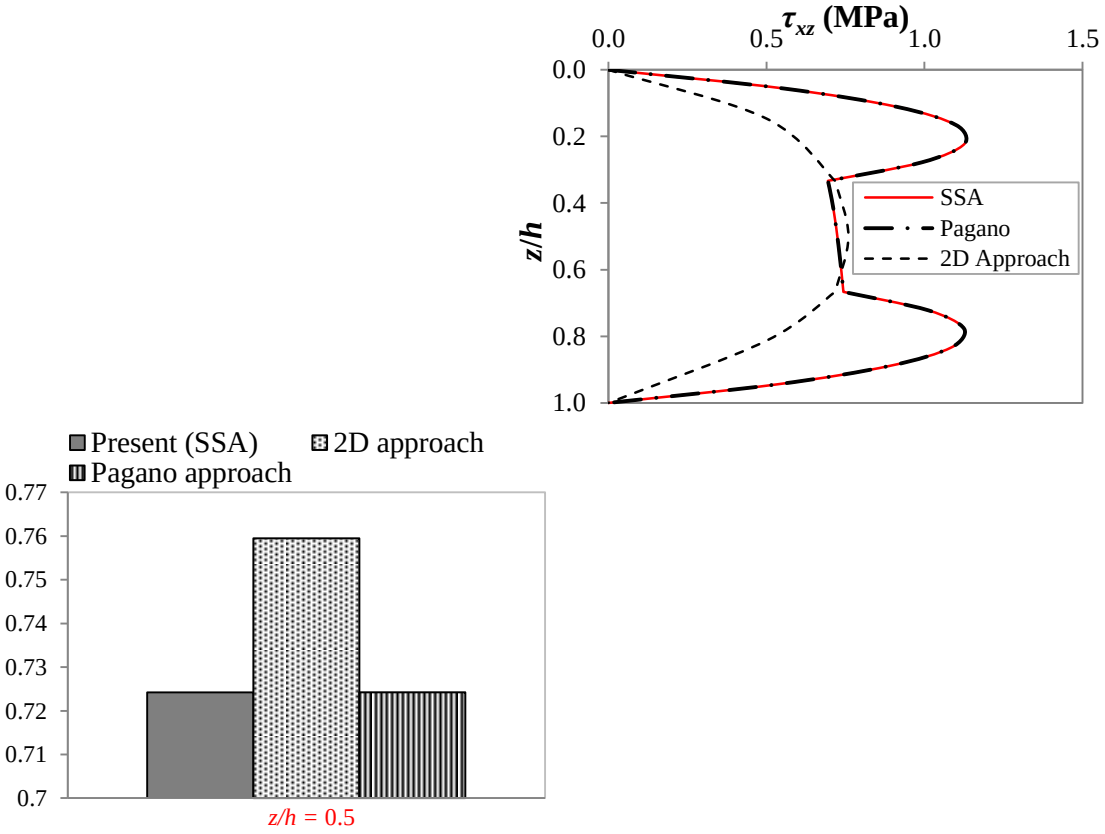

Figure 5-9 Out-of-plane shear stress τ_{xz} distribution through the thickness predicted by different plate approaches at z/h=0.5.

Table 5-3 Theoretical results for displacements (mm) and stress states (MPa) of the 3-ply CLT panel (h/a = 0.25).

	(x,y)	z	**SSA**	Pagano approach (Sturzenbecher and Hofstetter, 2011)	2D approach (Sturzenbecher and Hofstetter, 2011)
u	$(\frac{a}{2}, 0)$	*T	0.1246	0.1246	0.1360
		*B	-0.1240	-0.1240	-0.1360
v	$(0, \frac{b}{2})$	*T	0.1870	0.1870	0.2178
		*B	-0.2138	-0.2138	-0.2178
w	$(\frac{a}{2}, \frac{b}{2})$	*T	0.9943	0.9943	0.9652
		*B	0.9168	0.9168	0.9652
σ_x	$(\frac{a}{2}, \frac{b}{2})$	*T	-13.0319	-13.0320	-13.4500
		*B	12.2872	12.2870	13.4500
**σ_y	$(\frac{a}{2}, \frac{b}{2})$	*T	-10.1361	-10.1360	-10.2970
		*B	10.6190	10.6190	10.2970
τ_{xz}	$(\frac{a}{2},0)$	$h/2$	0.7242	0.7242	0.7595
τ_{yz}	$(0,\frac{b}{2})$	$h/2$	1.0865	1.0865	1.0596

* Where T and B are the top and bottom of the panel through the thickness respectively.
** The values of σ_y are the top and bottom of the 2nd layer (θ=90°).

Section 2.4.2 mentioned the limitations of the Sturzenbecher and Hofstetter (2011) analytical approach; in contrast, by using the SSA, σ_z is included in the solution. Also, there is no assumption for w and it can be calculated at any location through the thickness, as shown in Figure 5-10. From the same figure, also all the in- and out-of-plane stresses and displacements can be mapped by using the SSA. In most existing plate theories, the influence of the in-plane shear component is neglected (Sturzenbecher and Hofstetter, 2011) while the SSA can calculate τ_{xy} through the thickness of the plate, thus demonstrating the strength of the method. Furthermore, as can be noticed from the same figure, the stresses and the displacements are distributed through the thickness of the three plies of the CLT panel depending on ply orientation; it can also be observed that the distributions are non-linear through the thickness direction.

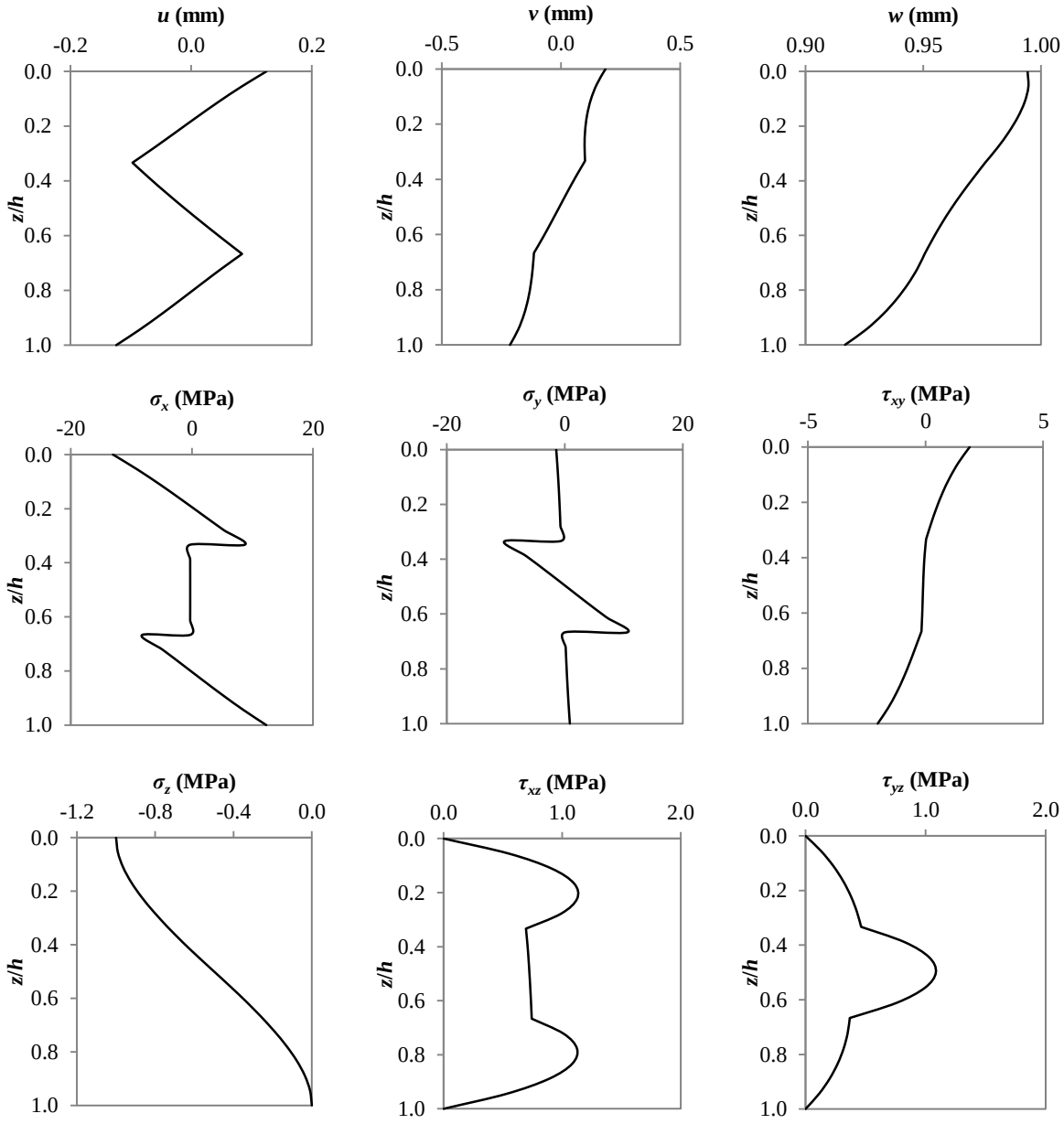

Figure 5-10 In- and out-of-plane displacements and stress states of the 3-ply CLT panel (h/a = 0.25) by the SSA.

5.3.1.1 Effect of thickness-to-width ratio (h/a) for Case Study 3

For CLT one of the most challenging issues is to obtain accurate results for thicker plates. By using the SSA, a key advantage of this approach can be utilised: its capability to provide an accurate solution for different thicknesses of the plate, as shown in Figure 5-11. This figure shows the effect of the thickness-to-width ratios (h/a) on the in-plane stresses σ_x. The behaviour of the stresses through the thickness is non-linear as h/a increases. Due to the assumptions of the 2D methods, there is always a limitation

relating to the maximum thickness of the plates to be analysed, saying h/a is less than 0.25 in Sturzenbecher and Hofstetter (2011). In contrast, the SSA can be applied to much thicker plates, which increases the range of CLT plates that can be studied.

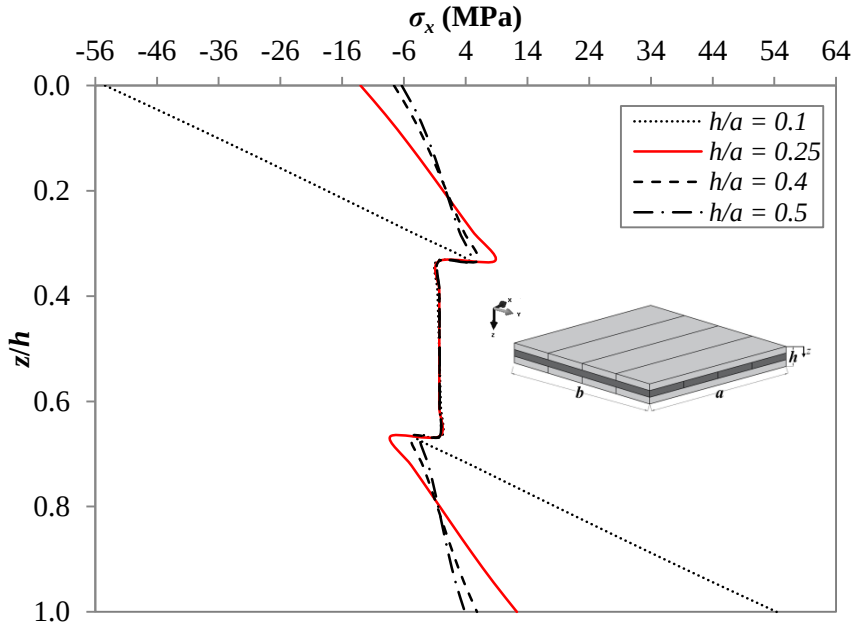

Figure 5-11 The effect of different h/a on the in-plane stress σ_x through the thickness of the 3-ply CLT panel.

After the 3-ply CLT panel has been studied analytically, the thicker plate with five plies will be explored in the next section.

5.3.2 Case study 4: 5-ply CLT panel

For this case study, the panel has the same geometry as that examined analytically by Sturzenbecher *et al*. (2010). The panel is symmetrical with five plies with the same set of elastic material parameters used for the timber plies as per section 5.2.2.

The panel is simply supported on all sides, as per Sturzenbecher *et al*. (2010), and the load on the top surface of the panel is a sinusoidal load with a maximum magnitude of 0.5 MPa ($q(x,y) = q_0 \sin(\pi x/a) \sin(\pi y/b)$ where q_0= 0.5 MPa), as shown in Figure 5-12. Each ply has a thickness of 30 mm, so the total plate thickness is 150 mm. The in-plane dimensions of the plate are $a = b$ =1500 mm and h/a is equal to 0.1.

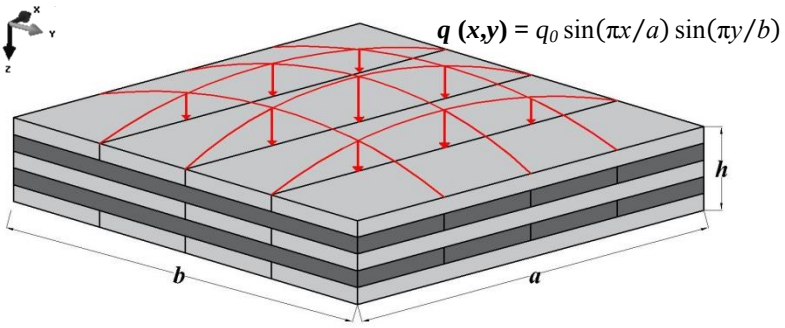

Figure 5-12 The geometry of the 5-ply CLT panel under sinusoidal load.

In Figure 5-13, the SSA is compared with CLPT and Pagano solutions for the in-plane and out-of-plane displacement (u and w). For both scenarios, the SSA gives a perfect agreement with the Pagano results. CLPT gives a linear distribution through the thickness, as shown in Figure 5-13(a). From Figure 5-13(b), it can be seen that, while the SSA and Pagano results have a good agreement, there is a large difference to the CLPT results, thus highlighting the limitations of the CLPT method.

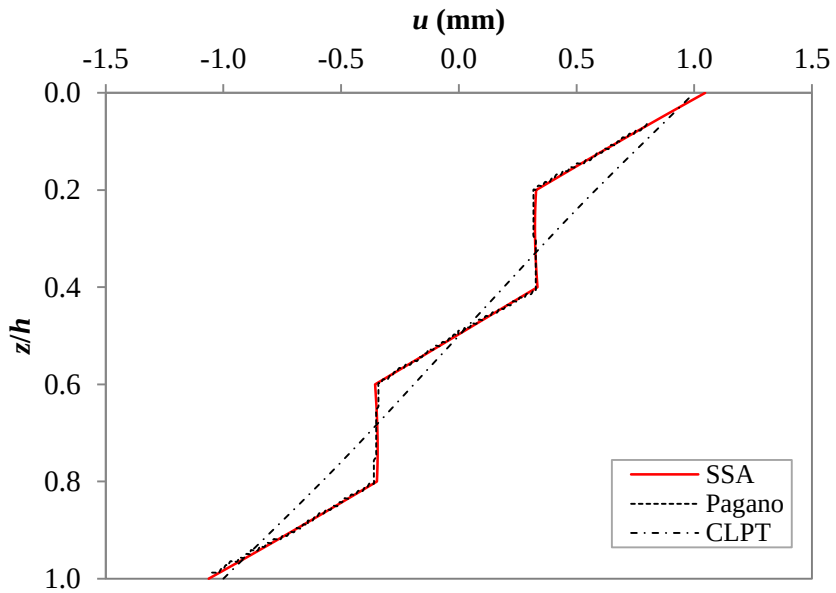

(a)

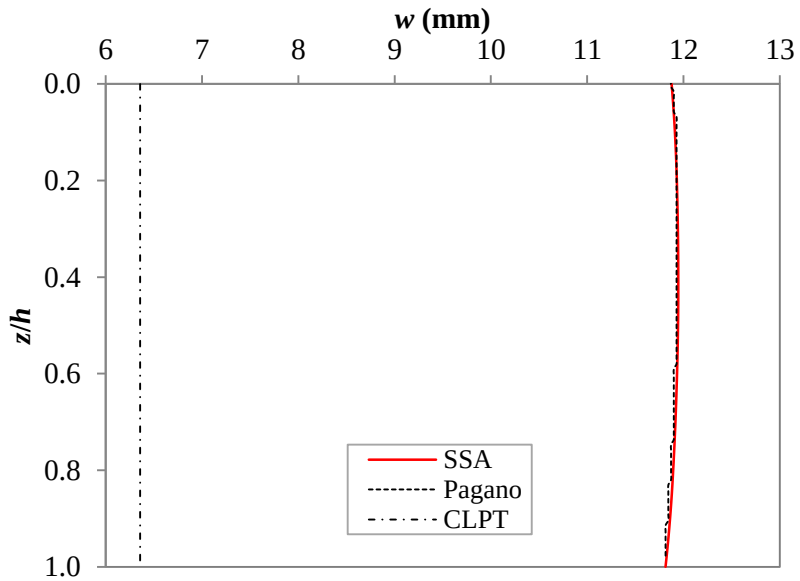

(b)

Figure 5-13 Displacement distribution through the thickness of the 5-ply CLT panel for (a) in-plane *u* and (b) out-of-plane *w* displacements.

In this case study, *h*/*a* is equal to 0.1. Thus, the plate is considered as a thin CLT panel. As the CLT becomes thicker (*h*/*a* = 0.5), the SSA is capable of accurately capturing all the elastic stresses and the displacement through the thickness, as shown in Figure 5-14.

From the same figure, the differences between the transverse shear stresses (τ_{xz} and τ_{yz}) for both CLT panel cases (thin and thick) are shown. For τ_{xz}, the thin plate shows that the maximum value will be in the middle of the third ply (0° ply), and the distribution through the other plies will be more linear. On the other hand, for the thicker plate, the non-linear behaviour and the distribution are shown through the thickness of the CLT panel and the maximum values are at the middle of each 0° ply (1st, 3rd and 5th ply). For τ_{yz}, as the maximum value shown for the thinner plate is at the middle of the 3rd ply when the plate becomes thicker, the non-linear behaviour becomes more obvious, and the maximum values are at the middle of the 2nd and 4th plies (90° plies).

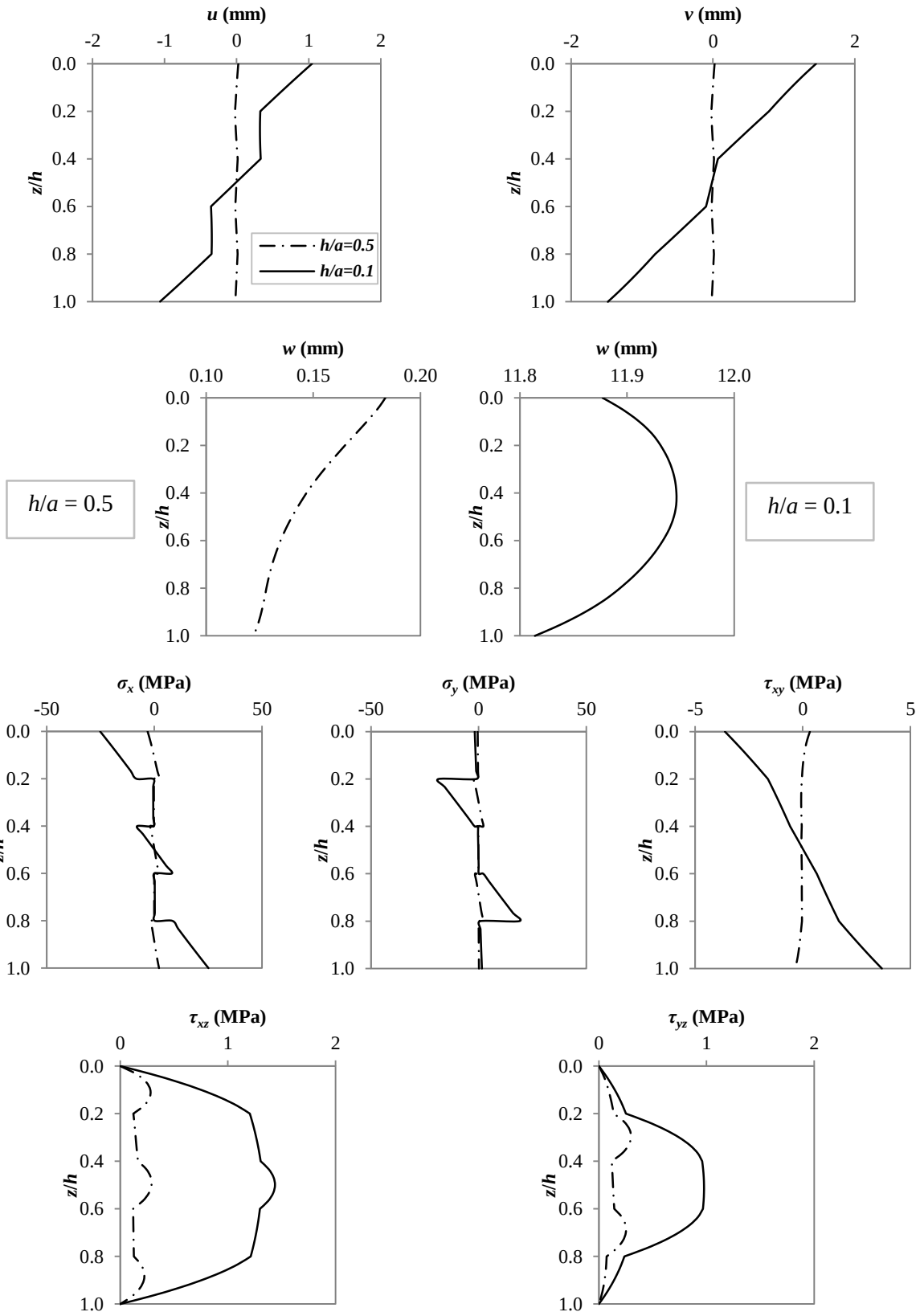

Figure 5-14 In- and out-of-plane displacements and stress states of the 5-ply CLT panel (h/a = 0.1 and 0.5) by the SSA.

In addition to the SSA method and other analytical solutions previously discussed, a simulation of the CLT panel using the commercially available finite element program ABAQUS will be presented.

5.4 FEM model of the CLT panel

In this section, three different case studies will be explored by using ABAQUS. The first two studies are three plies of CLT panel under different types of load. For the last study, the FEM model developed will be extended to a 5-ply beam of CLT under different boundary conditions and further checked against the corresponding experimental work by O'Dowd *et al*. (2016). Details are shown as follows.

5.4.1 Case Study 1: 3-ply CLT panel FEM model under sinusoidal load

To describe the bond connection between different plies, ABAQUS provides more than one approach for defining layer contact. Three modelling approaches will be explored under sinusoidal load. The first model in ABAQUS will be the composite Layup model. The second method is to define the contacted layers as a cohesive element and the last method is to define the connection as an interaction contact layer. Before applying these approaches for the analysis of the panel, mesh sensitivity, element types and simply supported boundary condition options will be explored.

In this section, the focused-on models have the same geometry (as shown in Figure 5-15), elastic material parameters, boundary condition and the types of load as that examined analytically by Sturzenbecher and Hofstetter (2011) and described in section 5.3.1.

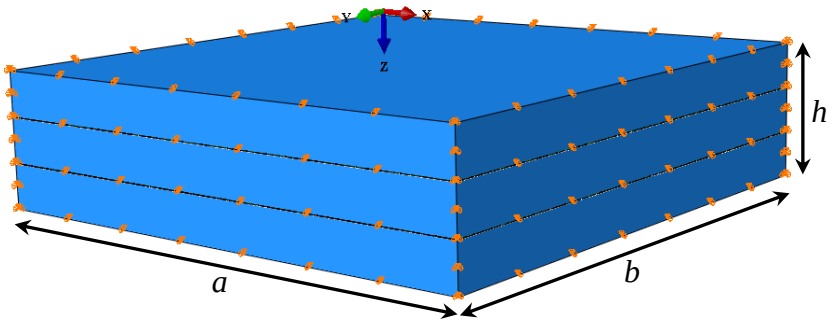

Figure 5-15 The geometry of the FEM model of a 3-ply CLT panel.

5.4.1.1 Mesh sensitivity study for Case Study 1

A mesh sensitivity study was undertaken to check which mesh size would be most appropriate for the analysis. Four mesh sizes were investigated comprising of equal-sided elements with dimensions of 3, 6, 12 and 24 mm. As shown in Figure 5-16, when the mesh density increases, the values of the in-plane stress σ_x with respect to the theoretical solution (derived from the SSA) will be more accurate. Although the 3 and 6 mm mesh sizes are giving close results to each other, and running the FEM model is time-consuming, as shown in Table 5-4, the 6 mm mesh size will be used in the current FEM analysis.

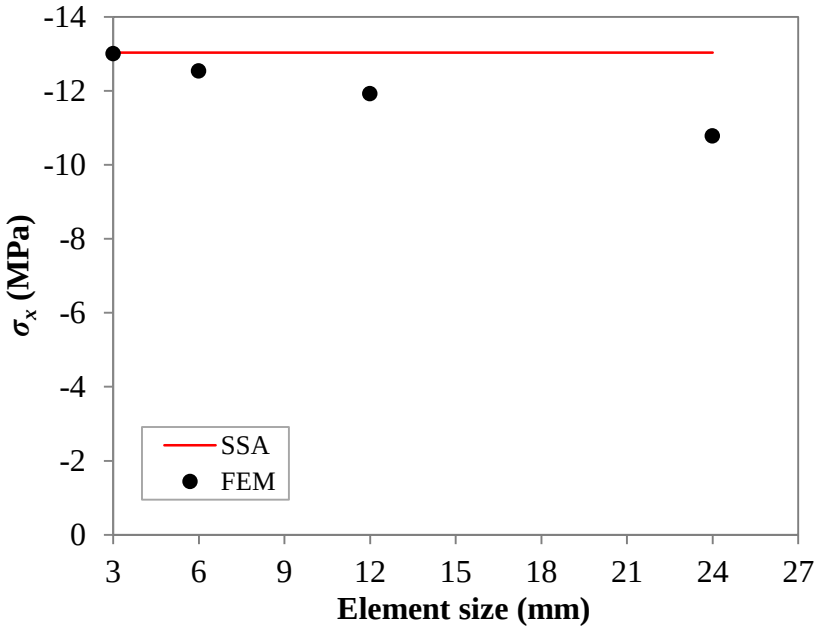

Figure 5-16 Different mesh size results of a single-ply plate for σ_x at z = 0.0 for h/a = 0.25.

Table 5-4 FEM models' running time for different mesh sizes for Case Study 1.

	Mesh 1 24 mm	Mesh 2 12 mm	Mesh 3 6 mm	Mesh 4 3 mm
Running time (s)	54	241	1332	11880

5.4.1.2 Choice of element types for Case Study 1

As outlined in Figure 5-17 and Table 5-5, two different solid elements have been studied (3D 8-node linear brick element (C3D8) and 3D 20-node linear brick element (C3D20)) (ABAQUS, 2013) and the results from these have been compared with the analytical results. Solid elements were used in this study instead of shell elements because of the former's ability to map all the displacements and stresses through the thickness of the plate. The most suitable solid element in terms of accuracy in comparison with the analytical solution is C3D20. Accordingly, this was adopted in the numerical model.

5.4.1.3 Boundary condition (BC) sensitivity for Case Study 1

The boundary conditions occupied a very important role in obtaining accurate FEM results. For simply supported edges, the ABAQUS program gives options to determine the BC. Figure 5-17 and Table 5-5 show two different options to create simply supported edges, as has been mentioned before, in section 4.4.3.4.

From Figure 5-17 and Table 5-5, the values of the displacements and the stresses are nearly the same as the SSA solution for the second boundary condition, BC2.

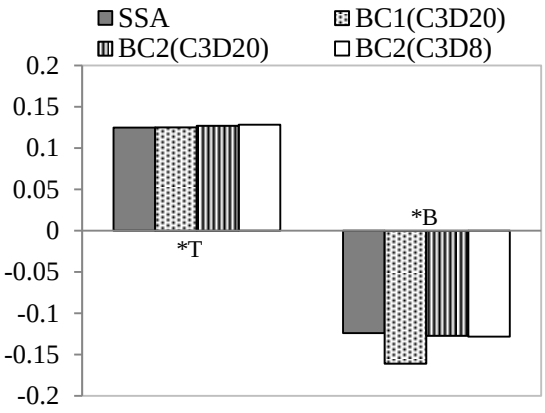

u at $(0,\frac{b}{2})$

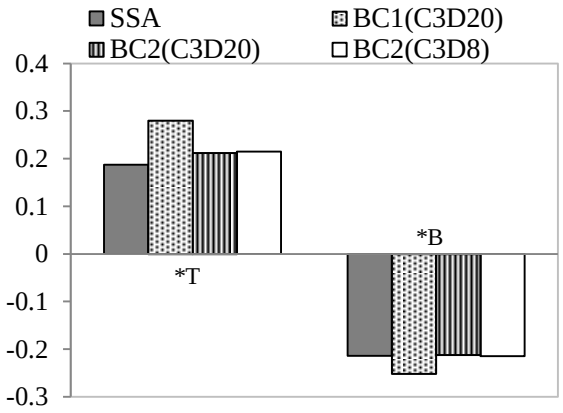

v at $(\frac{a}{2},0)$

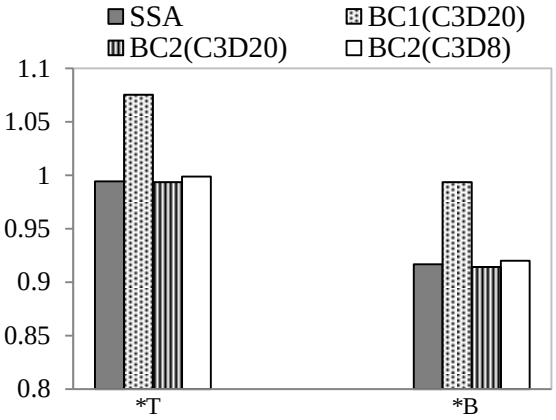

w at $(\frac{a}{2},\frac{b}{2})$

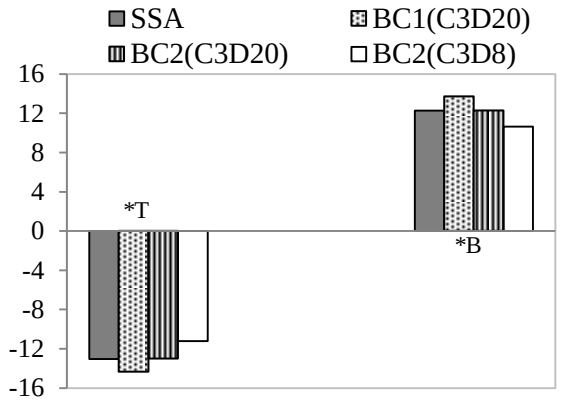

σ_x at $(\frac{a}{2},\frac{b}{2})$

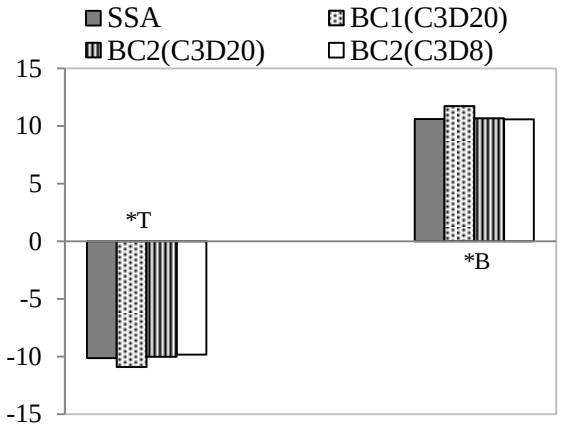

σ_y at $(\frac{a}{2},\frac{b}{2})$

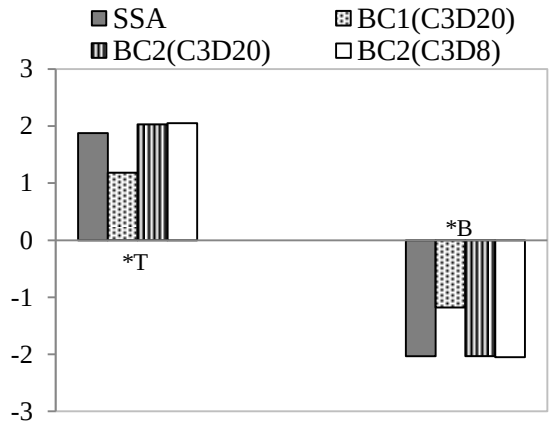

τ_{xy} at (0,0)

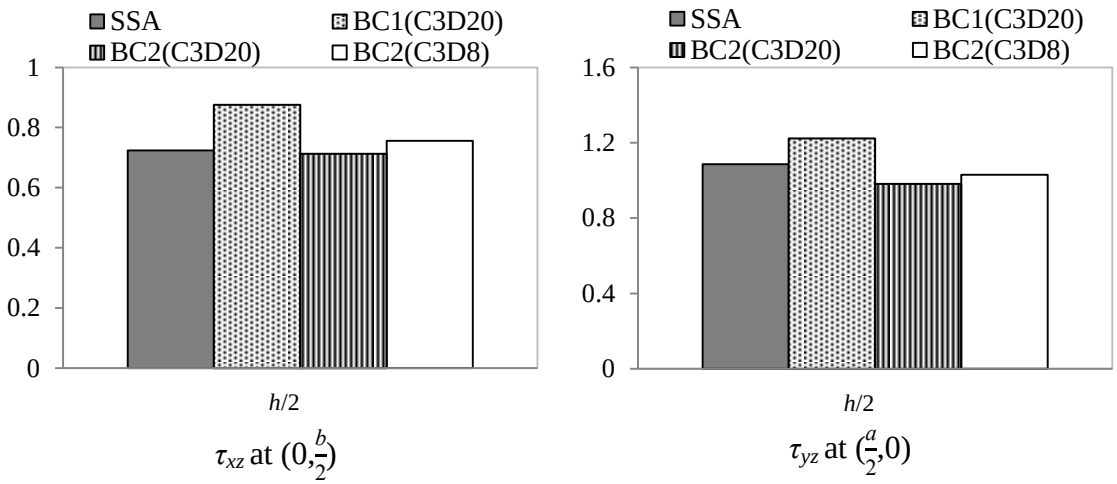

* Where T and B are the top and bottom of the panel through the thickness respectively.

Figure 5-17 SSA with FEM results on the displacements (mm) and stress states (MPa) of the 3-ply CLT panel for different element types and BCs (h/a = 0.25).

Table 5-5 The effect of the element type and BC sensitivity on the displacements (mm) and stresses (MPa) of 3-ply CLT panel (h/a = 0.25).

				FEM		
	(*x*,*y*)	***z***	**SSA**	**BC 1 (C3D20)**	**BC 2 (C3D20)**	**BC 2 (C3D8)**
u	$(\frac{a}{2},0)$	*T	0.1246	0.1251	0.1272	0.1283
		*B	-0.1240	-0.1607	-0.1272	-0.1283
v	$(0,\frac{b}{2})$	*T	0.1870	0.2801	0.2121	0.2148
		*B	-0.2138	-0.2520	-0.2121	-0.2148
w	$(\frac{a}{2},\frac{b}{2})$	*T	0.9943	1.0753	0.9936	0.9988
		*B	0.9168	0.9935	0.9143	0.9200
σ_x	$(\frac{a}{2},\frac{b}{2})$	*T	-13.0319	-14.3495	-13.0035	-11.2076
		*B	12.2872	13.7223	12.2756	10.6314
**σ_y	$(\frac{a}{2},\frac{b}{2})$	*T	-10.1361	-10.9284	-10.0436	-9.8312
		*B	10.6190	11.7134	10.6640	10.5847
τ_{xy}	**(0,0)**	*T	1.8764	1.1808	2.0314	2.0499
		*B	-2.0339	-1.1809	-2.0314	-2.0499
τ_{xz}	$(\frac{a}{2},0)$	*h*/2	0.7242	0.8756	0.7127	0.7553
τ_{yz}	$(0,\frac{b}{2})$	*h*/2	1.0865	1.2238	0.9827	1.0294

* Where T and B are the top and bottom of the panel through the thickness respectively.
** The values of σ_y are the top and bottom of the 2nd layer (θ=90°).

For detailed in-plane stress distribution σ_x through the thickness, Figure 5-18 shows σ_x for the two boundary conditions and accordingly with the results of the SSA. From this figure, both boundary condition options give a good distribution through the thickness when compared to the SSA, but BC2 is closer to the SSA distribution than BC1.

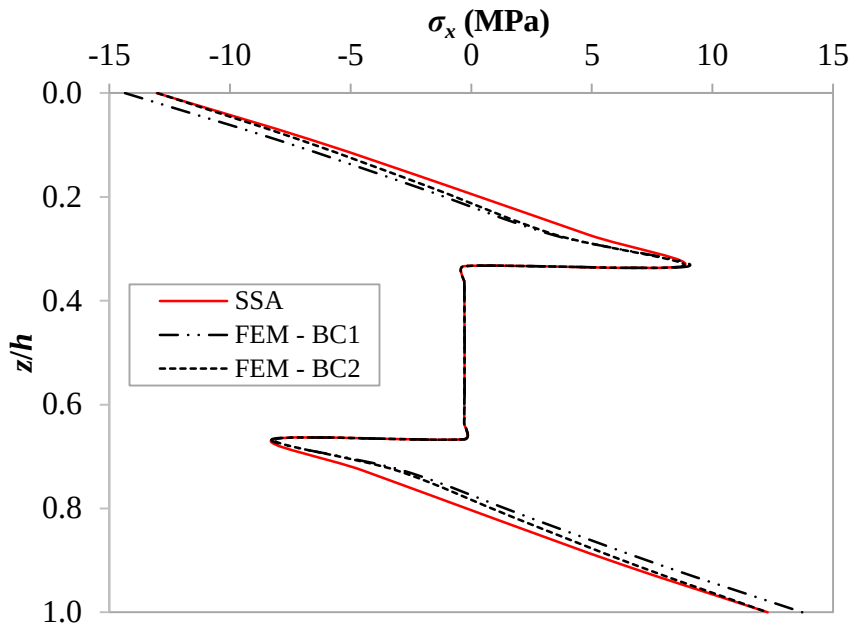

Figure 5-18 The effect of BC on the 3-ply CLT in-plane σ_x through the thickness of h/a = 0.25 (note: data is provided in Appendix C-Table C.2).

After choosing the optimum mesh size, element types and the suitable boundary condition for the simply supported CLT panel, three different options for interfacial connection to simulate the CLT panel will be presented in the following subsections.

5.4.1.4 Model 1: 3-ply CLT panel using the fully bonded model

In this model, as shown in Figure 5-19, the fully bonded model (Composite Layup) is chosen in ABAQUS to simulate three plies perfectly bonded in the CLT panel.

The fully bonded model (Composite Layup) in ABAQUS is designed to simulate a various number of plies in one composite model with perfect bonding between the different plies. By using this option in ABAQUS, the number of plies, the region of

each ply with the material properties and the fibre orientation angle should be specified (ABAQUS, 2013).

To obtain an accurate result, for CLT, the fibre orientation angle for each ply should be specified in a very accurate way and, for the case of CLT, should follow the sequence 0°, 90°, 0°, as shown in Figure 5-19. Also, the orientation angle should follow the reference orientation of the ply.

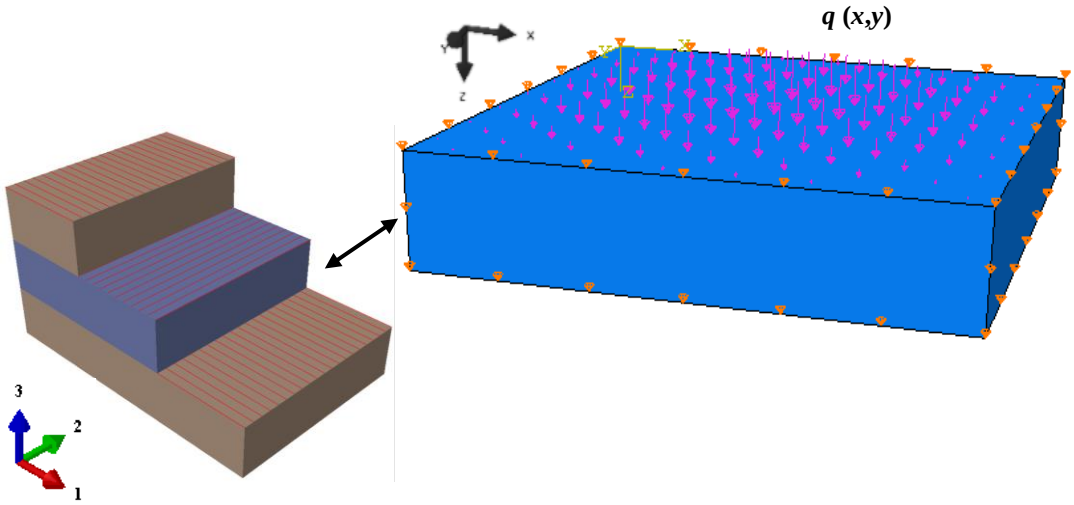

Figure 5-19 The FEM model for the 3-ply CLT panel under sinusoidal load and the grain orientation angles for each ply.

5.4.1.5 Model 2: 3-ply CLT panel using the cohesive element

In this model, the CLT plies will be modelled as separate plies and bonded by using cohesive elements such as glue or ties; this is defined as a mesh layer, as shown in Figure 5-20. The cohesive element is used to model adhesives between two components and to bind different interfaces although they do not have any degree of freedom other than that for displacement (ABAQUS, 2013).

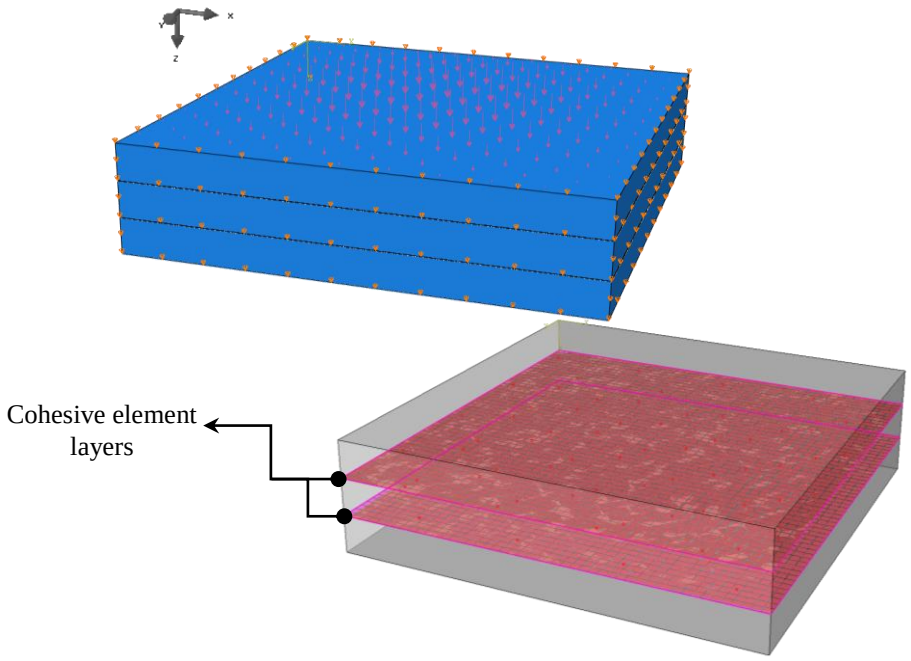

Figure 5-20 The FEM model for the 3-ply CLT panel with the cohesive element layers between the CLT plies.

In ABAQUS, three types of cohesive element are available, these being the elements for two-dimensional, three-dimensional and axisymmetric analyses (ABAQUS, 2013). In this model, the cohesive element to be used is an 8-node three-dimensional cohesive element (COH3D8).

In general, one of the most important factors in using this model is to define the cohesive element material property. Currently, the material property for the cohesive element is set as linear elastic traction. The elastic behaviour in ABAQUS is related to the nominal traction stress t and the strain of the cohesive element layer (the interface), as shown in equation (5-1). The nominal traction stress vector t consists of three components for a three-dimensional model, t_n, t_s and t_t, which represent the normal along the local 3-directions and two shear tractions along 1- and 2-directions.

$$\begin{Bmatrix} t_n \\ t_s \\ t_t \end{Bmatrix} = \begin{bmatrix} K_{nn} & K_{ns} & K_{nt} \\ K_{sn} & K_{ss} & K_{st} \\ K_{nt} & K_{ts} & K_{tt} \end{bmatrix} \begin{Bmatrix} \varepsilon_n \\ \varepsilon_s \\ \varepsilon_t \end{Bmatrix} \quad (5\text{-}1)$$

The elastic matrix [*K*] provides fully coupled behaviour between the normal and shear components. Note that, if the uncoupled behaviour exists, then the off-diagonal in the matrix will be equal to zero.

After defining the material properties of the cohesive element between the plies, the cohesive element itself will be defined as a mesh layer between the CLT plies and, for that, a section assigned to this element with the cohesive element's material property is assigned to this mesh element. Then, it is necessary to bond the different CLT plies by using tie constraints in ABAQUS. By this constraint, ABAQUS gives an option to choose one of the different surfaces to be the master and the other to be the slave and, by this tie (constraint), the plies will be tied together. In this model, as three plies of CLT plies are tied together, then two constraints are used.

5.4.1.6 Model 3: 3-ply CLT panel using contact interactions

In this model, the same procedure as used in the previous model is used to define different plies and define the bonding (glue) layer between the CLT plies. The difficulty in this model is how to define the contact interaction between the different plies, as shown in Figure 5-21.

As per the previous model, the cohesive element is a mesh element layer between the CLT plies with special properties (as the glue-type properties). However, for this model, the contact interactions between the CLT plies are directly applied and the material properties of the interaction can be defined and there is no need to create a section for the cohesive layer as in the previous case.

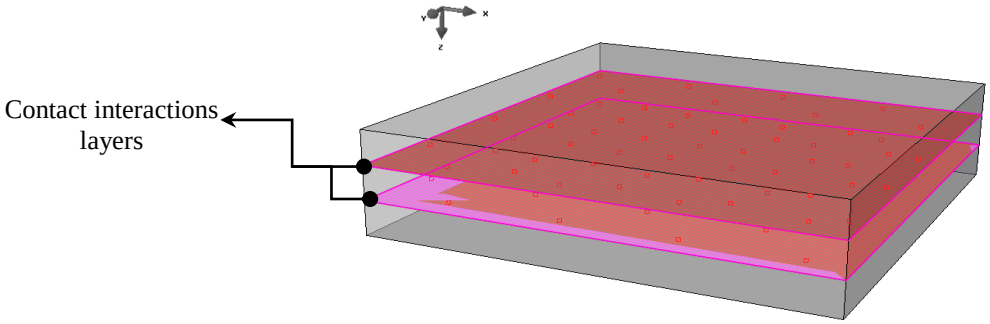

Figure 5-21 The FEM model for the 3-ply CLT panel with the contact interactions layers between the CLT plies.

5.4.1.7 Comparison of results between the different types of 3-ply CLT models

For the three models, the same mesh size and element types are used. In Figure 5-22 and Figure 5-4, the comparison between the three models with the SSA is shown. To recap, the first model (Model 1) is CLT with fully bonded model, the second one (Model 2) is CLT with the cohesive element and the final one (Model 3) is CLT with contact interactions. From this table, it is clear that models 2 and 3 give the same results except for the transverse normal shear stresses although they are very close to each other. Thus, Model 2 is more accurate than Model 1 in comparison with the SSA.

The SSA model adopts full connectivity between plies. It would, therefore, be expected that the full connectivity assumption of Model 1 would provide a closer match with the SSA model (taking SSA to be the benchmark based on its previously discussed favourable comparisons with Pagano, etc.). The fact that there is a notable difference demonstrates some of the shortcomings of the FEM in capturing the full behaviour of the plate; these are not solely attributed to the bond assumptions.

From the three displacements, the results show that, for Model 1, since full bond is assumed between the plies, the structure will be stiffer and the displacement will be less than the actual value. On the other hand, in Model 2, when the cohesive element is

used, the predicted behaviour of the CLT is theoretically more precise, especially for the transverse shear stresses τ_{xz} and τ_{yz}.

For the reasons mentioned above, Model 2 with cohesive elements between the CLT plies will be adopted for the following case study.

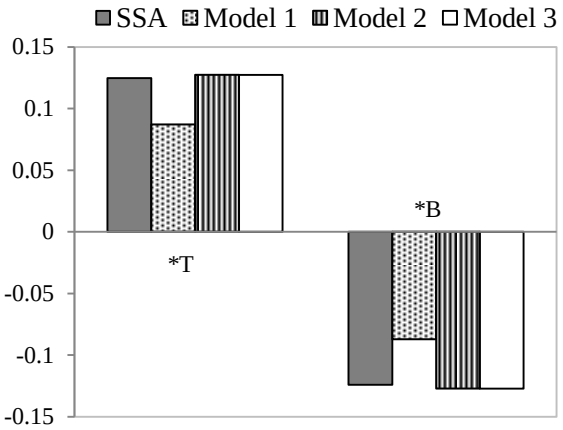

u at $(0,\frac{b}{2})$

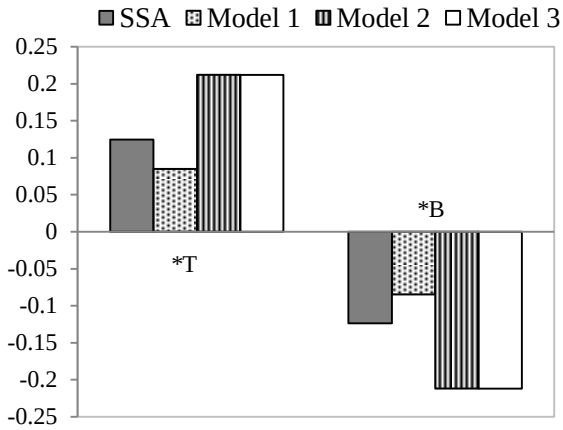

v at $(\frac{a}{2},0)$

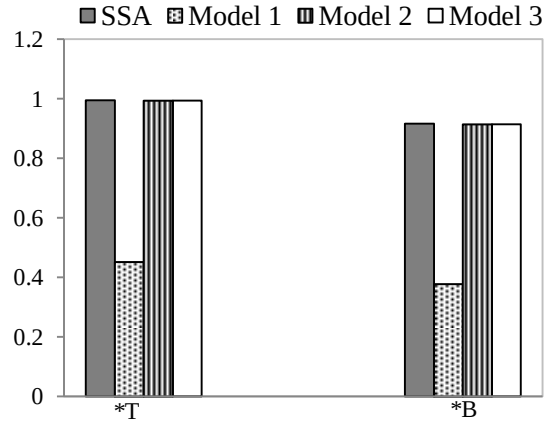

w at $(\frac{a}{2},\frac{b}{2})$

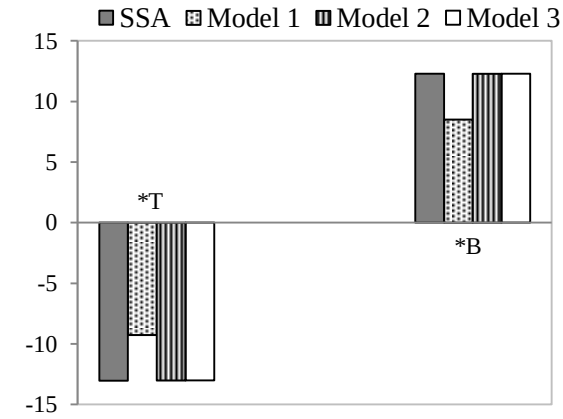

σ_x at $(\frac{a}{2},\frac{b}{2})$

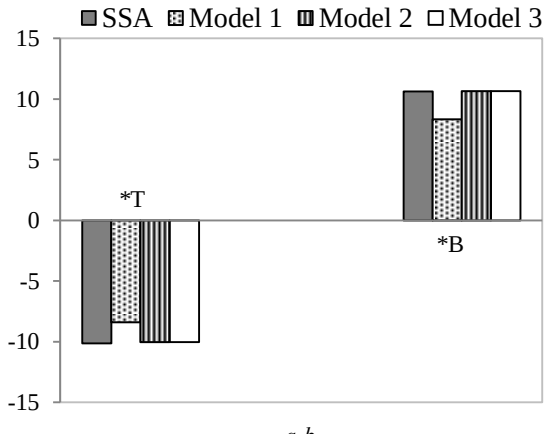

σ_y at $(\frac{a}{2},\frac{b}{2})$

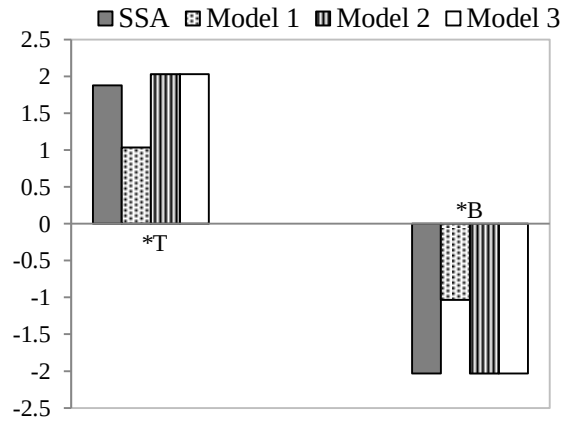

τ_{xy} at (0,0)

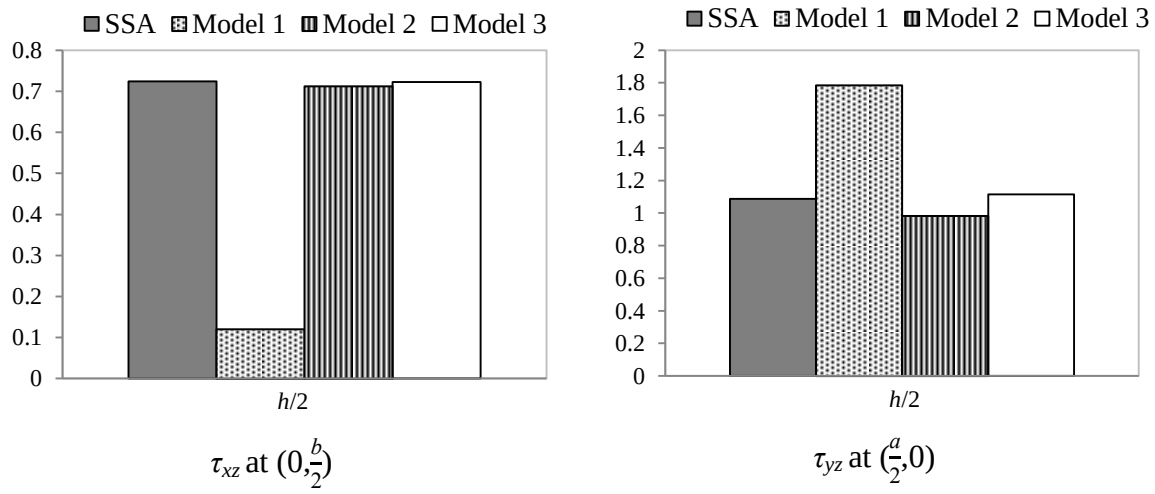

Figure 5-22 SSA with FEM results for different FEM model approaches for displacements (mm) and stress states (MPa) of the 3-ply CLT panel (h/a = 0.25).

Table 5-6 Different types of FEM model and SSA results for displacements (mm) and stress states (MPa) of the 3-ply CLT panel (h/a = 0.25; where a = 360 mm).

	(x,y)	z	**SSA**	***FEM		
				Model 1	**Model 2**	**Model 3**
u	$(\frac{a}{2},0)$	*T	0.1246	0.0871	0.1272	0.1272
		*B	-0.1240	-0.0871	-0.1272	-0.1272
v	$(0,\frac{b}{2})$	*T	0.1870	0.0848	0.2121	0.2120
		*B	-0.2138	-0.0848	-0.2121	-0.2121
w	$(\frac{a}{2},\frac{b}{2})$	*T	0.9943	0.4523	0.9936	0.9936
		*B	0.9168	0.3772	0.9143	0.9143
σ_x	$(\frac{a}{2},\frac{b}{2})$	*T	-13.0319	-9.2528	-13.0035	-13.0035
		*B	12.2872	8.5113	12.2756	12.2756
**σ_y	$(\frac{a}{2},\frac{b}{2})$	*T	-10.1361	-8.3951	-10.0436	-10.0436
		*B	10.6190	8.3277	10.6640	10.6640
τ_{xy}	$(0,0)$	*T	1.8764	1.0335	2.0314	2.0312
		*B	-2.0339	-1.0335	-2.0314	-2.0311
τ_{xz}	$(\frac{a}{2},0)$	$h/2$	0.7242	0.1208	0.7127	0.7223
τ_{yz}	$(0,\frac{b}{2})$	$h/2$	1.0865	1.7858	0.9827	1.1138

* Where T and B are the top and bottom of the panel through the thickness respectively.
** The values of σ_y are the top and bottom of the 2nd layer (θ=90°).
***All the FEM models are 3D 20-node linear brick element (C3D20) with mesh size 6 mm.

After all the sensitivity studies for the mesh size, element type and boundary condition have been explored, the 3D solid element (C3D20) with the cohesive element (COH3D8) with the finer mesh size is chosen. Figure 5-23 shows the comparison between the distribution of the in- and out-of-plane displacements along the *x* and *y*-axes for the SSA and FEM results at the top of the CLT panel. As can be observed from Figure 5-23, a good agreement is obtained.

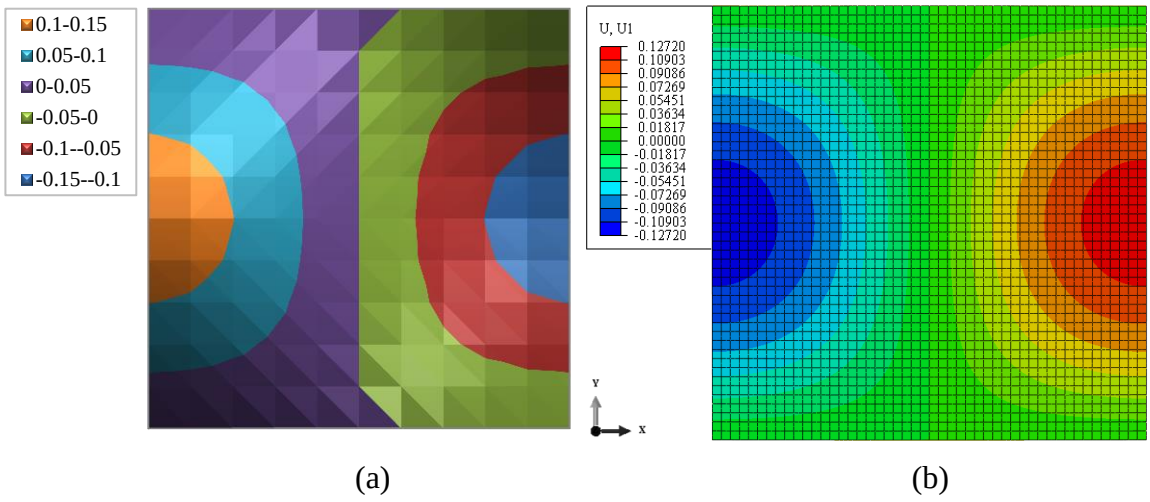

(a) (b)

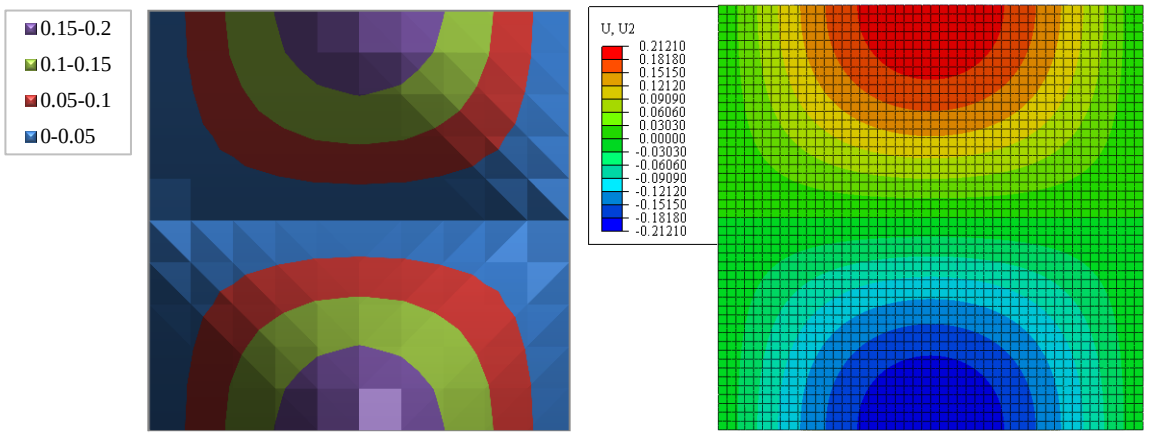

(c) (d)

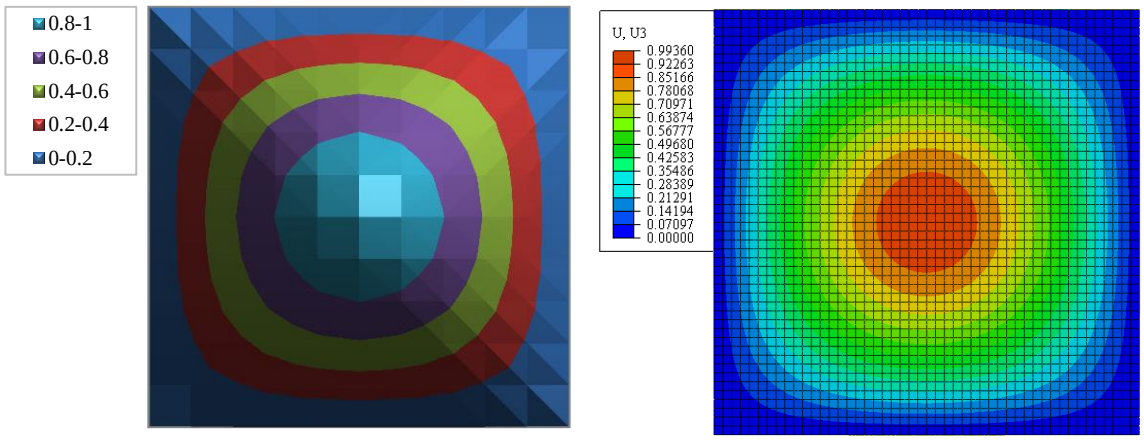

(e) (f)

Figure 5-23 The distribution along *x* and *y* of the in- and out-of-plane displacements for *h*/*a* = 0.25 at *z*=0. (a), (c) and (e) are the SSA values and (b), (d) and (f) are the FEM results for *u*, *v* and *w* (mm), respectively.

5.4.2 Case Study 2: 3-ply CLT panel under uniformly distributed load

In this section, the same number of plies and material properties of the 3-ply CLT panel are used as in Model 2 (section 5.4.1.5) with different types of load. A uniformly distributed load is used at the top of the plate (as shown in Figure 5-24) to show the effect of the number of Fourier series terms (*m* and *n*) on the SSA solution. As mentioned before, increasing the number of terms is one of the challenging points in using SSA. In the SSA models presented here, the *m* and *n* are chosen after load distribution sensitivity was studied, as shown in Figure 5-25. The high number of terms of the analytical solution is used for more accurate results.

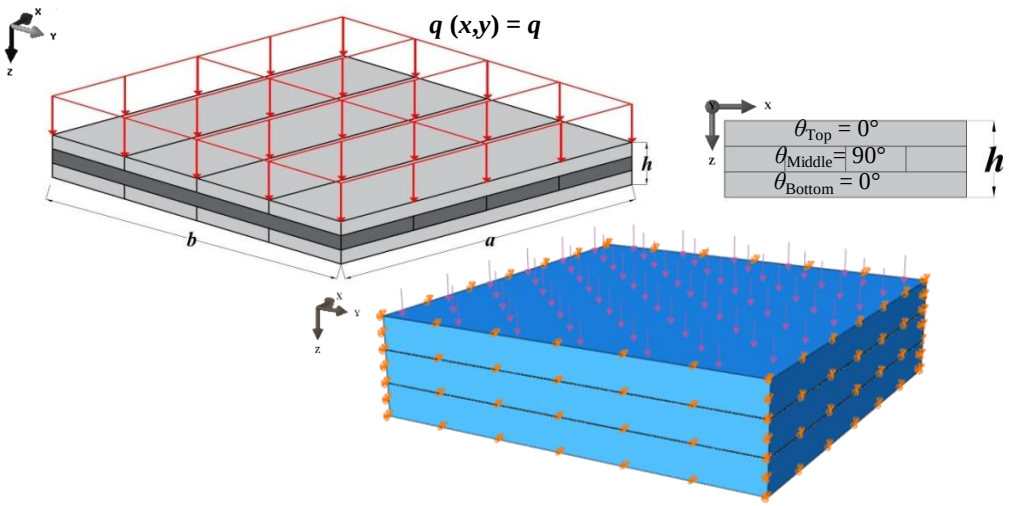

Figure 5-24 The geometry of the 3-ply CLT panel under uniformly distributed load and the grain orientation angles through *h* with the FEM model.

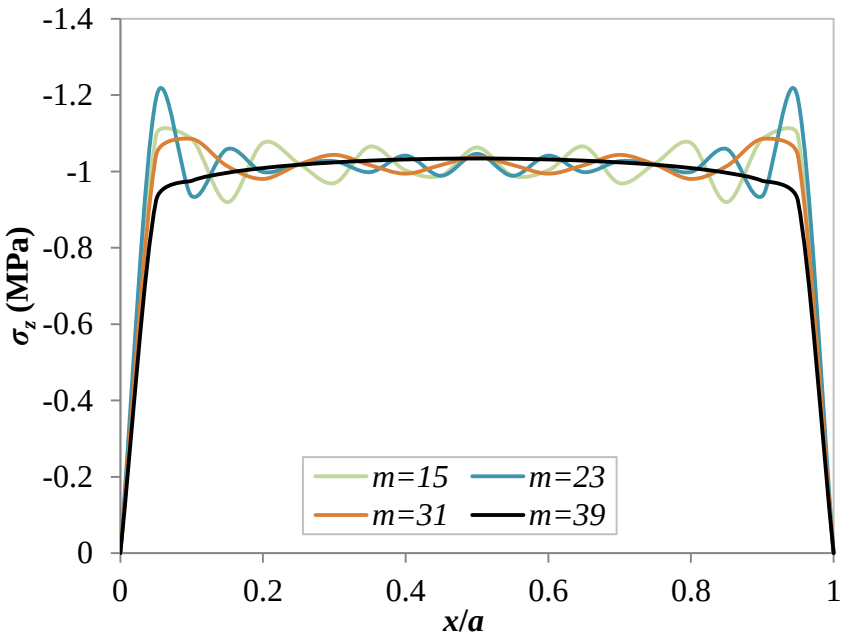

Figure 5-25 The load at the top ply (z=0) distribution along x/a for Case Study 2.

Table 5-7 shows the comparison between the SSA and the FEM results for all the displacements and the stress states for different locations. It can be clearly noticed that the FEM gives good agreement with the SSA for the three plies of the CLT.

For more detailed results through the thickness, Figure 5-26 and Figure 5-27 show the in-plane stress σ_x and the inter-laminar shear stresses τ_{xz} and τ_{yz} obtained from the SSA and the FEM through the thickness of the 3-ply CLT panel.

From the same table and from Figure 5-27, the FEM results show discontinuity of the inter-laminar stresses τ_{xz} and τ_{yz} at the interaction between the different plies (for example, in Table 5-7 and Figure 5-27 the bottom of the 1st ply for the SSA is equal to the top of the 2nd ply, but, for the FEM, it is not the case). As mentioned before, this is due to the fact that using solid elements in ABAQUS will lead to discontinuity of the transverse shear stresses at ply interfaces in the CLT as the transverse stresses are obtained from the displacement field not from the equilibrium equations (ABAQUS, 2013). Furthermore, the values of τ_{xz} should be equal to zero at the top and the bottom of

the plate, but for the FEM results they are not, and this has been mentioned before, in Chapter 4, section 4.4.4.

Table 5-7 In- and out-of-plane displacements (mm) and stress states (MPa) of the 3-ply CLT panel (h/a = 0.25) by SSA and FEM.

	(x,y)	# of the ply	z	SSA	**FEM		(x,y)	SSA	**FEM
u	$(\frac{a}{2},0)$	1st Ply	*T	0.2512	0.2167	v	$(0,\frac{b}{2})$	0.2954	0.3089
			*B	-0.1862	-0.2167			0.1811	0.1851
		2nd Ply	*T	-0.1862	-0.1543			0.1811	0.1851
			*B	0.1479	0.1543			-0.2025	-0.1851
		3rd Ply	*T	0.1479	0.1952			-0.2025	-0.1849
			*B	-0.2131	-0.1952			-0.3674	-0.3572
w	$(\frac{a}{2},\frac{b}{2})$	1st Ply	*T	1.9931	1.5113	σ_x	$(\frac{a}{2},\frac{b}{2})$	-18.2685	-18.0570
			*B	1.7317	1.5057			12.0051	12.0933
		2nd Ply	*T	1.7317	1.5065			-0.2387	-0.2352
			*B	1.6328	1.4721			-0.3774	-0.3708
		3rd Ply	*T	1.6328	1.4720			-11.8776	-11.6885
			*B	1.5621	1.4248			18.2443	18.1924
σ_y	$(\frac{a}{2},\frac{b}{2})$	1st Ply	*T	-1.8828	-1.8396	τ_{xy}	(0,0)	4.1017	4.3203
			*B	-0.7354	-0.7281			-0.2632	-0.2424
		2nd Ply	*T	-13.9692	-13.7273			-0.2632	-0.2424
			*B	14.7099	14.8148			-0.3209	-0.2919
		3rd Ply	*T	0.1310	0.1403			-0.3209	-0.2919
			*B	1.2603	1.2746			-3.6199	-3.6184
τ_{xz}	$(0,\frac{b}{2})$	1st Ply	*T	0.0000	-0.0604	τ_{yz}	$(\frac{a}{2},0)$	0.0000	0.0000
			*B	1.1439	1.2216			1.1590	1.1890
		2nd Ply	*T	1.1439	1.1490			1.1590	1.5002
			*B	1.2696	1.3339			0.6757	0.7091
		3rd Ply	*T	1.2696	1.3494			0.6757	0.6565
			*B	0.0000	0.0812			0.0000	0.0151

*Where T and B are the top and bottom of the panel through the thickness respectively.
**All the FEM models are 3D 20-node linear brick element (C3D20) with mesh size 6 mm.

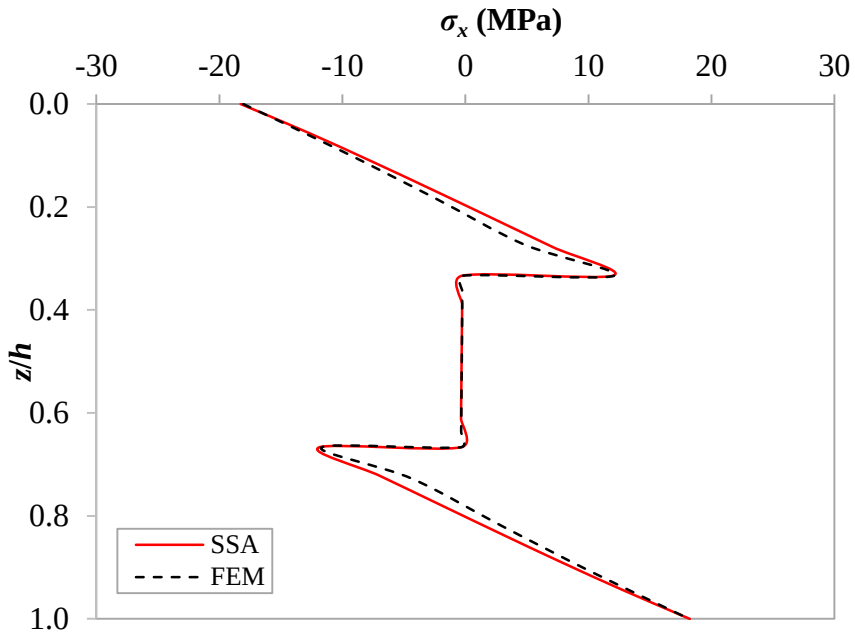

Figure 5-26 The SSA and FEM in-plane stress σ_x through the thickness of h/a = 0.25.

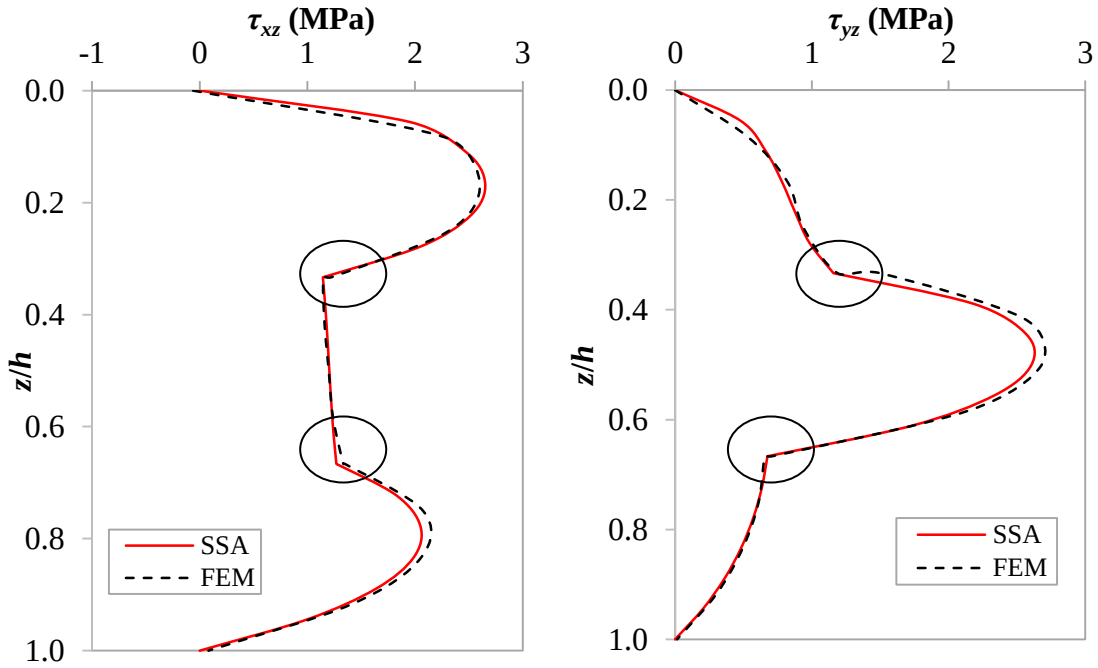

Figure 5-27 The SSA and FEM transverse shear stresses τ_{xz} and τ_{yz} through the thickness of the 3-ply CLT panel for h/a = 0.25.

After the FEM results have been validated with the SSA for the 3-ply CLT panel and the precise model that simulates the CLT in a good way with the suitable mesh size and element type has been chosen, the boundary condition for the CLT edges can be changed to include the 5-ply CLT beam. In this case study, the FEM model will be validated with the existing experiment by O'Dowd *et al.* (2016). This reference has already been mentioned in detail in Chapter 2, section 2.4.1; however, here, the FEM model will be validated with it and different parametric studies will be analysed.

5.4.3 5-ply CLT beam tested by O'Dowd *et al.* (2016)

O'Dowd *et al.* (2016) found the bending stiffness of CLT panels experimentally. They used three different specimen sizes to develop a detailed understanding of the accurate bending stiffness. The CLT panel examined in the test consisted of a five-lamina panel, with specimens from each lamina being removed and tested individually in order to define their properties to an accuracy greater than the declared grade strengths, not to mention the bias in the grade strength towards underestimating the properties, particularly for the non-grade determining properties. The material properties of the CLT reported in the experiment are shown in Figure 5-28 and Table 5-8. In this table, the modulus of elasticity *E* is measured by O'Dowd *et al.* (2016), and the other material properties are from BS EN 338 (2009).

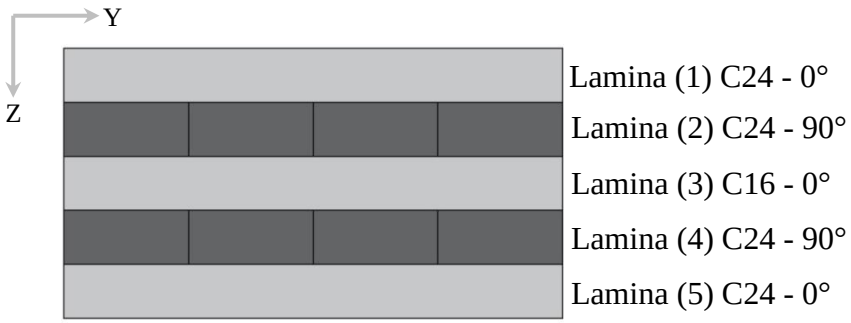

Figure 5-28 Timber gradient for each lamina.

Table 5-8 Material properties as per O'Dowd *et al.* (2016).

Lamina (1) = Lamina (5)	Lamina (3)	Lamina (2) = Lamina (4)
C24	**C16**	**C24**
E_1 = 11880 MPa	E_1 = 8980 MPa	E_1 = 14480 MPa
E_2 = 370 MPa	E_2 = 270 MPa	E_2 = 370 MPa
E_3 = 370 MPa	E_3 = 270 MPa	E_3 = 370 MPa
G_{12} = 690 MPa	G_{12} = 500 MPa	G_{12} = 690 MPa
G_{13} = 690 MPa	G_{13} = 500 MPa	G_{13} = 690 MPa
G_{23} = 50 MPa	G_{23} = 36 MPa	G_{23} = 50 MPa
ν_{12} = 0.44 ; ν_{13} = 0.44; ν_{23} = 0.64 (For all the laminas)		

In the O'Dowd *et al.* work, the specimen sizes are as follows: 1700×150 mm, 1700×200 mm and 1500×200 mm, and the total thickness is equal to 99 mm (each ply is 19 mm thick, the glue layer is 4 mm thick). In the current comparison study, only the first specimen size will be analysed (1700×150 mm). For the adhesive material, Polyurethane glue was used to bond the laminae together with the panel under out-of-plane load (BS EN 15425, 2008). In the experiment, the specimen exhibited approximately linear behaviour with the maximum load and corresponding deflection recorded being 35.30 kN and 25.83 mm respectively (O'Dowd *et al*., 2016).

The test set-up was based on that described in BS EN 408 (2012), as shown in Figure 5-29. The point loads are concentrated over a steel plate to minimise the localised stresses. The local displacement at the centre of the span is measured.

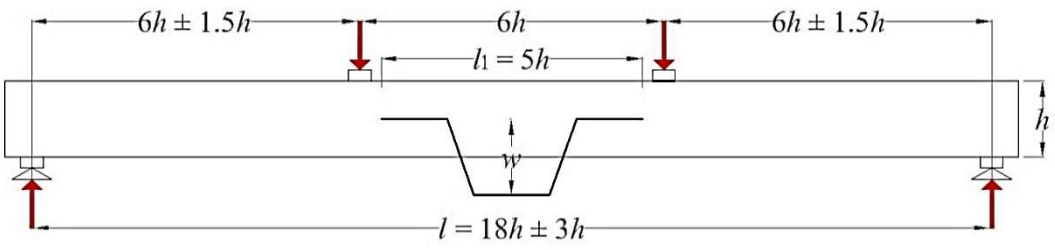

Figure 5-29 Four-point bending test according to BS EN 408 (2012).

For the FEM model in this study, a 3D 20-node element type with a cohesive element layer between the CLT plies and an element mesh size of 10.75 mm is used. The simulation results are shown in Figure 5-30.

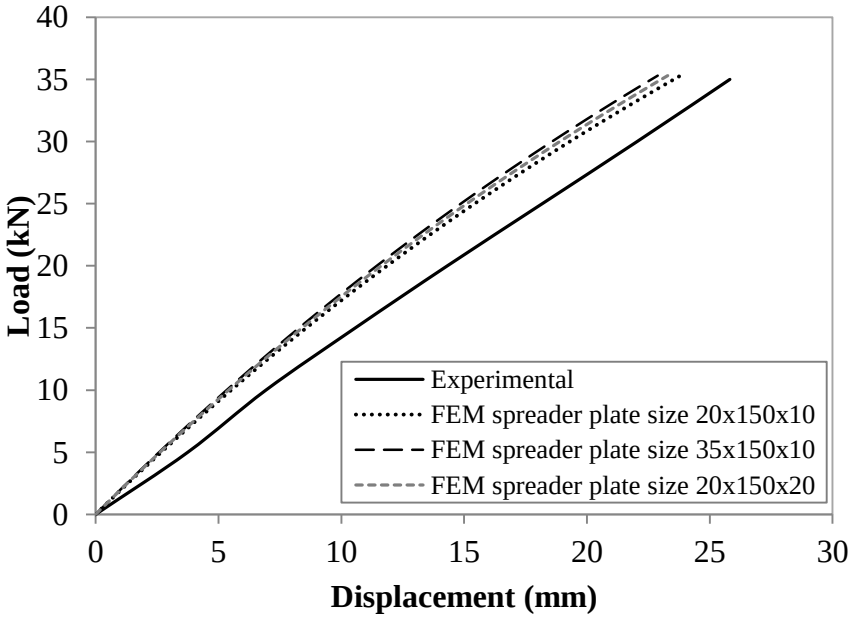

Figure 5-30 Load-displacement curves for the experimental and FEM models with different spreader plate sizes.

The dashed lines in Figure 5-30 are the FEM simulation results. Compared with the experimental test (solid line in Figure 5-30), the FEM model does give a fairly good agreement with the experimental work. Although this figure is showing the elastic load-displacement curves, the FEM curves are non-linear due to the involvement of the shear effect with the bending as the beam is thick. The level of accuracy is comparable with FEM models of CLT undertaken by others, as described in section 2.4.3. One source of error in the model is the exact geometry of the spreader plates under the load; this was estimated from photographs of the experiment.

As shown in Figure 5-29, BS EN 408 does allow a slight setting tolerance between the loading points and supports (note: all these components were steel). In the original experiment, the support bearings were rollers; see Figure 5-31. To understand the sensitivity of the model results to the estimated spreader plate size, a range of feasible

plate sizes were investigated by varying plate width and thickness. Three spreader plate sizes were examined, as shown in Figure 5-32.

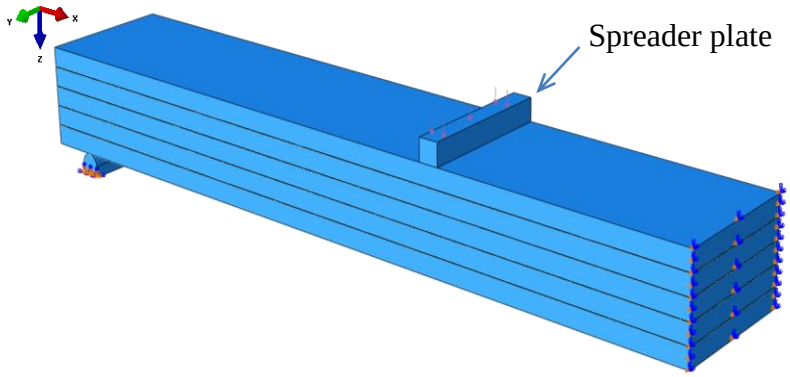

Figure 5-31 FEM model for the four-point bending test (note: the model is symmetric about the mid-span) (ABAQUS, 2013).

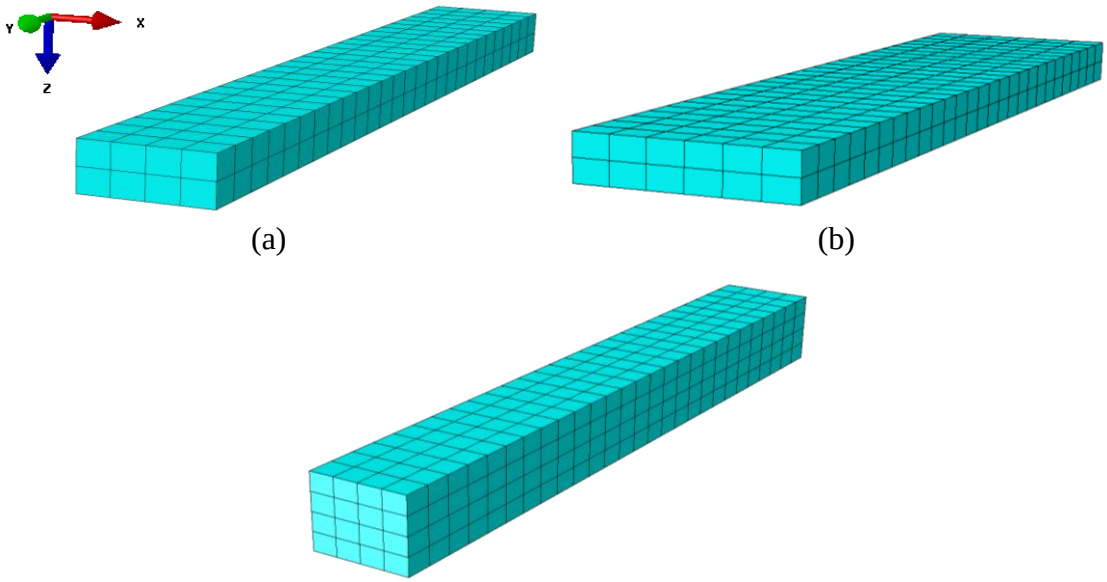

Figure 5-32 Three different spreader plate sizes (a) 150×20×10, (b) 150×35×10 mm and (c) 150×20×20 mm.

Table 5-9 and Figure 5-33 show the relative errors for the maximum displacement for different FEM models of spreader plate sizes. The negative values indicate that the FEM results underestimated the displacement values compared to the experimental data. Hence a stiffer response was predicted. As is shown, when the spreader plate sizes are smaller, the relative error becomes more reasonable and the FEM model gives more

accurate results. For the same width, the results are not greatly affected by the thickness of the spreader plate. The fact that the results are affected by the width of the plate is mainly due to the area change of the loading contact surface. For the case examined, the loading distribution is not affected by the thickness of the spreader plates.

Table 5-9 Relative errors of the spreader plate size on the displacements.

	Experimental (O'Dowd *et al.*, 2016)	**FEM (different spreader plate sizes)**		
		(a) Width: 20mm Thickness: 10mm	(b) Width: 35mm Thickness: 10mm	(c) Width: 20mm Thickness: 20mm
Maximum displacement *w* (mm)	25.830	23.808	22.882	23.804
Relative error (%)		7.83	11.41	7.84

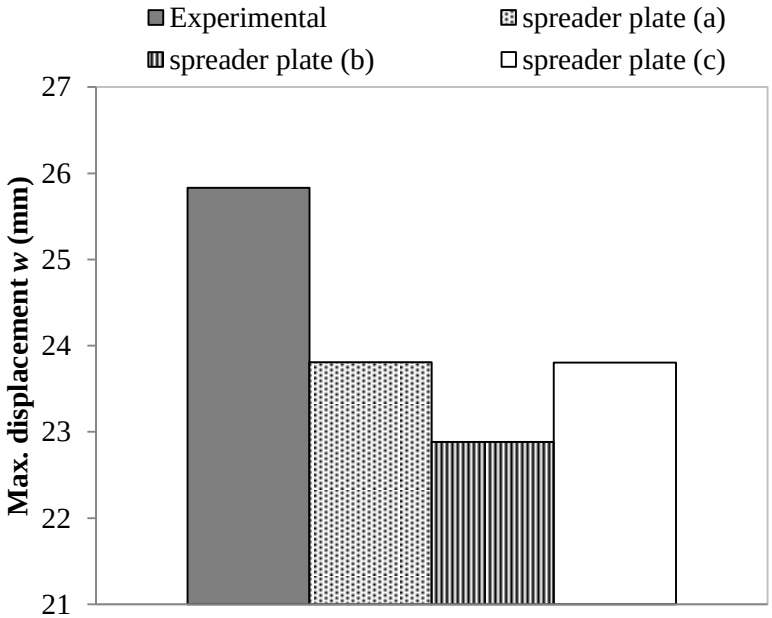

Figure 5-33 Maximum displacement values for the experimental and FEM models with different spreader plate sizes under the load.

Due to the uncertainty of the material properties of timber, upper and lower 5 percentiles of the modulus of elasticity are simulated in ABAQUS, as shown in Figure 5-34. From this figure, when the modulus of elasticity is 5% more, the model becomes stiffer within the same percentage of the changes in the modulus of elasticity.

On the other hand, the modulus of elasticity is 5% lower than the experiment; the displacement becomes closer to the experimental curve as the model becomes less stiff.

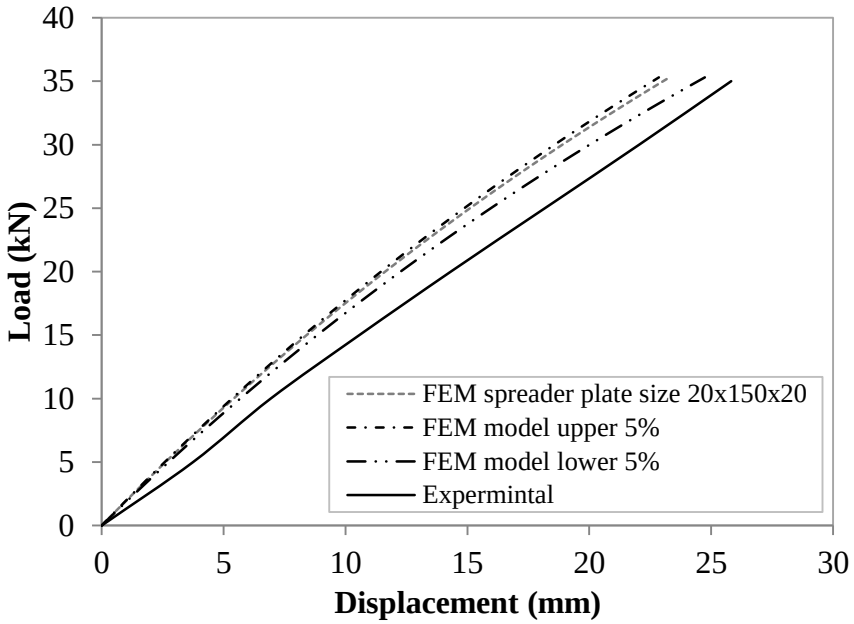

Figure 5-34 Load-displacement curves for the experimental and FEM models with upper and lower 5th percentiles of modulus of elasticity.

5.5 Concluding remarks

CLT panels were investigated as a novel application of the SSA. Existing analytical approaches for CLT panels have limitations in applicability and accuracy. The SSA has the potential to improve accuracy and range of applicability over these existing methods. Towards that, following validation of the SSA against the existing experimental results, an analytical and numerical investigation has been carried out for a simply supported orthotropic CLT panel under sinusoidal and uniformly distributed loads. In consideration of design, different failure criteria were applied to the CLT panels with a view to determining the structural adequacy of the 3-ply CLT panels. It was found that:

- By using the SSA, thicker CLT panels can be modelled and all the stresses and the displacements can be analysed at any location along *x* and *y* directions and through the thickness.

- By applying the SSA to the CLT panels, the transverse normal stress σ_z and the out-of-plane displacement w can be calculated exactly at any location through the thickness while the method used by Sturzenbecher and Hofstetter (2011) neglects σ_z and w is assumed to be constant through the thickness of the plate.
- The in-plane stresses τ_{xy} can be captured and plotted by using the SSA at any location along x, y and through the thickness directions of the panel accurately.
- For 3D analysis, the SSA and Pagano (1970) approaches under the current boundary condition give almost the same results for h/a equal to 0.25, as mentioned in section 5.3.1.
- The non-linear behaviour of the in-plane stresses σ_x through the thickness can be observed as the CLT becomes thicker.
- SSA provides accurate 3D solutions that guarantee continuous transverse stress distributions across the thickness of the CLT panels.
- FEM models were developed for a 3-ply CLT panel and a 5-ply CLT beam under different out-of-plane loads. The modelling is able to predict all the in- and out-of-plane displacements and stresses to a reasonable degree of accuracy. The FEM models were compared with the SSA and existing experimental data.
- The cohesive element mesh layer and the interaction contact models give almost the same results. They are more accurate than the fully bonded model compared to the SSA results as the benchmark.
- The FEM results show discontinuity of the inter-laminar stresses τ_{xz} and τ_{yz} at the interaction between the different plies; this problem is avoided with the SSA method.
- The developed FEM model compared with the existing experimental work by O'Dowd *et al.* (2016) can give a reasonable prediction of the maximum deflection of a CLT panel, taking into consideration the spreader plate dimensions. As the spreader plate sizes are smaller, the relative error between the experimental result and the

FEM model becomes more reasonable. For the same width, the loading distribution is not affected by the thickness of the spreader plates.

CHAPTER 6
NEW ANALYTICAL SOLUTIONS BY USING THE SSA AND THE APPLICATION TO CLT PANELS

6.1 Introduction

In the review of the literature discussed in section 3.4.2, it was explained that different boundary conditions using the state space approach have been studied by different researchers. Also, in the aforementioned chapter, an investigation was carried out on the SSA with regard to its potential application to CLT panels. So far, general exploration of the SSA method in relation to plates has been undertaken including the analysis of a simply supported rectangular plate and a comparison between the analytical results by using 3D SSA and the numerical results by using FEM. However, in this chapter; a novel analytical solution by using SSA for an orthotropic plate with three sides simply supported and one free edge will be covered. This represents the first time the SSA has been formulated for this particular boundary condition. In reality, this type of boundary condition may occur on CLT slabs supported by walls on three edges and spanning an opening on one edge, for example. In this chapter, the SSA together with a state transfer matrix using a programming code will be presented to investigate general homogenous orthotropic composite plate behaviour with the new boundary condition. All the detailed information surrounding formulation for the new boundary condition will be discussed.

The objective of this section is to develop and determine the theoretical solution and to satisfy the new boundary condition by analytical analysis.

For the SSA solution, it will consist of determining the displacements of a rectangular laminated plate by setting a general expression for the displacement field according to the boundary and loading conditions. Then, the displacement field is introduced to the

equations of equilibrium which are then solved. After that, the existing analytical solutions with the FEM will be compared with the SSA.

For a novel application, the new analytical solution will be applied to CLT under various types of load.

6.2 Formulation of the equation

Consider a homogenous orthotropic plate of length a, width b and uniform thickness h, while the boundary conditions for three sides of the plate are simply supported and one side is free, as shown in Figure 6-1, then the following boundary condition should be satisfied:

$$\begin{aligned} &\sigma_y = u = w = 0 && \text{at } y = 0 \text{ and } b \\ &\sigma_x = v = w = 0 && \text{at } x = 0 \\ &\sigma_x = \tau_{xy} = \tau_{xz} = 0 && \text{at } x = a \end{aligned} \tag{6-1}$$

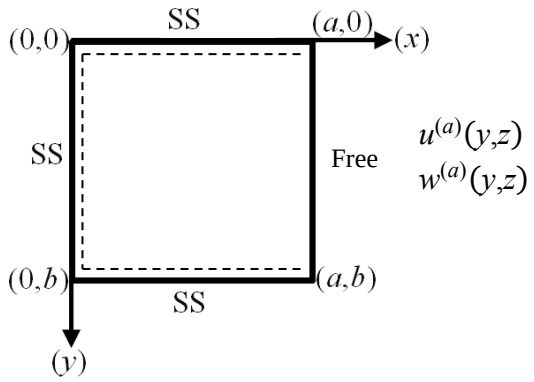

Figure 6-1 Boundary conditions of a plate.

In order to satisfy the boundary condition for a free edge at $x = a$, the in- and out-of-plane displacements have to be treated in such a way as to satisfy the free edge condition. The treatment considers the combination of the bending of a simply supported edge subjected to external transverse load and in-plane normal tractions along $x = a$. This traction causes in-plane displacements of the simply supported edges

to be equal to zero. This may have implications for deep plates where a degree of moment resistance could be developed at the plate edge.

To consider that, a function $u^{(a)}$ and $w^{(a)}$along the free edge will be added and the displacement functions of the plate are assumed as:

$$U = \overline{U} + f_1(x)u^{(a)} \tag{6-2}$$

$$V = \overline{V} + f_2(x)\beta u^{(a)} \tag{6-3}$$

$$W = \overline{W} + f_3(x)w^{(a)} \tag{6-4}$$

In order to satisfy the boundary conditions specified in equation (6-1), the following six state variables of the state vector can be expressed by Fourier series:

$$\begin{aligned}
\overline{u}(x,y,z) &= \sum_{m=1}\sum_{n=1} \overline{U}_{mn}(z)\cos(\zeta x)\sin(\eta y) \\
\overline{v}(x,y,z) &= \sum_{m=1}\sum_{n=1} \overline{V}_{mn}(z)\sin(\zeta x)\cos(\eta y) \\
\overline{w}(x,y,z) &= \sum_{m=1}\sum_{n=1} \overline{W}_{mn}(z)\sin(\zeta x)\sin(\eta y) \\
\overline{\tau}_{xz}(x,y,z) &= \sum_{m=1}\sum_{n=1} \overline{X}_{mn}(z)\cos(\zeta x)\sin(\eta y) \\
\tau_{yz}(x,y,z) &= \sum_{m=1}\sum_{n=1} Y_{mn}(z)\sin(\zeta x)\cos(\eta y) \\
\sigma_z(x,y,z) &= \sum_{m=1}\sum_{n=1} Z_{mn}(z)\sin(\zeta x)\sin(\eta y)
\end{aligned} \tag{6-5}$$

Here $\zeta = \frac{m\pi}{a}$ and $\eta = \frac{n\pi}{b}$ where m and n are the number of loops of the analytical solution in the x and y directions respectively.

Also, from equation (6-1), the out-of-plane stress τ_{xz} when $x=a$ should be equal to zero. To satisfy that, τ_{xz} will be as the following:

$$\tau_{xz} = \bar{\tau}_{xz} + f_4(x)x^{(a)} \tag{6-6}$$

From the above equations, $u^{(a)}$, $w^{(a)}$and $x^{(a)}$ are the unknown functions which can be determined and they have the following forms:

$$\begin{aligned} u^{(a)}(y,z) &= \sum_n u_n^{(a)}(z)\sin(\eta y) \\ w^{(a)}(y,z) &= \sum_n w_n^{(a)}(z)\sin(\eta y) \\ x^{(a)}(y,z) &= \sum_n x_n^{(a)}(z)\sin(\eta y) \end{aligned} \tag{6-7}$$

Also, the three in-plane stresses in the *x-y* plane can be calculated as follows:

$$\begin{Bmatrix} \sigma_x \\ \sigma_y \\ \tau_{xy} \end{Bmatrix} = \begin{bmatrix} C_2\frac{\partial}{\partial x} & C_3\frac{\partial}{\partial y} & -C_1 & 0 & 0 & 0 \\ C_3\frac{\partial}{\partial x} & C_4\frac{\partial}{\partial y} & -C_5 & 0 & 0 & 0 \\ C_6\frac{\partial}{\partial y} & C_6\frac{\partial}{\partial x} & 0 & 0 & 0 & 0 \end{bmatrix} \begin{Bmatrix} U \\ V \\ \sigma_z \\ \tau_{xz} \\ \tau_{yz} \\ W \end{Bmatrix} \tag{6-8}$$

From equation (6-8), the in-plane stresses:

$$\begin{aligned} &\sigma_x = C_2\frac{\partial U}{\partial x} + C_3\frac{\partial V}{\partial y} - C_1\sigma_z \\ &\sigma_x = C_2\frac{\partial}{\partial x}[\bar{U} + f_1(x)u^{(a)}] + C_3\frac{\partial}{\partial y}[\bar{V} + f_2(x)\beta u^{(a)}] - C_1\sigma_z \\ &\sigma_x = C_2[\frac{\partial \bar{U}}{\partial x} + \frac{\partial f_1(x)}{\partial x}u^{(a)}] + C_3[\frac{\partial \bar{V}}{\partial y} + f_2(x)\beta^2 u^{(a)}] - C_1\bar{Z} - C_1\sigma_z \\ &\sigma_x = \\ &-C_2\zeta\textstyle\sum_{m=1}\sum_{n=1}\bar{U}_{mn}(z)\sin(\zeta x)\sin(\eta y) - C_3\eta\sum_{m=1}\sum_{n=1}\bar{V}_{mn}(z)\sin(\zeta x)\sin(\eta y) - \\ &C_1\textstyle\sum_{m=1}\sum_{n=1}\bar{Z}_{mn}(z)\sin(\zeta x)\sin(\eta y) + \\ &C_2 f_1'(x)\textstyle\sum_n u_n^{(a)}(z)\sin(\eta y) - C_3\eta^2 f_2(x)\sum_n u_n^{(a)}(z)\sin(\eta y) \end{aligned} \tag{6-9}$$

$$\sigma_y = C_3 \frac{\partial U}{\partial x} + C_4 \frac{\partial V}{\partial y} - C_5 \sigma_z$$

$$\sigma_y = C_3 \frac{\partial}{\partial x} [\overline{U} + f_1(x) u^{(a)}] + C_4 \frac{\partial}{\partial y} [\overline{V} + f_2(x) \beta u^{(a)}] - C_5 \sigma_z$$

$$\sigma_y = C_3 [\frac{\partial \overline{U}}{\partial x} + \frac{\partial f_1(x)}{\partial x} u^{(a)}] + C_4 [\frac{\partial \overline{V}}{\partial y} + f_2(x) \beta^2 u^{(a)}] - C_5 \sigma_z$$

$$\sigma_y = \qquad (6\text{-}10)$$

$$-C_3 \zeta \sum_{m=1} \sum_{n=1} \overline{U}_{mn}(z) \sin(\zeta x) \sin(\eta y) - C_4 \eta \sum_{m=1} \sum_{n=1} \overline{V}_{mn}(z) \sin(\zeta x) \sin(\eta y) -$$

$$C_5 \sum_{m=1} \sum_{n=1} \overline{Z}_{mn}(z) \sin(\zeta x) \sin(\eta y) +$$

$$C_3 f_1'(x) \sum_n u_n^{(a)}(z) \sin(\eta y) - C_4 \eta^2 f_2(x) \sum_n u_n^{(a)}(z) \sin(\eta y)$$

$$\tau_{xy} = C_6 \frac{\partial U}{\partial y} + C_6 \frac{\partial V}{\partial x}$$

$$\tau_{xy} = C_6 \frac{\partial}{\partial y} [\overline{U} + f_1(x) u^{(a)}] + C_6 \frac{\partial}{\partial x} [\overline{V} + f_2(x) \beta u^{(a)}]$$

$$\tau_{xy} = C_6 [\frac{\partial \overline{U}}{\partial y} + f_1(x) \beta u^{(a)}] + C_6 [\frac{\partial \overline{V}}{\partial x} + \frac{\partial f_2(x)}{\partial x} \beta u^{(a)}]$$

$$\tau_{xy} = \qquad (6\text{-}11)$$

$$C_6 \eta \sum_{m=1} \sum_{n=1} \overline{U}_{mn}(z) \cos(\zeta x) \cos(\eta y) + C_6 \zeta \sum_{m=1} \sum_{n=1} \overline{V}_{mn}(z) \cos(\zeta x) \cos(\eta y) +$$

$$C_6 \eta f_1(x) \sum_n u_n^{(a)}(z) \cos(\eta y) + C_6 \eta f_2'(x) \sum_n u_n^{(a)}(z) \cos(\eta y)$$

To find the functions $f_1(x), f_2(x), f_3(x)$ and $f_4(x)$, equation (6-1) needs to be satisfied, so from this equation, at the simply supported edges, the values of $\sigma_x = v = w = 0$ at x=0 and σ_y, u and w at y=0, b are equal to zero. Also, at the free edge, the values of σ_x, τ_{xy} and τ_{xz} are equal to zero.

6.3 Boundary condition equations

The following procedures will show the determination of the functions.

When y = 0 and b

$$\sigma_y = [-C_3 \zeta \sum_{m=1} \sum_{n=1} \overline{U}_{mn}(z) \sin(\zeta x) - C_4 \eta \sum_{m=1} \sum_{n=1} \overline{V}_{mn}(z) \sin(\zeta x) -$$

$$C_5 \sum_{m=1} \sum_{n=1} \overline{Z}_{mn}(z) \sin(\zeta x) + C_3 f_1'(x) \sum_n u_n^{(a)}(z) - C_4 \eta^2 f_2(x) \sum_n u_n^{(a)}(z) = 0$$

$$U = \overline{U} + f_1(x)u^{(a)}$$

$$U = \sum_{m=1}\sum_{n=1} \overline{U}_{mn}(z)\cos(\zeta x)\sin(\eta y) + f_1(x)\sum_n u_n^{(a)}(z)\sin(\eta y)$$

$$U = [\sum_{m=1}\sum_{n=1} \overline{U}_{mn}(z)\cos(\zeta x) + f_1(x)\sum_n u_n^{(a)}(z)\,]\sin(\eta(0)) = 0$$

$$W = \overline{W} + f_3(x)w^{(a)}$$

$$W = \sum_{m=1}\sum_{n=1} \overline{W}_{mn}(z)\sin(\zeta x)\sin(\eta y) + f_3(x)\sum_n w_n^{(a)}(z)\sin(\eta y)$$

$$W = [\sum_{m=1}\sum_{n=1} \overline{W}_{mn}(z)\sin(\zeta x) + f_3(x)\sum_n w_n^{(a)}(z)\,]\sin(\eta(0)) = 0$$

When $x = 0$

$$\sigma_x = [-C_2\zeta\sum_{m=1}\sum_{n=1} \overline{U}_{mn}(z)\sin(\eta y) - C_3\eta\sum_{m=1}\sum_{n=1} \overline{V}_{mn}(z)\sin(\eta y) -$$

$$C_1\sum_{m=1}\sum_{n=1} Z_{mn}(z)\sin(\eta y)]\sin(\zeta(0)) + [C_2 f_1'(x)\sum_n u_n^{(a)}(z) - C_3\eta^2 f_2(x)\sum_n u_n^{(a)}(z)]\sin(\eta y)$$

$$= 0$$

$$[C_2 f_1'(x=0)\sum_n u_n^{(a)}(z) - C_3\eta^2 f_2(x=0)\sum_n u_n^{(a)}(z)]\sin(\eta y) = 0 \qquad (6\text{-}12)$$

$$V = \overline{V} + f_2(x)\beta u^{(a)}$$

$$V = \sum_{m=1}\sum_{n=1} \overline{V}_{mn}(z)\sin(\zeta x)\cos(\eta y) + f_2(x)\eta\sum_n u_n^{(a)}(z)\cos(\eta y)$$

$$V = \sum_{m=1}\sum_{n=1} \overline{V}_{mn}(z)\sin(\zeta x)(0) + f_2(x)\eta\sum_n u_n^{(a)}(z)\cos(\eta y) = 0$$

$$f_2(x=0)\sum_n u_n^{(a)}(z)\cos(\eta y) = 0 \qquad (6\text{-}13)$$

$$W = \overline{W} + f_3(x)w^{(a)}$$

$$W = \sum_{m=1}\sum_{n=1} \overline{W}_{mn}(z)\sin(\zeta x)\sin(\eta y) + f_3(x)\sum_n w_n^{(a)}(z)\sin(\eta y)$$

$$W = \sum_{m=1}\sum_{n=1} \overline{W}_{mn}(z)\sin(\zeta(0))\sin(\eta y) + f_3(x)\sum_n w_n^{(a)}(z)\sin(\eta y) = 0$$

$$f_3(x=0)\sum_n w_n^{(a)}(z)\sin(\eta y) = 0 \qquad (6\text{-}14)$$

When $x = a$

$\sigma_x =$

$$[-C_2\zeta\sum_{m=1}\sum_{n=1}\overline{U}_{mn}(z)\sin(\eta y) - C_3\eta\sum_{m=1}\sum_{n=1}\overline{V}_{mn}(z)\sin(\eta y) - C_1$$

$$\sum_{m=1}\sum_{n=1}\overline{Z}_{mn}(z)\sin(\eta y)]\sin(m\pi) + [C_2 f_1'(x)\sum_n u_n^{(a)}(z) - C_3\eta^2 f_2(x)\sum_n u_n^{(a)}(z)]\sin(\eta y) = 0$$

$$[C_2 f_1'(x=a)\sum_n u_n^{(a)}(z) - C_3\eta^2 f_2(x=a)\sum_n u_n^{(a)}(z)]\sin(\eta y) = 0 \quad (6\text{-}15)$$

$$\tau_{xy} = C_6\eta\sum_{m=1}\sum_{n=1}\overline{U}_{mn}(z)\cos(\zeta x)\cos(\eta y) + C_6\zeta\sum_{m=1}\sum_{n=1}\overline{V}_{mn}(z)\cos(\zeta x)\cos(\eta y) +$$
$$C_6\eta f_1(x)\sum_n u_n^{(a)}(z)\cos(\eta y) + C_6\eta f_2'(x)\sum_n u_n^{(a)}(z)\cos(\eta y) = 0$$

$$\tau_{xy} = [\eta\sum_{m=1}\sum_{n=1}\overline{U}_{mn}(z)\cos(\zeta x) + \zeta\sum_{m=1}\sum_{n=1}\overline{V}_{mn}(z)\cos(\zeta x) +$$
$$\eta f_1(x)\sum_n u_n^{(a)}(z) + \eta f_2'(x)\sum_n u_n^{(a)}(z)]\, C_6\cos(\eta y) = 0$$

$$[((\eta\sum_{m=1}\sum_{n=1}\overline{U}_{mn}(z) + \zeta\sum_{m=1}\sum_{n=1}\overline{V}_{mn}(z))(-1)^m) + \quad (6\text{-}16)$$
$$(f_1(x=a)\sum_n u_n^{(a)}(z) + f_2'(x=a)\sum_n u_n^{(a)}(z))\,\eta]C_6\cos(\eta y) = 0$$

$$\tau_{xz} = \sum_{m=1}\sum_{n=1}\overline{X}_{mn}(z)\cos(\zeta x)\sin(\eta y) + f_4(x)\sum_n x_n^{(a)}(z)\sin(\eta y) = 0$$

$$\sum_{m=1}\sum_{n=1}\overline{X}_{mn}(z)\cos(ma)\sin(\eta y) + f_4(x=\mathrm{a})\sum_n x_n^{(a)}(z)\sin(\eta y) = 0 \quad (6\text{-}17)$$

From equations (5-12) to (5-17), the summarised equations can be written as the following:

$$C_2 f_1'(x=0) - C_3\eta^2 f_2(x=0) = 0 \quad (6\text{-}18)$$

$$f_2(x=0) = 0 \quad (6\text{-}19)$$

$$f_3(x=0) = 0 \quad (6\text{-}20)$$

$$C_2 f_1'(x=a) - C_3\eta^2 f_2(x=a) = 0 \quad (6\text{-}21)$$

$$((\eta\sum_{m=1}\sum_{n=1}\overline{U}_{mn}(z) + \zeta\sum_{m=1}\sum_{n=1}\overline{V}_{mn}(z))(-1)^m) + \quad (6\text{-}22)$$
$$(f_1(x=a)\sum_n u_n^{(a)}(z) + f_2'(x=a)\sum_n u_n^{(a)}(z))\,\eta = 0$$

$$[\sum_{m=1}\sum_{n=1}\overline{X}_{mn}(z)(-1)^{m} + f_4(x=\mathrm{a})\sum_n x_n^{(a)}(z))\,]\sin(\eta y) = 0 \tag{6-23}$$

To satisfy all the conditions in equations (6-18) to (6-23), the following functions are chosen:

$$f_1(x) = \frac{C_3\eta^2}{C_2}\frac{a}{2}(ae^{(x/a)}-x) \tag{6-24}$$

$$f_2(x) = \frac{a}{2}(e^{(x/a)}-1) \tag{6-25}$$

$$f_3(x) = e^{(x/a)}-1 \tag{6-26}$$

For $f_4(x)$, when $x=0$, $f_4(x)$ should be equal to zero but when $x=a$, $f_4(x) \neq 0$.

$$f_4(x) = e^{(x/a)}-1 \tag{6-27}$$

Also, the unknown functions can be calculated as the following:

$$u_n^{(a)}(z) = \frac{(\eta\sum_{m=1}\sum_{n=1}\overline{U}_{mn}(z) + \zeta\sum_{m=1}\sum_{n=1}\overline{V}_{mn}(z))\,(-1)^m)}{(f_1(x=a)+f_2'(x=a))\eta} \tag{6-28}$$

$$w_n^{(a)}(z) = \overline{W}_{mn}(z) \tag{6-29}$$

$$x_n^{(a)}(z) = \frac{\sum_{m=1}\sum_{n=1}\overline{X}_{mn}(z)(-1)^m}{f_4(x=a)} \tag{6-30}$$

After finding all the functions, the following displacements can be found:

$$U = \sum_{m=1}\sum_{n=1}\overline{U}_{mn}(z)\cos(\zeta x)\sin(\eta y) + \frac{C_3\eta^2}{C_2}\frac{a}{2}(ae^{(x/a)}-x)\sum_n u_n^{(a)}(z)\sin(\eta y) \tag{6-31}$$

$$V = \sum_{m=1}\sum_{n=1}\overline{V}_{mn}(z)\sin(\zeta x)\cos(\eta y) + \frac{a}{2}(e^{(x/a)}-1)\eta\sum_n u_n^{(a)}(z)\cos(\eta y) \tag{6-32}$$

$$W = \sum_{m=1}\sum_{n=1}\overline{W}_{mn}(z)\sin(\zeta x)\sin(\eta y) + (e^{(x/a)}-1)\sum_n w_n^{(a)}(z)\sin(\eta y) \tag{6-33}$$

$$\tau_{xz} = \sum_{m=1}\sum_{n=1}\overline{X}_{mn}(z)\cos(\zeta x)\sin(\eta y) + (e^{(x/a)}-1)\sum_n x_n^{(a)}(z)\sin(\eta y) \tag{6-34}$$

Once the displacements are found, the in-plane and out-of-plane stresses can be calculated.

6.4 Solution of the equation

After satisfying all the boundary conditions, the governing equation needs to be checked and to be satisfied as the following:

$$\frac{\partial}{\partial z}\begin{Bmatrix} U \\ V \\ Z \\ X \\ Y \\ W \end{Bmatrix} = \begin{bmatrix} 0 & 0 & 0 & C_8 & 0 & -\alpha \\ 0 & 0 & 0 & 0 & C_9 & -\beta \\ 0 & 0 & 0 & -\alpha & -\beta & 0 \\ -C_2\alpha^2 - C_6\beta^2 & -(C_3+C_6)\alpha\beta & C_1\alpha & 0 & 0 & 0 \\ -(C_3+C_6)\alpha\beta & -C_6\alpha^2 - C_4\beta^2 & C_5\beta & 0 & 0 & 0 \\ C_1\alpha & C_5\beta & C_7 & 0 & 0 & 0 \end{bmatrix} \begin{Bmatrix} U \\ V \\ Z \\ X \\ Y \\ W \end{Bmatrix} \tag{6-35}$$

$$U = \overline{U} + f_1(x)u^{(a)}$$

$$\frac{\partial U}{\partial z} = \frac{\partial \overline{U}}{\partial z} + \frac{\partial u^{(a)}}{\partial z} f_1(x) = C_8[\overline{X} + f_4(x)x^{(a)}] - \alpha[\overline{W} + f_3(x)w^{(a)}] \tag{6-36}$$

$$\frac{\partial \overline{U}}{\partial z} = C_8\overline{X} - \alpha\overline{W} - \frac{\partial u^{(a)}}{\partial z} f_1(x) + C_8 f_4(x)x^{(a)} - f_3'(x)w^{(a)}$$

$$V = \overline{V} + f_2(x)\beta u^{(a)}$$

$$\frac{\partial V}{\partial z} = \frac{\partial \overline{V}}{\partial z} + \frac{\partial[\beta u^{(a)}]}{\partial z} f_2(x) = C_9 Y - \beta[\overline{W} + f_3(x)w^{(a)}] \tag{6-37}$$

$$\frac{\partial \overline{V}}{\partial z} = C_9 Y - \beta\overline{W} - \frac{\partial[\beta u^{(a)}]}{\partial z} f_2(x) - f_3(x)w^{(a)}$$

$$\frac{\partial Z}{\partial z} = -\alpha X - \beta Y = -\alpha[\overline{X} + f_4(x)x^{(a)}] - \beta Y = -\alpha\overline{X} - \beta Y - f_4'(x)x^{(a)} \tag{6-38}$$

$$X = \overline{X} + f_4(x)x^{(a)}$$

$$\frac{\partial X}{\partial z} = \frac{\partial \overline{X}}{\partial z} + \frac{\partial x^{(a)}}{\partial z} f_4(x)$$

$$\frac{\partial \overline{X}}{\partial z} = (-C_2\alpha^2 - C_6\beta^2)U - (C_3+C_6)\alpha\beta V + C_1\alpha Z - \frac{\partial x^{(a)}}{\partial z} f_4(x)$$

$$\frac{\partial X}{\partial z} = (-C_2\alpha^2 - C_6\beta^2)[\overline{U} + f_1(x)u^{(a)}] - (C_3+C_6)\alpha\beta[\overline{V} + g_1(x)\beta u^{(a)}] \tag{6-39}$$

$$+ C_1\alpha Z - \frac{\partial x^{(a)}}{\partial z} f_4(x)$$

$$\frac{\partial X}{\partial z} = (-C_2\alpha^2 - C_6\beta^2)[\overline{U}] - (C_3+C_6)\alpha\beta\,[\overline{V}] + C_1\alpha Z + (-C_2\alpha^2 - C_6\beta^2)f_1(x)u^{(a)} -$$

$$\frac{\partial x^{(a)}}{\partial z} f_4(x)$$

$$\frac{\partial Y}{\partial z} = -(C_3+C_6)\alpha\beta U +(-C_6\alpha^2-C_4\beta^2)V + C_5\beta Z$$

$$\frac{\partial Y}{\partial z} = -(C_3+C_6)\alpha\beta[\overline{U}+f_1(x)u^{(a)}] +(-C_6\alpha^2-C_4\beta^2)[\overline{V}+g_1(x)\beta u^{(a)}] + C_5\beta Z$$

$$\frac{\partial Y}{\partial z} = -(C_3+C_6)\alpha\beta[\overline{U}] +(-C_6\alpha^2-C_4\beta^2)[\overline{V}] + C_5\beta Z - (C_3+C_6)f_1'(x)\beta u^{(a)}+ (-C_6\alpha^2-C_4\beta^2)g_1(x)\beta u^{(a)} \quad (6\text{-}40)$$

$$\frac{\partial W}{\partial z} = C_1\alpha U +C_5\beta V + C_7 Z$$

$$\frac{\partial W}{\partial z} = \frac{\partial \overline{W}}{\partial z}+ \frac{\partial w^{(a)}}{\partial z}f_3(x) = C_1\alpha[\overline{U}+f_1(x)u^{(a)}]+C_5\beta[\overline{V}+g_1(x)\beta u^{(a)}] + C_7 Z \quad (6\text{-}41)$$

$$\frac{\partial \overline{W}}{\partial z} = C_1\alpha[\overline{U}] +C_5\beta[\overline{V}] + C_7 Z +C_1 f_1'(x)u^{(a)} +C_5 g_1(x)\beta^2 u^{(a)} - \frac{\partial w^{(a)}}{\partial z}f_3(x)$$

Rearranging equations (6-36) to (6-41) in a matrix form gives,

$$\frac{\partial}{\partial z}\begin{Bmatrix}\overline{U}\\ \overline{V}\\ Z\\ X\\ Y\\ \overline{W}\end{Bmatrix} = \begin{bmatrix} 0 & 0 & 0 & C_8 & 0 & -\alpha \\ 0 & 0 & 0 & 0 & C_9 & -\beta \\ 0 & 0 & 0 & -\alpha & -\beta & 0 \\ -C_2\alpha^2-C_6\beta^2 & -(C_3+C_6)\alpha\beta & C_1\alpha & 0 & 0 & 0 \\ -(C_3+C_6)\alpha\beta & -C_6\alpha^2-C_4\beta^2 & C_5\beta & 0 & 0 & 0 \\ C_1\alpha & C_5\beta & C_7 & 0 & 0 & 0 \end{bmatrix}\begin{Bmatrix}\overline{U}_{mn}(z)\cos(\zeta x)\sin(\eta y)\\ \overline{V}_{mn}(z)\sin(\zeta x)\cos(\eta y)\\ Z_{mn}(z)\sin(\zeta x)\sin(\eta y)\\ \overline{X}_{mn}(z)\cos(\zeta x)\sin(\eta y)\\ Y_{mn}(z)\sin(\zeta x)\cos(\eta y)\\ \overline{W}_{mn}(z)\sin(\zeta x)\sin(\eta y)\end{Bmatrix} +$$

$$\begin{Bmatrix} -\frac{\partial u^{(a)}}{\partial z}f_1(x) + C_8 f_4(x)x^{(a)} - f_3'(x)w^{(a)} \\ -\frac{\partial[\beta u^{(a)}]}{\partial z}f_2(x) - f_3(x)w^{(a)} \\ -f_4'(x)x^{(a)} \\ (-C_2\alpha^2-C_6\beta^2)f_1(x)u^{(a)} - \frac{\partial x^{(a)}}{\partial z}f_4(x) \\ -(C_3+C_6)f_1'(x)\beta u^{(a)} + (-C_6\alpha^2-C_4\beta^2)g_1(x)\beta u^{(a)} \\ C_1 f_1'(x)u^{(a)} + C_5 f_2(x)\beta^2 u^{(a)} - \frac{\partial w^{(a)}}{\partial z}f_3(x) \end{Bmatrix} \quad (6\text{-}42)$$

The above expression in equation (6-42) can be simplified as:

$$\frac{\partial}{\partial z}\begin{Bmatrix}\overline{U}\\ \overline{V}\\ Z\\ X\\ Y\\ \overline{W}\end{Bmatrix} = [\mathrm{G}].\begin{Bmatrix}\overline{U}\\ \overline{V}\\ Z\\ X\\ Y\\ \overline{W}\end{Bmatrix} + \overline{B} \tag{6-43}$$

The following first-order non-homogeneous ordinary differential equation of j^{th} can be determined for each combination of m and n:

$$\frac{d}{dz}\{R_{mn}(z)\}_j = D_j\{R_{mn}(z)\}_j + \{B_{mn}(z)\}_j \tag{6-44}$$

where

$$\{R_{mn}(z)\}_j = \begin{Bmatrix}\overline{U}_{mn}(z)\\ \overline{V}_{mn}(z)\\ Z_{mn}(z)\\ \overline{X}_{mn}(z)\\ Y_{mn}(z)\\ \overline{W}_{mn}(z)\end{Bmatrix}_j ; D_j = \begin{bmatrix} 0 & 0 & 0 & C_8 & 0 & -\zeta \\ 0 & 0 & 0 & 0 & C_9 & -\eta \\ 0 & 0 & 0 & \zeta & \eta & 0 \\ C_2\zeta^2+C_6\eta^2 & (C_3+C_6)\zeta\eta & C_1\zeta & 0 & 0 & 0 \\ (C_3+C_6)\zeta\eta & C_6\zeta^2+C_4\eta^2 & C_5\eta & 0 & 0 & 0 \\ -C_1\zeta & -C_5\eta & C_7 & 0 & 0 & 0 \end{bmatrix}$$

After solving all the above displacements and out-of-plane stresses, the in-plane stresses can be solved.

Once all the in- and out-of-plane displacements and stresses have been derived and solved by using the SSA, the results will be compared with different existing approaches.

6.5 Case Study 1: Antisymmetric cross-ply plate (two plies)

In the first part of this section, the new analytical solution results will be compared with different existing analytical solutions for different boundary conditions; this will include the existing 2D approaches that were examined analytically by Reddy (2004). Then, the FEM model will be simulated for the cross-ply 2-ply plate and the results will be compared with various analytical approaches.

6.5.1 Comparison with various analytical solutions

The focused-on panel has the same geometry as that examined analytically by Reddy (2004). The panel or plate is symmetrical with two plies of alternate orientation, i.e. [0/ 90]°, as shown in Figure 6-2. The in-plane dimensions of the plate are $a = b = 100$ mm and h/a is equal to 0.2. Here, a is the length of the plate along the x-axis, b is the dimension of the plate along the y-axis and h is the total thickness of the plate (z-axis), as shown in Figure 6-2. The set of elastic material parameters used for the plies is given as shown in Table 6-1, as per the reference (Reddy, 2004).

Table 6-1 Elastic material properties of the antisymmetric cross-ply plate (Reddy, 2004).

$E_1/E_2 = 25$
$G_{12} = G_{13} = 0.5\ E_2$
$G_{23} = 0.2\ E_2$
$v_{12} = v_{13} = v_{23} = 0.25$

Three sides of the plate are simply supported and there is one free edge, as per Reddy (2004), and the load on the top surface of the panel is a sinusoidal load, as shown in Figure 6-2.

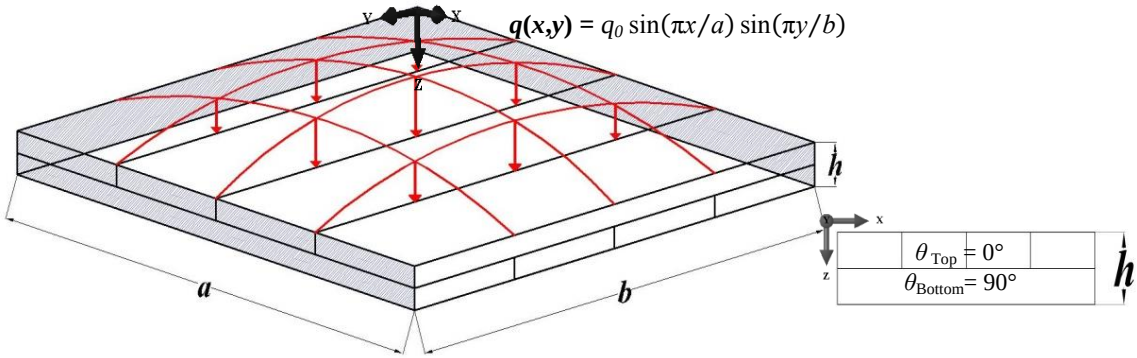

Figure 6-2 The geometry of the antisymmetric cross-ply plate under sinusoidal load and the orientation angles through *h*.

The different analytical approaches that are used here for comparison are Classical Laminated Plate Theory (CLPT), First-Shear Deformation Theory (FSDT) and Higher-Shear Deformation Theory (HSDT), and they are validated with the SSA. These theories are considered to be 2D plate theories, as mentioned before in Chapter 3 (section 3.2) in detail.

Table 6-3 shows the dimensionless results of different analytical approaches for the out-of-plane displacement w and the in-plane stresses σ_x and σ_y of the antisymmetric cross-ply for $a = b$ and $h/a = 0.2$. The values in Table 6-3 for the out-of-plane displacement w and in-plane stress σ_x will be at the top of the plate, and, for the in-plane stress σ_y, the resultant values will be at the bottom of the plate, as per Reddy (2004).

For w, σ_x and σ_y, the SSA results show good agreement with the existing 2D approaches, although, for w, the SSA shows higher values than the 2D approaches and the result is closer to the FSDT with a 7.5% relative error. Also, for the σ_x result, the SSA is closer to the CLPT with a 4.6% relative error. But, for the σ_y result, the SSA is closer to HSDT with a 3.5% relative error.

Table 6-2 Theoretical dimensionless results for displacements and stresses of the antisymmetric cross-ply for $a = b$ and $h/a = 0.2$.

	SSA	CLPT	FSDT	HSDT
$\frac{WE_2h^3}{b^4q_0}\times10^2$	2.526	1.471	2.335	2.211
$\frac{\sigma_x h^2}{b^2 q_0}\times10$	-5.113	-5.349	-4.430	-4.442
$\frac{\sigma_y h^2}{b^2 q_0}\times10$	-10.943	-9.837	-9.848	-11.324

Where E_2 is the modulus of elasticity along the *y*-axis, b is the dimension of the plate along the *y*-axis, h is the total thickness of the plate (*z*-axis) and q_0 is the out-of-plane load.

6.5.2 Antisymmetric cross-ply plate FEM results

In addition to the SSA method and other analytical solutions previously discussed, a simulation of the antisymmetric cross-ply plate using the commercially available finite element program ABAQUS is now presented. This section aims to compare the FEM results with the SSA results to provide more contexts for the SSA's capability in this application. The same plate as described in the previous section will be used for the numerical model. In the FEM model, the 3D 20-node linear brick element (C3D20) with the 8-node 3D cohesive element (COH3D8) (ABAQUS, 2013) between the antisymmetric cross-ply will be used, as shown in Figure 6-3. In terms of the mesh size, elements with a leading dimension of 0.125 mm were adopted.

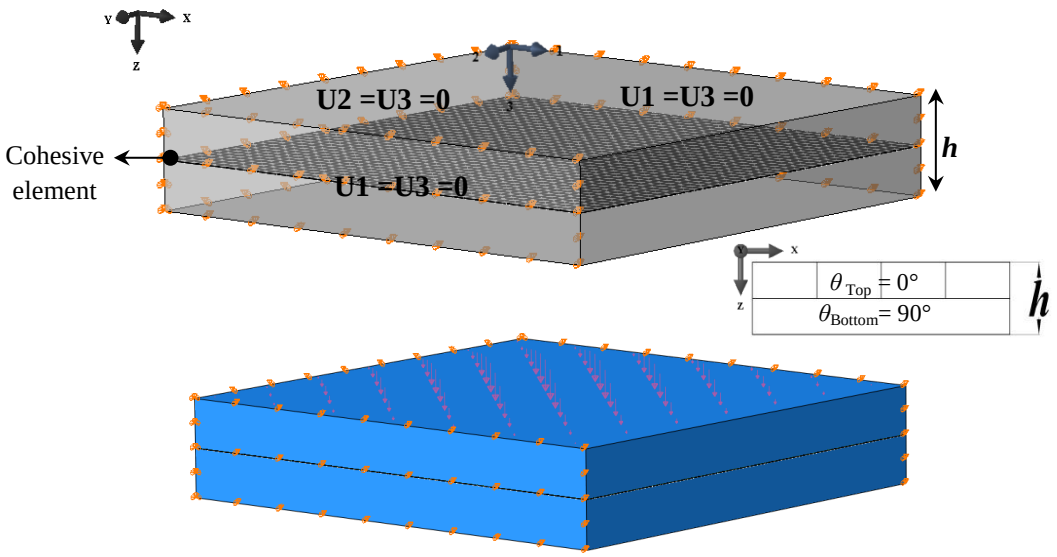

Figure 6-3 The FEM model of the antisymmetric cross-ply plate under sinusoidal load.

For the FEM results for the 2nd ply (90°), ABAQUS shows the results related to the local coordinate of each ply, as shown in Figure 6-4.

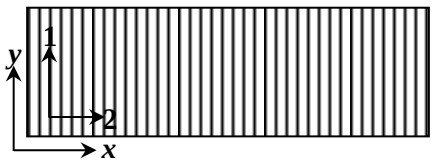

Figure 6-4 CLT 90° ply global and local coordinates.

In Figure 6-5 and Table 6-3, the FEM results are compared with the SSA and the other analytical results. The FEM results are very comparable with the SSA and the other analytical solutions and show the closest results to the SSA with a 4% relative error for the out-of-plane displacement w, 2% for σ_x and 0.5% for σ_y. Hence, to make a comparison with the SSA and the other analytical approaches, the FEM results for the second ply (90°) should be transferred to global coordinates, and then the stress distribution can be drawn, as shown in Figure 6-6. This figure shows the capability of the SSA and FEM to capture the in-plane stress σ_x through the thickness of the antisymmetric cross-ply plate.

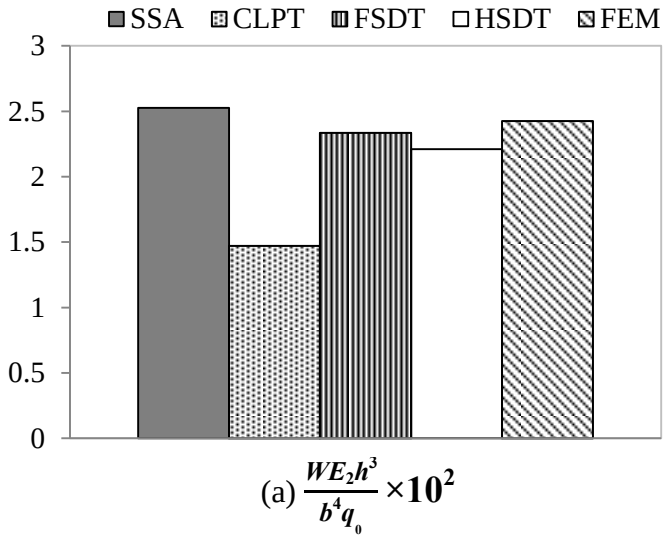

(a) $\frac{WE_2h^3}{b^4q_0}\times 10^2$

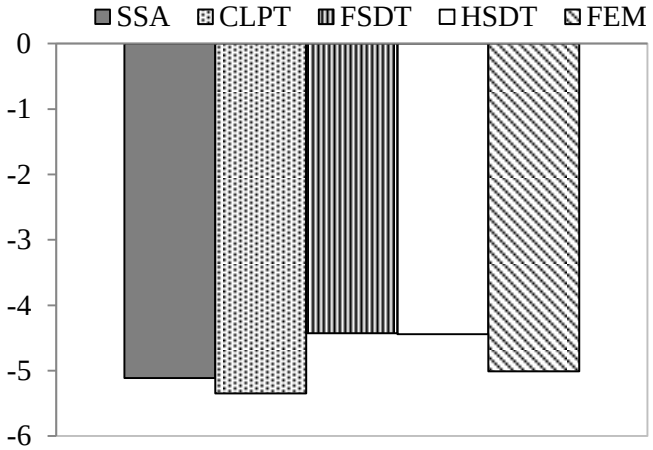

(b) $\frac{\sigma_x h^2}{b^2q_0}\times 10$

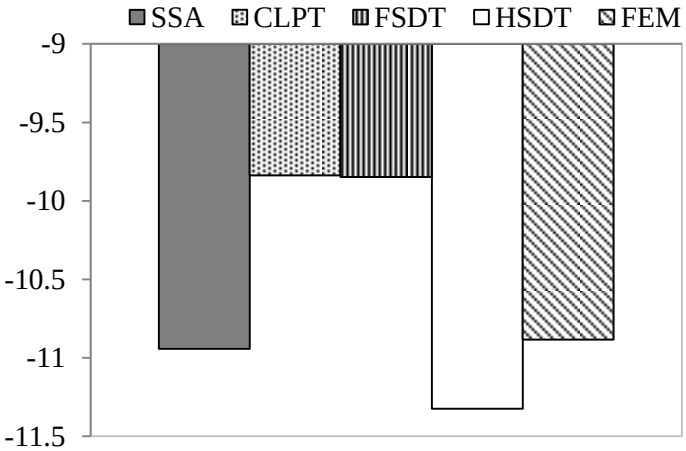

(c) $\frac{\sigma_y h^2}{b^2q_0}\times 10$

Figure 6-5 Theoretical and FEM results for out-of-plane displacements and in-plane stresses of the antisymmetric cross-ply for $a = b$ and $h/a = 0.2$.

Table 6-3 Theoretical dimensionless results for displacements and stresses of the antisymmetric cross-ply for $a = b$ and $h/a = 0.2$.

	SSA	CLPT	FSDT	HSDT	FEM
$\frac{WE_2h^3}{b^4q_0}\times10^2$	2.526	1.471	2.335	2.211	2.427
$\frac{\sigma_x h^2}{b^2q_0}\times10$	-5.113	-5.349	-4.430	-4.442	-5.010
$\frac{\sigma_y h^2}{b^2q_0}\times10$	-10.943	-9.837	-9.848	-11.324	-10.884

Where E_2 is the modulus of elasticity along the y-axis, b is the dimension of the plate along the y-axis, h is the total thickness of the plate (z-axis) and q_0 is the out-of-plane load.

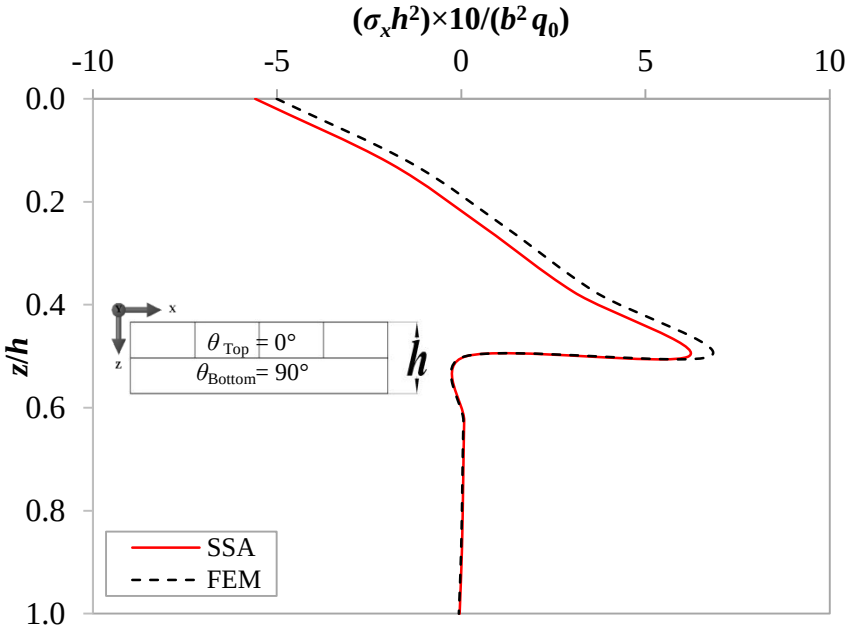

Figure 6-6 The SSA and FEM in-plane stress σ_x through the thickness of the antisymmetric cross-ply plate for $h/a = 0.2$.

After introducing the new analytical solution by using the SSA for a panel with three sides that are simply supported and one free edge in the previous section, and the results compared with the FEM, the SSA will be applied to CLT under different types of loads in the next section. Also, as the FEM results showed good agreement with the SSA, the

FEM will be adopted for the next section to model the CLT and for more comparison with the SSA results.

6.6 SSA applied to a CLT panel with three sides simply supported and one free edge

In this section, two case studies are explored. The first one is a 3-ply CLT panel under out-of-plane sinusoidal load; the plate in the second study has the same geometry but is under a transverse uniformly distributed load.

In this section, the two types of loads are chosen to show the effect of the number of Fourier series terms (*m* and *n*) on the SSA results. As for the sinusoidal load, *m* and *n* in the SSA solution are equal to 1, but for the uniformly distributed load, adding more Fourier series terms (*m* and *n*) will make the solution more theoretically accurate.

The panel in this section for the different case studies has three sides simply supported at x=0, y =0 and b and the free edge ts at x=a (as shown in Figure 6-7).

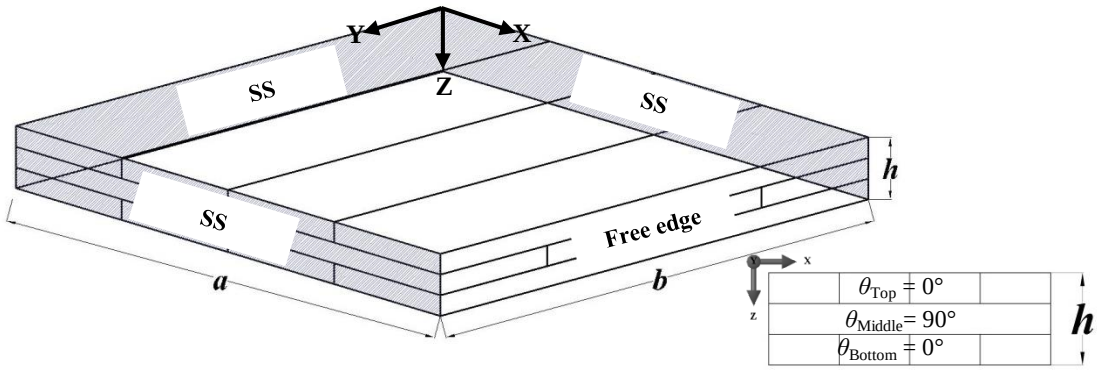

Figure 6-7 The geometry of the 3-ply CLT with three sides simply supported and a free edge.

From the previous chapter, the FEM results were compared with different existing analytical methods and were found to be in good agreement with them. Hence, from this point of view, after applying the SSA to the case studies, FEM simulation for each

case will be modelled and the results will be compared to check the accuracy of the SSA compared to the FEM.

6.6.1 FEM model of 3-ply CLT panels with three sides simply supported and a free edge

In this section, the FEM models will be the same as Chapter 4 with the same element type, mesh size and the types of model (the cohesive element layer between the CLT plies). The FEM models are a 3D 20-node linear brick element (C3D20) with mesh size 24 mm and an 8-node three-dimensional cohesive element (COH3D8) with three sides simply supported and a free edge.

6.6.1.1 Case Study 1: 3-ply CLT panel under sinusoidal load

The focused-on plate has the same geometry and the same material properties for the timber plies as that examined before, in section 5.3.1. The panel is symmetrical with three plies of alternate grain orientation, i.e. [0/90/0]°, as shown in Figure 6-8.

Each board or ply has a thickness of 30 mm so that the total plate thickness is 90 mm. The in-plane dimensions of the plate are $a = b = 360$ mm and h/a is equal to 0.25 as this is the thicker plate studied by Sturzenbecher and Hofstetter (2011). Here, a is the length of the plate along the x-axis, b is the dimension of the plate along the y-axis and h is the total thickness of the plate (z-axis), as shown in Figure 6-8.

The panel has three sides simply supported at $x=0$, $y=0$ and b and a free edge at $x=a$ (as shown in Figure 6-8) and the load on the top surface of the panel is a sinusoidal load with a maximum magnitude of 1 MPa ($q(x,y) = q_0 \sin(\pi x/a) \sin(\pi y/b)$ where $q_0 = 1$ MPa), as shown in Figure 6-8.

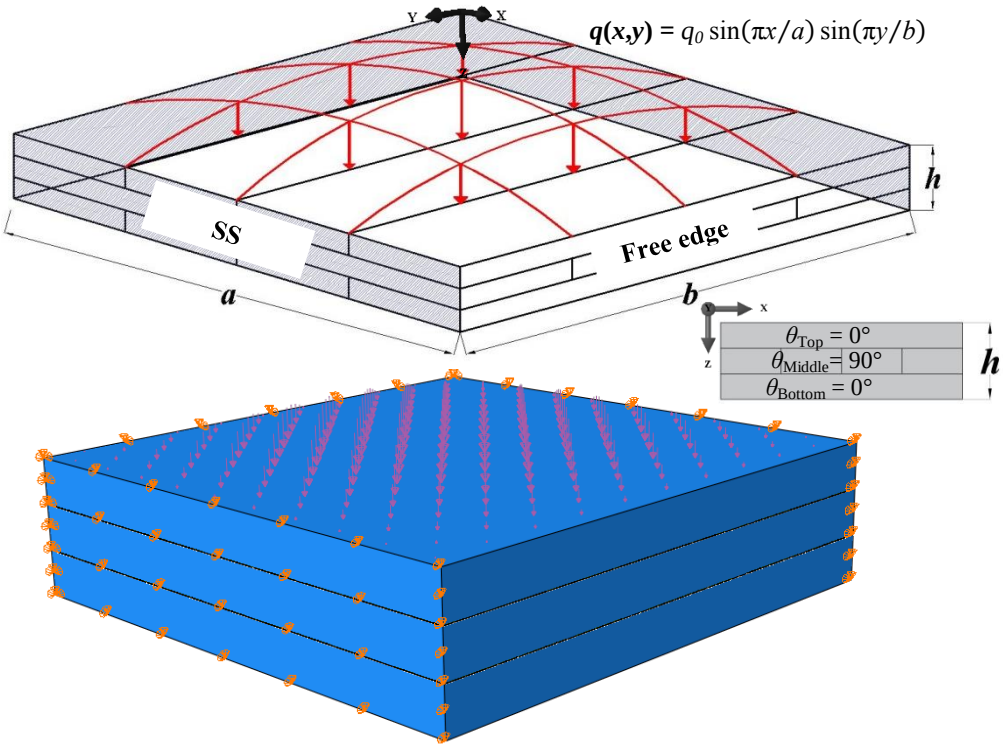

Figure 6-8 The geometry of the 3-ply CLT panel (three sides simply supported and a free edge) with the FEM models under sinusoidal load.

Table 6-4 shows the comparison between the SSA and the FEM results for all the in- and out-of-plane displacements and stresses for the 3-ply CLT panel under sinusoidal load.

In general, the SSA results give higher values than the FEM results for all the displacements and the stresses but still the results are very comparable to each other.

From the same table, the FEM shows discontinuity in the transverse shear stresses τ_{xz} and τ_{yz} between the plies. On the other hand, the SSA shows the continuity of the transverse shear stresses between the plies.

Table 6-4 In- and out- of plane displacements (mm) and stress states (MPa) of the 3-ply CLT panel (h/a = 0.25) by SSA and FEM under sinusoidal load.

	(x,y)	# of the ply	z	SSA	**FEM		(x,y)	SSA	**FEM
u	$(0, \frac{b}{2})$	1st Ply	*T	0.2458	0.2432	v	$(a,0)$	0.5786	0.5732
			*B	-0.0970	-0.0791			0.2452	-0.2450
		2nd Ply	*T	-0.0970	-0.0791			0.2452	0.2450
			*B	0.0830	0.0719			-0.2294	-0.2262
		3rd Ply	*T	0.0830	0.0719			-0.2294	-0.2262
			*B	-0.2398	-0.2373			-0.5525	-0.5489
w	$(a,\frac{b}{2})$	1st Ply	*T	2.1364	2.1174	σ_x	$(\frac{a}{2},\frac{b}{2})$	-9.4205	-9.2012
			*B	2.0978	2.0614			6.8563	6.6015
		2nd Ply	*T	2.0978	2.0614			-0.5742	-0.5730
			*B	2.0902	2.0562			0.4647	0.4734
		3rd Ply	*T	2.0902	2.0562			-6.1605	-5.9002
			*B	2.0617	2.0517			8.6928	8.5826
σ_y	$(a,\frac{b}{2})$	1st Ply	*T	-2.3705	-2.3310	τ_{xy}	$(0,0)$	3.4633	3.4270
			*B	-1.0488	-1.0314			0.42820	0.4000
		2nd Ply	*T	-21.9300	-22.7521			-0.4820	-0.4000
			*B	24.3113	23.6217			0.5483	0.5392
		3rd Ply	*T	0.7333	0.7316			-0.5483	-0.5392
			*B	1.9334	1.8996			-3.7150	-3.5900
τ_{xz}	$(0,\frac{b}{2})$	1st Ply	*T	0.0000	0.0237	τ_{yz}	$(\frac{a}{2},0)$	0.0000	0.0177
			*B	0.8334	0.8086			0.4640	0.4114
		2nd Ply	*T	0.8334	0.7745			0.4640	0.5258
			*B	0.8921	0.8613			0.3695	0.3750
		3rd Ply	*T	0.8921	0.8774			0.3695	0.3642
			*B	0.0000	0.0364			0.0000	0.0032

*Where T and B are the top and bottom of the panel through the thickness respectively.
**The FEM models are 3D 20-node linear brick element (C3D20) with mesh element size 6 mm.

6.6.1.2 Case Study 2: 3-ply CLT panel under Uniformly Distributed Load

In this section, the same geometry and the same material properties for the timber ply are used in the previous section with different types of load.

The plate is under uniformly distributed load, as shown in Figure 6-9, and all the in-plane and out-of-plane stresses and displacements will be shown and explored through the thickness of the three plies of CLT.

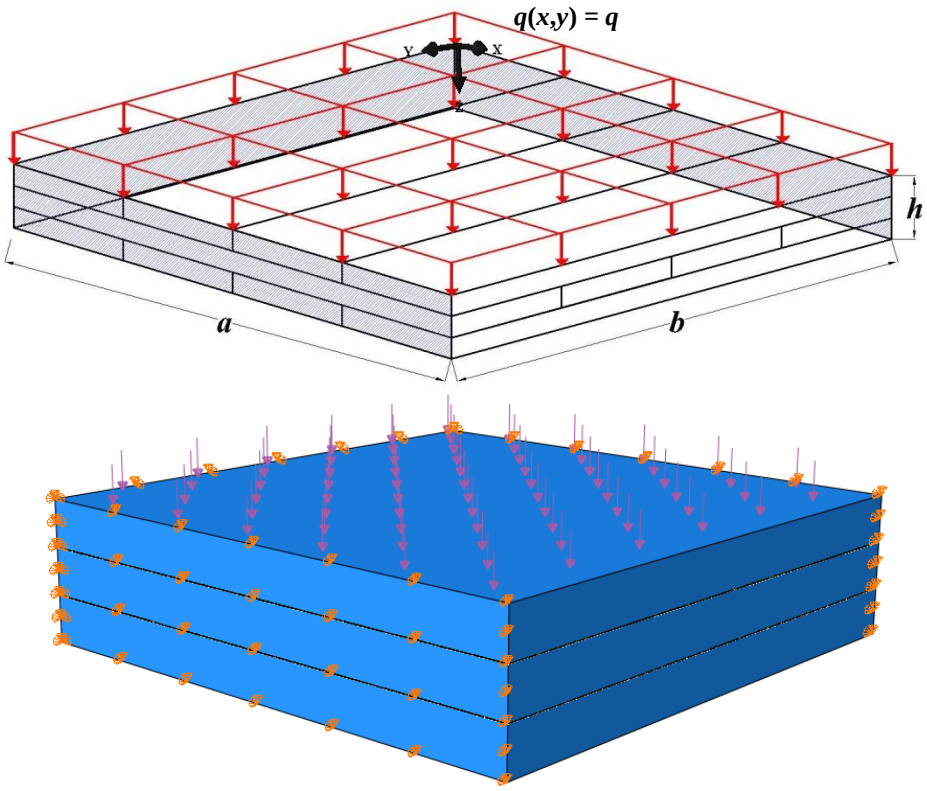

Figure 6-9 The geometry of the 3-ply CLT panel (three sides simply supported and a free edge) with the FEM models under uniformly distributed load.

From Table 6-5, all the in-plane and out-of-plane displacements and stresses are explored by using the SSA and FEM through the three plies of CLT. In general, the SSA results are higher than the FEM results, but still are very close to each other and give good agreement. Additionally, the values of the displacements and the stresses for the uniformly distributed load are approximate twice the values of the sinusoidal load from Table 6-4.

As mentioned before, in section 5.4.2, the same trends as the previous case study, the FEM shows discontinuity in the transverse shear stresses in between the plies; on the other hand, the SSA shows the continuity of the transverse shear stresses between the plies.

Table 6-5 In- and out- of plane displacements (mm) and stress states (MPa) of the 3-ply CLT panel (h/a = 0.25) by SSA and FEM under uniformly distributed load.

	(x,y)	# of the ply	z	SSA	**FEM		(x,y)	SSA	**FEM
u	$(0,\frac{b}{2})$	1st Ply	*T	0.4651	0.4618	v	$(a,0)$	1.1404	1.1259
			*B	-0.1602	-0.1203			0.5581	0.5567
		2nd Ply	*T	-0.1602	-0.1203			0.5581	0.5567
			*B	0.1125	0.1010			-0.4589	-0.4568
		3rd Ply	*T	0.1125	0.1010			-0.4589	-0.4568
			*B	-0.4492	-0.4492			-1.0868	-1.0713
w	$(a,\frac{b}{2})$	1st Ply	*T	4.5258	4.4845	σ_x	$(\frac{a}{2},\frac{b}{2})$	-10.8941	-10.8707
			*B	4.4804	4.4283			5.0770	4.4411
		2nd Ply	*T	4.4804	4.4283			-1.0180	-0.9961
			*B	4.3894	4.4141			0.4485	0.4267
		3rd Ply	*T	4.3894	4.4141			-5.3133	-4.4411
			*B	4.3890	4.3400			10.5695	10.8675
σ_y	$(a,\frac{b}{2})$	1st Ply	*T	-4.2652	-4.2241	τ_{xy}	$(0,0)$	7.6243	7.5607
			*B	-1.9857	-1.9811			0.5445	0.5410
		2nd Ply	*T	-46.2344	-46.0482			-0.5445	-0.5410
			*B	47.5175	47.5051			1.1608	1.1466
		3rd Ply	*T	1.3747	1.3369			-1.1608	-1.1466
			*B	3.7774	3.6138			-7.0645	-6.9494
τ_{xz}	$(0,\frac{b}{2})$	1st Ply	*T	0.0000	-0.0825	τ_{yz}	$(\frac{a}{2},0)$	0.0000	0.0000
			*B	1.4299	1.3969			1.1590	1.1890
		2nd Ply	*T	1.4299	1.2766			1.1590	1.5002
			*B	1.5870	1.4984			0.6757	0.7091
		3rd Ply	*T	1.5870	1.5286			0.6757	0.6565
			*B	0.0000	0.0836			0.0000	0.0151

* Where T and B are the top and bottom of the panel through the thickness respectively.
** The FEM models are 3D 20-node linear brick element (C3D20) with mesh element size 6 mm.

To show the capability of the SSA to capture the stress distribution through the thickness of the 3-ply CLT panel, Figure 6-10 shows the in-plane stress σ_x distribution through the thickness of the CLT panel by using the SSA and the FEM. The distribution of the SSA and the FEM shows very good agreement through the thickness.

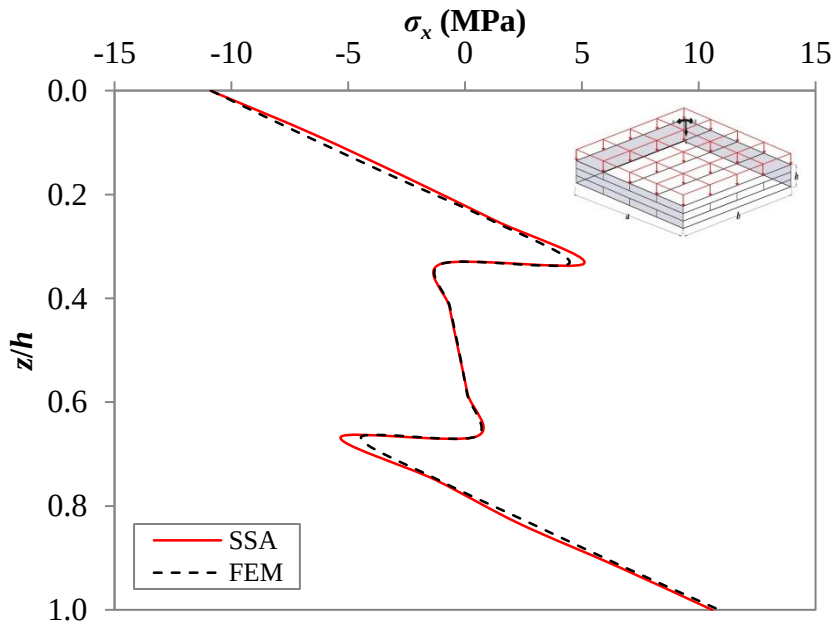

Figure 6-10 The SSA and FEM in-plane stress σ_x through the thickness of the CLT panel for h/a = 0.25 (note: data is provided in Appendix D-Table D.1).

6.7 Concluding remarks

In this chapter, a new analytical solution by the SSA for a plate with three sides simply supported and one free edge is derived; this solution takes into account all the independent elastic constants and satisfies all the governing and boundary condition equations (equations 6-5, 6-31 to 6-34 and 6-42). The new solution guarantees the continuity conditions of all inter-laminar stresses across interfaces between different layers and traction-free boundary conditions at the free edges.

For this new analytical solution by using the SSA, the MATHEMATICA code is an extension of the simply supported case in the previous chapters, as shown in Appendix A. Also, the code that has been developed can be applied to different material properties with different loading types.

Different analytical solutions for a generic composite material plate with the FEM model are compared with the new SSA solution, and the SSA results show good agreements with the other solutions with an overall relative error less than 10%.

After that, the new analytical solution was applied to the CLT panel under different types of loads and the FEM results gave good agreement with the SSA results, although the FEM underestimated the in- and out-of-plane stresses and displacement. Also, the continuity of the inter-laminar stresses across interfaces between the different CLT plies was shown using the SSA; on the other hand, the FEM showed the discontinuity of these stresses across the plies.

CHAPTER 7
CONCLUSIONS AND RECOMMENDATIONS FOR FUTURE STUDY

From the investigation of the existing experimental, analytical and numerical methods used to obtain accurate solutions for CLT panels in the literature review, the existing analytical approaches still have a need for improvement to overcome their limitations and to obtain more accurate results for thicker plates. Based on that, developing a new analytical solution is an active research topic. In this research, by using the SSA applied to CLT panels a more precise representation of the structural behaviour is obtained compared to the existing experimental, analytical and numerical methods. The comparison proved that the SSA is a good approach and gives good agreement for different boundary conditions under different out-of-plane loads for CLT and composite plates.

This chapter presents a summary of the main conclusions from the analytical and numerical investigations carried out in this work. Recommendations for future work are also given.

7.1 Analytical investigation for general composite simply supported plates

An analytical investigation has been carried out on a general composite simply supported rectangular plate with two types of loads by using 3D SSA. The SSA is a powerful three-dimensional approach and satisfies all the boundary conditions and the continuity at the interfaces. The analysis started with 1-ply under two different types of out-of-plane loading, and the results of the SSA and the Classical Plate Theory were compared and showed very good agreement. Then, by applying the SSA, it is found that the behaviour of the stresses through the thickness becomes non-linear, especially for plates with a higher thickness-to-width ratio (h/a). Furthermore, the finite element

models developed in ABAQUS give good agreement with the SSA after undertaking a parametric study for the element type, mesh size and the same boundary condition as the one used in the analytical solution. Although the SSA and the FEM results are comparable to each other, still more caution is required when using numerical results from the FEM when applied to real structural design and behaviour evaluation. The SSA solution was extended to more than one ply, and the SSA results were compared with different existing 2D approaches and found to give good agreement.

7.1.1 Experimental, analytical and numerical investigation of CLT panels

The SSA has been extended to consider laminated composite plates, and it is applied to Cross-Laminated Timber (CLT) as a laminated composite plate. Different case studies (3- and 5-ply CLT panels) are compared with the SSA experimentally, analytically and numerically, and the following conclusions can be drawn:

- Crucially, thicker CLT panels can be modelled and all the stresses and the displacements can be analysed at any location along x and y directions and through the thickness.

- The transverse-normal stress σ_z and the out-of-plane displacement w can be calculated exactly at any location through the thickness while the method used by Sturzenbecher and Hofstetter (2011) neglects σ_z and assumes w to be constant through the thickness of the plate.

- The in-plane stresses τ_{xy} can be accurately captured and plotted by using the SSA at any location along x, y and through the thickness directions of the panel.

- The SSA and Pagano (1970) approaches under all the simply supported boundary condition edges examined in this work give almost the same results for h/a equal to 0.25.

- The non-linear behaviour of the in-plane stresses σ_x through the thickness can be observed as the CLT becomes thicker.

- The SSA provides accurate 3D solutions that guarantee continuous transverse stress distributions across the thickness of the plates. Additionally, the state space method can give theoretically precise results for all in- and out-of-plane stresses and displacements for various thicknesses, from thin to very thick plates.

- Finite element modelling using ABAQUS shows the capability of the FEM to obtain a good agreement when compared with the SSA results for all the stresses and displacements of 3- and 5-ply CLT panels, although the FEM results for the plies using solid elements in ABAQUS will lead to discontinuity of the transverse shear stresses at ply interfaces (ABAQUS, 2013). Furthermore, the values of τ_{xz} should be equal to zero at the top and the bottom of the plate, but, for the FEM results, they are not. For the top of the plate the calculated error for the FEM results was 0.05 of the maximum value of $\tau_{xz,}$ and for the bottom of the plate, it was 0.07.

7.1.2 New analytical solutions by using the SSA and the application to CLT panels

A new analytical solution by SSA for a plate with three sides simply supported and a free edge is derived and explored to take into account all the independent elastic constants and satisfying all the governing and boundary condition equations as a novel work. The new solution guarantees the continuity conditions of all inter-laminar stresses across interfaces between different layers and traction-free boundary conditions at the free edges.

The different analytical solutions such as Classical Plate Theory (CLPT), First-order Shear Deformation Theory (FSDT) and Higher-order Shear Deformation Theory (HSDT) with the FEM model for a general composite plate with three sides simply supported and one free edge were compared with the new analytical solution by the SSA, and the results were comparable and gave good agreement, especially with the FEM. Also, the new analytical solution was applied to CLT with different types of loads. In addition to that, FEM models were developed and the results compared with the SSA.

7.2 Limitations of the research

The SSA in this application shows promise. Since the elastic behaviour and stress response of the CLT panels have been fully characterised, failure criteria and prediction of the load capacity for practical CLT panels can be assessed easily. However, there are a few associated limitations. The panel material properties have been considered as idealised elastic, as mentioned before, in section 2.1 (which from a design point of view is a reasonable approximation for timber). The present study focused on particular boundary conditions, i.e. all simply supported edges and three sides simply supported with a free edge. Although the SSA can be extended for other boundary conditions such as free and fixed supports, this requires more complex expressions and further refinement of the solution process for the governing state equation. As to the solution itself, theoretical precision of the SSA solution can be improved further by increasing the number of Fourier series terms (m and n) in the series expressions of the solution, as shown before, in sections 4.4.4 and 5.4.2.

Another limitation is that the SSA and the other existing analytical approaches used in this research assume full bond between the plies of the CLT panel and full bond between the boards in each ply. Although by using SSA, the bonding layers between

different plies could be considered, this requires further development. Also, this research does not consider the CLT behaviour for the long term, as both timber and the glues exhibit long-term visco-elastic behaviour under a sustained load as opposed to an instantaneous load.

7.3 Recommendations for future research

The following lists recommendations for future research that could be undertaken in the following areas:

- Since this research focuses on two different boundary conditions such as simply supported for all sides and three sides simply supported with a free edge for CLT panels, further investigation should be performed for other boundary conditions like three sides free with a clamped edge. In addition, other loading conditions could be considered.
- As previously stated, the SSA model presented in this work assumes full connectivity between plies. To understand the behaviour of the adhesive glue and the effect of it on the CLT plate behaviour, more detailed analysis of the bond between the CLT plies should be undertaken, taking into consideration the cohesive material between each board that forms the CLT panel.
- This research focused on out-of-plane behaviour. In-plane loads could be incorporated into the SSA formulation and buckling behaviour could be included. In parallel, boundary conditions simulating a CLT wall panel could also be formulated.
- CLT panels incorporating openings are necessary for practical structures; this could be further incorporated into the SSA formulation.

REFERENCES

ABAQUS, 2013. ABAQUS User's Manual, Version 6.13, Dassault Systémes Simulia Corp., Providence, Rhode.

Albostami, A., Wu, ZJ. and Cunningham, L.S. 2017. Structural behaviour of cross-laminated timber panels by the state space approach, *International Journal of Computational Methods and Experimental Measurements*, 8(4), 1-13.

American Institute of Timber Construction. 2012. *Timber construction manual*. John Wiley & Sons, Inc., New Jersy.

Bahar, L.Y. 1975. A state space approach to elasticity. *Journal of the Franklin Institute*, 299(1), 33-41.

Barlow, P. 1817. *An Essay on the strength and stress of timber*, 3rd edition, J. Taylor, London.

Bogensperger, T. and Jöbstl, R.A. 2015. Concentrated load introduction in CLT elements perpendicular to plane. *International Council for Research and Innovation in Building and Construction Working Commission W18 - Timber Structures Cib-W18*, 1-16.

Brandner, R. 2014. Production and technology of Cross-Laminated Timber (CLT): A state-of-the-art Report. *Focus Solid Timber Solutions - European Conference on Cross Laminated Timber (CLT)*, 3-36.

Brandner, R., Dietsch, P., Dröscher, J., Schulte-Wrede, M., Kreuzinger, H., Sieder, M., Schickhofer, G. and Winter S. 2015. Shear properties of cross laminated timber (CLT) under in plane load: test configuration and experimental study. *Proc-Cib*, 1-20.

BSI 2013. BS EN 14080:2013: *Timber structures - glued laminated timber and glued solid timber- requirements*, Milton Keynes, UK.

BSI 2008. BS EN 15425:2008: *Adhesives - one component polyurethane for load bearing timber structures- classification and performance requirements*, 3, Milton Keynes, UK.

BSI 2015. BS EN 16351:2015: *Timber structure - cross laminated timber-requirements*, Milton Keynes, UK.

BSI 2008. BS EN EN 1995-1-1 :2004+A: *Eurocode 5: Design of timber structures - Part 1-1: general - common rules and rules for buildings*, Milton Keynes, UK.

BSI 2010. BS EN 384:2009: *Structural timber-determination of characteristic values of mechanical properties and density*, Milton Keynes, UK.

BSI 2001. BS EN 386:2001: *Glued-laminated timber performance requirements and minimum production requirements*, (1109), Milton Keynes, UK.

BSI 2009. BS EN 338:2009: *Structural timber-strength classes*, 3, Milton Keynes, UK.

BSI 2012. BS EN 408:2010+A1: *Timber structures-structural timber and glued laminated timber-Determination of some physical and mechanical properties*, Milton Keynes, UK.

Carrera, E. 1996. C^0 Reissner-Midlin multilayered plate elements including zig-zag and interlaminar stress continuity. *International Journal for Numerical Methods in Engineering*, 39, 1797–1820.

Carrera, E. 1997. C^0_z requirements-models for the two dimensional analysis of multilayered structures. *Composite Structures*, 37(314), 373-383.

Carrera, E. 2003. Historical review of zig-zag theories for multilayered plates and shells. *Applied Mechanics Reviews*, 56(3), 287.

Cook, R. D. 1995. *Finite Element Modeling for Stress Analysis*, John Wiley &Sons Inc.

Czaderski, C., Steiger, R., Howald, M., Olia, S., Gülzow, A. and Niemz, P. 2007. Versuche und Berechnungen an Allseitig Gelagerten 3-Schichtigen Brettsperrholzplatten. *Holz als Roh - und Werkstoff*, 65(5), 383-402.

Ealias, J. and Mattam, J. 2013. Study of inter-laminar shear stress of composite structures. *International Journal of Emerging Technology and Advanced Engineering*, 3(8), 543-552.

Dinwoodie, J.M. 2000. *Timber: Its Nature and Behaviour*. 2nd edition, Taylor and Francis, London & New York.

Ealias, J. and Mattam, J. 2013. Study of Inter-laminar shear stress of composite structures. *International Journal of Emerging Technology and Advanced Engineering*, 3(8), 543-552.

Fan, J. and Ye, J. 1990. An exact solution for the statics and dynamics of laminated thick plates with orthotropic layers. *International Journal of Solids and Structures*, 26(7), 655-662.

FPInnovations 2013. CLT handbook canadian edition. *Journal of Chemical Information and Modeling*, 53, Canada.

Ghugal Y. M. and Shimpi R. P. 2002. A review of refined shear deformation theories of isotropic and anisotropic laminated plates. *Journal of Reinforced Plastics and Composites*, 21(9), 775.

Gordon, J.E. 1988. *The Science of Structures and Materials*. Scientific American Library, New York.

Guo, Y., Nagy, A.P. and Gürdal, Z. 2014. A layerwise theory for laminated composites in the framework of isogeometric analysis. *Composite Structures*, 107, 447-457.

Han, C. 2014. *3D State space analysis and free- edge effect of piezoelectric laminated thick plates*, PhD thesis, University of Manchester.

Harris, R. 2015. *Cross laminated timber, Wood Composites*. Elsevier Ltd.

Hochreiner, G., Fussl, J. and Eberhardsteiner, J. 2014. Cross-laminated timber plates subjected to concentrated loading: experimental identification of failure mechanisms. *Strain*, 50(1), 68-81.

Jairazbhoy, V.A., Petukhov, P. and Qu, J. 2008. Large deflection of thin plates in cylindrical bending -Non-unique solutions. *International Journal of Solids and Structures*, 45(11-12), 3203-3218.

Kamis, E. 2012. *Reinforced Polymer Laminated Composites*, PhD thesis, University of Manchester.

Kirchhoff, G. 1850. Uber das Gleichgewicht und die Bewegung einer elastischen Scheibe. *Journal f ̈ur die reine und angewandte Mathematik*, 40, 51–88.

Kreja, I. 2011. A literature review on computational models for laminated composite and sandwich panels. *Central European Journal of Engineering*, 1(1), 59-80.

Kutnar, A. and Muthu, S. 2016. *Environmental impacts of traditional and innovative forest-based bioproducts*, Hong Kong.

Forest Products Laboratory. 2010. *Wood handbook*. Madison, Wisconsin: Forest Products Laboratory.

Lekhnitskii, S. (1968), *Anisotropic Plates*, 2nd edition, Translated from the 2nd Russian Edited by SW Tsai and Cheron, Bordon and Breach.

Levinson, M. 1980. An accurate, simple theory of the statics and dynamics of elastic plates. *Mechanics research communications*, 7(6), 343-350.

Lewis, K., Basaglia, B., Shrestha, R. and Crews, K. 2016. The Use of Cross Laminated Timber for Long Span Flooring in Commercial Buildings. *World Conference on Timber Engineering*, 4-5.

McKenzie. 2000. *Design of structural timber*, MACMILLAN Press LTD, London.

Mindlin, R. 1951. Influence of rotatory inertia and shear on flexural motions of isotropic, elastic plates. *Journal of Applied Mechanics*, 18, 31-38.

Möhler, K. 1955. *Über das Tragverhalten von Biegeträger und Druckstäben mit zusamengestzten Querschnitten und nachgiebigen Verbindungsmitteln*. Technische Hochschule, Karlsruhe.

Murakami, H. 1986. Laminated composite plate theory with improved in-plane response. *Applied Mechanics Reviews*, 53, 661-666.

Nimbolkar, P. V. and Jain, I.M. 2015. Cylindrical Bending of Elastic Plates. *Procedia Materials Science*, 10, 793-802.

Noor, A.K. and Burton, W. 1990. Assessment of computational models for multilayered composite shells. *Applied Mechanics Reviews*, 43(4), 67-97.

O'Dowd, B., Cunningham, L. and Nedwell, P. 2016. Briefing : experimental and theoretical bending stiffness of Cross-Laminated Timber panels. *Proceedings of the Institution of Civil Engineers - Construction Materials*, 169(6), 277-281.

Oh, J.K., Lee, J.J. and Hong, J.P. 2015. Prediction of compressive strength of cross-laminated timber panel. *Journal of Wood Science*, 61(1), 28-34.

Onate, E. 1989. *Structural Analysis with the Finite Element Method - Linear Statics, Lecture Notes on Numerical Methods in Engineering and Sciences*. Dordrecht: Springer Netherlands.

Ozelton, E.C. and Baird, J.A. 2006. *Timber Designers Manual*. (Science, B.,Ed.), Blackwell Science.

Pagano, N.J. 1969. Exact solutions for composite laminates in cylindrical bending. *Composite Materials*, 3, 398-411.

Pagano, N.J. 1970. Exact solutions for rectangular bidirectional and sandwich plates. *Composite Materials*, 4, 20-34.

Pearson, H.R. 2014. *Cross-laminated timber panels incorporating angular material properties*, PhD thesis, University of Bath.

Rashed, Y.F. 2000. *Boundary element formulations for thick plates*, WIT press.

Reddy, J.N. 1993. An evaluation of equivalent-single-layer and layerwise theories of composite laminates. *Composite Structures*, 25(1-4), 21-35.

Reddy, J.N. 2004. *Mechanics of laminated composite plates and shells: theory and analysis*. CRC press.

Reissner, E. 1945. The effect of transverse shear deformation on the bending of elastic plates. *Journal of Applied Mechanics*, 12, 68-77.

Ren, J.G. 1986. Bending theory of laminated plate, *Composites Science and Technology*, 27(3), 225-248.

Ridley-Ellis, D., Stapel, P. and Bano, V. 2016. Strength grading of sawn timber in Europe: an explanation for engineers and researchers. *European Journal of Wood and Wood Products*, 74(3), 291-306.

Ritter, M. A. 1990. *Timber bridges: design, construction, inspection and maintenance*, (Service, F.,Ed.) *Book*, Washington.

Saavedra Flores, E.I., Dayyani, I., Ajaj, R.M., Castro-Triguero, R., DiazDelao, F.A., Das, R. and González Soto, P. 2015. Analysis of cross-laminated timber by computational homogenisation and experimental validation. *Composite Structures*, 121, 386-394.

Serrano, E. and Enquist, B. 2010. Compression strength perpendicular to grain in Cross-Laminated Timber (CLT), *WCTE*, 1-8.

Shahnewaz, M., Tannert, T., Alam, M.S. and Popovski, M. 2015. Experimental and finite element analysis of Cross Laminated Timber (CLT) panels. *First International Conference on Advances in Civil Infrastructure and Construction Materials*.

Sheng, H.Y. and Ye, J.Q. 2003. A three-dimensional state space finite element solution for laminated composite cylindrical shells. *Computer Methods in Applied Mechanics and Engineering*, 192(22-24), 2441-2459.

Sikora, K.S., McPolin, D.O. and Harte, A.M. 2016. Effects of the thickness of Cross-Laminated Timber (CLT) panels made from Irish Sitka spruce on mechanical performance in bending and shear. *Construction and Building Materials* , 116, 141-150.

Stauder, C. 2013. *Cross-Laminated Timber: an analysis of the Austrian industry and ideas for fostering its development in America*, Austria.

Stroud, K.A. 2013. *Engineering mathematics*. 7th edition, Industrial Press Inc., New York.

Sturzenbecher, R. and Hofstetter, K. 2011. Bending of cross-ply laminated composites: An accurate and efficient plate theory based upon models of Lekhnitskii and Ren. *Composite Structures*, 93(3), 1078-1088.

Sturzenbecher, R., Hofstetter, K. and Eberhardsteiner, J. 2010. Structural design of cross laminated timber (CLT) by advanced plate theories. *Composites Science and Technology*, 70(9), 1368-1379.

Sutton, A., Black, D. and Walker, P. 2011. *Cross-Laminated Timber An introduction to low-impact building materials, BRE publications*.

Thiel, A. and Schickhofer, G. 2010. CLTdesigner - A software tool for designing cross laminated timber elements: 1D-plate-design, *11th World Conference on Timber Engineering*, 2, 1742-1747.

Van De Kuilen, J.W.G., Ceccotti, A., Xia, Z. and He, M. 2011. Very tall wooden buildings with Cross-Laminated Timber. *Procedia Engineering*. 14, 1621-1628.

Vilguts, O.A., Serdjuks, D. and Pakrastins, L. 2015. Design methods of elements from Cross-Laminated Timber subjected to flexure. *Procedia Engineering*, 117(1), 10-19.

Vlasov, V. 1957. Method of initial functions in problems of theory of thick plates and shells. *Proceedings 9th of the International Congresses on Theoretical and Applied Mechanics*, Brussels, 321.

Wolfram Research 2016. Mathematica tutorial. Champaign, Illinois.

Wu, Z.J., Han, C. and Niu, Z. 2015. A 3D exact analysis of the boundary layer effect of asymmetric piezoelectric laminates with electromechanical coupling. *International Journal of Solids and Structures*, Elsevier Ltd, 72, 118-129.

Wu, Z.J. 1987. *Exact solution of orthotropic simply-supported rectangular plates under arbitrary loadings*, University of Hefei Technology, Hefei, China.

Wu, Z.J. and Wardenier, J. 1998. Further investigation on the exact elasticity solution for anisotropic thick rectangular plates. *International Journal of Solids and Structures*, 35(7-8), 747–758.

Xu, X., Sun, L. and Fan, X. 1995, Stress concentration of finite composite laminates weakened by multiple elliptical holes. *International Journal of Solids and Structures*, 32(20), 3001-3014.

Ye, J. 2003. *Laminated Composite Plates and Shells*. Springer London, London.

Zhou, J., Chui, Y.H., Gong, M. and Hu, L. 2017. Elastic properties of full-size mass timber panels: Characterization using modal testing and comparison with model predictions. *Composites Part B: Engineering*, 112, 203-212.

Appendix A

A.1 MATHEMATICA code for a single-ply orthotropic fully simply supported under uniformly distributed load (Case Study 3 - section 4.4.4)

```
E2=E3;E1=10*E3;
G12=0.6*E3;G23=0.5*E3;G13=G12;
v12=0.25;v13=0.25;v23=0.25;v21=v12*E2/E1;v32=v23*E3/E2;v31=
v13*E3/E1;
Q=1-v12*v21-v23*v32-v31*v13-2*v12*v23*v31;

C11=SetPrecision[E1*(1-
v23*v32)/Q,50];C12=SetPrecision[E1*(v21+v31*v23)/Q,50];C22=S
etPrecision[E2*(1-v13*v31)/Q,50];
C13=SetPrecision[E1*(v31+v21*v32)/Q,50];C33=SetPrecision[E3*
(1-v12*v21)/Q,50];C23=SetPrecision[E2*(v32+v12*v31)/Q,50];
C44=SetPrecision[G23,50];C55=SetPrecision[G13,50];C66=SetPrec
ision[G12,50];
C1=-(C13/C33);C2=C11-C13^2/C33;C3=C12-(C13 C23)/C33;C4=C22-
Subscript[C, 23]^2/C33;C5=-
(C23/C33);C6=C66;C7=1/C33;C8=1/C55;C9=1/C44;

Clear[E3,a,b,q,z0,h,z1];

U0 = 0;Uz= 0;V0= 0;Vz= 0;W0= 0;Wz= 0;
σX Top= 0;σX z= 0;σY Top= 0;σY z= 0;τXY Top= 0;τXY z= 0;ZTop
= 0;Z z = 0;Xg = 0;Y z = 0;

SumU0 = 0;SumUz= 0;SumV0= 0;SumVz= 0;SumW0= 0;SumWz= 0;
SumσX Top= 0;SumσX z= 0;SumσY Top= 0;SumσY z= 0;SumτXY Top=
0;SumτXY z= 0;SumZ z = 0;SumXg= 0;SumY z = 0;
Sumu02 =0;Sumuz2=0;Sumv02 =0;Sumvz2=0;Sumw02 =0;Sumwz2=0;
SumσzTop = 0;Sumσzz = 0 ;Sumτxz z = 0;Sumτyz z =0;

a=5;b =5;q=1;E3=1;h=1;
z0 =SetPrecision[1,50]; z1 =SetPrecision[h,50];x =0;y=0;

I6=SetPrecision[IdentityMatrix[6],50];

For[i=1, i <39,i+=2,m=i;
 For[ii=1, ii <39,ii+=2,n=ii;
  ZTop = SetPrecision[-((16 q)/(m n π2)),50]; LTop =
SetPrecision[(_{{ZTop},{0}, {0}}_),50]; LBottom =
SetPrecision[(_{{0},{0},{0}}_),50];ζ=SetPrecision[(m*π)/a,5
0];η=SetPrecision[(n*π)/b,50];

D01=(_{{0, 0, 0, C8E3, 0, -ζ},{0, 0, 0, 0, C9E3, -η},{0, 0,
0, ζ, η, 0},{(C2 ζ2+C6 η2)/E3, (C3+C6)ζ*η/E3, C1ζ, 0, 0, 0},
{(C3+C6)ζ*η/E3, (C6 ζ2+C4 η2)/E3, C5η, 0, 0, 0},{-C1ζ, -C5η,
C7E3, 0, 0, 0}}_);D0 = SetPrecision[D01,50];
```

```
eDz0=SetPrecision[MatrixExp[D0*z0],50];

L1=(_{{eDz0[[3,1]], eDz0[[3,2]], eDz0[[3,6]]},
     {eDz0[[4,1]], eDz0[[4,2]], eDz0[[4,6]] },
     {eDz0[[5,1]], eDz0[[5,2]], eDz0[[5,6]]} }_);

L2= (_{{eDz0[[3,3]], eDz0[[3,4]], eDz0[[3,5]]},
     {eDz0[[4,3]], eDz0[[4,4]], eDz0[[4,5]] },
     {eDz0[[5,3]], eDz0[[5,4]], eDz0[[5,5]]} }_);

X_Top = SetPrecision[LinearSolve[L1,(L_Bottom - L2.L_Top)],50] ;
U_0 = X_Top[[1,1]];
V_0 = X_Top[[2,1]];
W_0 = X_Top[[3,1]];

eDz1=SetPrecision[MatrixExp[D0*(z1/h)],50];
X_z =
SetPrecision[eDz1.(_{{U_0},{V_0},{Z_Top},{0},{0},{W_0}}_),50];

U_z = X_z[[1,1]];
V_z =  X_z[[2,1]];
Z_z =  X_z[[3,1]];
Xg =  X_z[[4,1]];
Y_z =  X_z[[5,1]];
W_z =  X_z[[6,1]];

u_02= SetPrecision[Cos[m Pi x/a] Sin[n Pi y/b]U_0 ,50];
u_z2=SetPrecision[Cos[m Pi x/a] Sin[n Pi y/b] U_z ,50];
v_02= SetPrecision[Sin[m Pi x/a] Cos[n Pi y/b]V_0 ,50];
v_z2=SetPrecision[Sin[m Pi x/a] Cos[n Pi y/b] V_z ,50];
w_02= SetPrecision[Sin[m Pi x/a] Sin[n Pi y/b]W_0,50];
w_z2=SetPrecision[Sin[m Pi x/a] Sin[n Pi y/b] W_z ,50];
σzTop =SetPrecision[Sin[m Pi x/a] Sin[n Pi y/b] Z_Top,50];
σzz = SetPrecision[Sin[m Pi x/a] Sin[n Pi y/b] Z_z ,50];
τxz z =SetPrecision[Cos[m Pi x/a] Sin[n Pi y/b]Xg ,50];
τyz z =SetPrecision[Sin[m Pi x/a] Cos[n Pi y/b]Y_z ,50];

σX Top =SetPrecision[(-C_2ζ/E3)(Sin[m Pi x/a] Sin[n Pi
y/b]U_0)+(-C_3η/E3)(Sin[m Pi x/a] Sin[n Pi y/b]V_0)-C_1
σzTop,50];
σY Top=SetPrecision[(-C_3ζ/E3)(Sin[m Pi x/a] Sin[n Pi
y/b]U_0)+(-C_4η/E3)(Sin[m Pi x/a] Sin[n Pi y/b]V_0)-C_5
σzTop,50];
τXY Top =SetPrecision[(C_6η/E3)(Cos[m Pi x/a] Cos[n Pi
y/b]U_0)+(C_6ζ/E3)(Cos[m Pi x/a] Cos[n Pi y/b]V_0),50];

σX z =SetPrecision[(-C_2ζ/E3)(Sin[m Pi x/a] Sin[n Pi
y/b]U_z)+(-C_3η/E3)(Sin[m Pi x/a] Sin[n Pi y/b]V_z)-C_1 σzz,50];
σY z=SetPrecision[(-C_3ζ/E3)(Sin[m Pi x/a] Sin[n Pi
y/b]U_z)+(-C_4η/E3)(Sin[m Pi x/a] Sin[n Pi y/b]V_z)-C_5 σzz,50];
```

```
τXY z =SetPrecision[(C6η/E3)(Cos[m Pi x/a] Cos[n Pi
y/b]Uz)+(C6ζ/E3)(Cos[m Pi x/a] Cos[n Pi y/b]Vz),50];

SumU0 = SetPrecision[SumU0 +U0,50];SumUz= SetPrecision[SumUz
+ Uz,50];
SumV0= SetPrecision[SumV0 + V0,50];SumVz= SetPrecision[SumVz
+ Vz,50];
SumW0= SetPrecision[SumW0 + W0,50];SumWz= SetPrecision[SumWz
+ Wz,50];
SumZz = SetPrecision[SumZz + Zz,50];
SumXg=SetPrecision[SumXg+Xg,50];
SumYz = SetPrecision[SumYz +Yz ,50];

Sumu02=SetPrecision[Sumu02+u02,50];Sumuz2=SetPrecision[Sumuz2+
uz2,50];
Sumv02=SetPrecision[Sumv02+v02,50];Sumvz2=SetPrecision[Sumvz2+
vz2,50];
Sumw02=SetPrecision[Sumw02+w02,50];Sumwz2=SetPrecision[Sumwz2+
wz2,50];
SumσzTop = SetPrecision[SumσzTop+σzTop,50];
Sumσzz = SetPrecision[Sumσzz +σzz ,50];
Sumτxz z = SetPrecision[Sumτxz z+τxz z,50];
Sumτyz z =SetPrecision[Sumτyz z+τyz z,50];
SumσX Top= SetPrecision[SumσX Top + σX Top,50];
SumσX z= SetPrecision[SumσX z + σX z,50];
SumσY Top= SetPrecision[SumσY Top + σY Top,50];
SumσY z= SetPrecision[SumσY z + σY z,50];
SumτXY Top= SetPrecision[SumτXY Top + τXY Top,50];
SumτXYz=SetPrecision[SumτXY z + τXY z,50];]]

Sumu02;
Sumuz2;
Sumv02;
Sumvz2;
Sumw02;
Sumwz2;
Sumσzz;
Sumτxz z;
Sumτyz z;
SumσX Top;
SumσX z;
SumσY Top;
SumσY z;
SumτXY Top
SumτXY z
SumXg;
SumYz;
```

A.2 MATHEMATICA code for a 3-ply CLT fully simply supported under uniformly distributed load (Case Study 2 - section 5.4.2)

```
E1=11000;E2=370;E3=370;
G12=690;G13=690;G23=50;
v12=0.44;v13=0.44;v23=0.64;v21=v12*E2/E1;v32=v23*E3/E2;v31=
v13*E3/E1;

Q=1-v12*v21-v23*v32-v31*v13-2*v12*v23*v31;
C11=SetPrecision[E1*(1-
v23*v32)/Q,50];C12=SetPrecision[E1*(v21+v31*v23)/Q,50];C22=S
etPrecision[E2*(1-v13*v31)/Q,50];
C13=SetPrecision[E1*(v31+v21*v32)/Q,50];C33=SetPrecision[E3*
(1-v12*v21)/Q,50];C23=SetPrecision[E2*(v32+v12*v31)/Q,50];
C44=SetPrecision[G23,50];C55=SetPrecision[G13,50];C66=SetPrec
ision[G12,50];

C1=-(C13/C33);C2=C11-C13^2 /C33;C3=C12-(C13 C23)/C33;C4=C22-
Subscript[C, 23]^2/C33;C5=-
(C23/C33);C6=C66;C7=1/C33;C8=1/C55;C9=1/C44;
C190=-(C23/C33);C290=C22-C23^2 /C33;C390=C12-(C13 C23)/C33;C490=C11-
Subscript[C, 13]^2/C33;C590=-
(C13/C33);C690=C66;C790=1/C33;C890=1/C44;C990=1/C55;

Clear[a,b,q,z0,z1 ];

sumUz30=0;sumVz30=0;sumWz30=0;sumZz30=0;sumXz130=0;sumYz30=0;sumσ
Xz30=0;sumσyz30=0;sumτXY30=0;sumσzz30=0;sumτxzz30=0;sumτyzz
30=0;sumUz60=0;sumVz60=0;sumWz60=0;sumZz60=0;sumσzz60=0;sumXz160
=0;sumτxzz60=0;sumYz60=0;sumτyzz60=0;sumσXz60=0;sumσyz60=0;s
umτXYz60=0;sumUz90=0;sumVz90=0;sumWz90=0;sumZz60=0;sumσzz90=0;s
umXz190=0;sumYz90=0;sumτxzz90=0;sumτyzz90=0;sumσXz90=0;sumσyz
90=0;sumτXYz90=0;

a=360;b=360;z0=30;z1=30;q=1;
x =a/2;y=b/2;

I6=SetPrecision[IdentityMatrix[6],50];

For[i=1, i <39,i+=2,m=i;
 For[ii=1, ii <39,ii+=2,n=ii;
ZTop=SetPrecision[-((16 q)/(m n π2)),50];
LTop=SetPrecision[(_{{ZTop},{0},{0}}_),50];
LBottom=SetPrecision[(_{{0},{0},{0}}_),50];

ζ=SetPrecision[(m*π)/a,50];η=SetPrecision[(n*π)/b,50];
```

```
D01=(_{{0, 0, 0, C8, 0, -ζ},{0, 0, 0, 0, C9, -η},{0, 0, 0,
ζ, η, 0},{C2 ζ2+C6 η2, (C3+C6)ζ*η, C1ζ, 0, 0, 0},{(C3+C6)ζ*η,
C6 ζ2+C4 η2, C5η, 0, 0, 0},{-C1ζ, -C5η, C7, 0, 0, 0}}_);
D0=SetPrecision[D01,50];

D090=(_{{0, 0, 0, C890, 0, -ζ},{0, 0, 0, 0, C990, -η},{0, 0,
0, ζ, η, 0},{C290 ζ2+C690 η2, (C390+C690)ζ*η, C190ζ, 0, 0, 0},
{(C390+C690)ζ*η, C690 ζ2+C490 η2, C590η, 0, 0, 0},{-C190ζ, -C590η,
C790, 0, 0, 0}}_);
D90=SetPrecision[D090,50];

eDz0=SetPrecision[MatrixExp[D0*z0],50];eDz90=SetPrecision[M
atrixExp[D90*z1],50];

pie1=SetPrecision[eDz90.eDz0,50];pie=SetPrecision[eDz0.eDz9
0.eDz0,50];

L1=(_{{pie[[3,1]], pie[[3,2]], pie[[3,6]]},
     {pie[[4,1]], pie[[4,2]], pie[[4,6]]},
     {pie[[5,1]], pie[[5,2]], pie[[5,6]]}}_);
L2 = (_{{pie[[3,3]], pie[[3,4]], pie[[3,5]]},
     {pie[[4,3]], pie[[4,4]], pie[[4,5]] },
     {pie[[5,3]], pie[[5,4]], pie[[5,5]]} }_);

XTop=SetPrecision[LinearSolve[L1,(LBottom - L2.LTop)],50] ;
U0=XTop[[1,1]];V0=XTop[[2,1]];W0=XTop[[3,1]];

Xz30=SetPrecision[SetPrecision[MatrixExp[D0*0],50].(_{
{U0},{V0},{ZTop},{0},{0},{W0}}_),50];

Uz30=Xz30[[1,1]];Vz30=Xz30[[2,1]];Zz30=Xz30[[3,1]];Xz130=Xz30[[4,1]
];Yz30=Xz30[[5,1]];Wz30=Xz30[[6,1]];

σXz30=SetPrecision[(-C2ζ)(Sin[m Pi x/a] Sin[n Pi
y/b]Uz30)+(-C3η)(Sin[m Pi x/a] Sin[n Pi y/b]Vz30)-C1(Sin[m Pi
x/a] Sin[n Pi y/b]Zz30),50];
σyz30=SetPrecision[(-C3ζ)(Sin[m Pi x/a] Sin[n Pi
y/b]Uz30)+(-C4η)(Sin[m Pi x/a] Sin[n Pi y/b]Vz30)-C5(Sin[m Pi
x/a] Sin[n Pi y/b]Zz30),50];
τXY30=SetPrecision[(C6η)(Cos[m Pi x/a] Cos[n Pi
y/b]Uz30)+(C6ζ)(Cos[m Pi x/a] Cos[n Pi y/b]Vz30),50];

σzz30=SetPrecision[Sin[m Pi x/a] Sin[n Pi y/b] Zz30,50];
τxzz30=SetPrecision[Cos[m Pi x/a] Sin[n Pi y/b] Xz130,50];
τyzz30=SetPrecision[Sin[m Pi x/a] Cos[n Pi y/b]Yz30,50];

Xz60=SetPrecision[SetPrecision[MatrixExp[D90*0].eDz0,50].(_{
{U0},{V0},{ZTop},{0},{0},{W0}}_),50];

Uz60=Xz60[[1,1]];Vz60=Xz60[[2,1]];Zz60=Xz60[[3,1]];Xz160=Xz60[[4,1]
];Yz60=Xz60[[5,1]];Wz60=Xz60[[6,1]];
```

```
σXz60=SetPrecision[(-C290ζ)(Sin[m Pi x/a] Sin[n Pi
y/b]Uz60)+(-C390η)(Sin[m Pi x/a] Sin[n Pi y/b]Vz60)-C190(Sin[m
Pi x/a] Sin[n Pi y/b]Zz60),50];
σyz60=SetPrecision[(-C390ζ)(Sin[m Pi x/a] Sin[n Pi
y/b]Uz60)+(-C490η)(Sin[m Pi x/a] Sin[n Pi y/b]Vz60)-C590(Sin[m
Pi x/a] Sin[n Pi y/b]Zz60),50];
τXYz60=SetPrecision[(C690η)(Cos[m Pi x/a] Cos[n Pi
y/b]Uz60)+(C690ζ)(Cos[m Pi x/a] Cos[n Pi y/b]Vz60),50];
σzz60=SetPrecision[Sin[m Pi x/a] Sin[n Pi y/b]Zz60,50];
τxzz60=SetPrecision[Cos[m Pi x/a] Sin[n Pi y/b] Xz160,50];
τyzz60=SetPrecision[Sin[m Pi x/a] Cos[n Pi y/b]Yz60,50];

Xz90=SetPrecision[SetPrecision[MatrixExp[D0*0].eDz90.eDz0,5]
.(_{ {U0},{V0},{ZTop},{0},{0},{W0}}_),50];

Uz90=Xz90[[1,1]];Vz90=Xz90[[2,1]];Zz90=Xz90[[3,1]];Xz190=Xz90[[4,1]
];Yz90=Xz90[[5,1]];Wz90=Xz90[[6,1]];

σXz90 =SetPrecision[(-C2ζ)(Sin[m Pi x/a] Sin[n Pi
y/b]Uz90)+(-C3η)(Sin[m Pi x/a] Sin[n Pi y/b]Vz90)-C1(Sin[m Pi
x/a] Sin[n Pi y/b]Zz90),50];
σyz90 =SetPrecision[(-C3ζ)(Sin[m Pi x/a] Sin[n Pi
y/b]Uz90)+(-C4η)(Sin[m Pi x/a] Sin[n Pi y/b]Vz90)-C5(Sin[m Pi
x/a] Sin[n Pi y/b]Zz90),50];
τXYz90 =SetPrecision[(C6η)(Cos[m Pi x/a] Cos[n Pi
y/b]Uz90)+(C6ζ)(Cos[m Pi x/a] Cos[n Pi y/b]Vz90),50];

σzz90= SetPrecision[Sin[m Pi x/a] Sin[n Pi y/b] Zz90,50];
τxzz90=SetPrecision[Cos[m Pi x/a] Sin[n Pi y/b] Xz190,50];
τyzz90=SetPrecision[Sin[m Pi x/a] Cos[n Pi y/b]Yz90,50];

Xz=SetPrecision[pie.(_{{U0},{V0},{ZTop},{0},{0},{W0}}_),50];
Uz =
Xz[[1,1]];Vz=Xz[[2,1]];Zz=Xz[[3,1]];Xz1=Xz[[4,1]];Yz=Xz[[5,1]]
;Wz=Xz[[6,1]];

sumUz30=Uz30+sumUz30;sumVz30=Vz30+sumVz30;sumWz30=Wz30+sumWz30;sumZz
30=Zz30+sumZz30;sumXz130=Xz130+sumXz130;sumYz30=Yz30+sumYz30;sumσXz3
0=σXz30+sumσXz30;sumσyz30=σyz30+sumσyz30;sumτXY30=τXY30+sum
τXY30;sumσzz30=σzz30+sumσzz30;sumτxzz30=τxzz30+sumτxzz30;su
mτyzz30=τyzz30+sumτyzz30;sumUz60=Uz60+sumUz60;sumVz60=Vz60+sumVz
60;sumWz60=Wz60+sumWz60;sumZz60=Zz60+sumZz60;sumσzz60=σzz60+sumσz
z60;sumXz160=Xz160+sumXz160;sumτxzz60=τxzz60+sumτxzz60;sumYz60=Y
z60+sumYz60;sumτyzz60=τyzz60+sumτyzz60;sumσXz60=σXz60+sumσXz6
0;sumσyz60=σyz60+sumσyz60;sumτXYz60=τXYz60+sumτXYz60;sumUz90
=Uz90+sumUz90;sumVz90=Vz90+sumVz90;sumWz90=Wz90+sumWz90;sumZz60=Zz60+
sumZz60;sumσzz90=σzz90+sumσzz90;sumXz190=Xz190+sumXz190;sumYz90=Y
z90+sumYz90;sumτxzz90=τxzz90+sumτxzz90;sumτyzz90=τyzz90+sumτy
zz90;sumσXz90=σXz90+sumσXz90;sumσyz90=σyz90+sumσyz90;sumτXY
z90=τXYz90+sumτXYz90;]]
```

sumU_{z30};
sumV_{z30};
sumW_{z30}
sumZ_{z30};
sumσzz30;
sumX_{z130};
sumτxzz30;
sumY_{z30};
sumτyzz30;
sumσXz30;
sumσyz30;
sumτXY30;

sumU_{z60};
sumV_{z60};
sumW_{z60};
sumZ_{z60};
sumσzz60;
sumX_{z160};
sumτxzz60;
sumY_{z60};
sumτyzz60;
sumσXz60;
sumσyz60;
sumτXYz60;

sumU_{z90};
sumV_{z90};
sumW_{z90};
sumZ_{z60};
sumσzz90;
sumX_{z190};
sumτxzz90;
sumY_{z90};
sumτyzz90;
sumσXz90;
sumσyz90;
sumτXYz90;

A.3 MATHEMATICA code for a 3-ply CLT three sides simply supported with a free edge under sinusoidal load (Case Study 1 – section 6.6.1.1)

```
E1=11000;E2=370;E3=370;
G12=690;G13=690;G23=50;
v12=0.44;v13=0.44;v23=0.64;v21=v12*E2/E1;v32=v23*E3/E2;v31=
v13*E3/E1;

Q=1-v12*v21-v23*v32-v31*v13-2*v12*v23*v31;
C11=SetPrecision[E1*(1-
v23*v32)/Q,50];C12=SetPrecision[E1*(v21+v31*v23)/Q,50];C22=S
etPrecision[E2*(1-v13*v31)/Q,50];
C13=SetPrecision[E1*(v31+v21*v32)/Q,50];C33=SetPrecision[E3*
(1-v12*v21)/Q,50];C23=SetPrecision[E2*(v32+v12*v31)/Q,50];
C44=SetPrecision[G23,50];C55=SetPrecision[G13,50];C66=SetPrec
ision[G12,50];

C1=-(C13/C33);C2=C11-C13^2/C33;C3=C12-(C13 C23)/C33;C4=C22-
Subscript[C, 23]^2/C33;C5=-
(C23/C33);C6=C66;C7=1/C33;C8=1/C55;C9=1/C44;
C190=-(C23/C33);C290=C22-C23^2/C33;C390=C12-(C13 C23)/C33;C490=C11-
Subscript[C, 13]^2/C33;C590=-
(C13/C33);C690=C66;C790=1/C33;C890=1/C44;C990=1/C55;

Clear[a,b,q,z0,z1 ];

a=360;b=360;z0=30;z1=30;q=1;
x =0;y=b/2;

I6=SetPrecision[IdentityMatrix[6],50];

m=1;n=1;
ZTop=SetPrecision[-1,50];
LTop=SetPrecision[(_{{ZTop},{0},{0}}_),50];
LBottom=SetPrecision[(_{{0},{0},{0}}_),50];
ζ=SetPrecision[(m*π)/a,50];η=SetPrecision[(n*π)/b,50];
D01=(_{{0, 0, 0, C8, 0, -ζ},{0, 0, 0, 0, C9, -η},{0, 0, 0,
ζ, η, 0},{C2 ζ2+C6 η2, (C3+C6)ζ*η, C1ζ, 0, 0, 0},{(C3+C6)ζ*η,
C6 ζ2+C4 η2, C5η, 0, 0, 0},{-C1ζ, -C5η, C7, 0, 0, 0}}_);
D0=SetPrecision[D01,50];
D090=(_{{0, 0, 0, C890, 0, -ζ},{0, 0, 0, 0, C990, -η},{0, 0,
0, ζ, η, 0}, {C290 ζ2+C690 η2, (C390+C690)ζ*η, C190ζ, 0, 0, 0},
{(C390+C690)ζ*η, C690 ζ2+C490 η2, C590η, 0, 0, 0},{-C190ζ, -C590η,
C790, 0, 0, 0}}_);
D90=SetPrecision[D090,50];

eDz0=SetPrecision[MatrixExp[D0*z0],50];eDz90=SetPrecision[M
atrixExp[D90*z1],50];
```

```
pie1=SetPrecision[eDz90.eDz0,50];pie=SetPrecision[eDz0.eDz9
0.eDz0,50];

L1=(_{{pie[[3,1]], pie[[3,2]], pie[[3,6]]},{pie[[4,1]],
pie[[4,2]], pie[[4,6]]},{pie[[5,1]],
pie[[5,2]],pie[[5,6]]}}_);
L2 = (_{pie[[3,3]], pie[[3,4]], pie[[3,5]]},{pie[[4,3]],
pie[[4,4]], pie[[4,5]]},{pie[[5,3]],
pie[[5,4]],pie[[5,5]]}}_);

X_Top=SetPrecision[LinearSolve[L1,(L_Bottom - L2.L_Top)],50]
;U_0=X_Top[[1,1]];V_0=X_Top[[2,1]];W_0=X_Top[[3,1]];

X_z30=SetPrecision[SetPrecision[MatrixExp[D0*0],50].(_{
{U_0},{V_0},{Z_Top},{0},{0},{W_0}}_),50];

U_z30SS=X_z30[[1,1]];V_z30SS=X_z30[[2,1]];Z_z30SS=X_z30[[3,1]];X_z130SS=X_z30[
[4,1]];Y_z30SS=X_z30[[5,1]];W_z30SS=X_z30[[6,1]];

σXz30SS=SetPrecision[(-C_2ζ)(Sin[m Pi x/a] Sin[n Pi
y/b]U_z30SS)+(-C_3η)(Sin[m Pi x/a] Sin[n Pi y/b]V_z30SS)-C_1(Sin[m
Pi x/a] Sin[n Pi y/b]Z_z30SS),50];
σyz30SS=SetPrecision[(-C_3ζ)(Sin[m Pi x/a] Sin[n Pi
y/b]U_z30SS)+(-C_4η)(Sin[m Pi x/a] Sin[n Pi y/b]V_z30SS)-C_5(Sin[m
Pi x/a] Sin[n Pi y/b]Z_z30SS),50];
τXY30SS=SetPrecision[(C_6η)(Cos[m Pi x/a] Cos[n Pi
y/b]U_z30SS)+(C_6ζ)(Cos[m Pi x/a] Cos[n Pi y/b]V_z30SS),50];
σzz30SS=SetPrecision[Sin[m Pi x/a] Sin[n Pi y/b] Z_z30SS,50];
τxzz30SS=SetPrecision[Cos[m Pi x/a] Sin[n Pi y/b]X_z130SS,50];
τyzz30SS=SetPrecision[Sin[m Pi x/a] Cos[n Pi y/b]Y_z30SS,50];

U_n30=SetPrecision[(-(η*U_z30SS+ζ*V_z30SS)*-1^m)/(((C_3 η2 a(a
Exp[a/a]-a))/(2C_2)+(Exp[a/a]/2))*η),50];
W_n30=SetPrecision[W_z30SS,50];
X_n30=SetPrecision[(-X_z130SS*-1^m)/(Exp[a/a]-1),50];

U_z30=SetPrecision[((U_z30SSCos[ζ x])1+((C_3 η2 a((a* Exp[x/a])-
x))/(2C_2)*U_n30))*Sin[η y],50]

V_z30= SetPrecision[((V_z30SS Sin[ζ x])+(a/2 ((Exp[x/a]-
1))*U_n30*η))*Cos[η y],50];

W_z30= SetPrecision[((W_z30SSSin[ζ x])+((Exp[x/a]-
1)*W_n30))*Sin[η y],50];

σxz30=SetPrecision[(-C_2ζ)(Sin[ζ x] Sin[η y]U_z30SS)+(-
C_3η)(Sin[ζ x] Sin[η y]V_z30SS)-C_1Sin[ζ x] Sin[η y]Z_z30SS+(C_2(C_3
η2 a((Exp[x/a])-1))/(2C_2)*U_n30*Sin[η y])-(C_3*(a/2*(Exp[x/a]-
1))*(η2)*U_n30*Sin[η y]),50];
```

```
σyz30=SetPrecision[(-C3ζ)(Sin[ζ x] Sin[η y]Uz30SS)+(-
C4η)(Sin[ζ x] Sin[η y]Vz30SS)-C5Sin[ζ x] Sin[η y]Zz30SS+(C3(C3
η2 a((Exp[x/a])-1))/(2C2)*Un30*Sin[η y])-(C4
*(a/2*(Exp[x/a]-1))*(η2)*Un30*Sin[η y]),50];

τXYz30=SetPrecision[((C6η)(Cos[ζ x] Cos[η
y]Uz30SS))+((C6ζ)(Cos[ζ x] Cos[η y]Vz30SS))+((C6η((C3 η2 a((a
Exp[x/a])-x))/(2C2)))(Un30*Cos[η y]))+((C6η
Exp[x/a]/2)(Un30*Cos[η y])),50];

τXZz30=SetPrecision[((Xz130SS Cos[ζ x])+((Exp[x/a]-
1)*Xn30))*Sin[η y],50];

Xz60=SetPrecision[SetPrecision[MatrixExp[D90*0].eDz0,50].(_{
{U0},{V0},{ZTop},{0},{0},{W0}}_),50];

Uz60SS=Xz60[[1,1]];Vz60SS=Xz60[[2,1]];Zz60SS=Xz60[[3,1]];Xz160SS=Xz60[
[4,1]];Yz60SS=Xz60[[5,1]];Wz60SS=Xz60[[6,1]];

σXz60SS=SetPrecision[(-C290ζ)(Sin[m Pi x/a] Sin[n Pi
y/b]Uz60SS)+(-C390η)(Sin[m Pi x/a] Sin[n Pi y/b]Vz60SS)-
C190(Sin[m Pi x/a] Sin[n Pi y/b]Zz60SS),50];
σyz60SS=SetPrecision[(-C390ζ)(Sin[m Pi x/a] Sin[n Pi
y/b]Uz60SS)+(-C490η)(Sin[m Pi x/a] Sin[n Pi y/b]Vz60SS)-
C590(Sin[m Pi x/a] Sin[n Pi y/b]Zz60SS),50];
τXYz60SS=SetPrecision[(C690η)(Cos[m Pi x/a] Cos[n Pi
y/b]Uz60SS)+(C690ζ)(Cos[m Pi x/a] Cos[n Pi y/b]Vz60SS),50];
σzz60SS=SetPrecision[Sin[m Pi x/a] Sin[n Pi y/b]Zz60SS,50];
τxzz60SS=SetPrecision[Cos[m Pi x/a] Sin[n Pi y/b]
Xz160SS,50];
τyzz60SS=SetPrecision[Sin[m Pi x/a] Cos[n Pi y/b]Yz60SS,50];

Un60=SetPrecision[(-(η*Uz60SS+ζ*Vz60SS)*-1m)/(((C390 η2 a((a*
Exp[a/a])-a))/(2C290)+(Exp[a/a]/2))*η),50];
Wn60=SetPrecision[Wz60SS,50];
Xn60=SetPrecision[(-Xz160SS*-1m)/(Exp[a/a]-1),50];

Uz60=SetPrecision[((Uz60SSCos[ζ x])+((C390 η2 a((a* Exp[x/a])-
x))/(2C290)*Un60))*Sin[η y],50];

Vz60=SetPrecision[((Vz60SS Sin[ζ x])+(a/2 ((Exp[x/a]-
1))*Un60*η))*Cos[η y],50];

Wz60=SetPrecision[(Wz60SSSin[ζ x]+((Exp[x/a]-1)*Wn60))*Sin[η
y],50];

σxz60=SetPrecision[(-C290ζ)(Sin[ζ x] Sin[η y]Uz60SS)+(-
C390η)(Sin[ζ x] Sin[η y]Vz60SS)-C190Sin[ζ x] Sin[η y]Zz60SS+(C290
(C390 η2 a((Exp[x/a])-1))/(2C290)*Un60*Sin[η y])-
(C390*(a/2*(Exp[x/a]-1))*η2*Un60*Sin[η y]),50];
```

σyz60=SetPrecision[(-C_{390}ζ)(Sin[ζ x] Sin[η y]U_{z60SS})+(-C_{490}η)(Sin[ζ x]Sin[η y]V_{z60SS})-C_{590}Sin[ζ x] Sin[η y] Z_{z60SS}+(C_{390}(C_{390} η2 a((Exp[x/a])-1))/(2C_{290})*U_{n60}*Sin[η y])-(C_{490}*(a/2*(Exp[x/a]-1))*η2*U_{n60}*Sin[η y]),50];

τXYz60=SetPrecision[((C_{690}η)(Cos[ζ x] Cos[η y]U_{z60SS}))+((C_{690}ζ)(Cos[ζ x] Cos[η y]V_{z60SS}))+((C_{690}η ((C_{390} η2 a((a Exp[x/a])-x))/(2C_{290})))(U_{n60}*Cos[η y]))+((C_{690}η Exp[x/a]/2)(U_{n60}*Cos[η y])),50];

τXZz60=SetPrecision[((X_{z160SS} Cos[ζ x])+((Exp[x/a]-1)*X_{n60}))*Sin[η y],50];

X_{z90}=SetPrecision[SetPrecision[MatrixExp[D0*0].eDz90.eDz0,50].(_{{U_0},{V_0},{Z_{Top}},{0},{0},{W_0}}_),50];

U_{z90SS}=X_{z90}[[1,1]];V_{z90SS}=X_{z90}[[2,1]];Z_{z90SS}=X_{z90}[[3,1]];X_{z190SS}=X_{z90}[[4,1]];Y_{z90SS}=X_{z90}[[5,1]];W_{z90SS}=X_{z90}[[6,1]];

σXz90SS =SetPrecision[(-C_2ζ)(Sin[m Pi x/a] Sin[n Pi y/b]U_{z90})+(-C_3η)(Sin[m Pi x/a] Sin[n Pi y/b]V_{z90})-C_1(Sin[m Pi x/a] Sin[n Pi y/b]Z_{z90}),50];
σyz90SS =SetPrecision[(-C_3ζ)(Sin[m Pi x/a] Sin[n Pi y/b]U_{z90})+(-C_4η)(Sin[m Pi x/a] Sin[n Pi y/b]V_{z90})-C_5(Sin[m Pi x/a] Sin[n Pi y/b]Z_{z90}),50];
τXYz90SS =SetPrecision[(C_6η)(Cos[m Pi x/a] Cos[n Pi y/b]U_{z90})+(C_6ζ)(Cos[m Pi x/a] Cos[n Pi y/b]V_{z90}),50];
σzz90SS= SetPrecision[Sin[m Pi x/a] Sin[n Pi y/b] Z_{z90},50];
τxzz90SS=SetPrecision[Cos[m Pi x/a] Sin[n Pi y/b] X_{z190},50];
τyzz90SS=SetPrecision[Sin[m Pi x/a] Cos[n Pi y/b]Y_{z90},50];

U_{n90}=SetPrecision[(-(η*U_{z90SS}+ζ*V_{z90SS})*-1^m)/(((C_3 η2 a(a Exp[a/a]-a))/(2C_2)+(Exp[a/a]/2))*η),50];
W_{n90}=SetPrecision[W_{z90SS},50];
X_{n90}=SetPrecision[(-X_{z190SS}*-1^m)/(Exp[a/a]-1),50];

U_{z90}=SetPrecision[((U_{z90SS}Cos[ζ x])+((C_3 η2 a((a* Exp[x/a])-x))/(2C_2)*U_{n90}))*Sin[η y],50];

V_{z90}= SetPrecision[((V_{z90SS} Sin[ζ x])+(a/2((Exp[x/a]-1))*U_{n90}*η))*Cos[η y],50];

W_{z90}= SetPrecision[((W_{z90SS}Sin[ζ x])+((Exp[x/a]-1)*W_{n90}))*Sin[η y],50];

σxz90=SetPrecision[(-C_2ζ)(Sin[ζ x] Sin[η y]U_{z90SS})+(-C_3η)(Sin[ζ x] Sin[η y]V_{z90SS})-C_1Sin[ζ x] Sin[η y] Z_{z90SS}+(C_2 (C_3 η2 a((Exp[x/a])-1))/(2C_2)*U_{n90}*Sin[η y])-(C_3 *(a/2*(Exp[x/a]-1))*(η2)*U_{n90}*Sin[η y]),50];

```
σyz90=SetPrecision[(-C3ζ)(Sin[ζ x] Sin[η y]Uz90SS)+(-
C4η)(Sin[ζ x] Sin[η y]Vz90SS)-C5Sin[ζ x] Sin[η y] Zz90SS+(C3
(C3 η2 a((Exp[x/a])-1))/(2C2)*Un90*Sin[η y])-(C4
*(a/2*(Exp[x/a]-1))*(η2)*Un90*Sin[η y]),50];

τXYz90=SetPrecision[((C6η)(Cos[ζ x] Cos[η
y]Uz90SS))+((C6ζ)(Cos[ζ x] Cos[η y]Vz90SS))+((C6η((C3 η2 a((a
Exp[x/a])-x))/(2C2)))(Un90*Cos[η y]))+((C6η
Exp[x/a]/2)(Un90*Cos[η y])),50];

τXZz90=SetPrecision[((Xz190SS Cos[ζ x])+((Exp[x/a]-
1)*Xn90))*Sin[η y],50];
```

Appendix B

B.1 The effect of different h/a on the in-plane stress (σ_x/q) through the thickness in Figure 4-12.

Table B.1 SSA and FEM results for different h/a on the in-plane stress (σ_x/q) through the thickness in Figure 4-12.

σ_x/q		
z/h	h/a = 0.2	
	SSA	FEM
0.00	-11.5818	-11.5783
0.07	-9.4761	-9.4888
0.13	-7.6747	-7.6724
0.19	-6.0681	-6.0783
0.25	-4.6628	-4.6614
0.32	-3.3722	-3.3810
0.38	-2.2007	-2.2001
0.44	-1.0756	-1.0840
0.50	0.0000	0.0000
	h/a = 0.35	
0.00	-4.1271	-4.1275
0.04	-3.4448	-3.4454
0.07	-2.8679	-2.8687
0.11	-2.3804	-2.3812
0.14	-1.9682	-1.9692
0.18	-1.6196	-1.6206
0.21	-1.3240	-1.3251
0.25	-1.0728	-1.0739
0.29	-0.8581	-0.8593
0.32	-0.6730	-0.6742
0.36	-0.5116	-0.5129
0.39	-0.3684	-0.3697
0.43	-0.2385	-0.2398
0.46	-0.1172	-0.1186
0.50	-0.0000	0.0000

σ_x/q		
z/h	h/a = 0.5	
	SSA	FEM
0.00	-2.3629	-2.3631
0.02	-1.9777	-1.9569
0.05	-1.6507	-1.6213
0.07	-1.3734	-1.3362
0.10	-1.1387	-1.0970
0.12	-0.9405	-0.8968
0.14	-0.7736	-0.7297
0.17	-0.6334	-0.5906
0.19	-0.5159	-0.4753
0.21	-0.4179	-0.3802
0.24	-0.3364	-0.3019
0.26	-0.2689	-0.2379
0.29	-0.2133	-0.1858
0.31	-0.1677	-0.1436
0.33	-0.1305	-0.1095
0.36	-0.1001	-0.1095
0.38	-0.0754	-0.0820
0.40	-0.0552	-0.0598
0.43	-0.0385	-0.0417
0.45	-0.0243	-0.0265
0.48	-0.0117	-0.0132
0.50	0.0000	0.0000

B.2 Out-of-plane displacement *w* distribution through the thickness of the plate with *h*/*a* = 0.2 in Figure 4-15

Table B.2 SSA and FEM results for out-of-plane displacement *w* distribution through the thickness of the plate with *h*/*a* = 0.2 in Figure 4-15.

$w.E_3/qh$		
z*/*h	**SSA**	**FEM**
0.00	13.7081	13.7163
0.11	13.7052	13.7152
0.21	13.6821	13.7062
0.30	13.6512	13.6909
0.38	13.6179	13.6709
0.45	13.5843	13.6473
0.52	13.5511	13.6209
0.59	13.5180	13.5926
0.65	13.4849	13.5626
0.71	13.4515	13.5312
0.76	13.4173	13.4982
0.82	13.3827	13.4632
0.86	13.3481	13.4257
0.91	13.3143	13.3847
0.94	13.2831	13.3390
0.97	13.2550	13.2871
1.00	13.2275	13.2274

B.3 Transverse shear stress τ_{xz} distribution through the thickness of the plate with h/a = 0.2 in Figure 4-16

Table B.3 SSA and FEM results for transverse shear stress τ_{xz} distribution through the thickness of the plate with h/a = 0.2 in Figure 4-16.

τ_{xz}/q		
z/h	**SSA**	**FEM**
0.00	0.0000	-0.0821
0.06	1.4712	1.4525
0.13	2.0784	2.0478
0.19	2.4912	2.4715
0.25	2.7928	2.7799
0.31	3.0067	2.9984
0.38	3.1429	3.1375
0.44	3.2067	3.2035
0.50	3.2006	3.1990
0.56	3.1249	3.1243
0.63	2.9763	2.9772
0.69	2.7508	2.7531
0.75	2.4403	2.4443
0.81	2.0330	2.0391
0.88	1.51123	1.5204
0.94	0.8483	0.8624
1.00	0.0000	0.0193

Appendix C

C.1 The in-plane stress σ_x by the SSA through the thickness for different *h*/*a* for Case Study 2 in Figure 5-6

Table C.1 The in-plane stress σ_x distribution through the thickness of different *h*/*a* for Case Study 2 by the SSA in Figure 5-6.

z*/*h	Ply #	***h*/*a***		
		0.1	**0.3**	**0.5**
0.00		-25.1230	-4.7848	-3.1036
0.05		-20.7819	-2.8880	-1.5669
0.10	1st ply	-16.5276	-1.1199	-0.2455
0.15		-12.3431	0.5833	0.9940
0.20		-8.2116	2.2831	2.2756
0.20		-0.5472	-0.1922	-0.1786
0.25		-0.5272	-0.2145	-0.1865
0.30	2nd ply	-0.5077	-0.2376	-0.1970
0.35		-0.4891	-0.2640	-0.2145
0.40		-0.4716	-0.2963	-0.2443
0.40		-8.0092	-2.9560	-1.8734
0.45		-3.9594	-1.3910	-0.8309
0.50	3rd ply	0.0735	0.1157	0.1052
0.55		4.1057	1.6168	1.0272
0.60		8.1530	3.1648	2.0255
0.60		0.1632	-0.0038	-0.0377
0.65		0.1811	-0.0297	-0.0512
0.70	4th ply	0.1996	-0.0542	-0.0628
0.75		0.2183	-0.0796	-0.0768
0.80		0.2371	-0.1085	-0.0975
0.80		8.3098	-1.9910	-1.6082
0.85		12.4250	-0.4345	-0.6593
0.90	5th ply	16.5912	1.1195	0.2264
0.95		20.8252	2.7185	1.1386
1.00		25.1441	4.4204	2.1698

C.2 The effect of BC sensitivity on the 3-ply CLT in-plane σ_x through the thickness of h/a = 0.25 in Figure 5-18

Table C.2 The in-plane stress σ_x distribution through 3-ply CLT thickness for different BC for h/a = 0.25 in Figure 5-18.

z*/*h	Ply #	**SSA**	**BC (1)**	**BC (2)**
0.00		-13.0319	-14.3495	-13.0035
0.09		-6.5675	-7.9704	-7.0386
0.18	1st ply	-0.7688	-2.1886	-1.6680
0.27		4.8556	3.3595	3.4837
0.33		8.7339	9.0228	8.7759
0.33		-0.2852	-0.2951	-0.2932
0.36		-0.2838	-0.2859	-0.2863
0.45	2nd ply	-0.2779	-0.2748	-0.2768
0.55		-0.2763	-0.2701	-0.2772
0.64		-0.2889	-0.2803	-0.2925
0.67		-0.2981	-0.2803	-0.2778
0.67		-8.1988	-8.2530	-8.1202
0.73		-4.4698	-2.8074	-3.0584
0.82	3rd ply	0.8704	2.4423	1.8032
0.91		6.3045	7.8411	6.7995
1.00		12.2872	13.7223	12.2756

Appendix D

D.1 The SSA and FEM in-plane stress σ_x through the thickness of the CLT panel for h/a = 0.25 in Figure 6-10

Table D.1 The SSA and FEM results for in-plane stress σ_x distribution through 3-ply CLT thickness for h/a = 0.25 in Figure 6-10.

z*/*h	Ply #	**SSA**	**FEM**
0.00		-10.8941	-10.8707
0.08		-6.5081	-7.0000
0.17	1st ply	-2.5293	-3.0000
0.25		1.2859	1.1342
0.33		5.0770	4.4411
0.33		-1.0180	-0.9961
0.42		-0.6690	-0.6472
0.50	2nd ply	-0.2854	-0.2636
0.58		0.1038	0.0819
0.67		0.4485	0.4267
0.67		-5.3133	-4.4411
0.75		-1.2568	-1.1342
0.83	3rd ply	2.2909	2.8051
0.92		6.5322	6.7570
1.00		10.5695	10.8675